EFFICIENT REMOVAL OF EMERGING MICRO-POLLUTANTS AND BACTERIA FROM TREATED WASTEWATERS USING SYNTHESISED NOVEL CLAY BASED NANOCOMPOSITES

A THESIS SUBMITTED IN PARTIAL FULFILLMENT OF THE REQUIREMENTS FOR THE DEGREE OF DOCTOR OF PHILOSOPHY

SWAGATA GOSWAMI

MZU REGISTRATION NUMBER: 2100003

Ph.D. REGISTRATION NUMBER: MZU/Ph.D/1613 of 06.11.2020

DEPARTMENT OF CHEMISTRY

SCHOOL OF PHYSICAL SCIENCES

JUNE, 2024

EFFICIENT REMOVAL OF EMERGING MICRO-POLLUTANTS AND BACTERIA FROM TREATED WASTEWATERS USING SYNTHESISED NOVEL CLAY BASED NANOCOMPOSITES

BY

SWAGATA GOSWAMI

Department of Chemistry

Under the supervision of

Prof. DIWAKAR TIWARI

and

Joint Supervision of

Dr. Lalhmunsiama

Dr. Rama Dubey

Submitted

In partial fulfillment of the requirement of the Degree of Doctor of Philosophy in Chemistry of Mizoram University, Aizawl.

MIZORAM UNIVERSITY
Department of Chemistry
(A DST-FIST Supported Department)
Tanhril, Aizawl, Mizoram. PIN: 796004

Thesis Certificate

This is to certify that the thesis entitled *'EFFICIENT REMOVAL OF EMERGING MICROPOLLUTANTS AND BACTERIA FROM TREATED WASTEWATERS USING SYNTHESISED NOVEL CLAY BASED NANOCOMPOSITES'* submitted by ***Miss Swagata Goswami*** for the degree of ***Doctor of Philosophy*** in the Mizoram University, Aizawl, Mizoram, embodies the record of original investigations carried out by her under my supervision. She has been duly registered and the thesis presented is worthy of being considered for the award of the Ph.D. degree. This work has not been submitted for any degree in any other university.

Dated:

(Prof. Diwakar Tiwari)
Supervisor

(Dr. Lalhmunsiama)
Joint Supervisor

(Dr. Rama Dubey)
Joint Supervisor

Tanhril Campus, Aizawl 796004 Phone: 9862323015
Fax : (0389) 233 0834 E-mail: diw_tiwari@yahoo.com

DECLARATION OF THE CANDIDATE

Mizoram University

June, 2024

I, Swagata Goswami, hereby declare that the subject matter of this thesis is the record of work done by me, that the contents of this thesis did not form the basis of the award of any previous degree to me or to do the best of my knowledge to anybody else, and that the thesis has not been submitted by me for any research degree in any other University/Institute.

This is being submitted to the Mizoram University for the degree of Doctor of Philosophy in Chemistry.

Dated:

(Swagata Goswami)

Candidate

(Prof. N. Mohondas Singh)
Head

(Prof. Diwakar Tiwari)
Supervisor

(Dr. Lalhmunsiama)
Joint Supervisor

(Dr. Rama Dubey)
Joint Supervisor

ACKNOWLEDGEMENT

I thank Almighty God for blessing me with health, strength, and knowledge to accomplish this work. Without his grace and mercy, this work would not have been possible.

I have great pleasure in expressing my gratitude to my supervisor, *Prof. Diwakar Tiwari*, Department of Chemistry, Mizoram University, and the Joint-supervisors *Dr. Rama Dubey,* Sc 'F', DRL, DRDO, and *Dr. Lalhmunsiama*, Department of Industrial Chemistry, Mizoram University. Their dedication and most of all their overwhelming attitude had been solely responsible for the completion of my work. They are always ready to provide a fresh perspective and scholarly advice during my entire tenure. Their timely advice, scrutiny, and scientific approach have greatly aided me in completing this work.

I sincerely extend my thank and gratitude to *Prof. N. Mohondas Singh*., Head, Department of Chemistry, MZU, and other faculty members viz., *Prof. Muthukumaran, R*., *Dr. Zodinpuia Pachuau, Dr. A. Bimolini Devi, Dr. Manjeet Singh, Dr. Joydeep Das,* and *Dr. R. Lalrempuia, Dr. G. Rajendro Kumar* for their constant encouragement and useful advice they have offered me throughout my academic career in the University. My heartfelt special thanks are extended to Dr. Ved Prakash Singh for his incentive and helpful suggestions in completing my research work.

I am grateful to acknowledge the close cooperation and support I received from all of my colleagues in the Department of Chemistry. I'd like to thank *Dr. J. Lalmalsawmi, Dr. R. Malsawmdawgnzela*, *Dr. Levia Lalthazuala, Dr. CVL Hmingmawia, Mr. Himangshu Dihingsia, Mr. Ricky Lalawmpuia, Mr.Sarikokba, Ms. Lalmalsawmdawngliani, Melody Lalhruaitluangi, Mr.*

Lalruatkima Ralte, Ms. Barsha Rabha, Ms. Hmingsangzuali and Mr. Vanhmingliana for assisting me with my laboratory work. It is my pleasure to mention the assistance of *Mr. Brojendro Singh Shagolsem*, Sr. Laboratory Technician, and *Mr. John Vanlalhruaia*, Technical Assistant, Chemistry Department.

My deepest gratitude to my parents and all my family members for their love and support during my tenure for the degree, as well as their comforts and prayers; I can't repay them entirely, but I thank and appreciate them from the bottom of my heart.

Swagata Goswami

TABLE OF CONTENTS

CHAPTER 3

3. RESULTS AND DISCUSSION

CHAPTER 4

List of figures:

List of Tables:

CHAPTER 1

INTRODUCTION

1. INTRODUCTION

1.1 Background

Life on Earth has been experiencing enormous risks during the last few decades including climate change and water pollution. These risks are further directly or indirectly linked to economic and social developments. Human health, happiness, and economic prosperity are indirectly impacted by the current global environmental impacts. Water demand is rising as a result of climate change, population growth, modernization, and environmental devastation (Dolan et al., 2021). All living things including human beings depend on water to survive. Therefore, the availability of enough sources of clean water is crucial for maintaining human well-being. Even though the earth is sometimes referred to as the "Blue Planet," there are frequent warnings about the global water shortage. About 2.5% of the total amount of water on earth is freshwater and the majority of water is present in the ocean. The amount of pure water that is available is limited to that which is stored in glaciers or underground (Otieno, 2018). Every living being needs clean water for drinking; in addition to drinking, the human requires clean water for leisure and aesthetic purposes. If water is polluted, it loses its aesthetic and economic worth and poses a risk to human and aquatic organisms. Chemical pollution of rivers and streams has become one of the most significant environmental problems of the past few decades. Chemical pollutants that enter rivers and streams pose severe damage to marine life. Although some types of water pollution might emerge from natural processes; however, most of it is caused by human activity (Shetty et al., 2023). The sources of water are underground (groundwater), lakes, and rivers, and the bulk of the recycles within these sources after we consume it or contaminate it. The term "wastewater" refers to the utilized water. If the water is not treated before being released into waterways, it seriously pollutes the environment (Kesari et al., 2021).

The conventional wastewater treatment plants (WWTPs) are not efficient enough to remove completely many persistent chemicals present in the wastewater. Pharmaceuticals or endocrine-disrupting chemicals (EDCs) have received serious concerns in recent decades due to their persistence in treated wastewater (Parida et al., 2021). From these WWTPs, treated wastewater leaked and ended up in the water bodies. Therefore, the harmful chemicals present in wastewater effluents and/or their metabolites and transformation products are found in surface waters, such as rivers, lakes, and seas. Therefore, the water pollutants present in WWTP effluents has become a major concern for the environmentalist in marine environment (Akpor & OTohinoyi, 2014).

An emerging problem for global water quality is the accumulation of micro- pollutants (MPs) and increase in their concentrations in the aquatic environment (UNESCO, 2023). The presence of a wide range of micro-pollutants *viz.*, pharmaceuticals and hormones (PPHs), personal care products (PCPs), and pesticides, in the aquatic environment and wastewater treatment plant (WWTP) effluents is a serious environmental concern (Mailler et al., 2016; Samal et al., 2022). Although these organic contaminants are present at low levels, however, they greatly impact the aquatic organisms, animals, and even human health (Sailo et al., 2017). Further, no statutory permissible limit is laid down by the regulatory agencies *i.e.,* EPA (Environmental Protection Agency) or WHO (World Health Organization) for these pollutants. However, these pollutants are identified as priority hazardous substances and commonly known as emerging micropollutants in aquatic environment (Geissen et al., 2015). Current wastewater treatment plants are not specifically designed to eliminate completely these persistent micropollutants and as a consequences various micropollutants along with their metabolites and trans-formation products are often detected in receiving water bodies (Richard et al., 2014, Rogowska et al., 2020).

Conventional secondary processes such as activated sludge and trickling filters are the most extensively used in the wastewater purification; however, these processes fail to remove several chemical compounds (Petrie et al.,

2015). It has been reported that the paracetamol and ibuprofen are efficiently removed from wastewater with the percentage removal of 99% and 72–100%, respectively, by conventional treatment methods (Ratola et al., 2012, Luo et al., 2014). On the other hand, the removal of sulfamethazine and carbamazepine from wastewater is less effective and the maximum percentage removal is 13% and 7–23%, respectively (Ratola et al., 2012). Therefore, a significant amount of pharmaceuticals, personal care products, surfactants, biocides, or flame retardants are released to the surface waters from WWTP (Petrie et al., 2015). Therefore, these emerging contaminants is gradually increased in the receiving waterbodies., viz., surface water, ground water or even in drinking water (Schäfer et al., 2010, Dai et al., 2011, Zhou et al., 2011). Therefore, it is necessary to instigate additional treatment technologies to remove these emerging micropollutants from the source i.e., the effluents of the WWTP.

The presence of different microbial pathogens in a partially treated wastewater sample is another concern and the development of antimicrobial resistance (AMR) has become a serious issue globally. According to the WHO reports, there are high levels of resistance among common microbes against antimicrobial agents (Murray et al., 2022). The spread of multi-drug resistant strains, especially *Pseudomonas*, *Klebsiella*, and *Acinetobacter*, has been confirmed towards the antibiotics such as fluoroquinolones, third-generation cephalosporins and carbapenem (Horcajada et al., 2019). Annually around 7,00,000 people die due to infections caused by such resistant strains. In the US, approximately 23,000 people die because of such diseases every year; in Europe, the estimated number is approximately 25,000 in a year (WHO, 2019). Therefore, many researchers focussed on newer effective antimicrobial agents to combat AMR. *Fecal coli* bacteria are present in human and animal feces and are relatively harmless to human intestines and *Escherichia coli* is the most common species of *Fecal coli* bacteria. The presence of these bacteria in a treated wastewater indicates the failure of disinfection process; however, their nonappearance does not necessarily ensures the nonexistence of pathogens (Khan & Gupta, 2020; Oram, 2020). The ultimate goal of

researchers/environmentalists is to obtain zero fecal coliform in the treated water prior to use it for various purposes. In order to prevent transmission of various diseases, the treated wastewaters need to comply the microbiological quality guidelines. Moreover, it has been reported that the removal of cyanobacterial toxins is an issue in conventional water treatment systems (Hitzfeld et al., 2000).

1.2. Micro-pollutants and biological pollutants

1.2.1 Micro-pollutants

Micro-pollutants are a diverse group of synthetic and natural substances found in the environment at very low concentrations, often in the range of nanograms to micrograms per liter. These include pharmaceuticals, personal care products, pesticides, industrial chemicals, and endocrine disrupting chemicals. Despite their minute concentrations, micropollutants can have significant adverse effects on ecosystems and human health due to their persistence, bioaccumulation potential, and biological activity. Several these chemicals disrupt endocrine systems in wildlife, contribute to antibiotic resistance, and contaminate drinking water supplies. Micropollutants poses varied challenges due to their widespread sources, complex chemical nature, and the limitations of conventional wastewater treatment processes in effectively removing them.

The present studies focused on some of potential micropollutants, including tetracycline, bisphenol A, ciprofloxacin, triclosan, and 17α-ethinylestradiol. Tetracycline and ciprofloxacin are widely used antibiotics that can contribute to antibiotic resistance when present in aquatic environments. Bisphenol A is an endocrine disruptor that interferes the hormone systems in both wildlife and humans. Triclosan, an antibacterial and antifungal agent found in many personal care products, persistent in the environment and has been shown to disrupt aquatic ecosystems. Similarly, the 17α-ethinylestradiol is a synthetic estrogen used in oral contraceptives, and a potent endocrine

disruptor that causes reproductive and developmental issues in aquatic organisms. Each of these micropollutants presents unique challenges for environmental management and underscores the need for advanced treatment technologies to mitigate their mobility from aquatic environment to biological environment.

1.2.1.1. Tetracycline

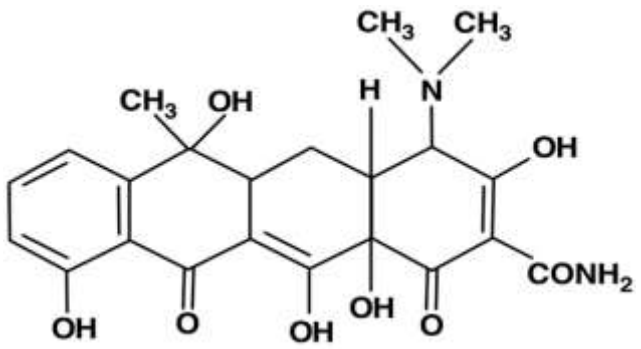

Figure 1.1: Structure of tetracycline

Tetracycline (TCH) [$C_{22}H_{24}N_2O_8$; mol. Wt. 444.435 g/mol; (4S,6S,12aS)-4-(dimethylamino)-1,4,4a,5,5a,6,11,12a-octahydro-3,6,10,12,12a-pentahydroxy-6-methyl-1,11-dioxonaphthacene-2-carboxamide)]. Tetracycline includes a naphthalene structure and widely prescribed antibiotics (Li et al., 2021).

Large amounts of antibiotics are continuously released into the environment through a variety of sources due to extensive usage of antibiotics by humans and live stocks (Wang et al., 2023). Tetracycline has been used to treat a variety of microbial infections, including anthrax, chlamydial infections, cholera, Lyme disease, and syphilis. It's also used to treat farm animals and domestic pets as veterinary medicine. Because of its effectiveness and low cost, TCH has become one of the most widely used antibiotics globally.

Statistics show that nearly 6000 tons of TCH are consumed annually in the United States and Europe, with global sales of $ 1.9 billion in 2014. Human and animal excretion of the substance in the form of urine, and feces, as well as improper disposal of expired medicines and leftovers, contribute to TCH entry into surface water (Aliyu et al., 2022). Since the TCH contributes to increased microbial resistance to similar antibiotics, removing mutant infection strains becomes difficult, if not impossible when conventional wastewater treatment processes are used (Mirsoleimani-Azizi et al., 2018). According to Sreejith et al. (2020) TCH has been detected in surface water in concentrations ranging from 0.23 to 5.32 mg/L. Significantly, the existence of a trace amount of TCH in the environment causes the emergence of antibiotic-resistant microorganisms to which humans are exposed through drinking water (Scaria et al., 2021).

1.2.1.2. Bisphenol A

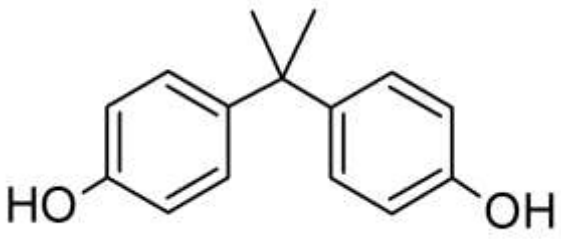

Figure 1.2: Structure of bisphenol A

Bisphenol A (BPA) [$C_{15}H_{16}O_2$; Molar mass: 228.291 g/mol; 4,4′-(Propane-2,2-diyl)diphenol] is an emerging contaminant that is often detected in natural waters at levels of ng/L or μg/L, making it a trace organic contaminant (Wang & Zhang, 2020). Bisphenol A (BPA) is an endocrine disruptive compound (EDC) that mimics or interfere with the endocrine or hormonal system (Metcalfe et al., 2022). BPA was first synthesized in 1891 by Dianin but its synthesis was first reported only in 1905 by Zincke (Rogers,

2023). BPA is widely used in the manufacture of thermal paper, food storage containers, baby bottles, reusable drink containers, toys, dish and laundry detergents, bar soaps, shampoo, shaving cream, face cleansers, sunscreen lotions, etc. Some effects of BPA on health are sexual dysfunction and fertility; metabolic disease, such as obesity; cancer (breast cancer, neuroblastoma); neurological effects (disruption of the dopaminergic system); cardiovascular diseases; thyroid disorders and asthma (Metcalfe et al., 2022). BPA alters plasma sex hormone levels in fishes and causes adverse effects in the development and reproduction of non-mammalian aquatic vertebrates, including reduced male hormones, testicular cell death, decreased sperm density, and motility, inhibition of spermatogenesis and egg production (Canesi & Fabbri, 2015).

As a monomer of many synthetic materials, bisphenol A has been widely used in diverse industries, for example, in synthesizing epoxy resins, polycarbonate, phenolic resins, polyester fibers, food cans, paint coatings, etc. The Brazilian government has banned the production and sale of plastic bottles containing bisphenol A since January 2012. Due to its high industrial yield and toxicological effect, bisphenol A has been listed as a priority pollutant in water treatment in many countries. Nowadays, most plastic containers and personal care products are produced without BPA. However, aquatic bodies are still contaminated with bisphenol A. Also, it has been reported that the BPA is able to reach the river waters mainly through leaching from BPA-based plastics or microplastics (Vilela et al., 2018).

1.2.1.3. Triclosan

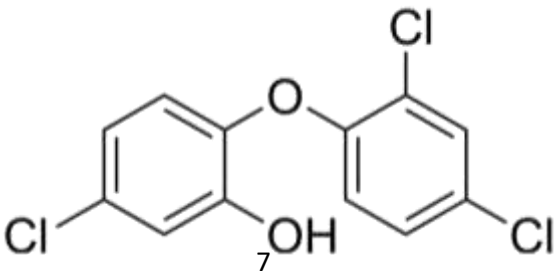

Figure 1.3: Structure of Triclosan

Triclosan (TCS) [$C_{12}H_7C_{l3}O_2$; Molar mass: 289.54 g/mol; 5-Chloro-2-(2,4-dichlorophenoxy)phenol] is a common biocide, used against Gram-negative and Gram-positive bacterium. It has extensive use in personal care products, including soaps, toothpaste, and chopping boards; therefore, triclosan has been detected in the aquatic ecosystem (Dhillon et al., 2015). Being lipophilic, triclosan accumulated in aquatic organisms on their prolonged exposures. Triclosan is detected in human breast milk, serum, urine samples, etc (Bever et al., 2018). Triclosan was initially reported as a pesticide in 1969, but it has been widely used in household products since the 1990s (US EPA, 2022). Triclosan is a well-known synthetic broad-spectrum antimicrobial agent, which inhibits the growth and activity of bacteria, viruses, and fungi. Studies have shown that triclosan inhibits enoyl-reductase involved in fatty acid synthesis in bacteria (Heath et al., 1999). At low doses, TCS acts as a bacteriostatic and at high doses as a bactericidal agent, therefore, it has been used as a major ingredient in personal care, veterinary, industrial, and household products. The extensive use of TCS provides many pathways for the compound to enter into the aquatic environment, and it is detected in sewage treatment plant effluents, surfaces, and groundwaters (Weatherly & Gosse, 2017). The physicochemical properties of TCS show the potential ability to accumulate in the environment; hence, there is a growing concern about the presence of triclosan in the environment and its potential impacts on wildlife and aquatic life (Dhillon et al., 2015). Antimicrobial soap contains 2% by weight of triclosan. The concentration of triclosan in personal care products is in the range of 0.1-0.3%. Studies show that exposure to triclosan leads to developmental and reproductive defects in infants (Weatherly & Gosse, 2017).

Triclosan has many biological effects associated with estrogen receptors. The compound leads to failure in implantation due to its ability to mimic estrogen in humans. Studies have shown that triclosan has estrogenic and androgenic properties in human breast cancer cells, which could potentially enhance the growth of cancer cells (Gee et al., 2008). Studies have shown that triclosan disrupts the thyroid hormone (TH) signaling and decreases serum T4 in male juvenile rats (Homburg et al., 2022). Triclosan structurally mimics thyroid hormones and binds to its receptors. Triclosan modulates thyroid hormone genes and blocks development in anurans (Veldhoen et al., 2006). Lin et al., (2014) reported that triclosan has the potential to damage DNA in freshwater invertebrate *Chironomus riparius* and increases the expression of the hsp27 gene. In vitro analysis of triclosan shows that it possesses intrinsic estrogenic and androgenic activity; it dislocates estradiol from ERs of MCF-7 human breast cancer cells and disturbs the testosterone from binding to the ligand-binding domain of the rat (Gee et al., 2008).

1.2.1.4. Ciprofloxacin

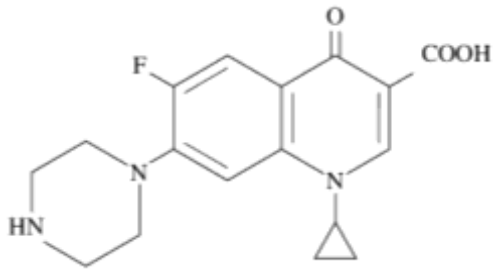

Figure 1.4: Structure of Ciprofloxacin

Ciprofloxacin (CIP) [$C_{17}H_{18}FN_3O_3$; Molar mass: 331.347 g/mol; IUPAC name: 1-Cyclopropyl-6-fluoro-4-oxo-7-(1-piperazinyl)-1,4-dihydro-3-quinolinecarboxylic acid. CIP is a broad-spectrum antibiotic and notably, antibiotics are the most widely used PCPPs (Igwegbe et al., 2021). Klein et al. analyzed antibiotic usage trends and drivers in 76 countries between 2000 and 2015. This study depicted about 65% (defined daily doses of 34.8 trillion)

increase in antibiotics consumption within the said period. Further, it was predicted that the global consumption of antibiotics could rise by 200% compared with 2015 data (if no policy changes are made) (Klein et al., 2018). Common side effects of taking CIP include nausea, vomiting, and diarrhoea. Severe side effects include an increased risk of tendon rupture, hallucinations, and nerve damage. The rates of side effects appear to be higher than some groups of antibiotics such as cephalosporins but lower than others such as clindamycin (Igwegbe et al., 2021). Ciprofloxacin (CIP) is among the leading fluoroquinolones (FQs) of choice and also the most widely used chemotherapeutic antibiotics worldwide. It was first marketed in 1987 and offers a broad spectrum antibacterial activity (Thai et al., 2023). CIP works by preventing the cellular replication of the bacteria and ultimately compromising their proliferation (Shariati et al., 2022). CIP in surface water has been found at levels ranging from 2.45 to 104 mg/L and 6.3 to 104 mg/L and from 7.0 to 104 to 0.1245 mg/L in hospital effluent (Igwegbe et al., 2021). The global concentration of CIP in surface water was reported to be within the range of 0.0018 nmol/L (Ngo et al., 2023) and a high value of 19 to 617 nmol/L. CIP like other antibiotics could accumulate in the body of organisms, thus posing a serious health threat. It is reported that CIP is one of the pharmaceutically active compounds (PhACs) that are majorly present as a contaminant in the pharmaceutical industry effluent (Samal et al., 2022). Due to the need for environmental protection and sustainable development, these effluents are treated in wastewater treatment plants for possible reuse or safe discharge into the environment. However, these pharmaceuticals, are often not eliminated by the treatment processes, thus, leading to pollution of the surface and groundwater system through water circulation. Therefore, CIP presence in the aquatic environment could cause severe toxicity to the aquatic flora and fauna species (Samal et al., 2022).

1.2.1.5. 17α-ethynylestradiol

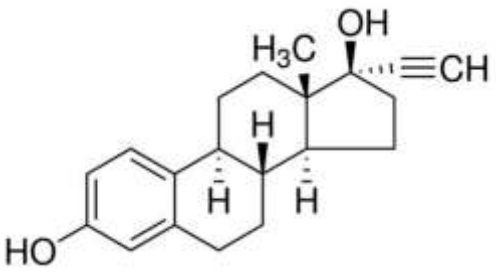

Figure 1.5: Structure of 17α-ethynylestradiol.

17α-ethynylestradiol (EE2) ($C_{20}H_{24}O_2$; Molar mass: 296.403 g/mol; Estra-1,3,5(10)-triene-3,17-diol, 17-ethynyl-) is a potential endocrine disrupting compounds (EDCs) and is extensively studied due to their potential negative effects on the endocrine systems of humans and wildlife (Ahn & Jeung, 2023). Among the known EDCs, EE2 as a synthetic estrogen with very strong estrogenic potency, has drawn much attention from environmentalists. The global annual consumption of EE2 in 1998 was around 1000 kg (Tang et al., 2021). The EE2 was first reported in Germany in January of 1938 and is quickly and clinically used as medication including prostate and breast cancers, chronic hemospermia, and induction of labor (Aris et al., 2014). As early as 1964, EE2 has been widely used as a steroid contraceptives that combined with different progestins. The biodegradability of EE2 in wastewater was first reported by Tabak and Bunch (1970). However, EE2 was not regarded as an important environmental trace contaminant until the 1990s. At present, the occurrence and fate in wastewater and other aquatic environment as well as its toxicological effects have received greater attention around the globe (Tang et al., 2021). Even at low concentration levels, EE2 poses adverse effects on fish such as feminization, induction of vitellogenin, reproduction disruption, decreased egg fertilization, and increased mortality (Armstrong et al., 2015). Among them, the most convincible study is that a collapse of fathead minnow fish population in a lake in Canada carried for seven years of field investigation on fish as exposed to 5–6 ng/L of EE2 (Kidd et al., 2007). Human excretion is

the major source of EE2 in municipal wastewater and several investigations showed that removals of EE2 from municipal WWTPs varied greatly, some studies found that the EE2 removal efficiencies are as high as 100% (Â. Almeida et al., 2020). Due to its potential adverse effect on human health, EE2 has been listed in the Japanese Drinking Water Quality Standard (Tang et al., 2021). In addition, Environmental Quality Standards suggested by the European Union showed EE2 as one priority micropollutant that might be regulated in Drinking Water Quality Standards of European countries in the future (Environmental Quality Standards-Ethinylestradiol, 2011). Surface water is the most important source of drinking water for most countries, thus contamination of surface waters with EE2 worldwide has attracted much attention. Although there have been plenty of studies on EE2 concentrations in surface waters there is a lack of systematic analysis of EE2 distributions among countries from a viewpoint of the global situation.

1.2.2. Biological pollutants

Various types of physical, chemical, and biological pollutants emerge from different sources causing the deleterious quality of water. Biological pollutants refer to the presence of various types of microbes and pathogens, especially viruses, bacteria, algae, protozoan, nematodes, insects, and their propagules (Maurya et al., 2020). There are a variety of pathogenic microorganisms, which causes various types of illness in humans. The bacteria that require organic carbon rather than carbon dioxide as a carbon source are called heterotrophic bacteria and most of the bacteria causing diseases in humans are heterotrophic. The presence of heterotrophs does not start a human health hazard, they assess the microbiological quality of the water and the effectiveness of water treatment (Larsson & Flach, 2021). Several methods are in progress for removing or inactivating waterborne pathogens (Lanrewaju et al., 2022). Chlorination is a common method of disinfection of potable water,

but it is found less effective for some microorganisms; e.g., *Cryptosporidium,* and thus, presents a challenge for removal of biological pollutants from water (Reed, 2013). The emerging number of resistant microbial strains toward the commonly applied physical and chemical disinfection methods and microbial composition of water are key factors in determining the transmission of emerging waterborne diseases. Thus, treatment methods for waterborne pathogens are assessed based on the amount, quality, and efficacy of the water since prolonged use of chlorine and chloramines encourages the growth of biofilm-forming organisms, such as *Mycobacterium*.

1.2.2.1. *Escherichia coli* (*E. coli*)

E. coli is a Gram-negative straight rod, occurring singly or in pairs, often motile by peritrichous flagella. In addition to the proteinaceous flagella, most strains have fimbriae (Pilli) or fibrillar proteins extending from the bacterial surface. Being facultative anaerobic, it possesses both a respiratory and a fermentative type of metabolism (Cooke, 1974). The optimum temperature required for growth is 37°C and well-dispersed turbidity is produced when grown in broth. According to the state of the lipopolysaccharide (LPS) of the outer membrane, strains are described as smooth (S) or rough (R). Smooth strains produce shiny convex colonies on culture media but on repeated subculture, results are rough and produce lustreless granular colonies and spontaneous agglutination in liquid media. The rough strains usually have lost their polysaccharide side chains due to mutations (Wang et al., 2005). Typical *E. coli* colonies are easy to recognize on certain differential media, for example, a characteristic metallic sheen is produced on commonly used media such as Eosin Methylene Blue Agar and Endo agar. The majority of its strains are lactose fermenters; however, some strains ferment lactose late or irregularly. Acid and gas are produced from a variety of carbohydrates with the production of pyruvate, which is further converted to lactic and formic acids. Part of this is then split by a complex hydrogenolyses system into equal amounts of carbon dioxide and hydrogen (Steinhilper et al., 2022). *E. coli* is

widely distributed in the intestine of humans and other warm-blooded animals (homeotherms, including birds and mammals) and is the predominant facultative anaerobe in the bowel, thus is often referred to as the colon bacillus. It is an essential part of the intestinal flora that maintains the physiology of the healthy host and plays a crucial role in food digestion by producing vitamin K from undigested food material (Feng et al., 2020). Although most strains of *E. coli* are not regarded as pathogens; they can be opportunistic pathogens that cause infections in immunocompromised hosts. However, there are also pathogenic strains, that cause serious infections in humans and animals. *E. coli* most commonly causes Urinary Tract Infections (UTI) especially in women. Certain strains of *E. coli* acquire virulence plasmids and produce endotoxins. Such strains are referred to as enterotoxic and enteroinvasive (Wolfe & Brubaker, 2015). In the 1890's the use of *E. coli* as an indicator of fecal contamination was proposed. This was based on the premise that *E. coli* is abundant in human and animal feces and is not usually found in other niches (Khan & Gupta, 2020). The contamination of soil and water by feces is considered a human health risk. Varied sources including droppings from humans, domestic animals, and wildlife as well as runoff from agricultural lands, inadequate septic systems, and sewage overflow are responsible for the ingress of these contaminants (Holcomb et al., 2020).

1.2.2.2. *Bacillus subtilis* (*B. subtilis*)

Bacillus subtilis is the type species of the genus *Bacillus* present in diverse environments ranging from air, water, soil, and even animal and human body surfaces. It is an isolated *Bacillus* species from environmental samples (Errington & van der Aa, 2020). *B. subtilis* was first isolated in 1835 by Ehrenberg who also named the bacterium, *Vibrio subtilis*, but it was later reclassified and named by Cohn in 1872 (Integrated Taxonomic Information System (ITIS), 2012). The species name ‘subtilis’ is a Latin word that means ‘slender’ indicating the long rod-shaped structure of the bacteria.

B. subtilis is considered an essential industrial bacterium as it is widely used in biotechnology due to the improved expression and secretion of enzymes by the bacteria (Earl et al., 2008). Besides, it is also used in food industries as flavor enhancers, sweeteners, and animal feed. B. subtilis are further classified into two subspecies *viz.*, *Bacillus subtilis* subsp. *subtilis* and *Bacillus subtilis* subspecies *spizizenii*. *B. subtilis* is the most studied Gram-positive bacterium as it is studied as a model organism for studies regarding bacterial chromosome replication and transformation. It is ubiquitous in distribution which is facilitated by the resistance of the bacteria to cold, heat, and common disinfectants (Su et al., 2020). Most *B. subtilis* species are non-pathogenic and are not associated with infections, but some strains have been associated with neoplastic diseases like fatal pneumonia and bacteremia, septicemia, and infections of necrotic axillary tumors in breast cancer. Some strains have also been implicated in foodborne illness and cases of bovine mastitis and ovine abortion (Ehling-Schulz et al., 2019). *B. subtilis* also produces an extracellular toxin called subtilisin, which is a proteinaceous compound capable of causing allergic reactions in some individuals. These reactions are often observed in immunocompromised individuals when they are exposed to such toxins regularly. The cases of allergies and hypersensitivity reactions, including dermatitis and respiratory distress, are often observed after the use of laundry products that are made with this toxin. The virulence of *B. subtilis*, and *B. subtilis* toxins, is relatively low and it has been suggested that the bacteria do not produce significant quantities of the enzymes or toxins (Gu et al., 2019).

1.2.2.3. *Pseudomonas aeruginosa* (*P. aeruginosa*)

Pseudomonas aeruginosa is a gram-negative, aerobic, non-spore-forming rod that is capable of causing a variety of infections in both immunocompetent and immunocompromised hosts (Qin et al., 2022). *P. aeruginosa* contains 12 other members in its family. Similar to other members of the genus, *P.*

aeruginosa is commonly found in soil, water, plants, and humans. Its predilection to cause infections among immunocompromised hosts, extreme versatility, antibiotic resistance, and a wide range of dynamic defence makes it an extremely challenging organism to treat in modern-day medicine (Chevalier et al., 2017). *Pseudomonas aeruginosa* is commonly found in the environment, particularly in freshwater. Reservoirs in urban communities include hot tubs, jacuzzis, and swimming pools. It can cause a wide array of community-acquired infections like folliculitis, and puncture wounds leading to osteomyelitis, pneumonia, otitis externa, and many others. It is an opportunistic pathogen and is also an important cause of nosocomial infections like ventilator-associated pneumonia, catheter-associated urinary tract infections, etc. Reservoirs in the hospital setting include potable water, taps, sinks, toothbrushes, icemakers, disinfecting solutions, sanitizers, soap bars, respiratory therapy equipment, endoscopes, and endoscope washers.

Pseudomonas aeruginosa infections are common in individuals with an immunocompromised state such as cystic fibrosis, bronchiectasis, neutropenia, burns, cancer, AIDS, organ transplant, uncontrolled diabetes mellitus, and ICU admissions. Individuals with invasive devices e.g., indwelling catheters or endotracheal tubes, are also at risk due to the organism's unique ability to form biofilms that are difficult to detect (Paprocka et al., 2022). *Pseudomonas aeruginosa* possesses many mechanisms for antibiotic resistance and a variety of virulence factors that collectively account for a broad spectrum of infections, increasingly challenging treatment for the resulting antimicrobial resistance. Multiple mechanisms have been identified for *Pseudomonas* antibiotic resistance, examples are intrinsic antibiotic resistance, efflux systems, and antibiotic-inactivating enzymes (Pang et al., 2019). The ability of *Pseudomonas* bacteria to form a biofilm is also an important mechanism with which it can increase antibiotic resistance and resist host defenses (Qin et al., 2022). This is especially important in cystic fibrosis patients, where most patients acquire the infection in the first year of life either from the environment or from healthcare facilities.

1.2.2.4. *Streptococcus pyogenes* (*S. pyogenes*)

Streptococcus pyogenes is a species of Gram-positive, aerotolerant bacteria in the genus *Streptococcus*. These bacteria are extracellular and made up of non-motile and non-sporing cocci (round cells) that tend to link in chains (Kanwal & Vaitla, 2023). They are clinically important for humans, as they are an infrequent, but usually pathogenic, part of the skin microbiota that can cause Group A streptococcal infection. *S. pyogenes* is the predominant species harbouring the Lancefield group A antigen and is often called group A *Streptococcus* (GAS) (Brouwer et al., 2023). The pathogen causes various infections, from minor, self-limiting illnesses like tonsillitis to serious, invasive diseases like necrotizing fasciitis, bacteremia, meningitis, pneumonia, streptococcal toxic shock syndrome (STSS), and endocarditis. The bacterium also causes immune-related severe sequelae in susceptible people, including rheumatic heart disease, acute rheumatic fever, and acute post-streptococcal glomerulonephritis (Cunningham, 2016). Compared to minor infections of the throat and skin, invasive and autoimmune diseases account for the majority of morbidity and mortality caused by *S. pyogenes* (Hand et al., 2020). Numerous virulence factors in *S. pyogenes* contribute to the organism's complicated pathogenicity. The *emm* gene, which codes for the M protein, fibronectin-binding protein, and collagen-binding protein, is the leading known virulence factor exposed on the cell surface of group A Streptococcus (GAS). These virulence factors establish host-pathogen interaction, determine antiphagocytic activity, and incite host immune responses. Antibiotic therapy is typically used to treat infections brought on by *S. pyogenes* (Castro & Dorfmueller, 2021). However, several instances of these diseases not responding to antibiotic therapy have been documented, making developing alternative antimicrobial medicines necessary (Murugaiyan et al., 2022). Additionally, among the *S. pyogenes* strains isolated worldwide between 1990 and 2000, 25 % and 38 % of strains were resistant to erythromycin and tetracycline, and 15% showed resistance to both (Khan et al., 2020)

1.3. Adsorption removal of water pollutants

Several techniques are in practice for water treatment at a small level or domestic scale. But, generally, the cost and maintenance of such household water treatment techniques is one of the major challenges to meeting the requirement of safe drinking water for everyone. Therefore, simplification and cost-cutting of such techniques is an important area of research. In this direction, the adsorptive purification of water for drinking purposes is gaining interest globally. Literature shows that it is one of the oldest yet widely used methods for water purification (Yoo et al., 2021). It is an established method that is used in a variety of separation and purification processes. Water treatment at the domestic level is one such process where the adsorption-based techniques have significant implications (Pillai, 2020). However, other techniques such as reverse osmosis, membrane separation, photo-oxidation, ozonolysis, etc., are energy intensive and need power to maintain water pressure (Malaeb & Ayoub, 2011; Osman et al., 2024)(REF). A review of the last 10 years of research papers on water purification shows that the use of an adsorption technique for the water treatment as compared to other techniques are maximum since this method is cost-effective method provides high removal efficiency (Talat, 2020).

Adsorption is one of the tertiary water treatment techniques, used for the removal of dissolved organic and inorganic pollutants from water (Rashed & Rashed, 2013). In this technique, the adsorbents play a critical role, and the potential of any adsorbent is determined by its specific surface area, porosity, surface functionality, selectivity, and adsorption kinetics. The efficiency of conventional adsorbents is often low due to insufficiency in one or more such properties. Nevertheless, nanomaterial (NMs) based adsorbents or nano adsorbents have a high specific surface area, well-defined porosity, and easy to modify surface structure (Awad et al., 2020). All these properties can be manipulated according to desired application, which collectively makes nano adsorbents as ideal materials for adsorptive removal of pollutants from water.

Such nano adsorbents can be easily incorporated into existing treatment methods in slurry reactors or adsorbers. Some of the nano-adsorbents are used in slurry reactors and in fixed-bed reactors, in powdered form (El-Sayed, 2020). In this process, the complete surface of the adsorbent is utilized for adsorption and yields better mass transfer reactions. These nanomaterials require separation unit for bulk separations. Therefore, the nanomaterials are introduced through the pellets/beads or porous granules and used in fixed bed reactors for making robust water purification system (Mekuye & Abera, 2023).

1.3.1. Natural clay materials

The low-cost natural materials are important for the cost-effective remediation of water contaminated with a variety of contaminants. The clays and their modified composites have been found to be either better or equivalent in contaminant adsorption capacity from water (Ewis et al., 2022). There are a variety of natural clays available around the globe, whose composition and properties varied widely from place to place and region to region. Some of natural clays possess high surface area, well defined porosity and, a large number of active; hence, utilized as efficient adsorbents (Barakan & Aghazadeh, 2020). Clays have unique physicochemical properties, which enables them to be used as excellent starting material to obtain the nanocomposite materials. Further, the layered clay is known as smectite and is widely used in synthesizing nanocomposite materials due to its applicability in structural modification, low cost, abundance, high sorption properties, and potential for ion exchange (Farias et al., 2022).

Clay minerals are generally categorized into different groups such as montmorillonite, smectite, kaolinite, illite, and chlorite. Attapulgite is palygorskite-type clay, and is a crystalloid hydrous magnesium-aluminium silicate mineral with a 2:1 ribbon-layer structure that is made up of one discontinuous octahedral layer and two continuous tetrahedral layers (Wang & Wang, 2019). It exhibits a high surface area due to its nanorod morphology and

the presence of microchannels and pores in its structure. Its application is further enhanced by its cation exchange capacity. Clays play an important role in the environment by acting as natural scavenger of pollutants by trapping cations and anions either through ion exchange or adsorption or both. Thus, clays invariably contain exchangeable cations and anions lying within the interlayers. The prominent cations and anions present within the clay structure are Ca^{2+}, Mg^{2+}, H^{+}, K^{+}, Na^{+}, Cl, and NO (Gopalapillai et al., 2013). These ions are often exchanged with other ions relatively easily without affecting the clay mineral structure. Large specific surface area, chemical and mechanical stability, layered structure, high cation exchange capacity (CEC), and so forth have made the clays excellent adsorbent materials (Pellenz et al., 2023).

1.4. Green Synthesis of Nanoparticles

Green nanotechnology is an area of interest having a significant focus on present-day scenarios with the objective of facilitating the manufacture of nanotechnology-based products that are eco-friendly and safer for all beings and with sustainable commercial viability (Pokrajac et al., 2021). The “green synthesis” of metal nanoparticles receives greater attention due to their various unique properties like optical, chemical, photochemical and electronic. Metal nanoparticles especially the noble metals have mainly been studied because of their strong optical absorption in the visible region caused by collective excitation of the free electron gas. Green synthesis of nanoparticles uses water commonly as an environment benign solvent, replacing toxic organic solvents. Biological entities have been reported as serving as both reducing and stabilizing agents for green synthesis metallic nanoparticles (Ghosh et al., 2021). Integration of green chemistry principles into nanotechnology is one of the key issues in nanoscience research. The inspiration for green chemistry and bioprocesses comes from nature through yeast, fungi, bacteria, and plant extracts in the synthesis of biocompatible metal and semiconductor nanoparticles (Kurhade et al., 2021). Innumerable physical and chemical synthetic approaches require high radiation, highly toxic reductants, and

stabilizing agents, which cause pernicious effects to both humans and marine life. In contrast, green synthesis of metallic nanoparticles is a one pot or single step eco-friendly bio-reduction method that requires relatively low energy to initiate the reaction, and, perhaps, cost effective (Philip, 2010).

Plant extracts have the potential to accumulate certain amounts of heavy metals in their diverse parts. Consequently, biosynthesis techniques employing plant extracts have gained increased consideration as a simple, efficient, cost-effective and feasible methods for synthesizing the nanoparticles (Skuza et al., 2022). These plant extracts can be utilized to reduce and stabilize the metallic nanoparticles in the "one-pot" synthesis process. Many researchers have employed green synthesis processes for preparation of metal/metal oxide nanoparticles via plant leaf extracts to further explore their various applications. Plants have biomolecules (like carbohydrates, proteins, and coenzyme) with exemplary potential to reduce metal salt into nanoparticles. Like other biosynthesis processes, gold and silver metal nanoparticles were first investigated in plant extract-assisted synthesis. Various plants [including Aloe vera (*Aloe barbadensis*), Oat (*Avena sativa*), alfalfa (*Medicago sativa*), Tulsi (*Ocimum sanctum*), Lemon (*Citrus limon*), Neem (*Azadirachta indica*), Coriander (*Coriandrum sativum*), Mustard (*Brassica juncea*) and lemon grass (*Cymbopogon flexuous*)] have been utilized to synthesize silver nanoparticles and gold nanoparticles.

1.4.1. Silver nanoparticles

Synthesized silver nanoparticles have a wide range of applications because of their remarkable physical and chemical properties. The ancient times, silver was used for making jewellery, utensils, dental alloy, photography, monetary currency, explosives, etc. (El-Nour et al., 2010). Silver is a basic, rare, and naturally occurring element on the earth, which is slightly harder than gold, very ductile, and malleable having the highest electrical and thermal conductivity with minimum contact resistance compared to all other metals AgNPs of smaller than 100 nm consist of about 10,000–15,000 silver atoms.

These nanoparticles are prepared by engineering the metallic silver into very ultrafine particles using various physical methods, which include spark discharging, solution irradiation, electrochemical reduction, and cytochemical synthesis (Zhang et al., 2016).

These silver nanoparticles provide significant pharmaceutical, clinical, biological, and immunological applications. They are used to prevent infection, in (burn and traumatic) wound dressings, diabetic ulcers, coating of catheters, dental works, scaffolds, and medical devices (Burdușel et al., 2018). Besides, silver nanoparticles are used as anticancer agents, and employed in the field of tissue engineering and in drug delivery. The chemical synthesis process of the Ag-NPs in solution usually employs the following three main components: (i) metal precursors, (ii) reducing agents (iii) stabilizing/capping agents. The formation of colloidal solutions from the reduction of silver salts involves two stages of nucleation and subsequent growth. Further, the size and shape of synthesized Ag-NPs are strongly dependent on these steps. Moreover, in the synthesis of monodispersed Ag-NPs with uniform size distribution, all nuclei are required to form at the same time. In this case, all the nuclei are likely to have the same or similar size, and then they have to grow uniformly in subsequent steps. The initial nucleation and the subsequent growth of initial nuclei are controlled by adjusting the reaction parameters such as reaction temperature, pH, precursors, reducing agents (i.e. $NaBH_4$, ethylene glycol, glucose) and stabilizing agents (i.e. PVA, PVP, sodium oleate) (Haider & Kang, 2015). Similarly, the physical approach synthesizes the metal nanoparticles by evaporation–condensation, which is carried out in a tube furnace at atmospheric pressure. However, in the case of using a tube furnace at atmospheric pressure, there are several drawbacks such as a large space of the tube furnace, high energy consumption for raising the environmental temperature around the source material, and time consuming for achieving thermal stability. A thermal-decomposition method was developed to synthesize Ag-NPs in powder form (Neelakandan & Thomas, 2018). The Ag-NPs are formed by the decomposition of an Ag^{+}–oleate complex, which was

prepared by a reaction with $AgNO_3$ and sodium oleate in a water solution, at a high temperature of 290°C. and an average particle size of the Ag-NPs was obtained *Ca*. 9.5 nm (Sadrolhosseini et al., 2015). When Ag-NPs are produced by chemical synthesis, three main components are needed: a silver salt (usually $AgNO_3$), a reducing agent (i.e. ethylene glycol) and a stabilizer or capping agent (i.e., PVP) to control the growth of the NPs and prevent them from aggregating. In the case of the biological synthesis of AgNPs, the reducing agent and the stabilizer are replaced by molecules produced by living organisms. These reducing and/or stabilizing compounds are utilized from bacteria, fungi, yeasts, algae or plants (Tran et al., 2013).

1.4.2. Applications of silver nanoparticles

Silver nanoparticles are utilized in cosmetic, medical and military applications due to their unique chemical and physical properties. Nanometre sized particles tend to exhibit very different properties than their bulk scaled counterparts. These silver nanoparticles are used for: (1) The purification and quality management of air, biosensing, imaging and drug delivery systems, (2) Biologically synthesized silver nanoparticles have many applications like coatings for solar energy absorption and intercalation material for electrical batteries, as optical receptors, as catalysts in chemical reactions, for biolabeling, and as antimicrobials, (3) Silver nanoparticles are cytotoxic hence, have tremendous applications in the field of high sensitivity biomolecular detection and diagnostics, antimicrobials and therapeutics, catalysis and micro-electronics, (4) It has some potential application like diagnostic biomedical optical imaging, biological implants (like heart valves) and medical application like wound dressings, contraceptive devices, surgical instruments and bone prostheses, (5) Many major consumer goods manufacturers already producing household items that utilize the antibacterial properties of silver nanoparticles. These products include nano silver lined refrigerators, air conditioners, and washing machines, (6) The antibacterial properties of silver nanoparticles have led to several new products such as nanoparticles embedded clothes, dryers,

and sheets to reduce clothing (socks) odors and antibacterial soap and toothpaste.

1.5. Review of literature

Polymeric adsorbents are of great technological and scientific interest owing to their properties like high surface area, selectivity and flexibility, tunable pore surface property, and improved performance for wastewater treatment processes (Pan et al., 2009). The significant efforts have been made over the years to develop highly selective and efficient adsorbent materials. It has been reported in a review that both natural and synthetic polymers exhibited enhanced removal efficiency when combined with different adsorbent materials, i.e., carbon-based materials, clays, and other inorganic adsorbents (Berber, 2020). Polymers in a composite structure showed good mechanical stability, provided additional binding sites for interaction with the adsorbates, and provided newer dimensions in water or air purification systems (Lodhi et al., 2022). Researchers have attempted to modify the polymer structures to achieve high removal performance, recyclability, and selectivity for many organic and inorganic pollutants (Sarojini et al., 2023; Zhao et al., 2018). A novel type of poly(maleic anhydride)-graft-poly(vinyl alcohol) functionalized magnetic nanoparticles were synthesized and its adsorption behavior for heavy metal ions as a function of pH was studied (Liu et al., 2020). Researchers are focusing on developing dendritic polymers, which are hyperbranched macromolecules with unique three-dimensional structures decorated with a huge number of reactive end groups (Sajid et al., 2018). These are relatively cost-effective and are easily functionalized over other substrates. These are widely used for the removal of inorganic and organic pollutants from polluted water. Zulfiqar et al. have reported the synthesis of palm oil bio-waste/ multiwalled carbon nanotubes reinforced polyvinyl alcohol hydrogels by a simple polymerization technique using N, N'- methylene bisacrylamide as a crosslinking agent and ammonium persulphate as an initiator (Zulfiqar et al., 2020). The resultant synthesized composite was applied for the adsorptive removal of Pb(II) from aqueous solutions in a batch adsorption mode, and the

monolayer adsorption capacity was achieved at 30.031 mg/g at pH 7.0. Starch-based magnetic polyurethane polymer was designed to remove tetracycline antibiotics from contaminated water (Okoli & Ofomaja, 2019). The adsorption mechanism was studied and suggested that π-π interaction and π- cation interactions are the predominant forces involved in the adsorption of tetracycline by the solid. Similarly, the material exhibits good stability since the sorption capacity is not greatly affected for 3 successive cycles. Magnetic β- β-cyclodextrin polymer is employed for its potential to remove various pollutants (bisphenol A, methylene blue, basic orange 2, rhodamine B, Cr(III), Pb(II), Zn(II), and Cu(II)) from aqueous solutions (Hu et al., 2020). The adsorption process is found to be dependent on solution pH, while the ionic strength and humic acid slightly affected the adsorption.

Clays play an important role in the generation of prebiotic components and in biological evolution. The large surface area of the natural clays accounts to adsorb efficiently the pollutants in aqueous medium (Williams, 2019). The particle size of clay mineral is typically below 2 μm while the surface area is as large as 800 m^2/g for montmorillonite (Kumari et al., 2021). In the natural environment, clays in soil and river sediments trap the pollutants. The clay adsorbs the anions, cations, non-ionic, and polar contaminants from natural water. These contaminants accumulate on clay surfaces and are retained through the processes of ion exchange, coordination, or ion-dipole interactions. Sometimes the pollutants are adsorbed by hydrogen bonding, van der Waals interactions, or hydrophobic interactions (Rafa et al., 2024). The strength of such interactions is determined by the particular structural and other features of the clay mineral (Srinivasan, 2011). The clay minerals in the environment interact with air, water, and soil, thereby regulating the occurrence and distribution of a large number of pollutants. Clays often contain Mg, Fe, Ti, Cr, and Zr with trace amounts of Be, V, Mn, Co, Ni, Zn, Mo, Ag, Cd, Sn, Tl, Pb, Bi as well as Cu, As, and Se (Ghosh & Chakraborty, 2023). The metals remain adsorbed to the clay surface and their release to the environment (air, water, soil) depends on factors like pH, temperature, precipitation, etc. Also, natural

weathering processes through clay-water, clay-air interactions, and other physical changes are responsible for the transport of contaminants between clay and the environment (Borst et al., 2020). Different types of clay minerals have been evaluated as adsorbents for metal ions and the results are very encouraging (Campillo-Cora et al., 2020). Clay-organic matter interactions are notably more intricate compared to clay-metal interactions, as they are influenced by a number of structural and stereochemical factors, in addition to environmental conditions (Regadío et al., 2020).

The mechanism associated with the removal of dissolved organic compounds (DOC) by attapulgite was studied elsewhere. The adsorption of DOC onto attapulgite proceeds in two steps as: a rapid external mass transfer of the DOC to the external surface of the attapulgite through film diffusion, and a low-rate intra-particle diffusion of DOC within the pores of the attapulgite. Moreover, the thermodynamic analysis showed that the process is exothermic in nature (Haddabi et al., 2015). The effect of equilibrium time, initial DOC concentration, solution pH, temperature, and attapulgite concentration on attapulgite's performance to absorb DOC is obtained extensively. The granular and powder attapulgite showed the maximum monolayer coverage of 31 mg/L and 65 mg/L, respectively. Further, the adsorption capacity was not significantly affected by variations in the oily water's pH. The pseudo-second-order model agrees well with the time dependence sorption. Both external mass transfer and intra-particle diffusion are dominant transport processes in the sorption. Liu et al. (2011) demonstrated the adsorption behavior of tetracycline (TCH), chloramphenicol (CAP), and sulfamethoxazole (SMX) on clay minerals, revealing that only TCH exhibited substantial adsorption to natural montmorillonite, kaolinite, and rectorite. Further, the adsorption equilibrium constant (kg/L) of TCH to natural montmorillonite is 332 at pH 3.0 and 108 at pH 7.0. Similarly, the adsorption and intercalation of ciprofloxacin on montmorillonite are studied and the cation exchange is the primary mechanism driving the adsorption of ciprofloxacin on montmorillonite (Wu et al., 2010). This implies that the interaction between ciprofloxacin and montmorillonite

involves the replacement of exchangeable cations within the montmorillonite by the ciprofloxacin molecules. The intercalation of ciprofloxacin onto the inter-layer of montmorillonite is also observed through the increase of basal spacing of the montmorillonite Benzalkonium chloride and triclosan are the commonly used biocides for cleaning products, cosmetics, and other household disinfectant products. These biocides have been known to raise severe environmental problems such as pathogen resistance and the existence of toxic compounds in reclaimed water. The removal of benzalkonium chloride and triclosan using surfactant-modified bentonite (dodecyltricetyl ammonium—bentonite/DTA-bentonite) was studied and results indicate that the modified bentonite has a relatively higher adsorption capacity toward triclosan than untreated bentonite. Organophilic cation facilitates the anchoring of hydrophobic triclosan, but slightly limits the adsorption of benzalkonium chloride by occupying the active cation exchange sites within the bentonite structure (Ong et al., 2014).

Organic compounds modifies the surface of clay minerals and other related layered silicates, mainly through the intercalation of these compounds at the surface of clay materials and the composite materials showed various applications in diverse area of research (Paiva et al., 2008). The combination of organo-clays with different polymers or biopolymers to create composites or nanocomposites have been widely studied (Amari et al., 2021; Basavegowda & Baek, 2021; Ismadji et al., 2015), and Table 1.1. summarizes various organo-clay materials and their applications in the removal of various contaminants in aqueous medium.

Table 1.1. Clay/organo-clay and polymer or biopolymers composites for the removal of various contaminants in aqueous medium.

Clay/Organo-clay	**Polymer/ biopolymer**	**Application**	**References**

Kaolinite	Polyvinyl alcohol	Removal of Pb(II)	(Unuabonah et al., 2012)
Wyoming montmorillonite	Polyacrylate	Removal of Fe(III)	(Natkański et al., 2012)
Bentonite	Chitosan	Removal of Ni(II) and d(II)	(Tirtom et al., 2012)
Montmorillonite	Cellulose acetate	Removal of Acid Scarlet anionic dye	(Zhou et al., 2012)
Montmorillonite	Chitosan	Removal of herbicide clopyralid	(Celis et al., 2012)
Na-montmorillonite	Ethylene propylene diene monomer (EPDM) rubber	Removal of Remacryl blue 3G–Basic blue 3, Nylson navy N-RBL–Acid blue 13, Remazol brilliant blue BB–Reactive blue 19, Samaron red 2BSL–Disperse red 60	(Hassan & El-Nemr, 2013)
Kaolin	Polyacrylic acid	Removal of brilliant green	(Shirsath et al., 2013)
Palygorskite	Cellulose	Removal of phenol	(Wu et al., 2014)
Sepiolite and	Polysacchari	Removal of	(Alcântara et al.,

palygorskite	des	Cu(II) and Pb(II)	2014)
Montmorillonite	Chitosan	Removal of Co(II)	(Wang et al., 2014)

Polyethylene glycol (PEG) is nontoxic, biocompatible, and soluble in water. PEG is widely used in pharmaceutical industries, biomaterial production, tissue culture, and is often employed as adsorbent in water treatment, oil spill cleanup, environmental monitoring etc. (Raina et al., 2021). Further, the polyethylene glycol is readily polymerized and provides functional groups in its structure (Ibrahim et al., 2022), that subsequently functionalized with vinyl groups at the chain-ends and these active vinyl groups are crosslinked to form PEG based superabsorbent hydrogel (Chapla et al., 2020). The preparation of nano clay filled composite hydrogels of poly acrylic acid and polyethylene glycol are synthesized by incorporating 0.5, 1.0 and 1.5 weight % nano size bentonite fillers. The hydrogels are employed in the adsorption of dye compounds. (Bhattacharyya & Ray, 2015). The adsorption experimental results indicate that nano clay filled composite hydrogels are excellent adsorbent for the removal of Congo red and methyl violet at wide range of dye concentrations.

A novel method synthesizes the composite material MMT@HTAB@PEG precursors to the surfactant, PEG and montmorillonite (MMT) and the material removes efficiently the methylene blue (MB) as a cationic dye and trypan blue (TB) as the anionic dye from aqueous solution under various parametric studies i.e., contact time, dye concentrations, temperature, and pH (Sardi et al., 2023). The surfactant's intercalation exfoliated the clay interlayers. Further, the MMT@HTAB@PEG shows the maximum adsorption capacities of 190.81 and 237.22 mg/g, respectively for TB and MB. Nanocomposites-based polystyrene sulfonate modified laterite (NCPML) employed in the removal of tetracycline from an aqueous solution. The electrostatic interactions between the negatively charged NCPML surface

and the zwitter ionic species of TCH and non-electrostatic interactions governed the adsorption mechanisms of TCH onto the NCPML. The pseudo-second-order model agrees well the sorption kinetics, and the Langmuir model fitted well to the adsorption isotherm of TCH onto NCPML. Moreover, the real water implications showed greater selectivity of TCH removal using the NCPML (Vu et al., 2020).

The sorption efficiency of PVP-coated silver nanoparticles in the removal of bisphenol-A and ketoprofen is influenced by the adsorbent dosage, contact time, temperature, and the presence of dissolved organic matter. Further, at pH 7.5 the bisphenol-A and ketoprofen removal attained a maximal adsorption capacity of 90.91 and 83.33 mg/g, respectively. Moreover, the nanocomposite material recycled and used for at least five adsorptive/desorptive cycles using methanol as desorptive solvent (Alizadeh Fard et al., 2017).

The synthesis of metal nanoparticles (especially gold and silver nanoparticles) using plants or plants' extracts (inactivated plant tissue, plant extracts and living plant) has received greater attention in recent time due to its efficiency and provides greener alternative methods (Zuhrotun et al., 2023). Synthesis of metal nanoparticles using plant extracts is very cost effective, and therefore used as an economic and valuable alternative for the large-scale production of metal nanoparticles (Md Ishak et al., 2019). Plant extracts act both reducing and capping agents in the nanoparticle synthesis. The bio-reduction of metal nanoparticles by combinations of biomolecules present in the plant extracts (e.g., enzymes, proteins, amino acids, vitamins, polysaccharides, and organic acids such as citrates) is environmentally benign. Many researchers have reported the biosynthesis of silver nanoparticles by plant leaf extracts and their potential applications (Giri et al., 2022; Karunakaran et al., 2023; Padhi & Behera, 2022; Vanlalveni et al., 2021).

Geranium leaf (*P. graveolens*) broth, when exposed to aqueous silver nitrate solution, resulted in extracellular enzymatic synthesis of stable crystalline silver nanoparticles. The bioreduction of the metal ions is fairly

rapid, and resulted in a high density of stable silver nanoparticles having the size of 16-40 nm. The proteins, terpenoids and other bio-organic compounds in the geranium leaf broth reduces the silver ions and stabilizes the nanoparticles (Shankar et al., 2003). The biosynthesis silver and gold using the precursors of their respective aqueous solutions i.e., $AgNO_3$ and $HAuCl_4$. Further, the synthesis of bimetallic core-shell nanoparticles of gold and silver by simultaneous reduction of Au and Ag ions using the broth of neem leaves (*A. indica*). The metal nanoparticles are stable in solution at least for 4 weeks of time and the nanoparticles are predominantly spherical and polydisperse with diameters in the range of 5 to 35 nm (Shankar et al., 2004).

The *Pinus desiflora*, *Diospyros kaki*, *Ginko biloba*, *Magnolia kobus* and *Platanus orientalis* leaves broth were utilized in the synthesis of stable silver nanoparticles with average particle size of 15 to 500 nm. In case of *M. kobus* and *D. kaki* (persimmon) leaf broth, synthesis rate and final conversion to silver nanoparticles was relatively rapid while raising the reaction temperature from 25°C to 95°C. However, the average particle size obtained by the *D. kaki* leaf broth was decreased from 50 nm to 16 nm while increasing the reaction temperature from 25°C to 95°C (Song & Kim, 2009). Another study reveals that the *M. Kobus* and *D. Kaki* synthesizes the metallic gold nanoparticles (5-300 nm) with different triangular, pentagonal, hexagonal, and spherical shapes within a few minutes (for up to 90% conversion at a reaction temperature of 95°C). It is suggested that the rate of synthesis of the nanoparticles is related to the reaction and incubation temperature, and increased temperature allowed nanoparticle growth at a faster rate. Moreover, increasing the temperatures and leaf broth concentrations, size of nanoparticles became smaller (Song & Kim, 2009).

The green tea (*Camellia sinensis*) extract synthesizes the gold nanoparticles and silver nanostructures in aqueous solution at ambient conditions. The concentrations of precursor metal ions and tea extract regulates the size, morphology and optical properties of the nanostructures. Further, increasing the amount of *C. sinensis* extract caused to increase the spherical

size of nanoparticles. This study suggests that phenolic acid-type biomolecules present in *C. sinensis* extract are responsible for synthesis and stabilization of silver and gold nanoparticles (Vilchis-Nestor et al., 2008). *Cinnamon zeylanicum* bark extract biosynthesizes the cubic and hexagonal silver nanocrystals (31-40 nm). The particle size distribution varied with variation in the dosage of *C. zeylanicum* bark extract. The number of particles increased with increasing dosage due to the variation in the number of reductive biomolecules. Small nanoparticles are formed at high pH and the shape of silver nanoparticles at high pH is more spherical in nature rather than ellipsoidal. Moreover, bactericidal effect of nano-crystalline silver nanoparticles was tested against *E. coli* strain, and various concentrations of nanoparticles i.e., 2, 5, 10, 25, and 50 mg/L inhibit 10.9, 32.4, 55.8, 82, and 98.8% of *E. coli*, respectively. The *C. zeylanicum* bark is rich in terpenoids (linalool, methyl, chavicol, and cugenol) and chemicals (cinnamaldehyde, ethyl cinnamate, and b-caryophyllene), contribute to its special aroma (Sathishkumar et al., 2009). Additionally, proteins are also present in the bark. The water-soluble organics within *C. zeylanicum* bark are responsible for the bioreduction of silver ions to nanosized Ag particles. Furthermore, proteins derived from *C. zeylanicum* bark caps the resulting nanoparticles either through free amine groups or cysteine residues, thereby stabilizing them in solution (Sathishkumar et al., 2009).

Silver nanoparticles (16-40 nm) are rapidly synthesized by introducing silver ions to leaf extract of *Datura metel*. The leaf extracts contain biomolecules including alkaloids, proteins/enzymes, amino acids, alcoholic compounds, and polysaccharides, which serve as both reductants that resist reacting with silver ions and scaffolds that guide the formation of silver nanoparticles in solution (Kesharwani et al., 2009). Quinol (alcoholic compound) and chlorophyll pigment is responsible for reduction of silver ions and stabilization of nanoparticles (Mittal et al., 2013).

The apiin compound extracted from henna leaves employed in synthesizing the anisotropic gold and quasi-spherical silver nanoparticles.

Secondary hydroxyl and carbonyl groups of apiin compound are responsible for the bioreduction of metal salts. In order to control the size and shape of nanoparticles, different amounts of apiin compound (as the reducing agent) is used. The nanoparticles are stable in water for 3 months, which is attributed to surface binding of apiin compound with the reduced materials (Kasthuri et al., 2009). Jha & Prasad (2010) used biotechnological method for production of silver nanoparticles. The *Cycas* leaf extract is used to produce stable silver nanoparticles. X-Ray data indicated that silver nanoparticles have face-centered cubic (fcc) unit cell structure. Phytochemicals such as polyphenols, glutathiones, metallothioneins (a family of cysteine-rich, low molecular weight proteins) and ascorbates are responsible for formation of the nanoparticles. Silver and gold nanoparticles are synthesized biologically by using *Sorbus aucuparia* leaf extract. The nanoparticles are found to be stable for more than 3 months. It was proposed that sorbate ion in the leaf extract of *S. aucuparia* encapsulated the nanoparticles and responsible their stability (Dubey et al., 2010).

The banana peels (*Musa paradisiaca*) extract shows potential in synthesizing of silver nanoparticles. The extract contains various biomolecules like phenolic compounds, flavonoids, and proteins, which possess reducing and stabilizing properties that serves as a novel source for synthesizing silver nanoparticles. The silver nanoparticles displayed antifungal activity against *C. albicans* and *C. lipolytica*, and antibacterial activity against *E. coli*, *Shigella sp*., *Klebsiella sp*. and *E. aerogenes* (Bankar et al., 2010). The monodispersed and spherical silver nanoparticles (3 nm) are biosynthesized using gum kondagogu (non-toxic polysaccharide derived as an exudate from the bark of *Cochlospermumgossy pium*). The carboxylate and hydroxyl groups are involved in complexation and bioreduction of silver ions into nanoparticles. This method is compatible with green chemistry principles as the gum serves a matrix for both bioreduction and stabilization of the synthesized nanoparticles. Due to the availability of low-cost plant derived biopolymer, this method is utilized for large-scale production of highly stable monodispersed

nanoparticles. The silver nanoparticles with an average size of 4.5 mm showed significant antibacterial effects against gram negative (*E.coli* and *P. aeruginosa*) and positive (*S.aureus*) bacteria (Kora et al., 2010). *Acalypha indica* (Euphorbiaccac) leaf extracts are employed for producing silver nanoparticles (20-30 nm). The silver nanoparticles have excellent antimicrobial activity against water borne pathogens *E. coli* and *V. cholera* (minimum inhibitory concentration (MIC) - 10 mg/ml) (Krishnaraj et al., 2010). The spherical silver nanoparticles are obtained using the leaf extract of *Euphorbia hirta,* a plant known for its medicinal properties. The antibacterial property of the silver nanoparticles was assessed through disk diffusion assay and silver nanoparticles show higher antibacterial activity against *B.cereus, S.aureus* whereas intermediated activity show against *E.coli, K.pneumoniae* and *P.aeruginosa* (Elumalai et al., 2010). Another study explored the impact of extracts derived from tissue cultures of callus and leaves of *Sesuvium portulacastrum* L., a saltmarsh plant, on the synthesis of antimicrobial silver nanoparticles using $AgNO_3$ as a substrate. The callus extract is able to produce silver nanoparticles efficiently. The silver nanoparticles are spherical shape with variable size ranging from 5 to 20 nm. The aromatic rings, geminal methyl and ether linkages, indicating the presence of flavones and terpenoids, which are responsible for the stabilization of the silver nanoparticles. The silver nanoparticles inhibit clinical strains of bacteria and fungi. The antibacterial activity is more distinct than anti-fungal activity (Nabikhan et al., 2010).

The review of literature reveals that the use of clay polymers in environmental remediation has shown promising in the adsorptive removal of micropollutants and decontamination of several bacterial contaminants. Clay-polymer-based adsorbents offer high surface area, structural stability, and versatile functionalization, making them effective for capturing various micropollutants from aquatic environments. The synergistic effects between the clay and polymer components enhances the adsorption capacity and selectivity, providing a robust material in environmental remediation.

Moreover, the incorporation of silver nanoparticles into clay-polymer matrices has opened newer technique for bacterial removal in water treatment. Therefore, the clay-polymer decorated with silver nanoparticles show dual-functional material enabling both adsorbing the micropollutants and inactivating the bacterial pathogens. Though the performance of clay-polymer and silver nanoparticle-incorporated clay-polymer adsorbents is promising, several challenges and considerations remain. The long-term stability and reusability of these materials, potential environmental impacts of nanoparticle leaching, and the scalability of synthesis methods are critical factors that need further investigation. Additionally, the development of sustainable and cost-effective production processes is essential for the practical application of these advanced materials in real water treatment scenarios.

1.6. Scope of the present investigation

There are serious concerns about the safety in the utilization of treated wastewater effluents due to the uncertainties in health risks resulting from the presence of low concentrations of micro-pollutants and microbiological contaminants in treated wastewater effluent. Numerous studies have been conducted during last couple of decades have showed that many micro-pollutants, as well as multiple viruses and other microorganisms, are only partially removed by treatment plants, and therefore, persist in TWW (Treated Wastewater). Although the concentrations of these contaminants are typically low (< 1 µg/L), however, they pose serious risks aspects, especially if bioconcentrated by crops or even by the human. Uncertainties about the risks associated with chronic exposure to chemicals in TWW and their possible additive or synergistic mixture effects, raise serious concerns about water reuse for agriculture or other household purposes.

There is also significant concern regarding the persistence of microorganisms (e.g., bacteria and viruses) in TWW and their ability to be transmitted to irrigated crops, resulting in risks to food safety and public health.

In light of both microbiological and micro-pollutants exposure risks associated with agricultural/or household purposes water reuse, the development of novel, cost-effective technologies for enhancing contaminant removal from treated wastewater is critically needed. Adsorption is recognized as a convenient and economical method because it facilitates the removal of numerous water pollutants using naturally abundant materials. Clays are widespread materials of natural origin, possessing various surface-active sites, exchangeable cations, as well as micro- and mesoporous structures that allow their applications in ion-exchange, adsorption and catalytic processes. To protect the environment, the clay minerals are widely used in the disposal and storage of hazardous chemicals. The capability of clay minerals to retain hazardous substances depends on their cation exchange capacity (CEC) since the process of retaining toxic materials mainly occurs by the adsorption or ion-exchange. Due to its high cation exchange capacity, clay minerals are very effective for the adsorption of cations from the solution, therefore different clays are successfully utilized for the removal of micropollutants from the aqueous media. Among the variety of clays, 2:1 type, smectite clay minerals received special interest due to its high surface area (up to 200 m^2/g), high cation exchange capacity and higher adsorption capacity compared to other clays. Modifying clay minerals with various surfactants is the most widely used physical method to prepare inorganic/organic hybrid materials and accordingly clay mineral–polymer nanocomposites (CPN). The modified clay materials exhibit remarkable improvements in certain properties such as increased strength and heat resistance, decreased gas permeability and flammability. Noble metal nanoparticles mainly silver nanoparticles (AgNPs) are widely utilized as these are found to be useful in many aspects including antibacterial, antibiofilm, drug delivery systems, diagnostic tools, and personal care products and cosmetics. The antibacterial activity of AgNPs against a broad spectrum of bacteria is well-known. AgNPs have been conjugated to different molecules with antibacterial activity in order to obtain synergic effects, such as poly(ethyleneimine), amoxicillin, polysaccharides, peptides, surfactants, and polymers.

Therefore, the aim of the current research is to develop clay-polymer composites using two different types of hydrophilic polymers viz., PEG and PVP with the attapulgite clay framework. The functionalized, low-cost material was then applied for the elimination of tetracycline, bisphenol A, ciprofloxacin, triclosan and EE2 from aqueous solutions under different physico-chemical parametric studies. The batch reactor operations along with multiple parametric investigations allowed to propose a plausible mechanism involved at the solid/solution interface. Additionally, the operation of the column reactor offers the solids loading capacity for these contaminants under dynamic conditions, which is helpful for actual implications of materials in the wastewater treatment plan or even for scaling up laboratory data to large-scale treatment. Further, silver nanoparticles were synthesized from *Artocarpus heterophyllus* (Jackfruit) leaf extract and incorporated with the clay-polymer composite to access the antimicrobial activity of the bacteria present in water.

CHAPTER 2

METHODOLOGY

1. METHODOLOGY

2.1 Materials and apparatuses

2.1.1 Chemicals

All chemicals and reagents obtained are analytical grade or equivalent and are utilized without further purification. Table 2.1 provides detailed information on all the chemicals used in the present work.

Table 2.1: List of chemicals used for the experimental works.

Sl. No.	Chemicals used	Chemical Formula	CAS Number	Company
1	Tetracycline hydrochloride	$C_{22}H_{24}N_2O_8.HCL$	64-75-5	MERCK, India
2	Bisphenol A	$C_{15}H_{16}O_2$	80-05-7	Sigma Aldrich, USA
3	Ciprofloxacin	$C_{17}H_{18}FN_3O_3$	85721-33-1	Sigma Aldrich, USA
4	17 α-ethynylestradiol	$C_{20}H_{24}O_2$	57-63-6	Sigma Aldrich, USA
5	Triclosan	$C_{12}H_7Cl_3O_2$	3380-34-5	Sigma Aldrich, USA
6	Poly(ethylene glycol)	$H(OCH_2CH_2)NOH$	25322-68-3	MERCK, India
7	Poly(4-vinyl	$C_{14}H_{10}Cl_2NNaO_2$	26222-40-2	Sigma

	pyridine-co-styrene)			Aldrich, USA
8	Sodium Alginate	NaC_6H_7O	9005-38-3	SDFCL, India
9	Calcium chloride	$CaCl_2$	10043-52-4	MERCK, India
10	Ethanol	CH_3CH_2OH	64-17-5	Qualigens Fine Chemicals, India
11	Sulphuric acid	H_2SO_4	7664-93-9	HiMEDIA, India
12	Hydrochloric acid	HCl	7647-01-0	Merck, India
13	Glycine	$C_2H_5NO_2$	56-40-6	HiMEDIA, India
14	Sodium hydroxides	NaOH	1310-73-2	HiMEDIA, India
15	Disodium hydrogen phosphate anhydrous	Na_2HPO_4	7558-79-4	Merck, India
16	Ethylenediamine - tetraacetic acid	$C_{10}H_{16}N_2O_8$	60-00-4	Qualigens Fine Chemicals, India
17	Oxalic Acid	$C_2H_2O_4$	144-62-7	MERCK, India
18	Magnesium sulphate heptahydrate	$MgSO_4.7H_2O$	10034-99-8	Loba Chemie, India

19	Calcium chloride dihydrate powder	$CaCl_2.2H_2O$	10035-04-8	MERCK, India
20	Manganese (II) chloride anhydrous	$MgCl_2$	7773-01-5	MERCK, India
21	Nickel (II) chloride anhydrous	$NiCl_2$	7718-54-9	MERCK, India
22	Silver sulfate	Ag_2SO_4	10294-26-5	MERCK, India

2.1.2. Attapulgite clay, *Artocarpus heterophyllus*, and natural water samples

Artocarpus heterophyllus leaves are collected from the Mizoram University, Mizoram (India). The attapulgite clay (ATTP) was mined close to Bhuj, Gujarat (India), and collected for the present investigation. The clay was rinsed multiple times with distilled water (DW), dried at 100°C in a hot-air oven (Relitech Co., India), and ground to a fine powder (BSS No. 325) (British Standard Sieve). The natural water samples were collected from sources spread over four distinct locations in the Aizawl district of Mizoram (India). Each place is described in Table 2.2. The water samples are filtered using Whatman filter paper (pore size 20 μm) before employing it for further use. Several physicochemical parametric investigations of these water samples are conducted and included in Table 2.3. The water quality was tested using a multiparameter (Hanna Multiparameter Waterproof Meter; Model: HI98194) that evaluated a range of parameters, including pH, conductivity, resistivity, salinity, and total dissolved solids. A multiphotometer (Hanna Instruments,

USA; Model: H183300) was used to analyze the dissolved sulfate, phosphate, fluoride, and nitrate in the real water samples using the standard photometers reagents of phosphate, fluoride, nitrate, and sulfate as HI93713-0, HI93729-0, HI93728-0, HI9751-0, respectively. Further, the water samples were examined for various elements, using an AAS (Atomic Absorption Spectrometer), (Model: AA-7000 Series, Shimadzu, Japan) instrument. The NPOC (Non-purgeable Organic Carbon) and IC (Inorganic Carbon) are obtained using the TOC analyzer (Shimadzu, Model: TOC-VCPH/CPN, Japan). Furthermore, the real water samples were spiked with tetracycline, ciprofloxacin, bisphenol A, triclosan, and 17 α-ethynylestradiol and the efficacy of nanocomposites are examined in the removal of these pollutants in natural water samples.

Table 2.2: Details of GPS coordinates of natural water samples collected from different locations in Aizawl, Mizoram, India.

Location	Source	GPS Coordinates
Chite Veng (Aizawl)	Municipal wastewater	Latitude: 23.735687 Longitude: 92.733666
Lengpui (Aizawl)	Stream water	Latitude: 23.830385 Longitude: 92.625835
MZU water supply	Supply water	Latitude: 23.4416 Longitude: 92.4010
SIPMIU (Aizawl)	Treated wastewater	Latitude: 23.630385 Longitude: 92.435735

2.1.3. Materials and instrumentation

Sartorius (Arium Mini Plus UV Lab) water purification system was used for purifying the water. The purified water was used for preparing all the experimental solutions. All the weighing is conducted using an electronic balance (HPB220, Wensar, India). A pH–meter (Thermo Scientific, Model: Orion 2 Star, pH Benchtop) was utilized for pH measurements. The pH meter was calibrated using a standard buffer solution having pH 4.0, 7.0, and 12.0.

Glass beads (0.5 mm to 1 mm and 3-4 mm) were obtained from HiMedia, India for packing of glass column (Omnifit® SolventPlus™ Chromatography Columns with Two Fixed Endpieces; 1 cm inner diameter and 12 cm of length). The sorptive solution of the pollutant was pumped upward using a peristaltic pump (KrosFlo Research I Peristaltic Pump, Spectrum Laboratories Inc., California, USA). Syringe filters with a porosity of 0.45 μm and a diameter of 25 mm were obtained from Whatman, USA. Tetracycline, bisphenol A, triclosan, ciprofloxacin, and EE2 were analyzed using a UV-Vis spectrophotometer (Shimadzu Model: UV 1800, Japan). The calibration curves were obtained using the standard sorptive solutions of 1.0, 5.0, 10.0, 15.0, 20.0, and 25.0 mg/L for tetracycline, bisphenol A, triclosan, ciprofloxacin, and EE2. The λ_{max} was measured at 271.5 nm for ciprofloxacin, 287 nm for EE2, 280 nm for triclosan, 275 nm for BPA, and 276 nm for tetracycline. The solid materials were annealed in an electronic furnace (Nabertherm; 30-3000°C; P330; Germany). The samples were dried using a hot-air oven (Relitech Co., India).

A scanning electron microscope (SEM; JEOL, JSM 7100F; Oxford Xmax), and transmission electron microscope (TEM; JEOL, JEM 2100; Oxford Xtreme) were used for obtaining the surface morphologies of materials. Furthermore, the elemental composition was determined using energy-dispersive X-ray (EDX, Oxford instruments X-MaxN) spectroscopy in

conjunction with a scanning electron microscope (SEM). The FT-IR data of solids were collected using a Fourier transform infrared spectrometer (FT-IR-Shimadzu, Model: IR Affinity-1S, Japan). An X-ray diffraction (XRD) spectrometer (X'Pert PRO, MPD, PANalytical, Netherlands) was used to obtain the X-ray diffraction pattern of solids. The specific surface area and pore volumes of solids were obtained using a BET (Brunauer-Emmett-Teller) surface area analyzer (3 Flex version 4.03, Micromeritics, USA). Surface elemental compositions of the nanocomposites were measured by an X-ray photoelectron spectroscopy (XPS) (Shimadzu AXIS Supra, Kratos, UK).

2.1.4. Reagents

The stock solutions of tetracycline, bisphenol A, triclosan, ciprofloxacin, and EE2, each having a concentration of 50 mg/L, were prepared by dissolving their appropriate amount in purified water and by successive dilutions of stock solutions the required concentrations of are obtained. The pH of the experimental solutions was adjusted to freshly prepared solutions of 0.1 mol/L HCl or 0.1 mol/L NaOH.

2.2. Methods

2.2.1. Preparation procedure of the nanocomposite solids

Attapulgite clay (ATTP) was thoroughly rinsed with deionized water before drying at 100ºC to eliminate sand particles and other particulate impurities. The dried ATTP was sieved (BSS No. 325), and the clay was thermally activated using a fixed-bed electrical furnace for 2 hrs at 400ºC. The temperature was raised at a rate of 5ºC/minute. Further acid activation of the clay was carried out using 1.0 M HCl at room temperature with constant stirring for 2 hrs. The slurry was filtered and repeatedly rinsed with distilled

water until the filtrate's pH was neutral. It was then dried at 80ºC and put in a glass bottle. For grafting with polymers, two hydrophilic polymers are used, *viz*., poly(ethylene glycol) (PEG) and poly(1-vinylpyrrolidone-co-styrene) (PVP).

2.2.1.1. PVP-incorporated attapulgite clay (ATTP@PVP)

0.3 g of PVP was dissolved in 100 mL of ultrapure water, and agitated at room temperature for 1 hr, followed by sonication for 1 hr, ensuring complete dissolution of PVP. In parallel, a beaker contains 7 g of ATP in 100 mL of water and a magnetic stirrer agitates the suspension for 1 hr followed by ultrasonication for 90 mins at room temperature. Finally, the solution of PVP is introduced in the ATP suspension carefully, and a magnetic stirrer stirs the solution mixture for 48 hrs. The PVP expands within the ATP pores and grafts with the clay network. Further, repeated washing using the purified water removes the non-grafted PVP. The centrifugation of suspension separates the solid. Repeated washings of solid give the ATTP@PVP solid.

2.2.1.2 PEG-incorporated attapulgite clay (ATTP@PEG)

The *in-situ* reaction enables the grafting of polyethylene glycol (PEG) with the activated clay. At ambient temperature, a mixture of 0.8 g of PEG and 100 mL of purified water was agitated for an hour to mix the PEG in water. Further, the suspension of PEG is sonicated in a sonicator bath for 1 hr before mixing it with the clay sample. In parallel, 10 g of ATTP in 100 mL of water was agitated for 1 hr in a beaker at ambient temperature followed by sonication for 90 mins in a sonicator bath. Further, the clay slurry was mixed with the PEG solution, and a homogeneous slurry was obtained, and agitated for 48 hrs. The ATTP@PEG composite was obtained and washed with an excess of purified water that removed the residual polymer.

2.2. Synthesis of Ag-NPs

Fresh and healthy leaves of *Artocarpus heterophyllus* (Jackfruit) were collected locally and rinsed thoroughly with tap water followed by purified water to remove the dust particles. The leaves are chopped into small pieces and dried at room temperature. A 250 mL beaker takes the 10 g of these finely cut leaves mixed with 100 mL of purified water, and the mixture boils at 80ºC for 20 mins. Filter paper (Whatman No. 1) filters the leaf extract, and the clear extract is stored in an Erlenmeyer flask at 4°C. Sterility conditions were upheld throughout the experiments to ensure the efficacy and accuracy of results. Further, a 150 mL Erlenmeyer flask takes 6 mL of 1 mM silver sulfate (Ag_2SO_4) solution and slowly introduces the 30 mL leaf extract. The extract readily reduces the Ag^+ ions to Ag^0 and forms its colloidal solution, which is pale yellow. The UV-Vis spectra further confirm the formation of colloidal Ag^0(NPs).

2.2.2. Preparation of ATTP@PEG/Ag⁰ and ATTP@PVP/Ag⁰ nanocomposites

The two clay-polymer composites, ATTP@PEG and ATTP@PVP decorated with the biosynthesized silver nanoparticle. 10 g of ATTP@PEG or ATTP@PVP is taken in 100 mL of water and the mixture is agitated for 1 hr in a beaker at ambient temperature followed by sonication for 90 mins in a sonicator bath. 30 mL of previously prepared Ag colloidal solution is added and further agitated for 24 hrs at 50ºC in the beaker containing the ATTP@PVP or ATTP@PEG slurry. The mixture was washed with distilled water, cleaned, and dried at 60ºC to get the Ag-NP decorated ATTP@PVP or ATTP@PEG nanocomposites.

2.2.3. Synthesis of clay-polymer nanocomposites beads

1 g of Na-alginate powder with 75 mL of distilled water is agitated vigorously to obtain a homogenized solution, and then 5 g of ATTP@PEG or/ ATTP@PVP powder is mixed in it. The slurry is allowed to stir for 2 hrs. A small tip with a 0.2 cm hole is introduced at the bottom of a separating funnel

filled with the slurry. The slurry was carefully dropped from the separating funnel into a beaker containing 2% $CaCl_2$ solution under the stirring condition. This entails the uniform formation of spherical beads of solid. The nanocomposite materials beads remained in the solution for 4 hrs and separated from the $CaCl_2$ solution. The purified water washes the beads, and a drying oven dries it at 70ºC for 4 hrs. These beads are further used for column reactor operations.

2.3. Characterization of the materials

The surface morphology of ATTP, ATTP@PEG, ATTP@PVP, ATTP@PEG/Agº and ATTP@PVP/Agº are obtained using the scanning electron microscope (SEM) (Operational condition: SEI Resolution: 15 kV, 46 Magnification: 10-1000000, Accelerating Voltage: 0.2-30 kV, Probe Current: 1 pA to 400 nA and Electron Gun used: In-Lens Schottky field emission gun). Furthermore, the elemental composition was determined using energy-dispersive X-ray spectroscopy. Similarly, to understand of the surface morphology, shape, and size of nanocomposites was obtained using a transmission electron microscope (TEM). The solid powder was dispersed in isopropyl alcohol by sonication and drop cast on the TEM grid. The grid was dried in a vacuum desiccator and then coated with gold (2.0 nm). The sample was analyzed using the secondary electron detector at 30 kV acceleration voltage.

The materials *viz.*, ATTP, ATTP@PEG, ATTP@PVP, ATTP@PEG/Agº and ATTP@PVP/Agº were characterized by the Fourier transform infrared spectrometer (FT-IR). The sample holder was cleaned with chloroform and about 10 mg of the powder solid sample was placed in the sample holder. The solid was exposed to infrared light from the FT-IR instrument that ranges in wavenumber range of 10,000 to 100 cm^{-1}. The molecules in the sample transform the absorbed radiation into rotational and/or vibrational energy. The resultant signal, which appears as a spectrum at the detector in wavenumbers

ranging from 4000 cm^{-1} to 400 cm^{-1}, represents the sample's molecular fingerprint. Because each molecule or chemical structure provides a distinct spectral fingerprint, FT-IR analysis is a useful technique for identifying specific molecules. To determine the phase structure, particle size, Miller indices and lattice parameters of power materials, an X-ray diffraction (XRD) spectrometer was used. The X-ray diffraction data were collected at a scan rate of 0.033 of 2θ illuminations and with the generator set to 30 mA and 40 kV.

A BET surface area analyzer based on liquid nitrogen adsorption/desorption isotherms was used to perform the BET analyses. The results provide the material's physical structure such as specific surface area, pore size, and pore volumes. The surface area of material is often correlated with various properties such as shelf-life, dissolution rates, moisture retention, and catalytic activity. Moreover, the X-ray photoelectron spectroscopy (XPS) was utilized for obtaining the XPS data of the modified materials before and after the sorption of TCH and BPA. This enables to obtain greater insights of the interaction of sorbate ions with the nanocomposite solids. The contact angle of the ATTP, ATTP@PEG and ATTP@PVP samples were measured with using an optical goniometer (Attension, Theta Lite 100, DKSH Korea Ltd. Korea).

2.3.1. pH_{PZC} determination of the powder material

The pH level at which the net surface charge on the solid surface is zero is known as the point of zero charge pH (pH_{PZC}). The surface has a net positive charge when the pH is less than pH_{PZC} and a net negative charge when the pH is more than pH_{PZC}. Determining these solids' point of zero charge is useful for understanding the adsorption process. The pH drift method was used to determine the solid's $pH_{PZC.}$ In a series of 100 mL of 0.1 M NaCl was dissolved in CO_2-free purified water. The CO_2 was degassed by bubbling the nitrogen gas for 5 mins and covered with parafilm paper to prevent further reabsorption of CO_2 gas. To a series of 100 mL of 0.1 M NaCl solutions taken in different narrow-mouth bottles 0.1 M HCl or 0.1 M NaOH solutions were used to adjust the solution pH from 2.0 to 11.0. In each bottle, 0.1 g of the solid was added, and it was sealed tightly and stirred for 24 hrs at 25°C. The solutions' final pH

was recorded and a graph was drawn between $pH_{Initial}$ and pH_{Final}, and the zero charge was obtained at the point where this curve and the linear $pH_{Initial}$ = pH_{Final} plot intersects each other.

2.4. Batch reactor experiments

The adsorption of pollutant is carried out for various parametric conditions *viz*., the effects of sorptive pH, initial sorptive concentrations, contact time, background electrolytes, and co-existing ion under the batch operations. The parametric studies provide insights of the sorption mechanism and demonstrates the mechanism involved at the solid/solution interface (Zhao et al., 2022). By dissolving the appropriate and accurate amounts of pollutant in purified water, the stock solutions of 50 mg/L of tetracycline, bisphenol A, triclosan, ciprofloxacin and EE2 in 1.0 L of each sorptive solutions were prepared. To improve the solubility of these pollutants in purified water, the solutions were subjected for sonication for 5 mins. The sequential dilution achieves the required concentration of pollutant in the batch reactor trials. 0.05 g of the solid sample is taken with 25 mL of 10 mg/L sorptive solutions to study the adsorption of tetracycline, bisphenol A, triclosan, ciprofloxacin and EE2. The pH of the sorptive solution was adjusted by the dropwise additions of 0.1 mol/L HCl / 0.1 mol/L NaOH solutions. Rotary flask shaker (Scientech, India) was used to equilibrate the solution mixture for 24 hrs at 25°C. A 0.45 µm syringe filter was used to filter the equilibrated solution. The bulk sorptive concentration of tetracycline, bisphenol A, triclosan, ciprofloxacin and EE2 were measured by using a UV-Vis spectrophotometer at the wavelengths of 276 nm, 275 nm, 280 nm, 271.5 nm and 287 nm, respectively, for these micro-pollutants. Equation 2.1 was used to calculate the removal efficiency.

$$\text{Removal efficiency (\%)} = \frac{C_0 - C_e}{C_0} \times 100 \qquad \text{..... (2.1)}$$

where C_o and C_e are the initial and final sorptive concentrations, respectively

2.4.1. Effect of pH

The pH of a solution is a crucial variable as it significantly impacts on various parameters such as the rate of dissociation and the speciation of these pollutant molecules. The dissociation of functional groups of adsorbents, and the charge on the surface of the adsorbent depends on the solution pH (Ambaye et al., 2020). The sorptive solution pH for tetracycline, bisphenol A, triclosan, ciprofloxacin and EE2 were maintained in the range of pH 2.0 and 10.0. The sorptive solution with the sorbent is equilibrated at constant temperature of 25°C for 24 hrs to achieve apparent equilibrium between the solid/solution interface. The sorption tests were carried out as already demonstrated previously in Chapter 2, section 2.4 of the batch reactor operations. The findings are presented as percentage removal (%) of pollutant against sorptive solution pH.

2.4.2. Effect of sorptive concentration

The initial sorbate concentrations provides the driving force to overcome the mass transfer resistance at the liquid-solid interface, and enables the sorption rate. (Brandani, 2021). Additionally, it facilitates the use of equilibrium state adsorption isotherm models to demonstrate the type of interaction involved at the solid/solution interface as well to optimize the removal capacities based on isotherms' assumptions. Therefore, a systematic sorption studies were conducted varying the sorbate initial concentrations.

The initial concentrations of tetracycline, bisphenol A, triclosan, ciprofloxacin and EE2 is varied from 1.0 mg/L to 25.0 mg/L at pH of 3.5, 6.06, 4.0 ,7.0, and 6.08 respectively for the tetracycline, bisphenol A, triclosan, ciprofloxacin and EE2 in the removal of these pollutants at these concentrations. The sorptive solutions were equilibrated with the sorbent for 24

hrs at constant temperature of 25°C in the shaker. The detailed sorption procedure is given in Chapter 2, section 2.4. The results are presented as a function of the initial sorptive concentrations against the removal efficiency (%).

2.4.3. Adsorption isotherm modeling

In order to optimize the design of an adsorptive removal system to remove pollutants from solutions, it is important to establish the most appropriate correlation for the equilibrium state data. An accurate mathematical description of equilibrium adsorption data is indispensable for reliable prediction of adsorption parameters and quantitative comparison of adsorption behavior for different adsorbent systems within any given system.

2.4.3.1. Langmuir adsorption isotherm

Langmuir adsorption isotherm is based on the assumption that adsorbate are homogeneously dispersed on the surface of the adsorbent and that there is no lateral interactions and steric hindrance between the adsorbed molecules, even on adjacent sites. In its derivation, Langmuir isotherm refers to homogeneous adsorption; each molecule has constant enthalpies and sorption kinetic energy, and all sites have identical affinity for the adsorbate (Swenson & Stadie, 2019). The linearized form of Langmuir adsorption model (Guo & Wang, 2019) is used for the evaluation of maximum uptake (q_o) at varied initial concentrations (Equation 2.2):

$$\frac{C_e}{q_e} = \frac{1}{q_0 b} + \frac{C_e}{q_0} \qquad \ldots (2.2)$$

where q_e is the amount of solute adsorbed per unit weight of adsorbent (mg/g) at equilibrium; C_e is the equilibrium bulk sorptive concentration (mg/L); q_o is the Langmuir monolayer adsorption capacity, i.e., the amount of solute occupy the available sites per unit mass of solid sample or monolayer capacity (mg/g) and b is the Langmuir constant (L/mg).

2.4.3.2. Freundlich adsorption isotherm

Freundlich adsorption isotherm illustrates the relationship between the non–ideal and reversible adsorption, with no restriction to the monolayer coverage. Freundlich isotherm assumed multilayer adsorption, with uneven dispersion of adsorption heat and attractions over the heterogeneous surface. Currently, Freundlich isotherm is broadly employed in heterogeneous surfaces and binding sites with discrete energies relying on multilayer adsorption and equilibrium (Kalam et al., 2021). The linearized form of Freundlich equation (Osmari et al., 2013) is shown in Equation 2.3:

$$logq_e = \frac{1}{n} logC_e + logK_f \qquad \text{…….....} (2.3)$$

where q_e and C_e are the amount adsorbed (mg/g) and bulk sorptive concentration (mg/L) at equilibrium, respectively, and K_f and 1/n are the Freundlich constants referring to adsorption capacity (mg/g) and adsorption intensity or surface heterogeneity, respectively.

2.4.4. Effect of contact time

In wastewater treatment, the study of sorption kinetics is crucial because it provides important insights into the reaction pathways and makes it possible to determine the mechanism of sorption processes (Etuk et al., 2021). It is observed that the nature of the adsorbent, its accessible active sites, and the accessibility of the pollutants to the active sites are all factors that affect the

removal of pollutants to reach their apparent equilibrium state, which varies from one pollutant to another. To create effective wastewater treatment facilities, it is crucial to forecast the rate at which the pollutant is removed from aqueous solutions. The impact of contact time was investigated over a wide range of time while maintaining initial sorptive concentrations of 10.0 mg/L. The outcome of the studies is shown as percent removal of pollutants against the contact time.

2.4.5. Adsorption kinetic modeling

A reasonable explanation for the mechanisms and kinetics involved in the uptake of pollutants by the employed materials, the kinetic modeling is conducted with the known kinetic models. The reaction orders of adsorption systems based on the capacity of the adsorbents and the reaction orders based on solution concentration are previously reported in numerous kinetic models (Lima et al., 2015).

The most popular kinetic models for describing the adsorption of a solute from an aqueous solution are the pseudo-first-order and pseudo-second-order equations. The pseudo-second-order kinetic model describes the chemisorptive type uptake, which are primarily caused by valency forces and ion exchange between the adsorbent and adsorbate (Ho, 2006).

2.4.5.1. Pseudo-first-order kinetic model

PFO kinetic is known as the Lagergren rate equation. In this model, the difference between the amount of adsorbate adsorbed on adsorbents at equilibrium is determined by the adsorption process. When one of the reactants is present in extreme excess or is kept at a constant concentration in relation to the other component, the reaction is demonstrated with pseudo-first order

kinetics (Revellame et al., 2020). Equation (2.4), is the pseudo-first-order kinetic model in its linear form, which is applied to fit the time dependence sorption data. The pseudo–first–order kinetic model, which is theoretically derived by the Lagergren show the properties of the Langmuir rate at initial times of adsorption or close to equilibrium.

$$q_t = q_e(1 - e^{k_1 t}) \qquad \text{..... (2.4)}$$

where q_t and q_e are the amount of sorbate removed at time t and removal capacity at equilibrium, respectively, k_1 is the rate constant for pseudo-first order kinetics. Excel 'add-ins' Solver was used with user-defined functions to minimize the residuals between the model-calculated and model-measured values.

2.4.5.2. Pseudo-second-order kinetic model

Based on the presumption that chemisorption is the rate-limiting phase, the pseudo-second-order kinetic model predicts the adsorption mechanism. In this condition, the adsorption rate is dependent on adsorption capacity not on concentration of adsorbate. Equation (2.5) represents the pseudo-second-order kinetic equation (Haerifar & Azizian, 2013). Similarly, theoretical studies indicate that the rate coefficient of pseudo-second-order model, i.e., k_2 is virtually a complex function of the initial concentration of the sorbing species

$$q_t = \frac{k_2 q_e^2 t}{1 + k_2 q_e t} \qquad \text{... (2.5)}$$

where q_t and q_e are the amount of sorbate removed at time 't' and removal capacity at equilibrium, respectively, k_2 is the rate constant for pseudo-second-order kinetics.

2.4.6. Effect of background electrolyte

The nonspecific and specific adsorption are distinguished using the background electrolyte concentrations. Physisorption, also known as non-specific adsorption, that involves relatively weaker forces and forming outer-sphere complexes, whereas chemically adsorbed inner-sphere complexes, more selective, and less reversible reactions are characteristics of specific adsorption (Hamdi et al., 2022). Ionic strength as the background electrolyte concentrations showed a significant impact on outer sphere complexes, which simply include electrostatic interactions, but inner-sphere complexes, which involve considerably stronger covalent or ion-exchange showed insignificant impact (Wiesner et al., 2006). Furthermore, the ionic strength also governs electrostatic interaction. Thus, by raising the ionic strength of the sorptive solution, whether electrostatic forces or the physisorption, is decreased significantly since the background ions created a surface charge layer at the solid surface and caused screening effect. A systematic sorption studies were conducted varying the background electrolyte concentrations of NaCl from 0.0001 to 0.1 mol/L in the sorptive solutions with the pollutants' concentration of 10.0 mg/L. The solution pH of tetracycline, bisphenol A, triclosan, ciprofloxacin and EE2 were maintained at 3.5, 6.0, 4.0 ,7.0, and 6.08 respectively. A solid dose of 2.0 g/L was introduced to the sorptive solutions to equilibrate it for 24 hrs. The sorption process is demonstrated previously Chapter 2, section 2.4. Further, the percentage removal of pollutants is presented as a function of background electrolyte concentrations.

2.4.7. Effect of co-existing ions

It is very important to investigate the effect of co-existing ions on the adsorption of adsorbate because a variety of ions are likely to present in polluted water and may compete with adsorbate for binding sites on the surface

of the adsorbent. The sorption of micro-pollutants tetracycline, bisphenol A, triclosan, ciprofloxacin and EE2 at pH 3.5, 6.0, 4.0 ,7.0, and 6.08 respectively were performed separately in the presence of various cations and anions, and the sorptive solutions were given a solid dosage of 2.0 g/L to equilibrate for 24 hrs. 50.0 mg/L was used as the coexisting ion concentrations. The anions used are ethylenediaminetetraacetic acid (EDTA), oxalic acid, glycine, and phosphate, while the cations are manganese (II), magnesium (II), calcium (II), and nickel (II).

2.4.8. Column reactor studies

Column experiments are carried out using a glass column (1 cm inner diameter and 12 cm long) filled with 0.25 g or 1.0 g of ATTP@PEG/ATTP@PVP beads (placed in the middle of the column) for the removal of micro-pollutants, *viz*; tetracycline, bisphenol A, ciprofloxacin, triclosan and EE2. The column is packed with small sized glass beads, and sand below and above of the nanocomposite beads. The initial sorptive concentrations were kept at 10.0 mg/L, with tetracycline, bisphenol A, ciprofloxacin, triclosan and EE2's pH of 3.5, 6.0, 7.0, 4.0 and 6.08, respectively. A peristaltic pump was used to pump sorptive solution from the bottom of column at a constant flow rate of 1.0 mL/min. Fraction Collector, collects the effluent solution of column. The collected effluents are filtered using a 0.45 μm syringe filter, and their concentrations are measured using an UV-Vis spectrophotometer.

The breakthrough curve is obtained by plotting curve between the column data (C_e/C_o) and the throughput volume (L). Further, using the Thomas equation (Equation 2.6) (Barros et al., 2013), the breakthrough data are further used to estimate the loading capacity of column for the pollutants under dynamic conditions.

$$\frac{C_e}{C_o} = \frac{1}{1+e[K_T\,(q_o m - C_o V)]/Q} \qquad \text{... (2.6)}$$

where C_e and C_o are the concentrations of effluent and influent solutions of tetracycline, bisphenol A, ciprofloxacin, triclosan or EE2; K_T refers to the Thomas rate constant (L/min/mg); q_o is the maximum amounts of pollutants loaded (mg/g) in the column under the specified column conditions; m is the amount of adsorbent taken in column (g); V is the throughput volume (L); and Q is the flow rate of pumped pollutant's solution (L/min). The column data is then fitted to a non-linear Thomas equation using the least square fitting method to estimate two unknown variables, i.e., K_T and q_o. Microsoft Excel 'add-ins' Solver was used with user-defined functions to minimize the residuals between the model-calculated and model-measured values.

2.4.9. Application of the nanocomposites in the natural water matrix

The sorption experiments are carried out using the natural water samples collected from different water sources in various regions of the Aizawl district, Mizoram to assess the practical implacability of the synthesized material in the removal of these pollutants in natural water samples. The studies make it possible to model the sorption process onto a realistic water matrix. Using a Mult photometer instrument, several water quality parameters, including pH, conductivity, resistivity, salinity, total dissolved solids, phosphate, sulphate, nitrate, and fluoride, were measured for these water samples. Using an atomic absorption spectrometer, the metal concentrations of Fe, Zn, Mn, Ca, Pb, and Cu were determined. The inorganic carbon and NPOC values of the real water samples were obtained using a TOC analyzer. As a stock solution, real water is spiked with tetracycline, bisphenol A, triclosan, ciprofloxacin and EE2 to make it 10.0 mg/L. The pH of the pollutant solutions was adjusted by the dropwise

addition of 0.1 mol/L HCl or 0.1 mol/L NaOH. The pH was adjusted to 3.5, 6.0, 4.0 ,7.0, and 6.08 tetracycline, bisphenol A, triclosan, ciprofloxacin and EE2, respectively. Further, 2.0 g/L solid was introduced and the sorption experiments are performed as demonstrated previously Chapter 2, Section 2.4. The equilibrated solutions are filtered with the syringe filter and subjected for the micro-pollutant's concentration measurements. The bulk sorptive concentration of tetracycline, bisphenol A, triclosan, ciprofloxacin and EE2, are measured using UV-Visible spectrophotometer.

2.4.10. Regeneration and reusability

The desorption studies of tetracycline, bisphenol A, triclosan, ciprofloxacin and EE2 using ATTP@PEG and ATTP@PVP are performed using the hydrochloric acid (HCl) at room temperature and the concentration of the acid was varied from 0.005 to 0.1 mol/L in order to optimize the suitable HCl concentration to desorb the pre-adsorbed tetracycline, bisphenol A, triclosan, ciprofloxacin and EE2 from ATTP@PEG and ATTP@PVP. The sorption experiment is carried out as described in batch experiment section 2.4. The sorption experiment is conducted for these micro-pollutants (tetracycline, bisphenol A, triclosan, ciprofloxacin and EE2) at the concentration of 10.0 mg/L using the ATTP@PEG and ATTP@PVP solids. 100 mg of ATTP@PEG and ATTP@PVP is introduced in different polyethylene bottles containing 50 mL of micro-pollutant and kept in automatic shaker for 24 hrs. It is then centrifuged and the equilibrated solutions are analysed for micro-pollutant concentrations using the UV-Visible spectrophotometer. Further, the 50 mL of HCl having various concentrations (i.e., 0.005, 0.01, 0.05 and 0.1 mol/L) are introduced into different polyethylene bottles to desorb the pre-adsorbed pollutants. The desorption is performed in automatic shaker for 60 mins to desorb the pre-adsorbed tetracycline, bisphenol A, triclosan, ciprofloxacin and EE2. The solution is then centrifuged and the supernatant solution is analysed for obtaining the pollutant concentrations using UV-Visible Spectrophotometer. The percentage desorption is then calculated using equation 2.7. The studies

showed that the 0.01 mol/L HCl is most suitable to desorb the studied pollutants from ATTP@PEG or ATTP@PVP solids. The regenerated material is washed with purified water for several times and dried in an oven at 60°C. Further, the next adsorption-desorption studies are performed for all the five micro-pollutants using ATTP@PEG and ATTP@PVP solids. The reusability test is conducted for six adsorption-desorption cycles.

$$\% \text{ Desorption} = \frac{\text{Concentration of pollutant desorbed}}{\text{Concentration of pollutant adsorbed}} \times 100 \qquad \text{..... (2.7)}$$

2.4.11. Stock Cultures and Culture Media

All microbial strains cited were provided by DSMZ, Deutsche Sammlung von Mikroorganismen und Zellkulturen GmbH (German Collection of Microorganisms and Cell Cultures). *Bacillus subtilis* (MTCC 2415), *Pesudomonas aeruginosa* (MTCC 1688), *Escherichia coli* (ATCC 25922) and *Streptococcus pyogenes* (ATCC 12204) were maintained frozen (−80ºC) and transferred monthly on TSA (Tryptone Soya Agar) made of 15 g/L tryptone, 5 g/L soya peptone, 5 g/L NaCl, and 15 g/L neutralized bacteriological agar.

2.4.12. Antibacterial susceptibility testing

The Agar well diffusion assay performs the preliminary antibiotic effectiveness of pristine attapulgite, ATTP@PVP/Agº and ATTP@PEG/Agº nanocomposite. The test bacteria are grown in nutritional broth for 24 hrs to reach a colony-forming unit (CFU) density of 10^8 cells/mL. The Luria-Bertani (LB) agar plates with 100 µL of each bacteria culture are used for plating. Following solidification, wells (5 mm in diameter) are drilled with a sterilized cork borer and stocked with various concentrations of ATTP@PEG/Agº (2.0, 4.0, 6.0, or 8.0 mg) against *Bacillus subtilis* and *Pseudomonas aeruginosa;* ATTP@PVP/Agº (2.0, 4.0, 6.0, or 8.0 mg) against *Escherichia coli* and *Streptococcus pyogenes* and 8.0 mg of pristine attapulgite against all the four

bacterial strains. The sizes of the inhibitory zones are measured in millimetres (mm) after incubation of plates for 18 hrs at 37°C.

2.4.13. Antimicrobial activity test by dynamic contact method

All bacterial pre-inoculum cultures are grown for 24 hrs at 37ºC in 20 mL of Nutrient Broth (made of 1 g/L beef extract; 5 g/L neutralized peptone; 2 g/L yeast extract; 5 g/L NaCl) subjected to horizontal shaking at 100 rpm. The nanocomposite materials (ATTP@PEG/Agº and ATTP@PVP/Agº) are placed in contact with a microbial liquid suspension, subjected to vigorous shaking in order to assure the best contact between bacteria and sample. At 0.5, 4, 8, 12 and 24 hrs of contact, the bacterial concentration (CFU/mL) of the microbial suspension is determined by plating serial dilution on plate count agar to obtain the overall number of bacteria (CFU—Colony Forming Units). For the antibacterial tests the specific conditions are used as given below:

(i) microbial liquid suspension: 5 mL of 5% Nutrient Broth in phosphate buffer (0.3 mM, pH 7.2) inoculated with 10^{-8} CFU/mL bacteria;
(ii) total flask volume: 25 mL;
(iii) sample incubation: 24 hrs at 37ºC under vigorous shaking;
(iv) quantity of tested material: 2.0, 4.0, 6.0, 8.0 mg of ATTP@PVP/Ag^0 and ATTP@PEG/Agº nanocomposites tested in triplicate;
(v) control samples: bacteria growth was tested on flasks only containing inoculated broth media and distilled water. All the samples are subjected to sterilization by autoclave.

The bacteria percentage reduction of the samples is calculated as follows:

$$P = \frac{100(b-a)}{b} \qquad \ldots\ldots\ldots\ldots (2.8)$$

where P is the percentage removal (%), a is the number of bacterial cells that remained after treatment with nanocomposite for 24 hrs, and b is the number of bacterial cells before treatment with the nanocomposite.

2.4.14. Effect of pH on bacterial removal

The culture grown overnight is divided into 5 mL separate samples, with each mL holding 8 $\log_{10}$CFU of bacteria. The material ATTP@PVP/Ag^0 follows two cycles of centrifugation at 2000 g for 10 mins. The pellets obtained are again re-suspended in a solution containing 0.5 % NaCl. The pH of the final bacterial suspensions is then varied to 4.0, 7.0, and 9·0 using either HCl or NaOH solutions, and samples are triplicated to obtain the average value at pH conditions. Following 7 h incubation period at 37ºC with 150 rpm shaking, the samples and controls are collected for their microbial CFU counts. The effect of pH is compared to the same bacterial culture, which is not subjected to pH adjustment (growth control) both with and without the addition of ATTP@PVP/Ag^0.

CHAPTER 3

RESULTS AND DISCUSSION

3. RESULTS AND DISCUSSION

1. PHYSICO-CHEMICAL PARAMETRIC ANALYSIS OF NATURAL WATER SAMPLES

The four natural water samples are collected from various water sources *viz.*, municipal wastewater, stream, supply water and treated wastewater from different parts of Aizawl, Mizoram (India). These water samples are tested for several physio-chemical parametric results are given in Table 3.1. The pH of the samples is almost neutral and ranged from 7.0 to 8.2. The natural water samples contain a substantial amount of inorganic carbon, a lesser content of non-purgeable organic carbon (NPOC) i.e., 1.73, 0.976, 1.679 and 1.043 mg/L, respectively for the Municipal wastewater (Chite Veng, Aizawl), MZU Water supply, SIPMUI Treated water and Lengpui stream water. Copper, aluminum, lead, and nickel are present in trace amounts in these water samples. However, relatively high content of calcium and magnesium is detected in these water samples. Varied but relatively high concentrations of calcium and magnesium are found, and lying between 3.0 to 136.0 mg/L and 4.5 to 16.0 mg/L, respectively, for Ca and Mg in these different natural water samples. The presence of high inorganic carbon with Ca and Mg indicated that the water is contained with carbonates and bicarbonates of calcium and magnesium. Phosphate is present at its low values i.e., 0.56, 0.2, 0.250, and 0.4 mg/L for Municipal wastewater (Chite Veng, Aizawl), MZU Water supply, SIPMUI Treated water and Lengpui stream, respectively and sulphate is also within the permissible level i.e., 8.0, 1.0, 2.0, and 4.5 mg/L respectively for the Municipal wastewater (Chite Veng, Aizawl), MZU Water supply, SIPMUI Treated water and Lengpui stream water samples.

Table 3.1: Physico-chemical quality parameters of four natural water samples

Natural water	**TOC (mg/L)**	**Cations (mg/L)**	**Anions**	**Physical properties**
Municipal wastewater (Chite Veng, Aizawl)	NPOC:1.739 TC: 17.86 IC: 15.554	Cu: BDL Ca: 65.0 Pb: 0.35 Ni: BDL Al: BDL Fe: BDL Mg: 12.0	Sulphate: 8 mg/L Phosphate: 0.56 mg/L Nitrate: 2.0 µg/L	pH: 7.15 Salinity: 0.09 PSU Oxd. & red. Potential: 170.7 MV Resistivity: 0.0043 $M\Omega cm^{-1}$ Conductivity: 219 μScm^{-1} TDS: 111 ppm
MZU Water supply, (Aizawl)	NPOC: 0.976 TC: 8.443 IC: 7.466	Cu: BDL Ca: 3.4589 Pb: 0.0442 Ni: BDL Al: BDL Mg: 11.0	Sulphate: 1 mg/L Phosphate: 0.2 mg/L Nitrate: 20 µg/L	pH: 7.9 Salinity: 0.07 PSU Oxd. & red. Potential: 194.5 MV Resistivity: 0.0078 $M\Omega cm^{-1}$ Conductivity: 129 μScm^{-1} TDS: 65 ppm
SIPMUI Treated water	NPOC: 1.679 TC:	Cu: BDL Ca: 136.0 Pb: 0.35	Sulphate: 2 mg/L Phosphate:	pH: 7.9 Salinity: 0.12 PSU

(Aizawl)	16.862 IC: 14.506	Ni: BDL Al: BDL Mg: 16.0	2.50 mg/L Nitrate: 5.7 µg/L	Oxd. & red. Potential: 204.8 MV Resistivity: 0.0044 MΩcm^{-1} Conductivity: 257 µScm^{-1} TDS: 113 ppm
Lengpui stream	NPOC:1.043 TC: 16.731 IC: 16.004	Cu: BDL Ca: 35.0 Pb: 0.10 Ni: BDL Al: BDL Mg: 4.5	Sulphate: 4.5 mg/L Phosphate: 0.4 mg/L Nitrate: 4.0 µg/L	pH: 7.0 Salinity: 0.21 PSU Oxd. & red. Potential: 203.1 MV Resistivity: 0.002 MΩcm^{-1} Conductivity: 214 µScm^{-1} TDS: 113 ppm

*BDL= Below detection limit

2. CHARACTERISATION OF MATERIALS

3.2.1. Scanning electron microscopy (SEM) with energy-dispersive X-ray spectroscopy (EDX)

SEM photographs of the pristine attapulgite clay (ATTP), ATTP@PEG, ATTP@PVP, ATTP@PEG/Ag^{0} and ATTP@PVP/Ag^{0} are given in Figure 3.1 (a-e), respectively. Attapulgite clay (ATTP) exhibits a fibrous crystal structure.

The individual fibers are thin and elongated, resembling microscopic needles/rods. These fibrous particles interlock and intertwine, forming three-dimensional networks in the clay matrix. Attapulgite clay shows porous structure contained with micro to mesopores on it (Figure 3.1 (a)). The composite materials ATTP@PEG and ATTP@PVP show a thicker and more heterogeneous solid surface. The polymers, PEG and PVP have grown on the surface of attapulgite (Figure 3.1 (b-c)). This is due to the self-polymerization of the polymers within the clay's internal and external surfaces. On the other hand, the nanocomposites (ATTP@PEG/Ag^0 and ATTP@PVP/Ag^0) show the distinct presence of Ag nanoparticles, that are spatially distributed on the surface of the solids (Figure 3.1 (d-e)). The Ag-NPs are spherical and not aggregated at the surface.

Furthermore, the SEM-EDX spectrum of ATTP, ATTP@PEG, ATTP@PVP, ATTP@PEG/Ag^0 and ATTP@PVP/Ag^0 are shown in Figure3.1(f-i) along with the quantitative data (weight and atomic percentages) included in Table 3.2. The EDX results revealed that these solids contained the common elements of Si, Al, Mg, C, O, Na, Ca, N, K. The specific chemical formula for attapulgite is complex and can be described as $(MgAl)_2Si_4O_{10}(OH)\cdot 4(H_2O)$ (Elbassyoni et al., 2020). This formula indicates that it is composed of various elements (Mg, Al, Si, and O) in specific ratios according to their X-rays analysis (EDAX): Mg (6.33%), Si (18.91%), Al (4.15%) and O (57.91%). Also, an additional peak of the Ag is obtained in the EDX spectrum of ATTP@PEG/Ag^0 and ATTP@PVP/Ag^0, confirming the existence of Ag in the nanocomposite solid.

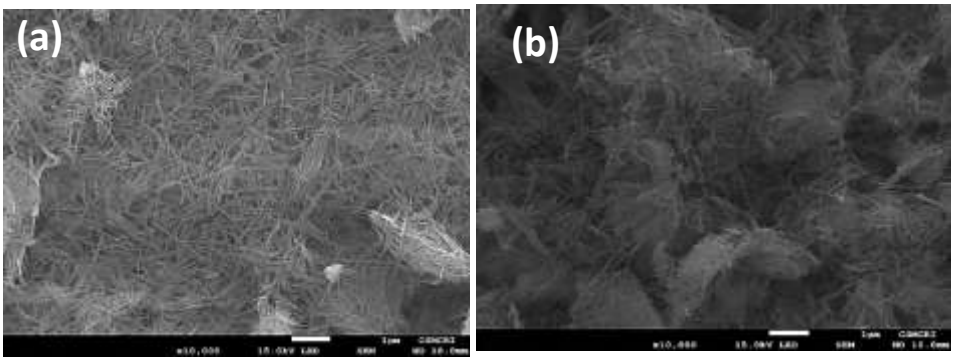

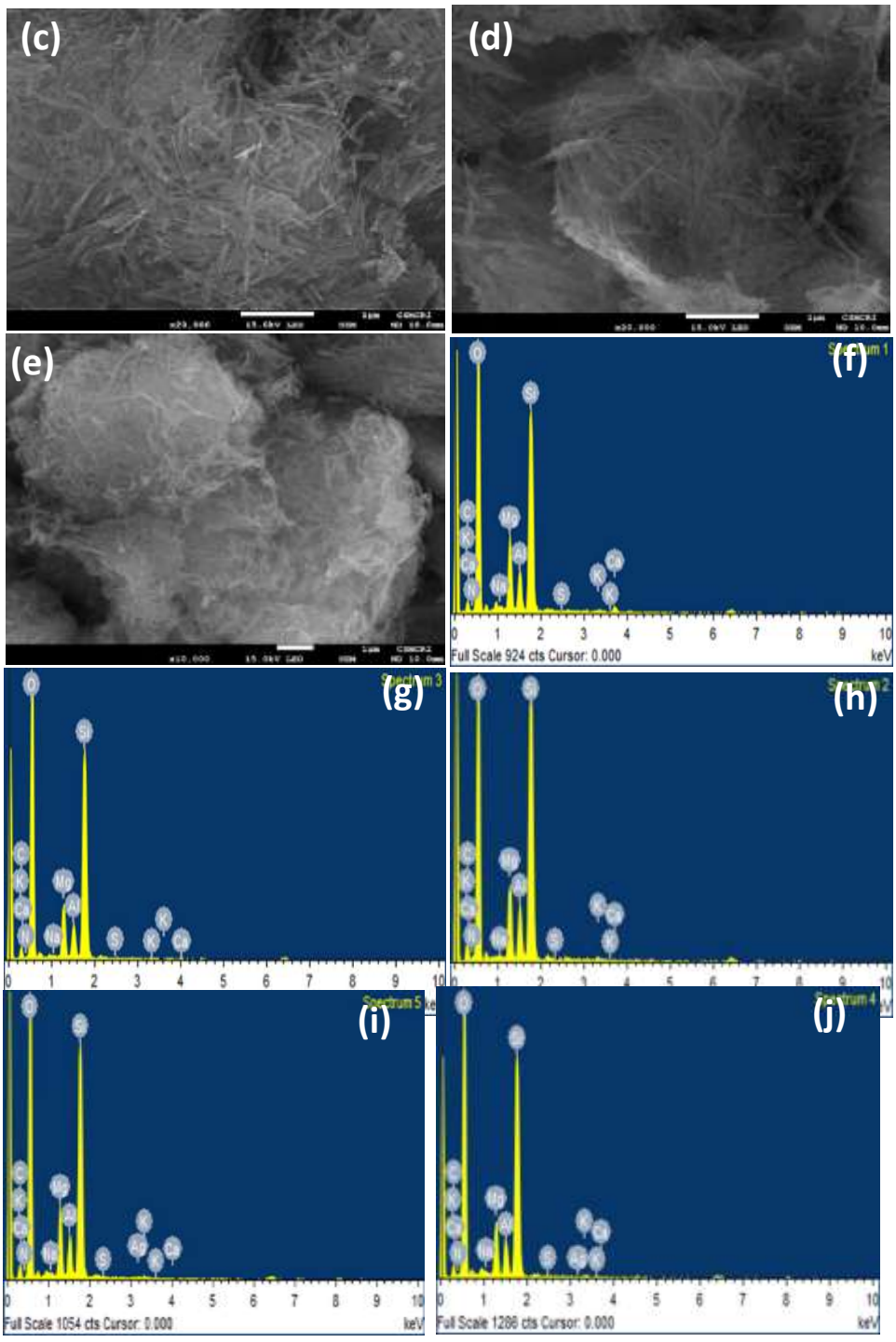

Figure 3.1: SEM micrographs of **(a)** ATTP; **(b)** ATTP@PEG; **(c)** ATTP@PVP; **(d)** ATTP@PEG/Ag^0 and **(e)** ATTP@PVP/Ag^0; and EDX spectra of **(f)** ATTP; **(g)** ATTP@PEG; **(h)** ATTP@PVP; **(i)** ATTP@PEG/Ag^0 and **(j)** ATTP@PVP/Ag^0.

Table 3.2: Weight and atomic percentage of the elements present in the ATTP, ATTP@PEG, ATTP@PVP, ATTP@PEG/Ag^0 and ATTP@PVP/Ag^0 solid samples using the SEM/EDX analysis.

Elements	**Weight %**				
	ATTP	**ATTP @PEG**	**ATTP @PEG/ Ag^0**	**ATTP@ PVP**	**ATTP@P VP/Ag^0**
C K	9.94	11.64	13.99	14.81	13.69
O K	57.91	60.14	54.47	54.44	58.70
N K	0.38	0.26	0.23	1.63	0.66
Na K	0.07	0.09	0.17	0.04	0.02
Al K	4.15	2.72	2.98	3.17	2.53
Si K	18.91	20.01	20.20	20.66	19.27
K K	0.34	0.17	0.21	0.20	0.39
Mg K	6.33	4.85	5.72	5.12	4.57
Ca K	2.03	0.15	0.02	0.05	0.08
Ag L	-	-	0.05	-	0.13

Elements	Atomic %				
	ATTP	ATTP@ PEG	ATTP@ PEG/Ag⁰	ATTP@ PVP	ATTP@ PVP/Ag⁰
C K	15.35	17.79	20.12	21.19	19.53
O K	63.20	64.14	60.98	58.46	62.86
N K	0.48	0.33	0.28	2.00	0.81
Na K	0.05	0.06	0.13	0.03	0.01
Al K	3.04	1.75	1.91	2.02	1.61
Si K	11.76	12.35	12.42	12.64	11.75
K K	0.15	0.08	0.09	0.09	0.17
Mg K	5.55	2.46	4.07	3.62	0.06
Ca K	0.45	0.07	0.01	0.02	3.22
Ag L			0.01		0.02

3.2.2. Transmission electron microscopy (TEM)

TEM micrographs for the surface morphology of attapulgite clay (ATTP), ATTP@PEG, ATTP@PVP, ATTP@PEG/Ag⁰ and ATTP@PVP/Ag⁰ are shown in Figure 3.2. (a-g). Additionally, the ATTP@PEG/Ag⁰ and ATTP@PVP/Ag⁰ shows the distinct presence of silver nanoparticles (Figure. 3.2. (b-c)). Furthermore, the Image J software obtains the d-spacing value and the average particle size of the Ag-NPs. The Ag-NPs are spherical and have an average size of around 41.18 nm for ATTP@PEG/Ag⁰ and the size of about 30.91 nm for ATTP@PVP/Ag⁰. Figure. 3.2. (f-g) shows the fringes of the Ag-

NPs, which calculates the d-spacing and is 0.24 nm for ATTP@PEG/Ag⁰ and 0.211 nm for ATTP@PVP/Ag⁰. A prior investigation reveals that spherical Ag nanoparticles are uniformly dispersed on the polypyrrole/attapulgite matrix and mean particle size of 40 nm (Zang et al., 2016).

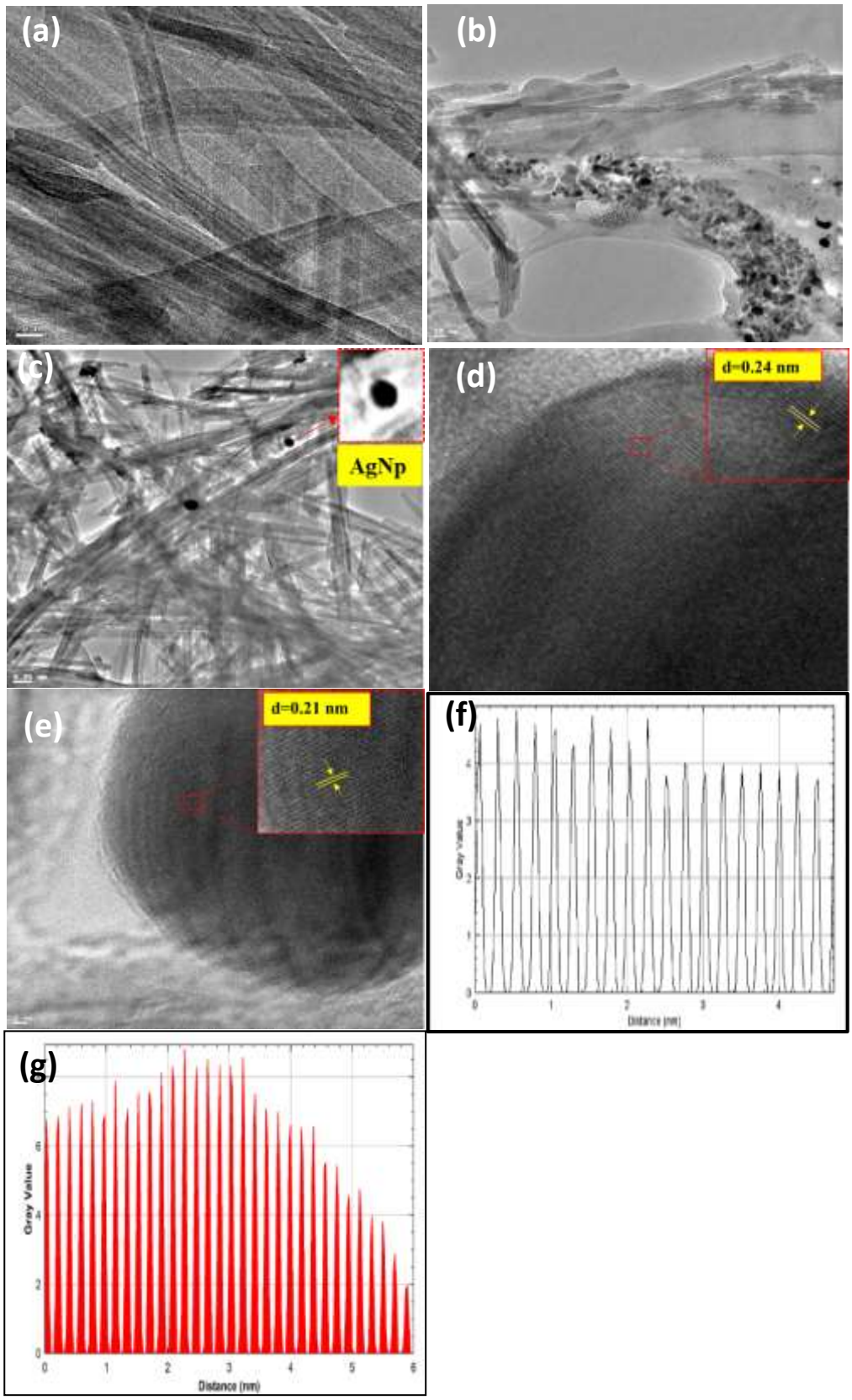

Figure 3.2. Transmission electron microscope pictures of (a) pristine attapulgite (ATTP); (b) ATTP@PEG/Agº; (c) ATTP@PVP/Agº; (d) d-spacing of ATP@PEG/Agº; (e) d-spacing of ATP@PVP/Agº; (f) particle size distribution of ATP@PEG/Agº; and (g) particle size distribution of ATP@PVP/Agº.

3.2.2. X-ray Diffraction (XRD)

The XRD patterns of attapulgite and the composites, i.e., ATTP@PEG, ATTP@PVP, ATTP@PEG/Ag^0 and ATTP@PVP/Agº are shown in Figure 3.3. (a-b). The XRD pattern of pristine clay exhibit the major diffraction peaks at 2θ values of 8.3º, 19.7º, and 27.3º which inferred the diffraction planes of (110), (040), and (400), respectively, of the natural attapulgite clay (Mohammed et al., 2020). Further, the diffraction peaks occurred at 2θ values of 29.57º, 39.26º, 43.38º, 47.47º, and 48.67º is due to the Miller indices of (104), (113), (202), (204), and (116), respectively, of calcite ($CaCO_3$) present in the ATTP clay. Further, the ATTP@PEG showed predominant diffraction peaks at 2θ values of 19.81º and 24.19º having diffraction planes of (120) and (032) of PEG (Jayaramudu et al., 2016). Further, the ATTP@PEG/Ag^0 solid showed additional diffraction peaks at 2θ values of 38.19º, 46.18º, 67.74º, and 77.70º denoted to the characteristic planes of (111), (200), (220), and (311), respectively, for Ag(NPs) (Kumar et al., 2011).

On the other hand, the XRD pattern of ATTP@PVP showed distinct peaks at 2θ values of 13.84º, 19.83º, and 21.21º, which is due to the presence of PVP (Li et al., 2001). Moreover, the ATTP@PVP/Ag^0 showed characteristic diffraction peaks of the Ag(NPs), predominantly occurred at 2θ values of 38.1º, 46.2º, 67.74º and 77.70º corresponding to the planes at (111), (200), (220), and (311), respectively (Thangamani & Bhuvaneshwari, 2022).

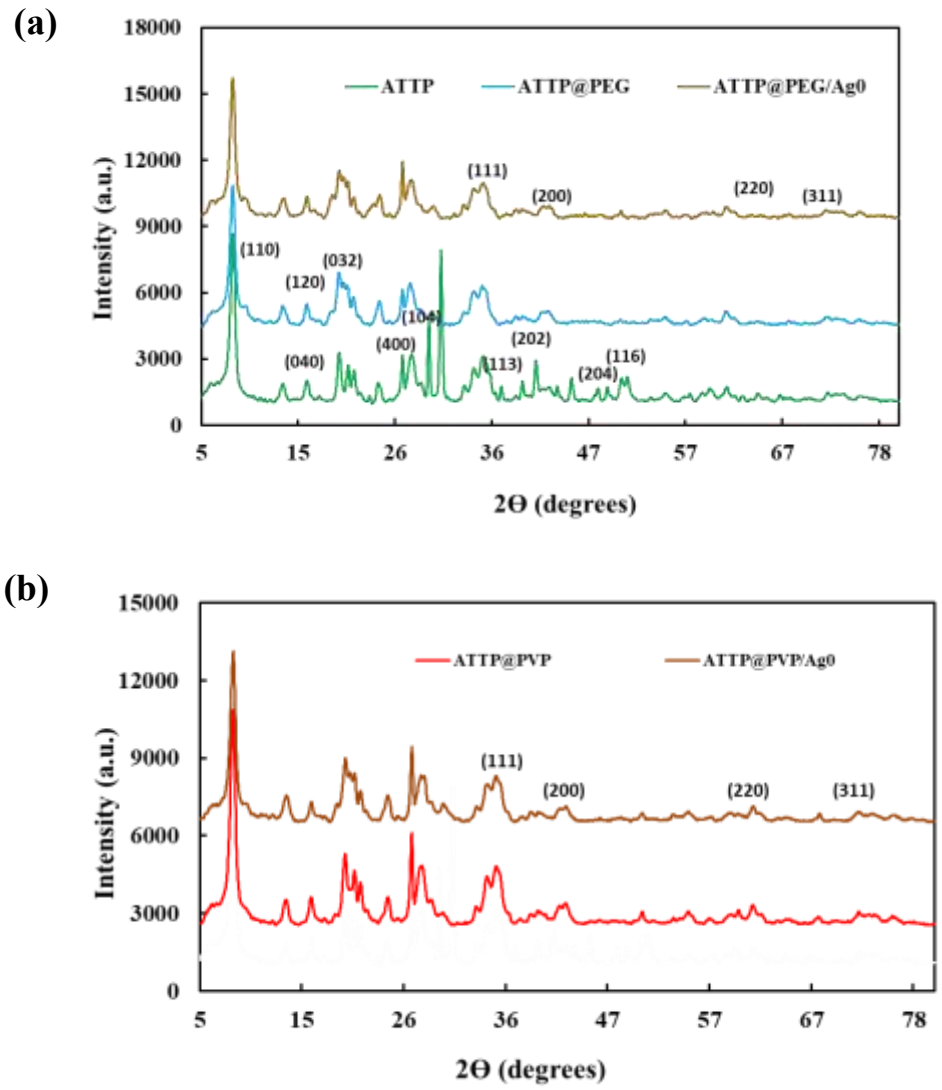

Figure 3.3: X-ray diffraction pattern of ATTP, ATTP@PEG, ATTP@PVP, ATTP@PEG/Ag^0 and ATTP@PVP/Ag^0 solids.

3.2.3. Fourier-transform infrared spectroscopy (FT-IR)

In order to determine the functional groups of the nanocomposites (ATTP, ATTP@PEG, ATTP@PVP, ATTP@PEG/Ag^0 and ATTP@PVP/Ag˚), the FT-IR spectra results are presented in Figure 3.4. Al^{3+} cations in

dioctahedral coordination (Al_2OH) and water coordinated to Mg along the fibers contribute to the vibration of hydroxyl (-OH) groups at 3614 cm^{-1} and 3546 cm^{-1} (Li et al., 2022). In addition, a broad peak around 848 cm^{-1} due to the asymmetric stretching vibrations of Si-O-Al. The acid activation eliminates the carbonate impurities; hence, the ATTP@PEG FT-IR spectrum disappears carbonate bands at 1423 cm^{-1} and 877 cm^{-1} (So et al., 2020). The ether groups in PEG's C-O stretching modes (ATTP@PEG) are responsible for the considerably higher peak intensity at 1092 cm^{-1} (Jafarpour et al., 2021). The PEG chains grafted with the hydroxyl (-OH) groups on the clay surface. The acid treatment caused carbonate vibrations to disappear at 1422 cm^{-1} and 876 cm^{-1} in the pristine clay. Further, the ATTP@PVP shows that peak at 1660 cm^{-1} represents the carbonyl (C=O) group (Dhumale et al., 2012). Compared to the free C=O stretching band of PVP, the absorption peaks of ATTP@PVP/Ag°, the peak shifts slightly towards the lower wave number due to the coordination between Ag^{+} ions and carbonyl oxygen (Song et al., 2014). The backbone of PVP comprises carbon-carbon (C-C) bonds; hence, the peaks related to C-C stretching are typically present in the range of 1000-1200 cm^{-1}. PVP contains amide (CONH) groups since a broad peak at 3549 cm^{-1} is due to the stretching vibrations of the N-H bonds (Zidan et al., 2019).

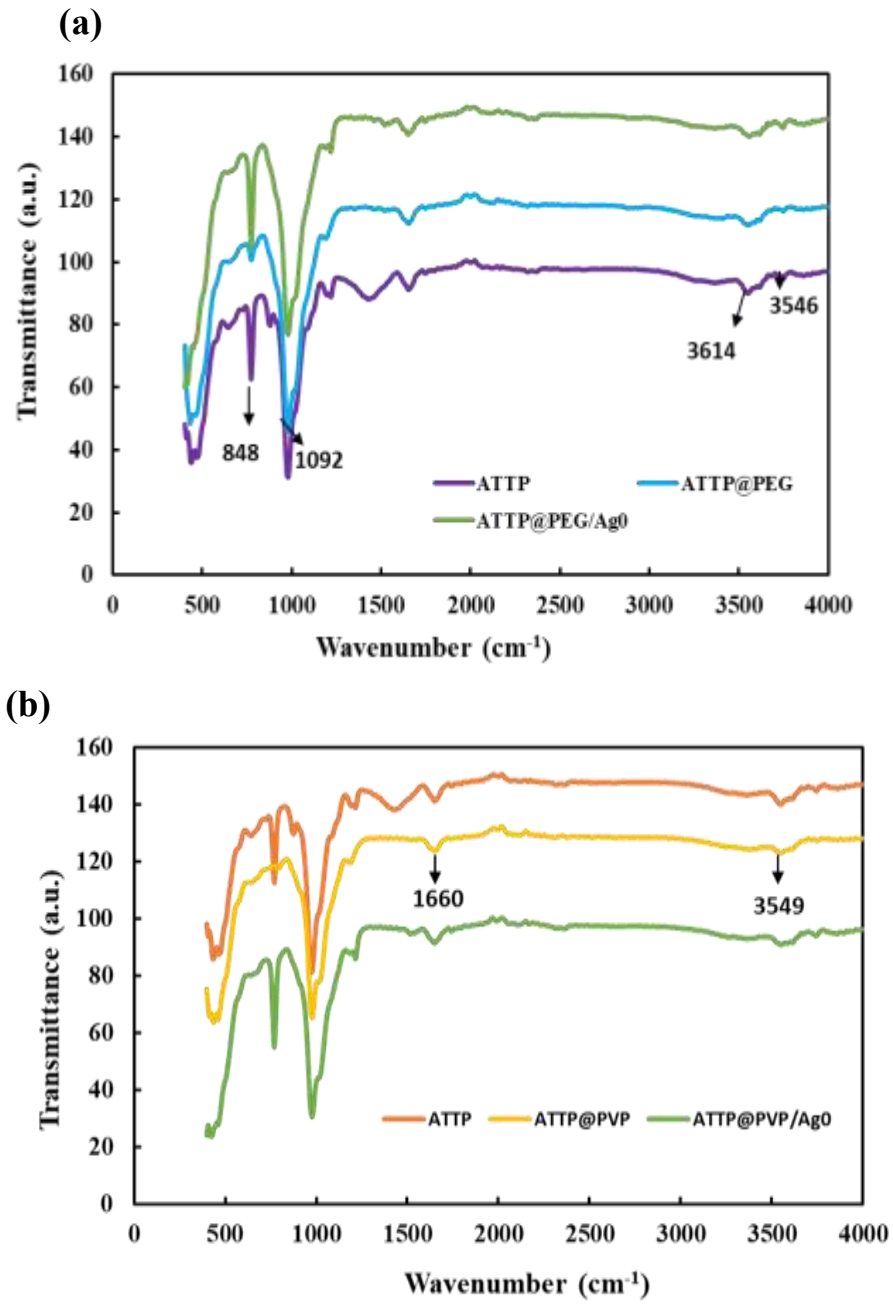

Figure 3.4. FT-IR spectra of (a) ATTP, ATTP@PEG and ATTP@PEG/Ag^0 (b) ATTP, ATTP@PVP and ATTP@PVP/Ag^0 solids.

3.2.4. Brunauer-Emmett-Teller (BET)

The specific surface area, pore size, and pore volume for ATTP, ATTP@PEG, ATTP@PVP, ATTP@PEG/Ag⁰ and ATTP@PVP/Ag^0 were determined using the Brunauer, Emmett, and Teller (BET) method, as shown in Table 3.3. Figure 3.5 (a). shows the N_2 adsorption/desorption isotherms for all the nanocomposites. Materials possessed type-IV isotherms having H3 hysteresis loops, with wedge-shaped pores (Buttersack, 2019). The BET-specific surface areas of ATTP, ATTP@PEG, ATTP@PVP, ATTP@PEG/Ag⁰ and ATTP@PVP/Ag^0 are 85.55, 100.01, 203.79, 88.46, and 107.37 m^2/g, respectively. The specific surface area of ATTP@PEG and ATTP@PVP are higher than that of pristine ATTP with small pore diameter and low pore volume. It is possible that the increased surface area is the result of a uniform coating and the penetration of a polymeric chain into the clay intergallery, which tends to widen the interspacing and therefore enlarge the surface area. However, the surface area decreased comparatively for ATTP@PEG/Ag⁰ and ATTP@PVP/Ag^0 due to the silver nanoparticles having predominantly occupied some of the pores of ATTP@PEG and ATTP@PVP. It was previously reported that an Ag/PVP-modified clay hybrid sample had an increase in the clay surface area as PVP molecules were incorporated into the interlayer space of MMT to make MMT form intercalation structure compared to bare MMT (Shi et al., 2011). More significantly, the mesoporous area has a high density of pores and promotes the N_2 adsorption process due to the composite's accessible pores (Oraon et al., 2016). Furthermore, Figure 3.5 (b). shows the ATTP, ATTP@PEG, ATTP@PVP, ATTP@PEG/Ag⁰ and ATTP@PVP/Ag⁰ pore width distributions versus the different pore volumes. All the materials fall in the pore width range between 2-50 nm, exhibiting a mesoporous structure (Buttersack, 2019).

Table 3.3: BET surface area, BJH adsorption pore volume, adsorption average pore diameter, and BJH desorption pore width for the ATTP, ATTP@PEG, ATTP@PVP, ATTP@PEG/Ag^0 and ATTP@PVP/Ag^0 solids.

Parameters	**ATTP**	**ATTP @PEG**	**ATTP @PVP**	**ATTP @PEG/Ag^0**	**ATTP @PVP/Ag^0**
BET-specific surface area (m^2/g)	85.55	100.01	203.79	90.46	107.37
Pore volume BJH adsorption (cm^3/g)	0.442	0.566	0.505	0.459	0.475
Average pore diameter (Å)	210.27	229.25	104.11	231.93	180.77
BJH desorption pore width (Å)	188.37	181.18	135.66	177.10	156.30

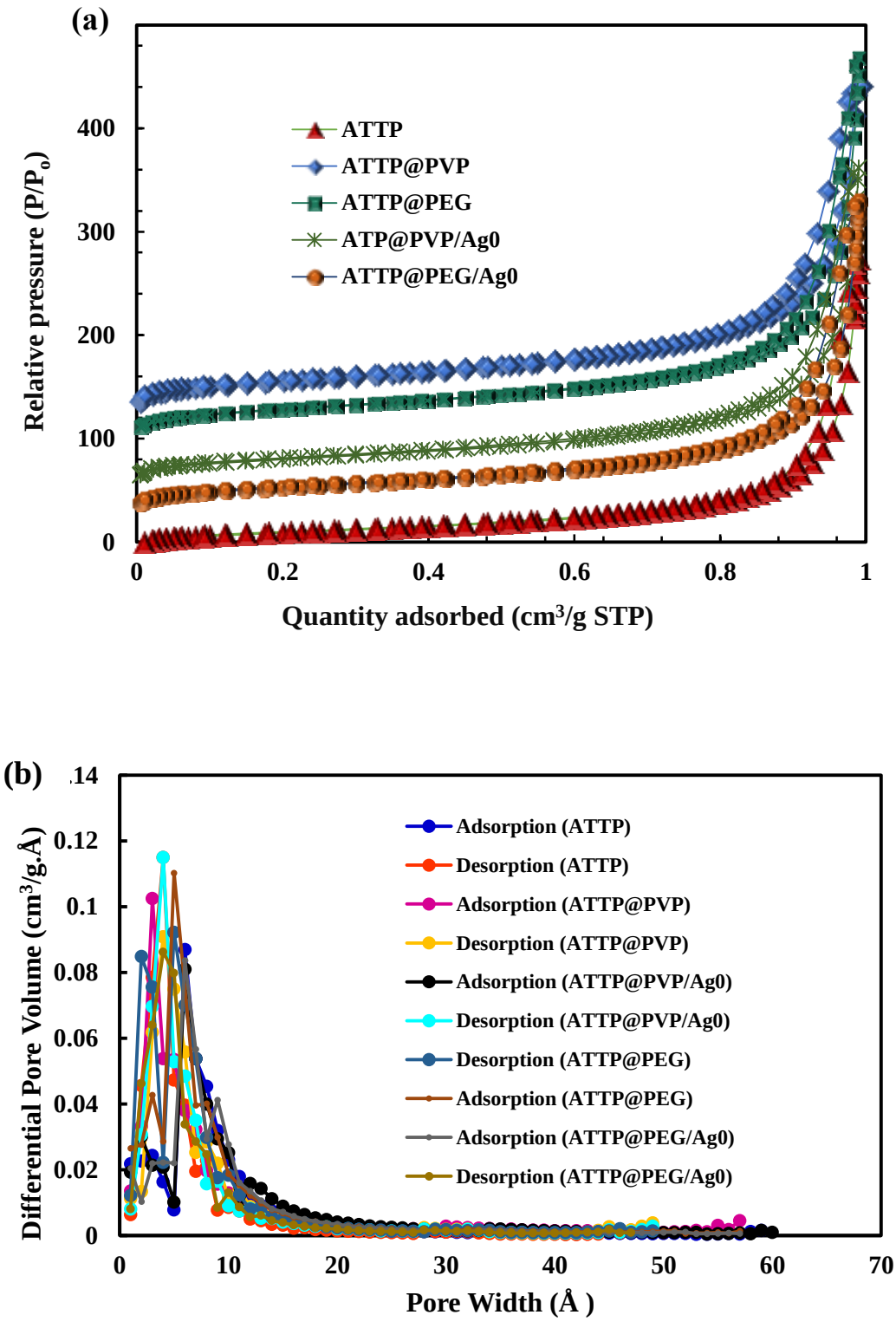

Figure 3.5: (a) N_2 adsorption-desorption isotherms obtained for ATTP, ATTP@PVP, ATTP@PEG, ATTP@PEG/Ag⁰ and ATTP@PVP/Ag⁰; and **(b)**

pore size distribution of ATTP, ATTP@PVP, ATTP@PEG, ATTP@PEG/Ag⁰ and ATTP@PVP/Ag⁰ solids.

3.2.5. X-ray photoelectron spectroscopy (XPS)

The XPS spectra of the ATTP@PEG/Ag⁰ and ATTP@PVP/Ag⁰ nanocomposites determine the presence of silver nanoparticles with their oxidation states. The O(1s), N(1s), C(1s), and Ag (3d) peaks in solids were visible in the XPS spectrum (Figure 3.6 (a-b)). Also resolved and shown in Figure 3.6 (a-b) (inset) are the photopeak of the Ag(3d). The nanocomposites 3d Ag photoelectron peaks are visible in the spectra. A pair of 3d peaks representing the elemental zerovalent silver's $3d_{5/2}$ and $3d_{3/2}$ energy levels occurred at the binding energies of 368.4 eV and 374.1 eV, respectively (Ghodake et al., 2020). Therefore, this confirms the presence of silver in its reduced state in ATTP@PEG/Ag⁰ and ATTP@PVP/Ag⁰ nanocomposites.

(a)

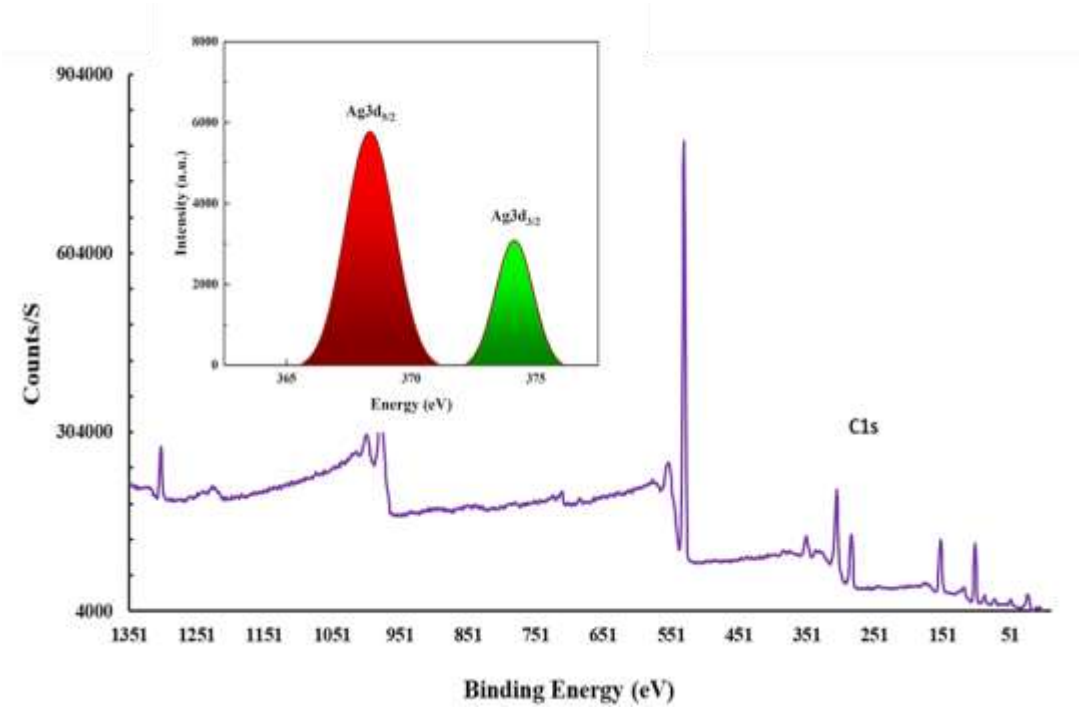

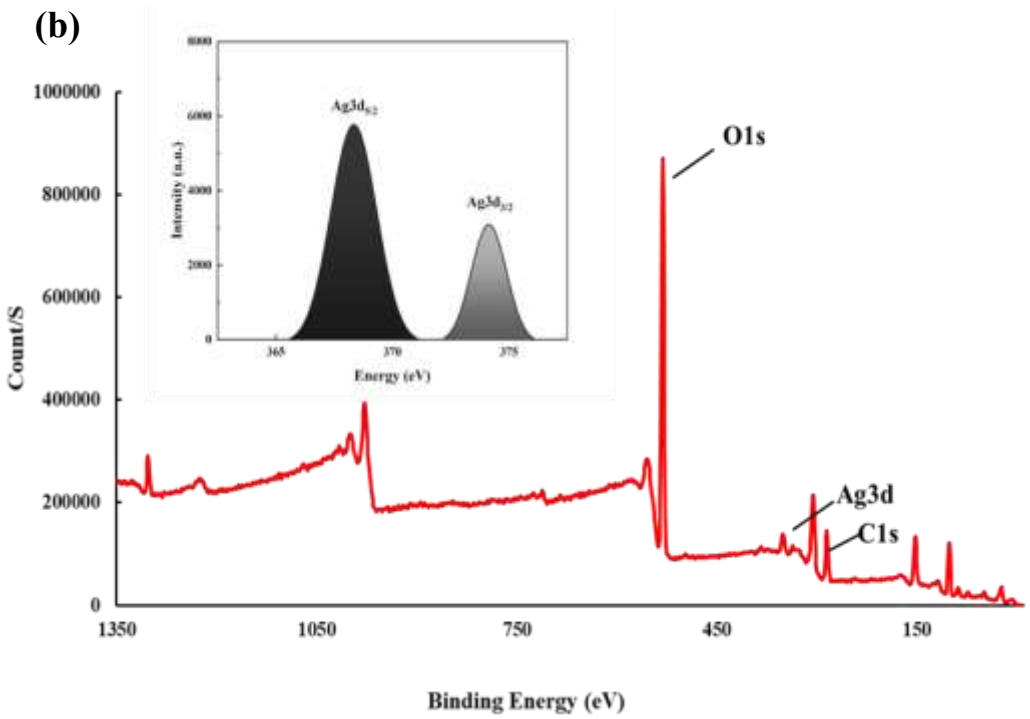

Figure 3.6: High-resolution XPS spectra for **(a)** ATTP@PEG/Ag⁰ and **(b)** ATTP@PVP/Ag⁰. [Inset: High-resolution XPS spectra for Ag 3d].

3.2.6. Contact angle measurement

Figure 3.7 illustrates the contact angle measurements for ATTP, ATTP@PEG, and ATTP@PVP composites. The sessile drop technique was employed, utilizing a 2 µL volume of chloroform as the testing liquid to evaluate the wettability of the prepared samples. Pristine attapulgite clay presents a contact angle of 64º, indicating moderate wetting behavior. The observed increase in contact angles to 100.9º and 102.9º for ATTP@PEG and ATTP@PVP composites suggests the composite's hydrophobic nature. This enhancement implies the presence of hydrophobic interactions between the micropollutants and the ATTP@PEG and ATTP@PVP composites, constituting the primary mechanistic pathway in removing these pollutants.

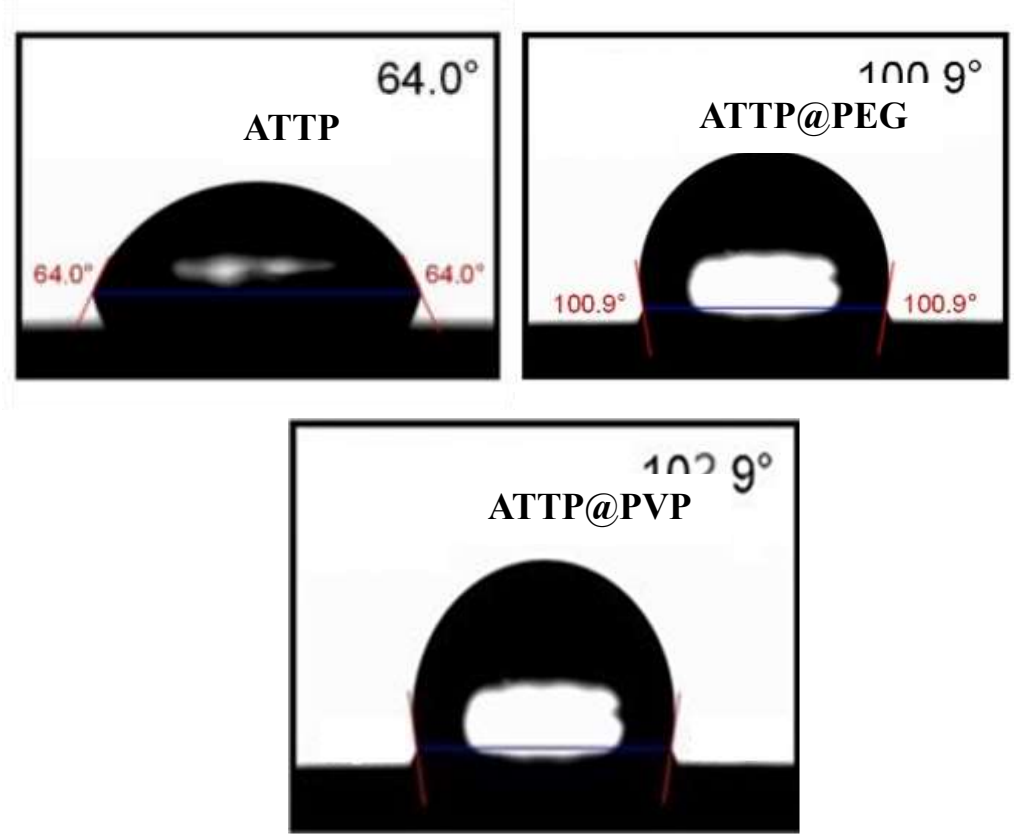

Figure 3.7. The contact angles of ATTP, ATTP@PEG, and ATTP@PVP composites.

3.2.7. Point of zero charge (pH_{PZC}) values

The pH_{PZC} of the ATTP, ATTP@PVP, ATTP@PEG, ATTP@PEG/Ag^0 and ATTP@PVP/Ag^0 solids were obtained and are shown graphically in Figure 3.8 and the values are given in Table 3.4.

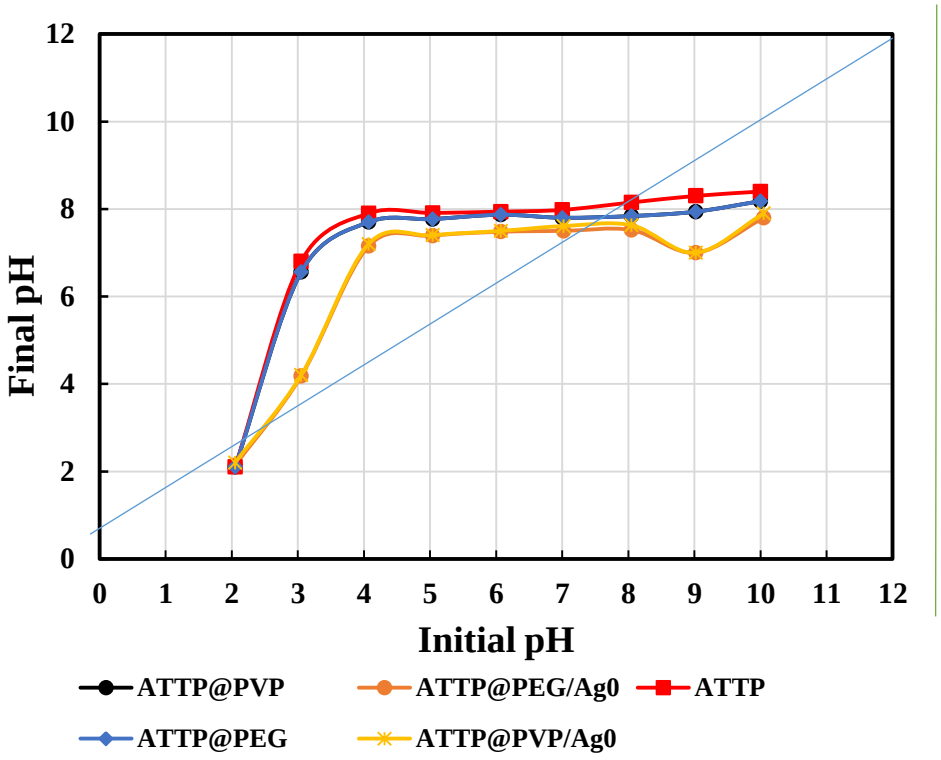

Figure 3.8: Plot of initial pH versus final pH for ATTP, ATTP@PEG, ATTP@PVP, ATTP@PEG/Ag⁰ and ATTP@PVP/Ag⁰ solids.

Table 3.4. The pH_{PZC} values of the ATTP, ATTP@PEG, ATTP@PVP, ATTP@PEG/Ag° and ATTP@PVP/Ag^0.

Samples	**pH_{PZC}**
ATTP	8.0
ATTP@PEG	7.8
ATTP@PVP	7.7
ATTP@PEG/Ag^0	7.5
ATTP@PVP/Ag^0	7.63

3. BATCH REACTOR STUDIES FOR TETRACYCLINE, BISPHENOL A, CIPROFLOXACIN, TRICLOSAN AND 17α-ETHINYLESTRADIOLE

3.3.1. Effect of pH

3.3.1.1. Tetracycline (TCH)

The effect of pH on the removal of tetracycline using ATTP@PEG, ATTP@PVP, ATTP@PEG/Ag⁰ and ATTP@PVP/Ag⁰ along with pristine attapulgite is performed at a wide pH range (pH 2.0 to 10.0) using the tetracycline concentration 10.0 mg/L. Results are presented as in Figure 3.9. It is notable that the percentage removal of tetracycline by ATTP@PEG, ATTP@PVP, ATTP@PEG/Ag⁰ and ATTP@PVP/Ag⁰ are significantly increased compared to the pristine attapulgite. The figure demonstrates that the lower pH region (~2-4) relatively favors the uptake of TCH by ATTP, and a maximum uptake occurred at pH 3.1 of 50.2%. However, a further increase in pH (>4.0) caused a gradual decrease in TCH uptake by ATTP, and at pH ~10.0, ATTP removes only 17.3% of TCH. In contrast, the high percentage removal of tetracycline (*Ca* 92.6% & *Ca* 85.5%) by ATTP@PEG and ATTP@PEG/Ag⁰ solids showed almost constant removal efficiency up until the pH 8.0 and further increase in pH had caused a slight decrease in percentage removal of tetracycline. On the other hand, the proportion of TCH removal by the ATTP@PVP and ATTP@PVP/Ag^0 solids shows very high removal efficiency (*Ca.* 82%) until pH 7.0, followed by a slight decrease in it. Moreover, these two solids, ATTP@PVP, and ATTP@PVP/Ag^0, show a comparable removal efficiency for the TCH removal; however, the ATTP@PVP/Ag^0 shows a slightly lower removal efficiency than the ATTP@PVP throughout the studied pH.

The pH_{PZC} values of ATTP, ATTP@PEG, ATTP@PVP, ATTP@PEG/Ag^0 and ATTP@PVP/Ag^0 are 8.0, 7.8, 7.7, 7.5 and 7.63, respectively. These solids possess almost similar pH_{PZC} values; however, the ATTP@PEG, ATTP@PVP, ATTP@PEG/Ag^0 and ATTP@PVP/Ag^0 show significantly enhanced removal efficiency of TCH compared to ATTP. The material carries a net negative charge at pH > pH_{PZC} and a positive charge at pH< pH_{PZC}. Similarly, the speciation of TCH showed the pk_a values of TC (pk_a^1: 3.3, pk_a^2: 7.7, and pk_a^3: 9.7) (Zhang et al., 2014) and the speciation results are given in Figure 3.10. The cationic species of TCH exists (TCH_3^+ or $TCH_3^{+\,0\,0}$), at lower pH~3.3. Further, with an increase in pH (pH~ 3.3 to 7.7), TC predominates with zwitterion (TCH^0 or $TCH^{0\,+\,-}$) by the deprotonation from the phenolic diketone sites of TCH. Further, the anionic species (TCH^- or $TCH^{+\,-\,-}$) of TCH exists at pH>7.6, which dissociated to dianionic species (TCH^{2-} or $TCH^{0\,-\,-}$) of TCH at pH> 9.7. The pH range (~3-8) favors the removal of TCH which is due to two reasons: (i) in this pH region, the positively charged surface of solid attracts the negatively charged species (partly or fully) of TCH molecules, and (ii) the hydrophobic nature of surface attracts the TCH molecules with relatively stronger Van der Waals forces at the surface. These results in an enhanced uptake of TCH by the ATTP@PEG, ATTP@PVP, ATTP@PEG/Ag^0 and ATTP@PVP/Ag^0 solids. However, a slight decrease in the uptake of TCH by these solids at pH>8.0 is primarily due to the mechanism proposed in (i), causing the slight electrostatic repulsion between both the negatively charged species of TCH and solids. However, a significant uptake of TCH even at pH>8.0 is due to the organophilic attraction of TCH molecules by the solid surfaces (Thanhmingliana et al., 2015). Similar outcomes were reported on the adsorption of tetracycline onto Fe-Mt (Wu et al., 2016).

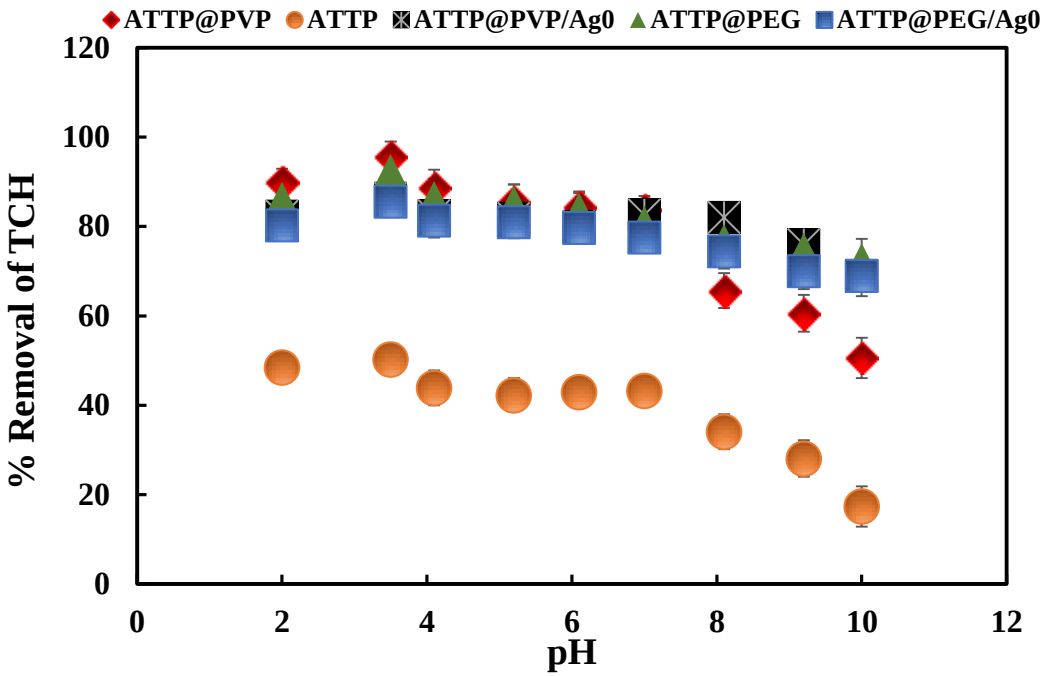

Figure 3.9: Percentage removal of tetracycline by pristine attapulgite and ATTP@PEG, ATTP@PVP, ATTP@PEG/Ag⁰ and ATTP@PVP/Ag⁰ as a function of pH ([TCH]: 10.0 mg/L; Solid dose: 2.0 g/L; Temperature: 25⁰C).

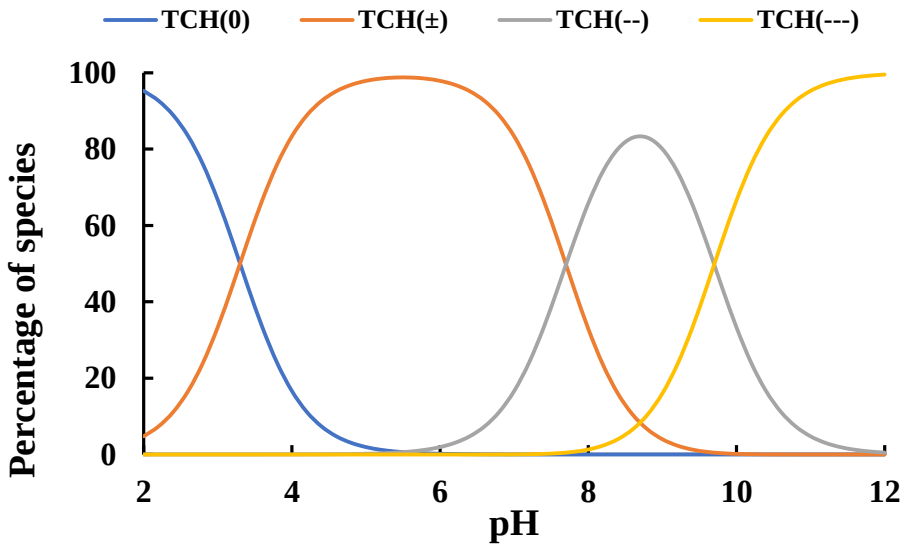

Figure 3.10: Percentage distribution of tetracycline (TCH) as a function of pH ([TCH]: 10.0 mg/L; Temperature: 25°C).

3.3.1.2. Triclosan (TCS)

The pH dependent removal of triclosan was conducted at wide range of pH 2.0 to 10.0. The percentage removal of triclosan using ATTP@PEG, ATTP@PVP, ATTP@PEG/Ag^0 and ATTP@PVP/Ag^0 along with the pristine attapulgite is illustrated in Figure 3.11. The pristine clay attapulgite showed relatively high uptake at lower pH~3.0, however, further increase in pH caused significant decrease in percentage uptake of triclosan and reached very low removal at neutral pH~7.0. Therefore, the pristine attapulgite showed very limited implications in the elimination of triclosan from aqueous solution. However, the removal of triclosan is almost unaffected using ATTP@PEG, ATTP@PVP, ATTP@PEG/Ag^0 and ATTP@PVP/Ag^0 solids as the pH increased from *Ca*. pH 2.0 to 7.01. However, the removal of triclosan was decreased abruptly with further increase in pH (pH>7.0) and attained to low removal percentage at *Ca.* pH 10. The elimination of triclosan is almost constant within the pH<7.0. Triclosan is having the acid dissociation constant values as pk_{a1}: 7.90 and pk_{a2}: 8.1 (San-rom et al., 2020). Therefore, the speciation of triclosan is conducted and presented in Figure 3.12 also reported previously (Tiwari et al., 2020). It is evident from the speciation studies that triclosan is predominantly present as uncharged species at pH<7.0. However, pH>7.0, the dominant species are anionic species (i.e., TCS^-or TCS^{2-}). Therefore, very high uptake of triclosan at pH<7.0 is primarily due to the hydrophobic nature of the nanocomposites towards the triclosan. The strong hydrophobic interactions between the triclosan molecules and organo-modified clay had enabled for enhanced elimination of triclosan. Similar, removal behaviour was reported previously in the removal of triclosan by kaolinite and montmorillonite (Behera et al., 2010). However, the increase in pH>7.0, a rapid decrease in percentage elimination of triclosan by the ATTP@PEG, ATTP@PVP, ATTP@PEG/Ag^0 and ATTP@PVP/Ag^0 is observed. This is due to the fact that the anionic species of triclosan and negatively charged solid surface caused strong repulsive forces which retarded significantly the sorption of triclosan.

Generally, a high removal percentage of triclosan at neutral pH conditions are providing an optimum pH condition indicating ATTP@PEG, ATTP@PVP, ATTP@PEG/Ag⁰ and ATTP@PVP/Ag⁰ in the treatment strategies for efficient removal of triclosan from water bodies at neutral pH conditions.

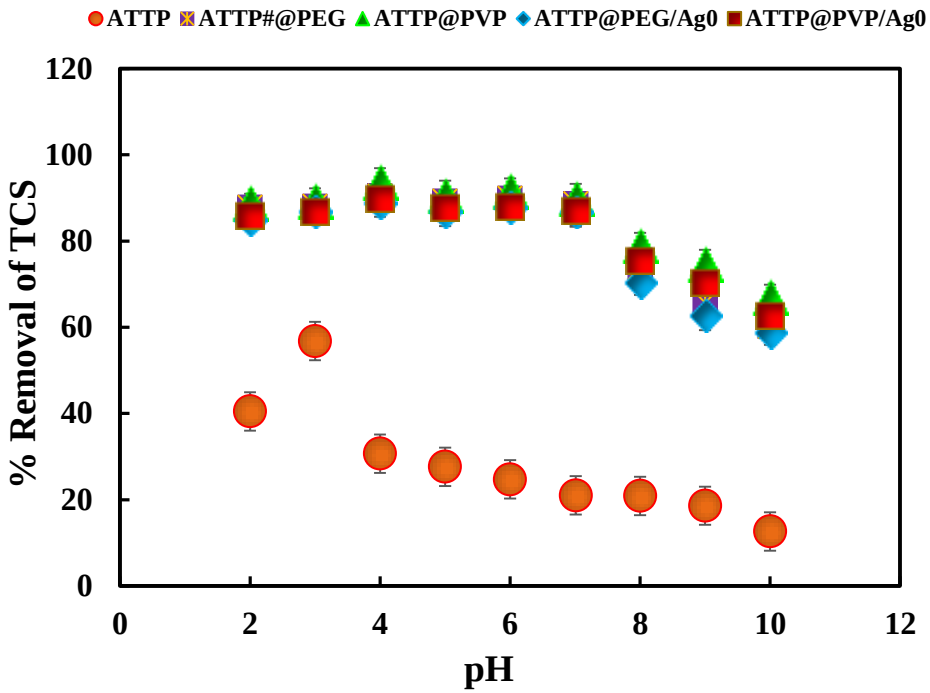

Figure 3.11: Percentage removal of triclosan (TCS) by pristine attapulgite and functionalized materials (ATTP@PEG, ATTP@PVP, ATTP@PEG/Ag⁰ and ATTP@PVP/Ag⁰) as a function of pH ([TCS]:10.0 mg/L; Solid dose: 2.0 g/L: Temperature: 25⁰C).

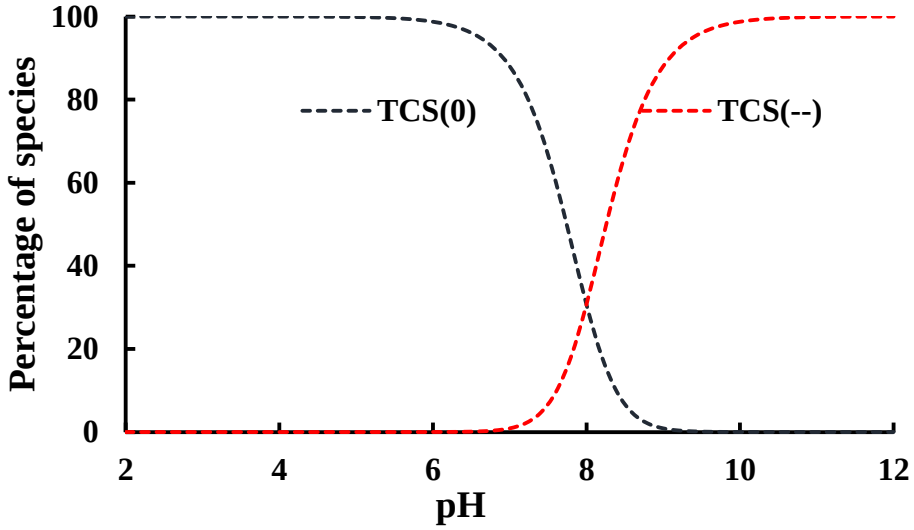

Figure 3.12: Percentage distribution of triclosan (TCS) as a function of pH ([TCS]: 10.0 mg/L; Temperature: 25°C).

3.3.1.3. 17α-ethinylestradiol (EE2)

The pH dependence sorption of 17α-ethinylestradiol (EE2) is illustrated in Figure 3.13. Figure reveals that the elimination of EE2 by the ATTP is quite low within the studied pH (pH 2.0 to 10.0). A maximum of *Ca* 42.9% of EE2 was recorded at pH 6.08. However, using the polymer and Ag^0 grafted attapulgite solids i.e., ATTP@PEG, ATTP@PVP, ATTP@PEG/Ag^0 and ATTP@PVP/Ag^0 showed significantly enhanced elimination of EE2 within the studied pH (2.0 to 10.0). It is further noted that a maximum of *Ca* 86.4, 88.9, 84.2 and 85.3% of EE2 was eliminated using the ATTP@PEG, ATTP@PVP, ATTP@PEG/Ag^0 and ATTP@PVP/Ag^0 solids, respectively at around pH 6.08. According to research conducted on EE2, the acid dissociation constant (pk_a) is 10.5 (H. He et al., 2022) (Figure 3.14). As a result, the EE2 at pH>>10.5 carries a net negative charge and exists as a neutral species at pH<10.5. On the other hand, the pH_{PZC} (point of zero charge) of ATTP@PEG, ATTP@PVP, ATTP@PEG/Ag^0 and ATTP@PVP/Ag^0 is obtained as 7.8, 7.7, 7.5 and 7.63,

respectively. Therefore, the hydrophobic interaction is the driving force responsible for a high percentage removal of EE2 using these solids in a wide pH range. The hydrophilic polymers introduced within the attapulgite sheets provide enhanced hydrophobicity with the organophilic nature which intended to attract the EE2 molecules and enabled a high uptake of EE2. Moreover, the dense grafted structure ATTP@PEG, ATTP@PVP, ATTP@PEG/Ag⁰ and ATTP@PVP/Ag⁰ has enabled significantly to trap the EE2 from aqueous solutions and enhanced the elimination of EE2. A similar result shows removing EE2 using dense silane-functionalized bentonite material (Malsawmdawngzela & Tiwari, 2022).

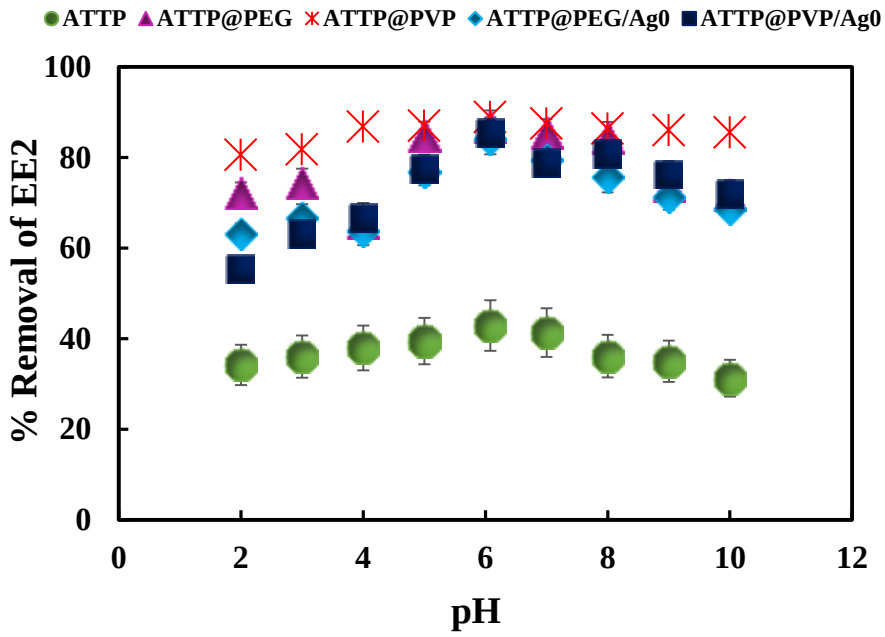

Figure 3.13: Percentage removal of EE2 by pristine attapulgite and functionalized attapulgite solids (ATTP@PEG, ATTP@PVP, ATTP@PEG/Ag⁰ and ATTP@PVP/Ag⁰) as a function of pH ([EE2]: 10.0 mg/L; Solid dose: 2.0 g/L: Temperature: 25ºC).

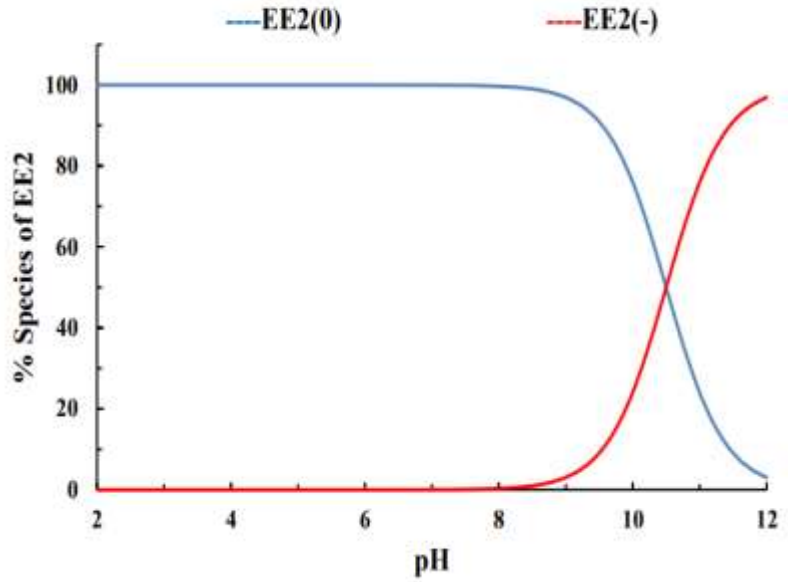

Figure 3.14: Percentage distribution of 17α-ethinylestradiol (EE2) as a function of pH ([EE2]: 10.0 mg/L; Temperature: 25°C).

3.3.1.4. Ciprofloxacin (CIP)

Figure 3.15 shows the percentage removal of CIP as a function of solution pH. Further, the speciation of CIP at various pH levels is crucial for understanding the percentage removal of CIP at varied pH. The pH-dependent study reveals that relatively higher uptake of CIP occurred at pH 7.0 with 95.8% and 94.4% by the ATTP@PEG and ATTP@PVP, respectively. The pH_{PZC} of attapulgite, ATTP@PEG, ATTP@PVP, ATTP@PEG/Ag^0 and ATTP@PVP/Ag^0 are 8.0, 7.8, 7.7, 7.5 and 7.63 respectively. Accordingly, the material carries negative charges at $pH>pH_{PZC}$. However, $pH<pH_{PZC}$ carries net positive charge. The speciation studies of CIP is shown in Figure 3.16 and CIP has two pk_a values corresponding to 6.1 and 8.7 (Jiang et al., 2013). The

species of CIP are cationic (CIP^+) at pH 6.1, zwitterionic ($CIP^{\pm}$) at pH 6.1-8.7, and anionic (CIP^-) at pH 8.7 (Cheikh et al., 2023). As a result of their oppositely charged surfaces, the pH range of 6.1- 8.9 favours the attraction between the adsorbent particles and adsorbate molecules. Because the carboxyl group has lost protons, the CIP molecule is in an anionic state at a pH above 8.9. In addition, the solid possesses a hydrophobic nature with organophilic interactions with the sorbing species and eventually enhances the sorption of CIP by these nanocomposite solids. Similar removal behaviour was reported for the adsorption of ciprofloxacin onto PAC@Fe_3O_4-MN (Al-Musawi et al., 2021).

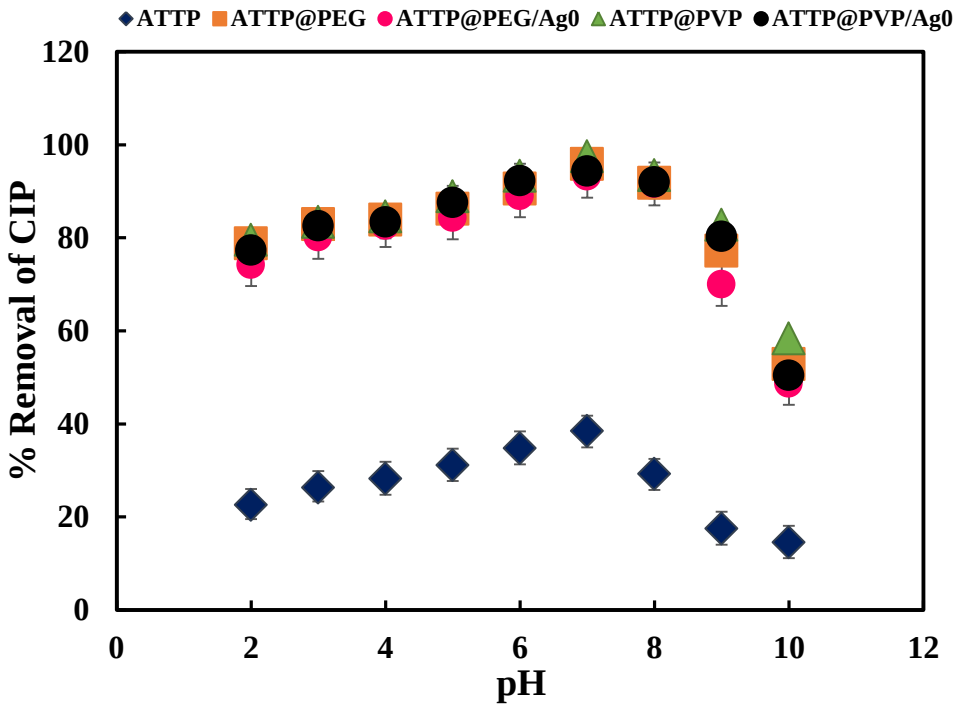

Figure 3.15: Percentage removal of CIP by pristine attapulgite and functionalized attapulgite solids (ATTP@PEG, ATTP@PVP, ATTP@PEG/Ag^0 and ATTP@PVP/Ag^0) as a function of pH ([CIP]: 10.0 mg/L; Solid dose: 2.0 g/L: Temperature: 25ºC).

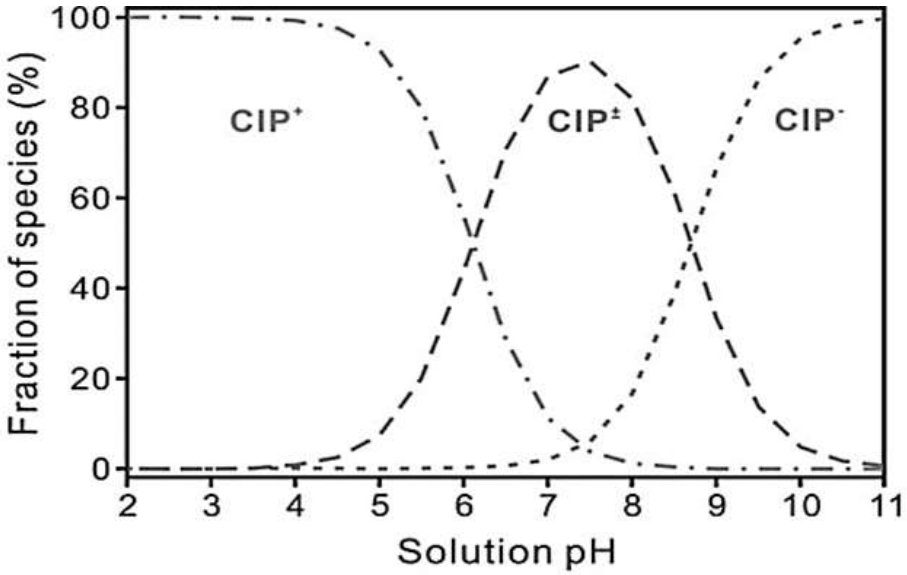

Figure 3.16: Percentage distribution of ciprofloxacin (CIP) as a function of pH ([CIP]: 10.0 mg/L; Temperature: 25°C) (Jiang et al., 2013).

3.3.1.5. Bisphenol A (BPA)

Similarly, the elimination of BPA was studied using ATTP, ATTP@PVP, ATTP@PEG, ATTP@PEG/$Ag^{0,}$ and ATTP@PVP/Ag^{0}, solid materials with a pH from 2.0 to 10.0. As seen in Figure 3.17. the BPA removal (%) stays fairly constant, around 88%, between pH 6.0–8.0, hence there is low pH dependency in this range. However, adsorption efficiency showed a significant decrease at pH values higher than 9.0.

The speciation of BPA, as shown in Figure 3.18., indicates that the BPA predominates to its neutral species at pH 3~9 and turns to its negative species at pH >9.0 since the pk_a^1 and pk_a^2 values of BPA are 9.59 and 10.2, respectively (Park et al., 2014). Relatively high uptake of the BPA, even at low pH (2.0), is explicable due to the hydrophobic interactions between the BPA molecule and solids, enabling stronger Van der Waals forces. An increase in pH from 2.0 to 6.0) favors further the uptake of BPA due to the mixed effect of electrostatic attraction of BPA by the solid surface since a slight increase in electronegativity of BPA, which brings the BPA molecules closer to the surface

and enables stronger hydrophobic interactions. These interactions prevail within the pH region 6.0-8.0 and keep a very high uptake of BPA by these solids. However, a further increase in pH>8.0 gradually decreases the uptake of BPA, primarily because the negatively charged surface of solids repels the negatively charged BPA molecules, leading to a decrease in BPA uptake. Nevertheless, it is interesting to observe that even at a high pH of 10.0, these nanocomposites can remove a higher percentage of BPA due to the predominant hydrophobic interactions between the solid and sorbate molecules. These results indicate that the hydrophobic interactions are the predominant driving force enabling high uptake of BPA by these nanocomposites. These results follow the previous results demonstrated elsewhere (Silva, et al., 2022). Spectrogel® type-C removes relatively less BPA at lower pH and attains a maximum uptake around pH 9.0, and it declines at pH > 9.0. Similarly, the mixed effect of hydrophobic and electrostatic attractions governs the mechanism of BPA removal by the organoclay (Malsawmdawngzela & Tiwari, 2022).

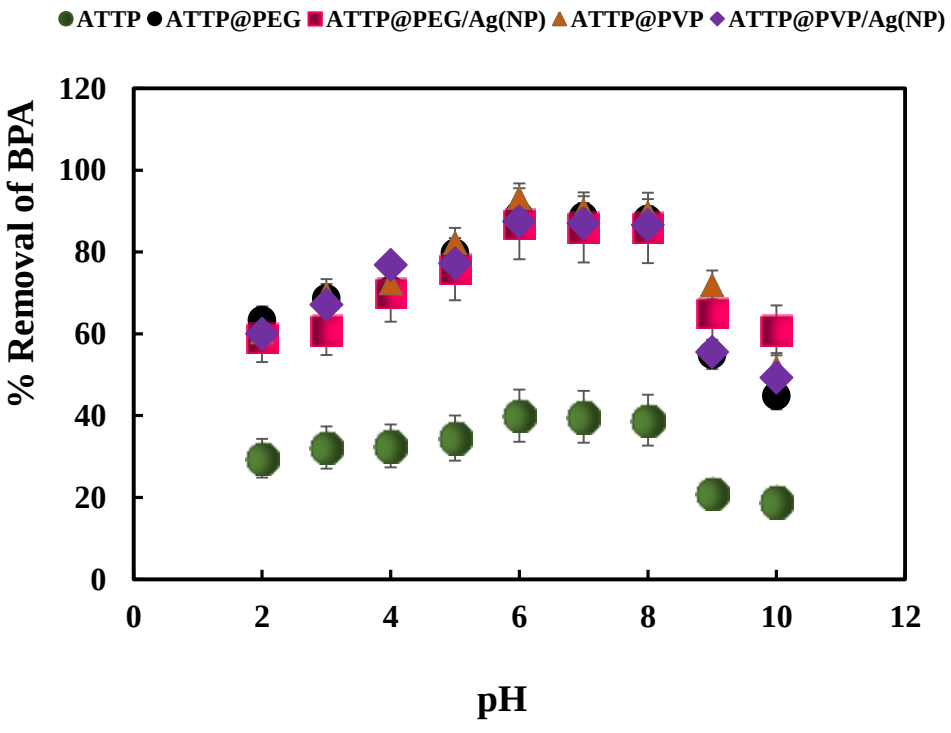

Figure 3.17: Percentage removal of BPA by pristine attapulgite and functionalized attapulgite solids (ATTP@PEG, ATTP@PVP, ATTP@PEG/Ag⁰ and ATTP@PVP/Ag⁰) as a function of pH ([CIP]: 10.0 mg/L; Solid dose: 2.0 g/L: Temperature: 25⁰C).

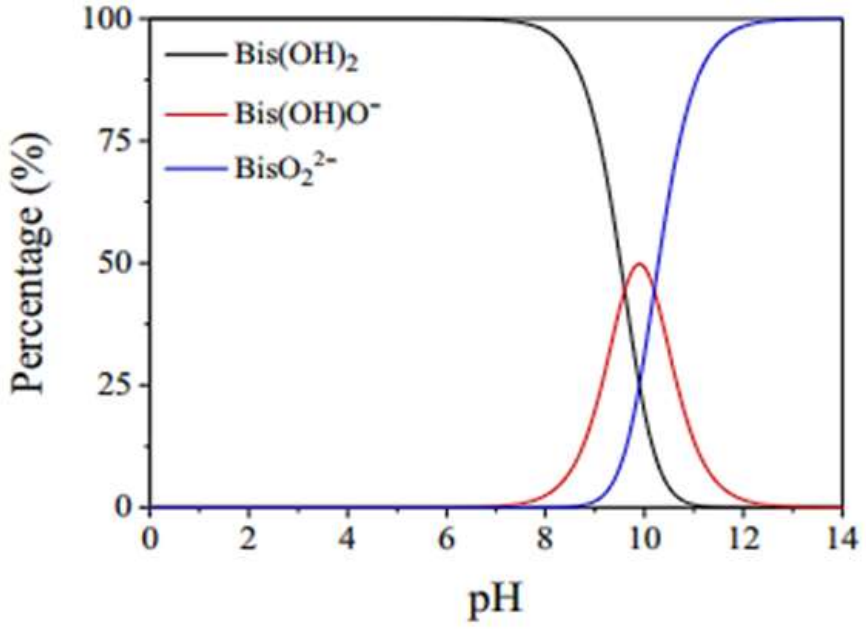

Figure 3.18: Percentage distribution of bisphenol A (BPA) as a function of pH ([BPA]: 10.0 mg/L; Temperature: 25°C).

3.3.2. Effect of sorptive concentration

3.3.2.1. Tetracycline (TCH)

The percentage removal of tetracycline using ATTP@PEG and ATTP@PVP at various initial concentrations are shown in Figure 3.19. It is noteworthy that very high percentage removal of tetracycline was obtained within the studied concentration range (1.0 to 25.0 mg/L) using the ATTP@PEG and ATTP@PVP solids. The percentage removal of tetracycline at the initial concentration of 1.0 mg/L is 93.2% and 95.8% for ATTP@PEG and ATTP@PVP materials. In this sorption process, it is assumed that the initial concentration of the adsorbate act as a driving force to pass through the

sorption barrier at the solid-solution interface; hence, the amount of tetracycline uptake was extensively enhanced from 1.3 to 10.98 mg/g and 1.36 to 13.58 mg/g and for ATTP@PEG and ATTP@PVP, respectively, while increasing the initial concentration of tetracycline from 1.0 to 25.0 mg/L. The higher uptake of tetracycline at fairly high initial concentrations reaffirmed the strong affinity of ATTP@PEG and ATTP@PVP solids towards the tetracycline.

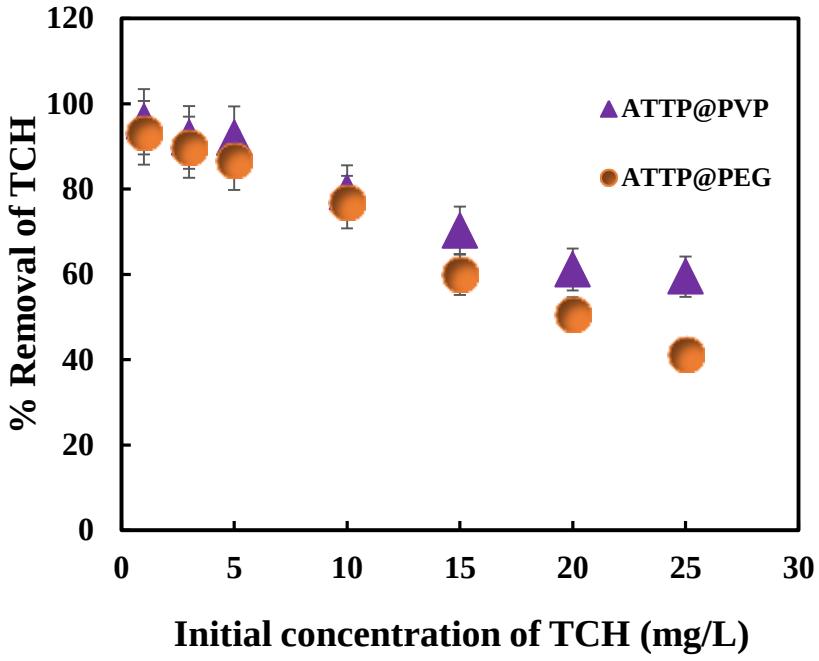

Figure 3.19: Percentage removal of tetracycline by the ATTP@PEG and ATTP@PVP materials as a function of initial tetracycline concentrations (pH: 3.5; Solid dose: 2.0 g/L: Temperature: 25°C).

3.3.2.2. Triclosan (TCS)

The sorption performance of ATTP@PEG and ATTP@PVP materials towards the triclosan is obtained by varying the triclosan concentrations from 1.0 to 25.0 mg/L (pH: 4.0) at solid dose of 2.0 g/L. Results are plotted with initial sorptive concentration against the percentage removal of triclosan and illustrated in Figure 3.20. Results inferred that the percentage elimination of triclosan is almost unaffected within the studied sorptive concentrations. This

implied high affinity of ATTP@PEG and ATTP@PVP towards triclosan. Quantitatively, increasing the concentration of triclosan from 1.0 to 25.0 mg/L the removal efficiency is only decreased from 92.0 to 84.3% using ATTP@PEG and from 96.0 to 82.1% using ATTP@PVP solids.

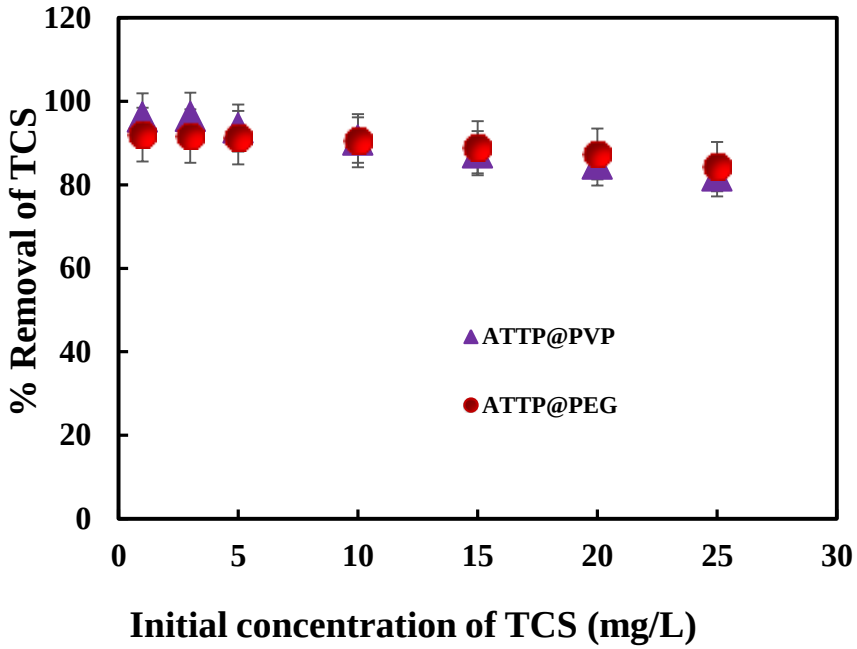

Figure 3.20: Percentage removal of triclosan by the ATTP@PEG and ATTP@PVP solids as a function of initial triclosan concentrations (pH: 4.0; Solid dose: 2.0 g/L: Temperature: 25°C).

3.3.2.3. 17α-ethinylestradiol (EE2)

The relationship between the initial EE2 concentration (1.0 to 25.0 mg/L) and percentage removal of EE2 by the ATTP@PEG and ATTP@PVP materials is obtained at pH 6.08 and solid dose 2.0 g/L. The results are illustrated in Figure 3.21. Results indicated that increasing the concentration of EE2, the percentage elimination of EE2 is decreased slightly. Increasing concentration of EE2 from 1.0 to 25.0 mg/L the corresponding decrease in percentage elimination of EE2 is from 90.0 to 78.3% for ATTP@PEG and 92.8

to 81.6% for ATTP@PVP solids. Similar to other micro-pollutants, the high percentage uptake of EE2 even at high concentration of EE2 inferred the high affinity of ATTP@PEG and ATTP@PVP materials for EE2 and potential sorbing materials for decontamination of water contaminated with various micro-pollutants.

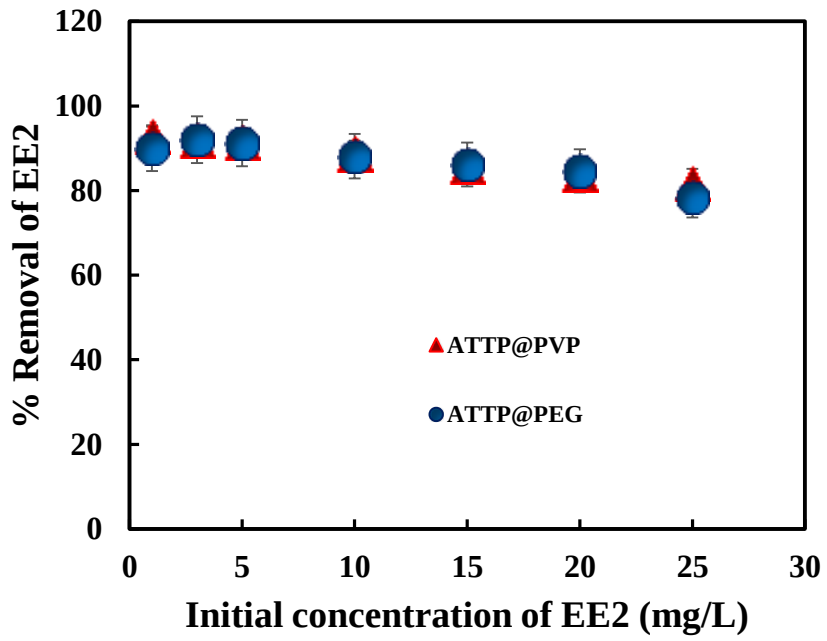

Figure 3.21: Percentage removal of EE2 by the ATTP@PEG and ATTP@PVP solids as a function of initial EE2 concentrations (pH: 6.08; Solid dose: 2.0 g/L: Temperature: 25ºC).

3.3.2.4. Ciprofloxacin (CIP)

The concentration dependence sorption of ciprofloxacin using ATTP@PEG and ATTP@PVP, respectively was performed by varying the concentrations of CIP from 1.0 to 25.0 mg/L; pH 7.0 for ATTP@PEG and ATTP@PVP and the results are shown in Figure 3.22. Increasing the concentration of CIP from 1.0 to 25.0 mg/L, the percentage removal was

decreased from 98.3 to 90.3% using ATTP@PEG and 97.9 to 88.8% using ATTP@PVP. The high removal percentage of CIP even at high concentrations by the functionalized solids ATTP@PEG and ATTP@PVP inferred the high affinity of these pollutants towards the solids.

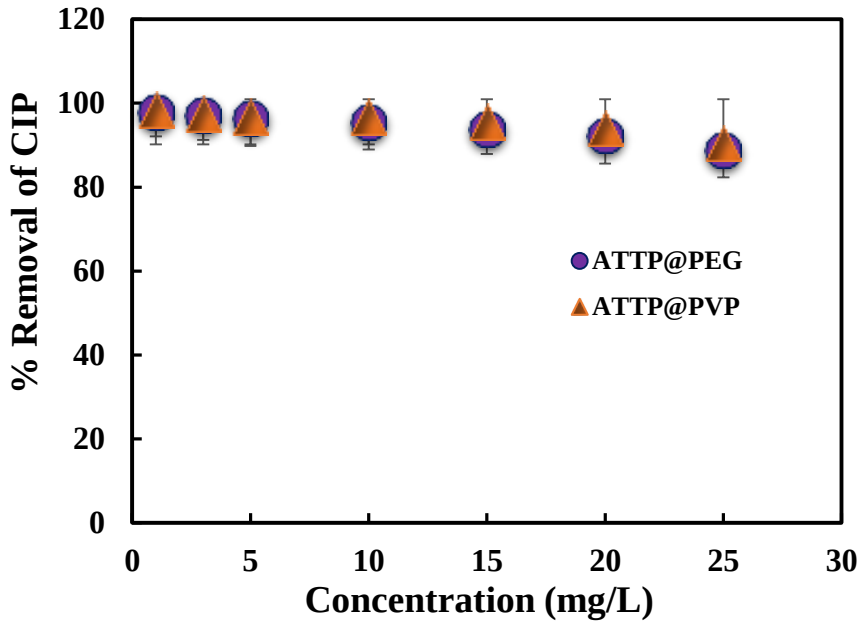

Figure 3.22: Percentage removal of CIP by the ATTP@PEG and ATTP@PVP solids as a function of initial EE2 concentrations (pH: 7.0; Solid dose: 2.0 g/L: Temperature: 25ºC).

3.3.2.5. Bisphenol A (BPA)

Similarly, the concentration dependence removal of BPA was conducted at pH 6.06 to estimate the efficiency and adsorption capacity of the modified materials towards BPA. The concentration dependence percentage removal by the ATTP@PEG and ATTP@PVP is illustrated in Figure 3.23. It is observed that ATTP@PVP attained high percentage removal of BPA at varied concentrations of BPA. Increasing the initial BPA concentrations from 1.0 to 25.0 mg/L did not affect the percentage removal. At the initial concentration of 25.0 mg/L, the ATTP@PEG removed 66.3% and ATTP@PVP removed 60.7% of BPA respectively. These findings indicated that ATTP@PEG and

ATTP@PVP materials are highly efficient for the removal of BPA from aqueous solutions.

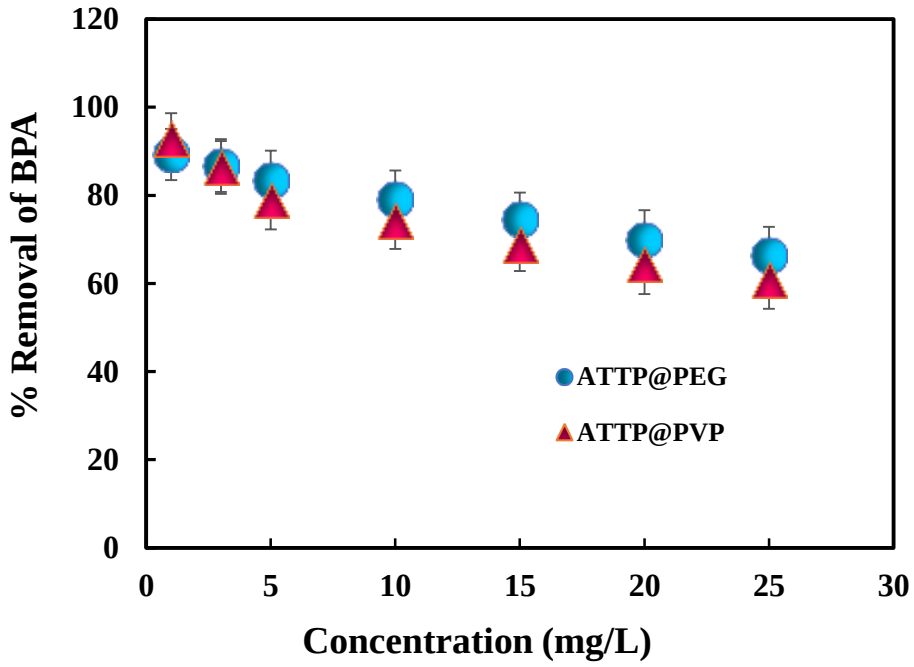

Figure 3.23: Percentage removal of BPA by the ATTP@PEG and ATTP@PVP solids as a function of initial BPA concentrations (pH: 6.06; Solid dose: 2.0 g/L: Temperature: 25ºC).

3.3.3. Adsorption isotherm studies

The equilibrium state sorption data acquired for varying sorptive concentrations at constant pH and temperature is further used to determine the adsorption isotherms especially the Langmuir and Freundlich adsorption isotherms.

3.3.3.1. Adsorption isotherm modelling for tetracycline, triclosan, EE2, ciprofloxacin and bisphenol A

Result obtained from the concentration dependent study of tetracycline by the ATTP@PEG and ATTP@PVP is utilized to study the adsorption

isotherm models viz., Langmuir and Freundlich adsorption isotherms (Malsawmdawngzela et al., 2022) and fitting results are presented graphically in Figure 3.24. The isotherm constants i.e., Langmuir monolayer sorption capacity (q_o), Langmuir constant (b) and Freundlich constants (K_f and 1/n) are hence, estimated and returned in Table 3.5. Since higher value of R^2 is obtained for Langmuir adsorption isotherm for tetracycline using ATTP@PEG and ATTP@PVP, which inferred the applicability of Langmuir adsorption isotherm in the adsorption of tetracycline by these solids. The applicability of the Langmuir isotherm specifies that monolayer coverage of the solid surfaces by tetracycline molecules and the active sites are homogeneously distributed on the surface (Zhang et al., 2018). The Langmuir monolayer capacity (q_o) is relatively high, indicating the high chemical affinity of tetracycline towards the ATTP@PEG and ATTP@PVP solids. The Langmuir monolayer capacity is found to be 10.98 and13.58 mg/g respectively for ATTP@PEG and ATTP@PVP. Previously, it was reported that the sorption of tetracycline onto different montmorillonite SAz-1 (Ca-MMT containing 98% smectite), SWy-2 (Na-MMT containing 95% smectite), SHCa-1 (low-charge Li-bearing trioctahedral smectite) and SYn-1 (synthetic mica-MMT containing 95% mica-MMT) followed the Langmuir adsorption isotherm having removal capacity of 468, 404, 38 and 243 mg/g, respectively (Chang et al., 2014). Moreover, higher values of (1/n) and (b), Freundlich and Langmuir constants respectively indicated that the material has strong affinity towards tetracycline.

Table 3.5. Langmuir and Freundlich constants estimated for sorption of tetracycline using ATTP@PEG and ATTP@PVP solids.

	Langmuir constant			**Freundlich constant**		
Materials	**q_o (mg/g)**	**b (L/mg)**	**R^2**	**1/n**	**K_f (mg/g)**	**R^2**
ATTP@PVP	13.58	0.505	0.992	0.445	4.02	0.979
ATTP@PEG	10.98	0.899	0.999	0.425	4.01	0.917

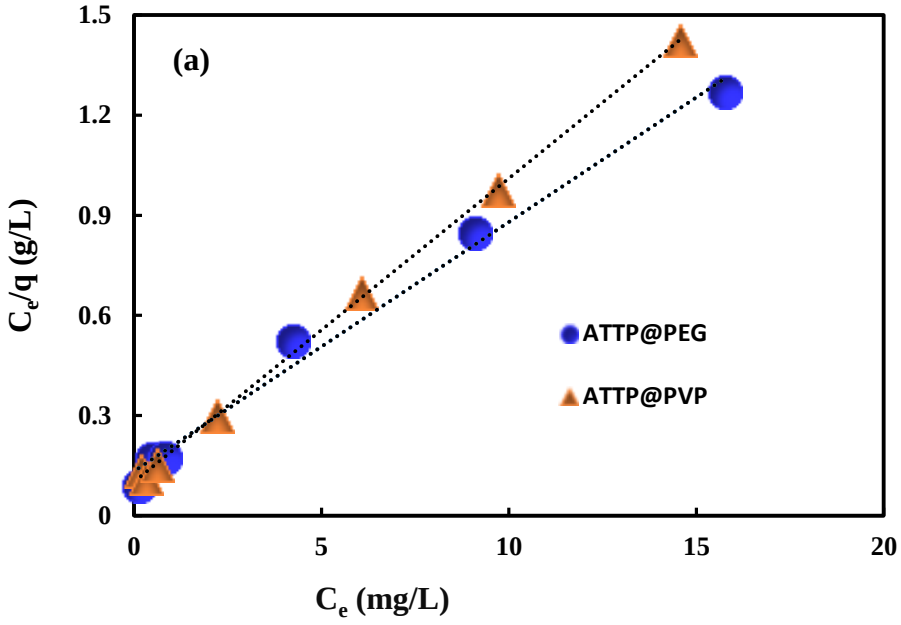
(a)
1.5
1.2
0.9
0.6
0.3
0
0
5
10
15
20
C_e/q (g/L)
C_e (mg/L)
ATTP@PEG
ATTP@PVP

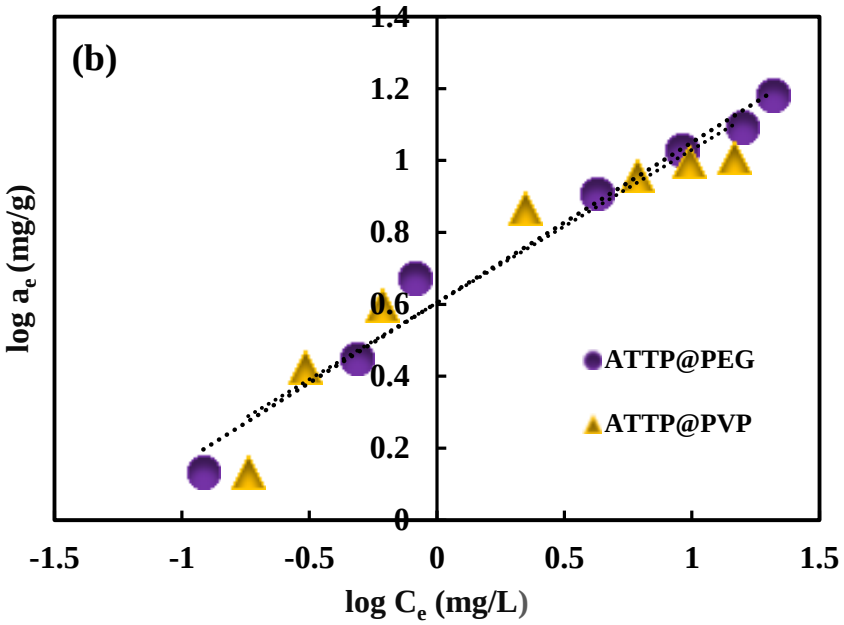
(b)
1.4
1.2
1
0.8
0.6
0.4
0.2
0
-1.5
-1
-0.5
0
0.5
1
1.5
log a_e (mg/g)
log C_e (mg/L)
ATTP@PEG
ATTP@PVP

Figure 3.24: Fitting of concentration dependence data to (a) Langmuir adsorption; and (b) Freundlich adsorption isotherms in the sorption of tetracycline by ATTP@PEG and ATTP@PVP solids.

Furthermore, the equilibrium sorption data obtained for triclosan is utilized for plotting the sorption modelling studies i.e., the Langmuir and Freundlich adsorption isotherms (Lee et al., 2012). The graphs were plotted for these two isotherms and shown in Figure 3.25. The unknown constants i.e., Langmuir monolayer adsorption capacity (q_o), Langmuir constant (b) along with the Freundlich constants (K_f and 1/n) are estimated and given in Table 3.6. The isotherm studies showed that the removal of triclosan using ATTP@PEG and ATTP@PVP solids followed Langmuir adsorption isotherm better than Freundlich adsorption isotherm. Langmuir isotherm suggests that the adsorption sites of ATTP@PEG and ATTP@PVP solids have strong interactions with triclosan and the triclosan molecules are forming the monolayer onto the solid surfaces (Phuekphong et al., 2020). The high value of Langmuir monolayer capacity (q_o) indicates the high affinity of triclosan towards ATTP@PEG and ATTP@PVP solids. The Langmuir monolayer adsorption capacity (q_o) was found to be 39.06 and 25.90 mg/g for ATTP@PEG and ATTP@PVP, respectively. It is worth noted that a very high monolayer capacity was obtained for triclosan using the functionalized materials. Further, relatively high values obtained for Langmuir constant (b) and Freundlich constant (K_f) indicated the strong affinity of ATTP@PEG and ATTP@PVP towards triclosan in aqueous media.

Table 3.6. Langmuir and Freundlich isotherm constants estimated for the sorption of triclosan using ATTP@PEG and ATTP@PVP solids

	Langmuir constant	**Freundlich constant**

Materials	q_o (mg/g)	b (L/mg)	R^2	1/n	K_f (mg/g)	R^2
ATTP@PVP	25.90	0.81	0.99	0.600	9.64	0.982
ATTP@PEG	39.06	0.31	0.997	0.787	8.37	0.989

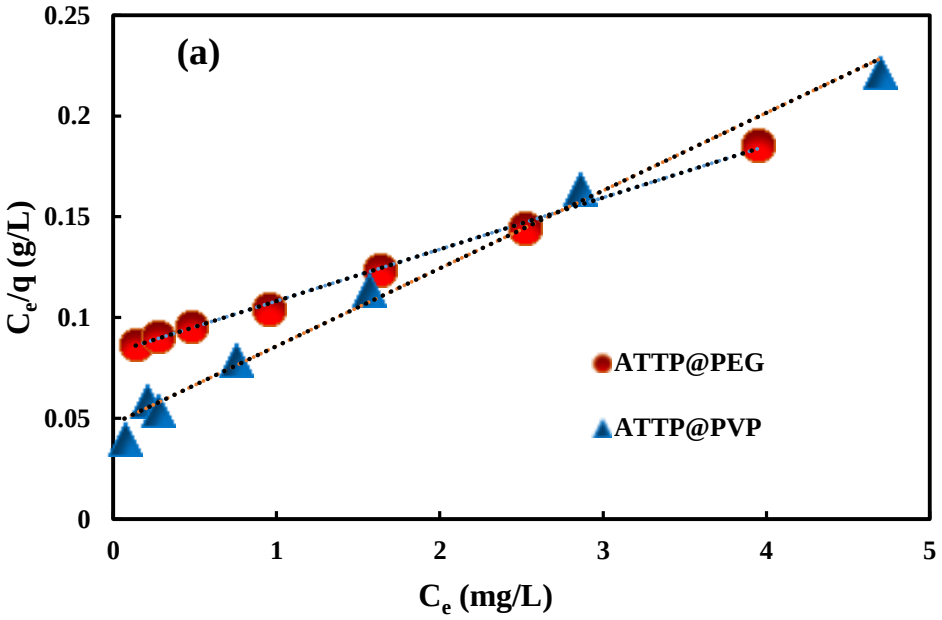

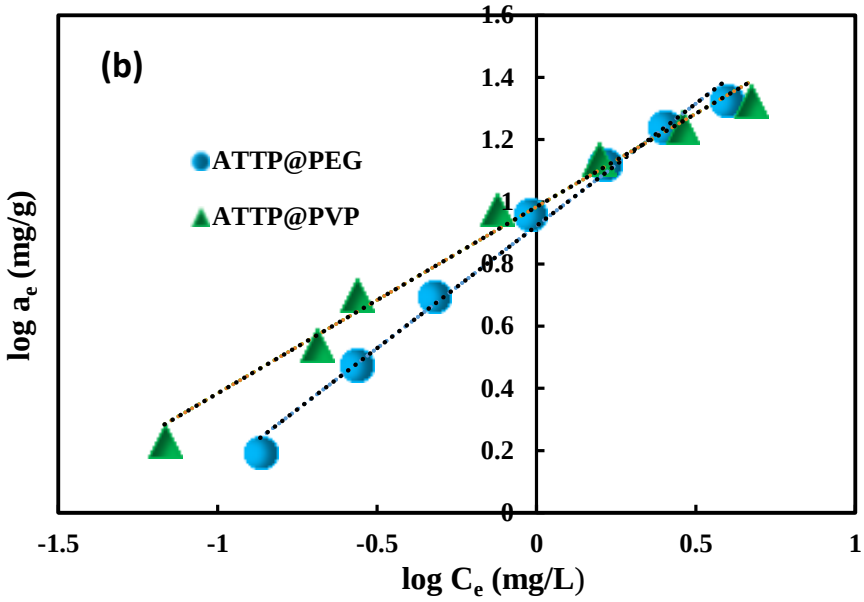

Figure 3.24: Fitting of concentration dependence data to the (a) Langmuir adsorption; and (b) Freundlich adsorption isotherms in the sorption of triclosan by the ATTP@PEG and ATTP@PVP solids.

Similarly, the linear form of Langmuir and Freundlich isotherms is utilized for isotherm modelling for the adsorption of EE2 by the ATTP@PEG and ATTP@PVP solids and the results are illustrated in Figure 3.26. The unknown constants are estimated and presented in Table 3.7. The results showed that the equilibrium sorption data obtained for the removal of EE2 is reasonably fitted well to the Langmuir adsorption model compared with Freundlich isotherm model. This result further indicates the surface homogeneity of the ATTP@PEG and ATTP@PVP in the removal of the EE2. The high value of Langmuir monolayer sorption capacity (q_o) indicates the strong affinity of triclosan towards ATTP@PEG and ATTP@PVP. The high value of Langmuir monolayer capacity 29.32 and 30.48 mg/g is obtained for the EE2 using ATTP@PEG and ATTP@PVP materials, respectively. The sorption of 17β-estradiol, 17α-ethinylestradiol and bisphenol A on tea leaves (TLH) and granular activated carbon (GAC) also followed Langmuir adsorption isotherm model. Moreover, the maximum adsorption capacities are 3.46, 2.44 and 18.35 mg/g using TLH and 4.01, 2.97 and 16.26 mg/g using GAC for the adsorption of 17α- estradiol, 17α- ethinylestradiol and bisphenol A

	Langmuir constant	**Freundlich constant**

,

r

e

s

pectively (Ifelebuegu et al., 2015).

Materials	q_o (mg/g)	b (L/mg)	R^2	1/n	K_f (mg/g)	R^2
ATTP@PVP	30.48	0.19	0.999	0.688	7.65	0.996
ATTP@PEG	29.32	0.40	0.982	0.680	4.62	0.973

Table

3.7. Langmuir and Freundlich adsorption isotherm constants estimated for the sorption of EE2 by the ATTP@PEG and ATTP@PVP solids

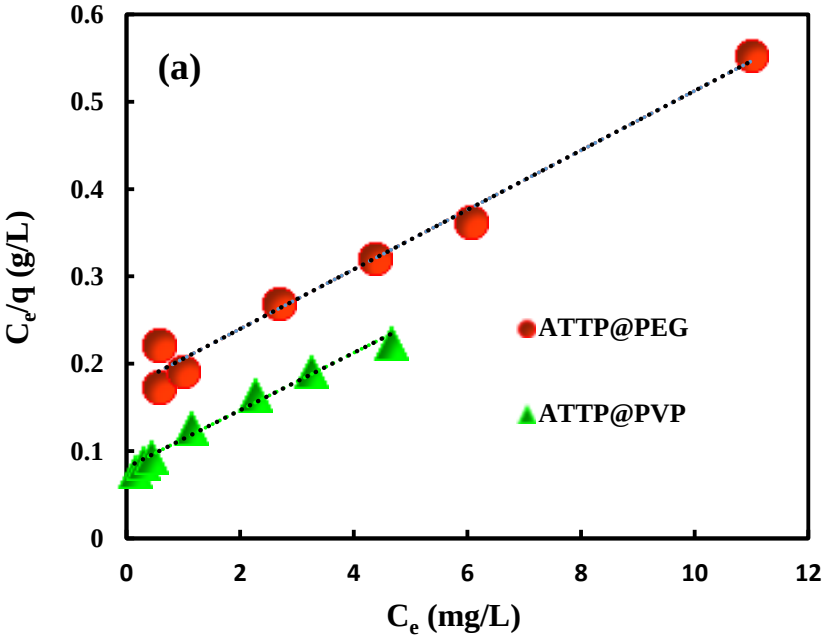

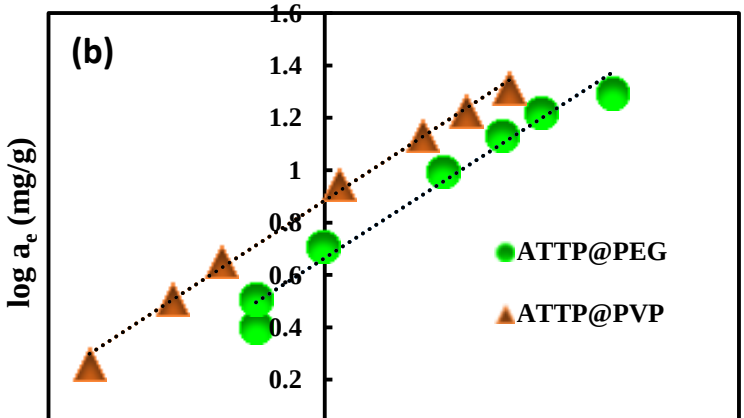

Figure 3.26: Fitting of concentration dependence data to the (a) Langmuir adsorption; and (b) Freundlich adsorption isotherms in the sorption of EE2 by the ATTP@PEG and ATTP@PVP materials.

The two adsorption isotherm models, Langmuir and Freundlich are derived from the results of the concentration-dependent study and are shown in Figure 3.27. The values for the isotherm constants, which include Freundlich constants (K_f and 1/n), Langmuir monolayer sorption capacity (q_o), and Langmuir constant (b), are calculated and are shown in Table 3.8. Since the Langmuir adsorption isotherm for CIP yielded a more excellent value of R^2, this implied that the isotherm follows the systems under study. Moreover, the maximum monolayer adsorption (q_o) of CIP were 28.17 and 28.98 mg/g showed high adsorption capability of the ATTP@PEG and ATTP@PVP material against this micro-pollutant. Similarly, the sorption of 17-ethinylestradiol using reduced graphene oxide-magnetic composite follows the Langmuir adsorption isotherm (Luo et al., 2017).

	Langmuir constant	**Freundlich constant**

Table 3.8. Langmuir and Freundlich adsorption isotherm constants estimated for the sorption of CIP by the ATTP@PEG and ATTP@PVP solids.

Materials	q_o (mg/g)	b (L/mg)	R^2	1/n	K_f (mg/g)	R^2
ATTP@PVP	28.98	0.79	0.99	0.70	9.19	0.98
ATTP@PEG	28.17	0.67	0.99	0.63	9.16	0.98

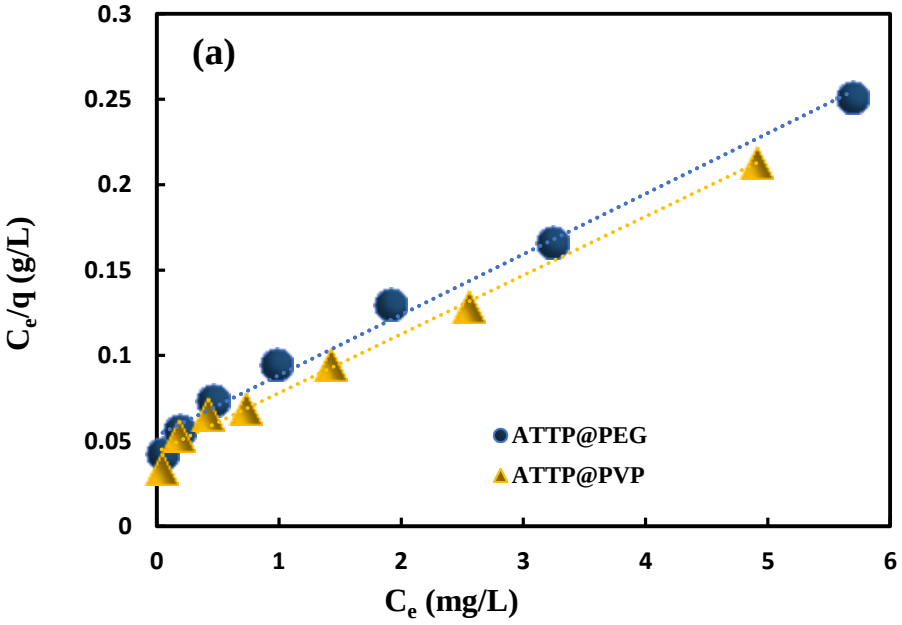

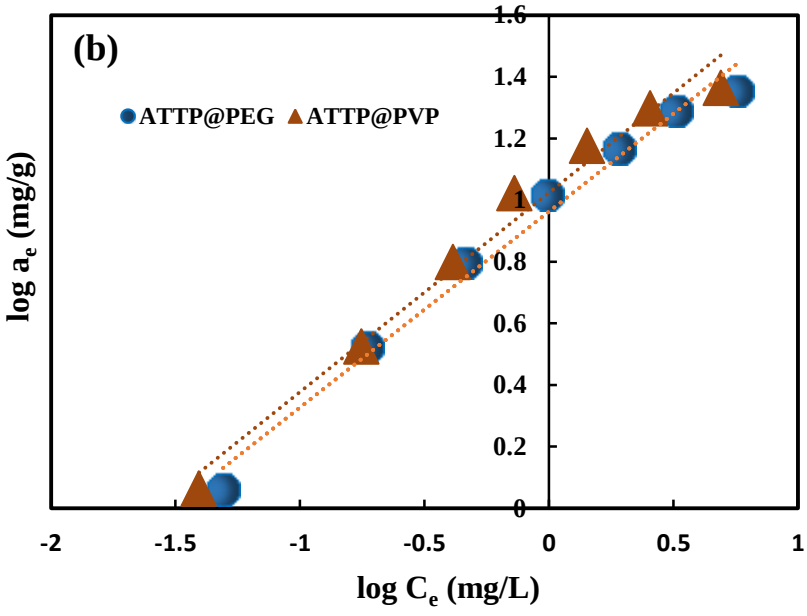

Figure 3.27: Fitting of concentration dependence data to the (a) Langmuir adsorption; and (b) Freundlich adsorption isotherms in the sorption of CIP by the ATTP@PEG and ATTP@PVP materials.

Result obtained from the concentration-dependent study of bisphenol A by the ATTP@PEG and ATTP@PVP is utilized to study the adsorption isotherm models viz., Langmuir and Freundlich adsorption isotherms and fitting results are presented graphically in Figure 3.28. The isotherm constants i.e., Langmuir monolayer sorption capacity (q_o), Langmuir constant (b) and Freundlich constants (K_f and 1/n) are hence, estimated and returned in Table 3.9. Since higher value of R^2 is obtained for Langmuir adsorption isotherm for bisphenol A using ATTP@PEG and ATTP@PVP, which inferred the applicability of Langmuir adsorption isotherm in the adsorption of BPA by these solids. The applicability of the Langmuir isotherm specifies that monolayer coverage of the solid surfaces by bisphenol A molecules and the active sites are homogeneously distributed on the surface. The Langmuir monolayer capacity (q_o) is relatively high, indicating the high chemical affinity of BPA towards the ATTP@PEG and ATTP@PVP solids. The Langmuir monolayer capacity is found to be 22.37 and 14.08 mg/g respectively for ATTP@PEG and ATTP@PVP.

	Langmuir constant	**Freundlich constant**

Table 3.9. Langmuir and Freundlich adsorption isotherm constants estimated for the sorption of BPA by the ATTP@PEG and ATTP@PVP solids.

Materials	q_o (mg/g)	b (L/mg)	R^2	1/n	K_f (mg/g)	R^2
AT						0.97
AT						0.98

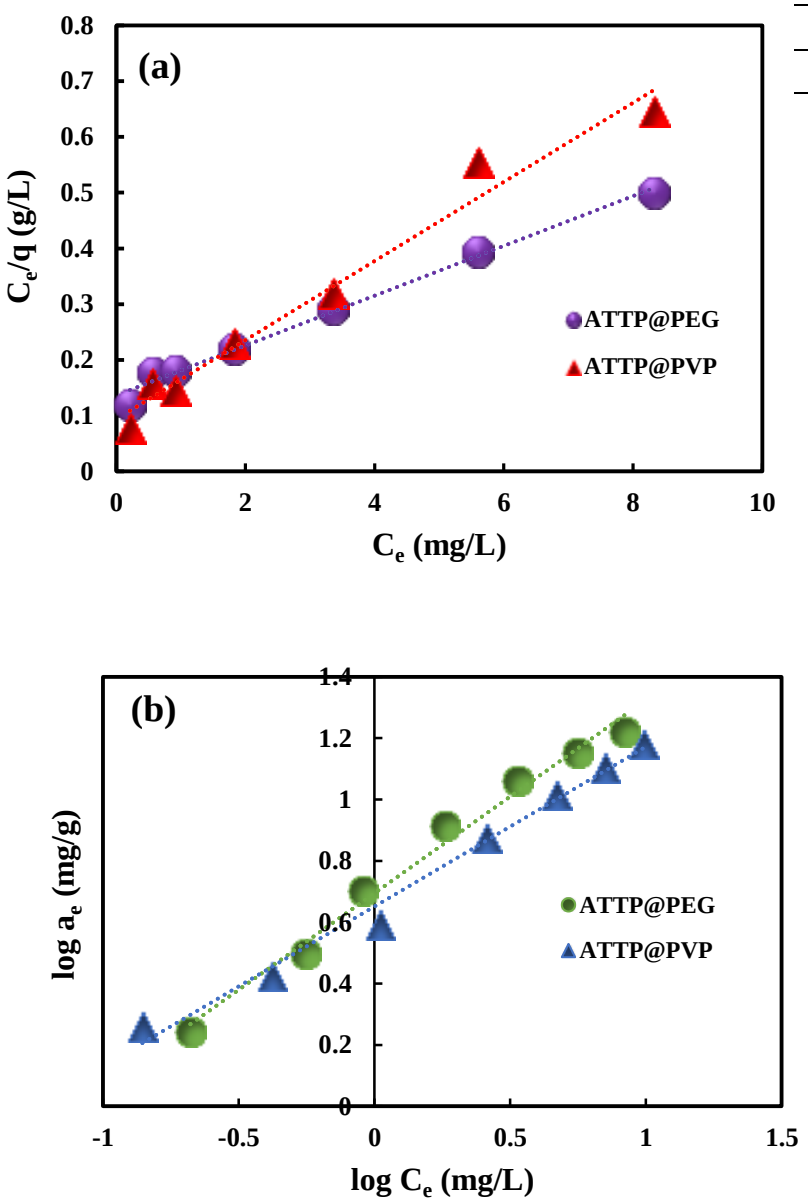

Figure 3.28: Fitting of concentration dependence data to the (a) Langmuir adsorption; and (b) Freundlich adsorption isotherms in the sorption of BPA by the ATTP@PEG and ATTP@PVP material.

3.3.4. Effect of contact time

3.3.4.1. Tetracycline (TCH)

The extent of tetracycline (TCH) adsorbed by the ATTP@PEG and ATTP@PVP are obtained at different time intervals 5 to 360 mins and the percentage removal of tetracycline by these solids are presented as a function of time in Figure 3.29. A fast uptake of tetracycline by these solids is observed during the initial period of contact and within 5 mins of contact, *Ca* 36.7 and 52.0% of tetracycline are adsorbed using ATTP@PEG and ATTP@PVP, respectively. This inferred that the rate of adsorption of tetracycline by these solids is significantly high. This is primarily due to the fact that extent of active sites are relatively more at the functionalized materials surface during the initial period of time which enabled fast aggregation of tetracycline molecules onto the solid surface (Lalhmunsiama et al., 2015). However, further increase in time, the rate of sorption slowed down and an apparent equilibrium is attained within 180 mins of contact for tetracycline using ATTP@PEG and ATTP@PVP. This result signifies the materials are useful and efficient at least for the elimination of tetracycline from aqueous wastes.

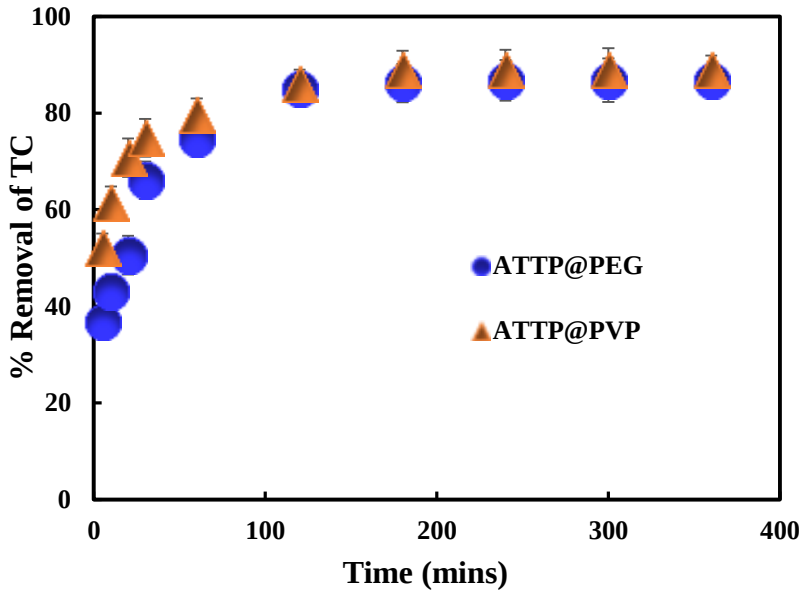

Figure 3.29: Effect of contact time in the removal of tetracycline by the ATTP@PEG and ATTP@PVP solids ([TCH]: 10.0 mg/L; pH: 3.5; Solid dose: 2.0 g/L; Temperature: 25°C).

3.3.4.2. Triclosan (TCS)

The uptake of triclosan by ATTP@PEG and ATTP@PVP solids was studied at different interval of time between 1 to 420 mins and the time dependent removal of these at various contact time are shown as in Figure 3.30. It is observed that during the initial period of contact, the uptake of triclosan by ATTP@PEG and ATTP@PVP was very fast and it was observed that *Ca* 40 and *Ca* 42.1% of triclosan were removed by the ATTP@PEG and ATTP@PVP, respectively within 5 mins of contact. Further, increase in time caused for gradual increase in percentage removal of triclosan by these solids and apparent sorption equilibrium was achieved within 180 mins and 240 mins of contact for triclosan using ATTP@PEG and ATTP@PVP. The fast uptake of triclosan suggested that the materials possessed greater affinity towards triclosan and is a potential solid to be employed in waste water treatment plants. Previously it was reported that the maximum time to reach the sorption equilibrium for the sorption of triclosan using biomass, Phaeodactylum tricornutum was 180 mins (Santaeufemia et al., 2019).

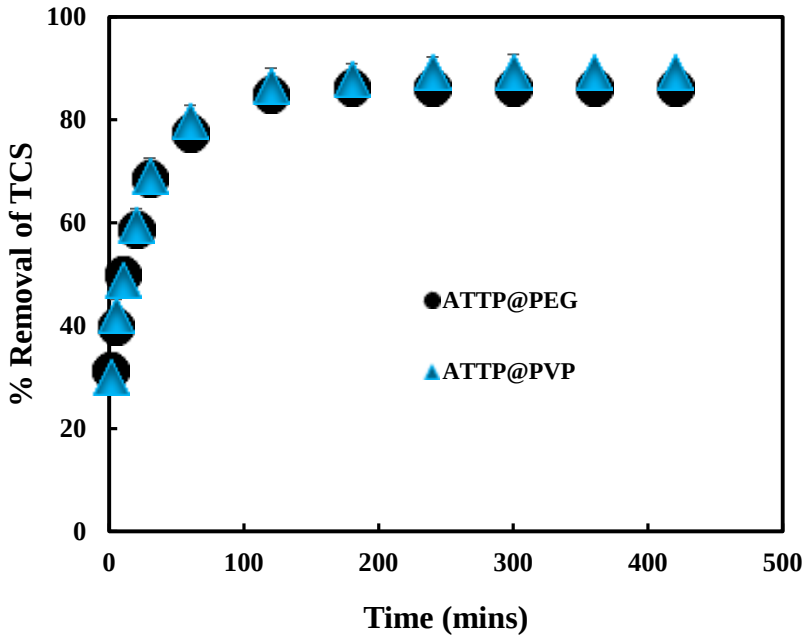

Figure 3.30: Effect of contact time in the removal of triclosan by the ATTP@PEG and ATTP@PVP solids ([TCS]: 10.0 mg/L; pH: 4.0; Solid dose: 2.0 g/L; Temperature: 25°C).

3.3.4.3. 17α-ethinylestradiol (EE2)

The percentage elimination of EE2 by the ATTP@PEG and ATTP@PVP solids at different time intervals was obtained and returned in Figure 3.31. The percent removal of EE2 by both the materials was rapid during initial period of contact and *Ca* 52.5 and 55.2% of EE2 was removed within just 10 mins of time by the ATTP@PEG and ATTP@PVP materials, respectively. Further, the sorption of EE2 onto these synthesized materials was saturated just within 180 mins of contact. This indicated that the surface active sites of these two functionalized materials saturated within 180 mins and no further removal of EE2 was obtained even after 420 mins of contact. These results further inferred that both the materials possessed high affinity for the attenuation of EE2 and its applicability in treatment of wastewater.

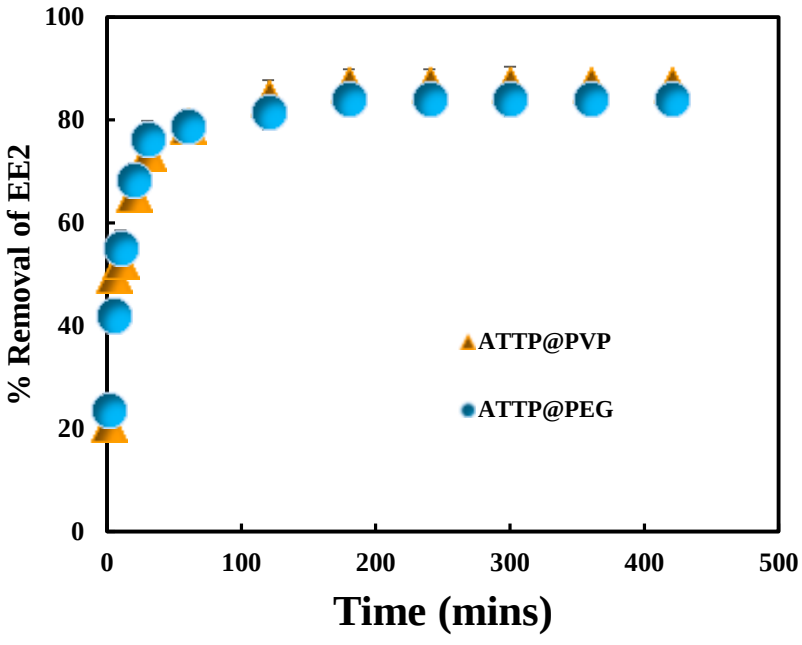

Figure 3.31: Effect of contact time in the removal of EE2 by the ATTP@PEG and ATTP@PVP solids ([EE2]: 10.0 mg/L; pH: 6.08; Solid dose: 2.0 g/L; Temperature: 25°C).

3.3.4.4. Ciprofloxacin (CIP)

At varied times (5 - 360 mins), the amount of CIP absorbed by ATTP@PEG and ATTP@PVP is measured at pH 7.0. As shown in Figure 3.32. the ATTP@PEG and ATTP@PVP rapidly adsorbs the CIP; within 5 mins, more than 50% of these micro-pollutants aggregated on the surface. The initial rate of adsorption for both the materials was notably high, which is mainly due to the number of active sites being comparatively higher at the ATTP@PEG and ATTP@PVP surfaces during the early contact time, which facilitated the quick accumulation of CIP molecules onto the solid surfaces. However, the sorption rate decreases with time, and within 180 mins of contact reaches the equilibrium. Results show that ATTP@PEG and ATTP@PVP effectively removes CIP from aqueous wastes.

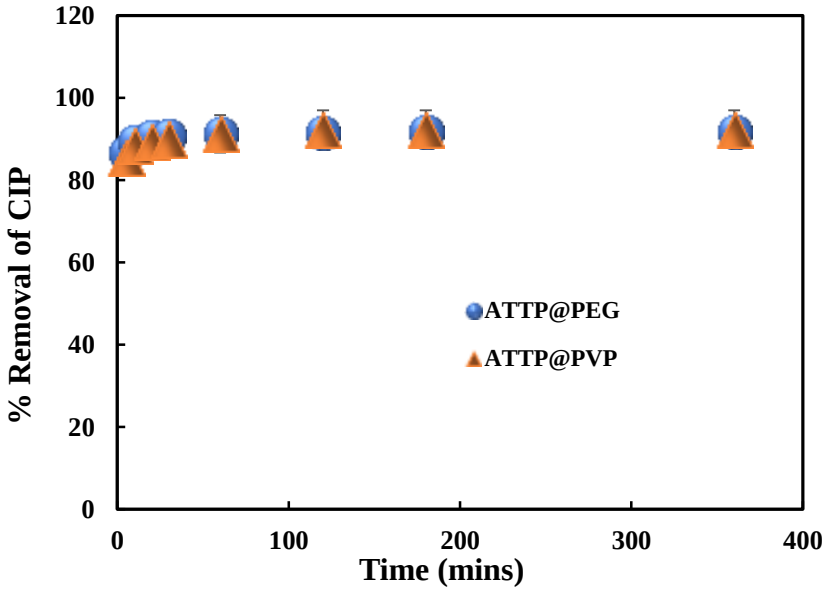

Figure 3.32: Effect of contact time in the removal of CIP by the ATTP@PEG and ATTP@PVP solids ([CIP]: 10.0 mg/L; pH: 7.0; Solid dose: 2.0 g/L; Temperature: 25°C)

3.3.4.5. Bisphenol A (BPA)

BPA removal with respect to time onto ATTP@PEG and ATTP@PVP is conducted by varying the contact time from 5 to 360 mins at pH 6.06 using the initial concentration of 10.0 mg/L for both pollutant solutions. Figure 3.33 graphically depicts the percentage uptake BPA by ATTP@PEG and ATTP@PVP as a function of time. The results demonstrate that during the early stage of interaction (i.e., 5 mins only), both ATTP@PEG and ATTP@PVP quickly adsorb the BPA. Moreover, almost an apparent sorption equilibrium was attained within 240 mins of contact for ATTP@PEG and *Ca* 180 mins using the ATTP@PVP. This indicated that both the solids are reasonably efficient in removing BPA from an aqueous medium. Similarly, the effect of time on the removal of BPA using the clay modified with hexadecyltrimethylammonium bromide (HDTMA) also showed that the sorption equilibrium was attained in 180 mins of contact (Issaoui et al., 2020).

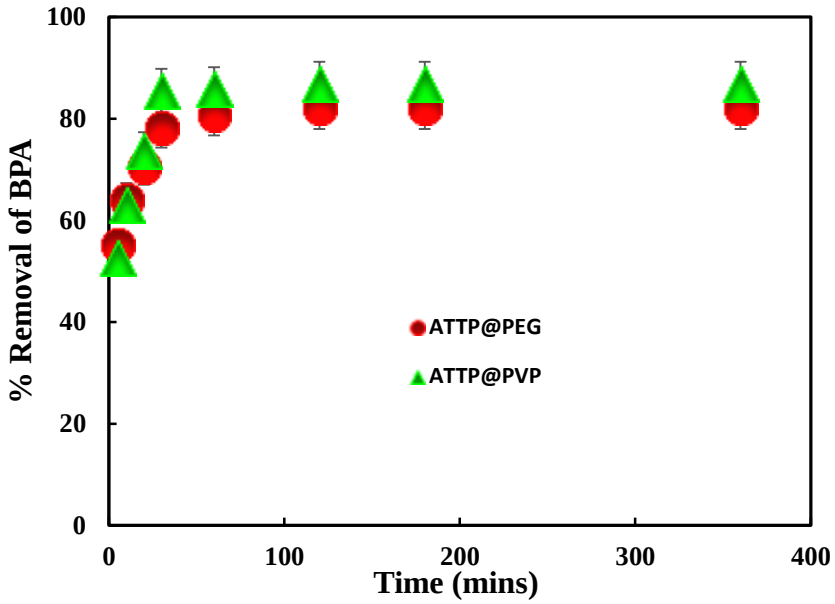

Figure 3.33: Effect of contact time in the removal of BPA by the ATTP@PEG and ATTP@PVP solids ([BPA]: 10.0 mg/L; pH: 6.06; Solid dose: 2.0 g/L; Temperature: 25°C).

3.3.5. Kinetic modelling studies

The time dependence data is further employed to deduce the sorption kinetics in the sorption of these pollutants using the solids. The two kinetic models viz., pseudo-first order (PFO) and pseudo-second order (PSO) (Azizian, 2004) equations were utilized for its linear fitting. A linear least square fitting method is conducted for the estimation of unknown parameters along with the rate constant values. Further, the linear fitting enables to estimate the unknown constant involved in the basic equations i.e., the sorption capacity of solid for the specific pollutant.

3.3.5.1. Tetracycline (TCH)

The time dependence sorption data of tetracycline is utilized to study the kinetics of sorption by employing pseudo-first order (PFO) pseudo-second order (PSO) rate kinetics. The simulation results are illustrated graphically as in Figure 3.34. Moreover, the estimated parameters are returned in Table 3.10. Table 3.10 showed that the uptake of tetracycline by ATTP@PEG and ATTP@PVP followed the PSO kinetics model rather than PFO model expressed by the higher correlation coefficients (R^2) for pseudo-second-order. The removal capacity of tetracycline is relatively high which pointed the potential applicability of the materials towards the removal of tetracycline from aqueous wastes. Further, the well-fitting of PSO with the sorption data indicated that tetracycline species were captured on the surface of the materials with the strong forces. Sorption of tetracycline onto Na-montmorillonite (Na-Mt) modified with carboxymethyl-chitosan is better fitted to the PSO kinetics (Ahamad et al., 2020). Previously, the sorption of tetracycline and 17α–ethynylestradiol using various hybrid material at different contact time were

	PFO Model			PSO Model		
Materials	**q_e (mg/g)**	**k_1 (min^{-1})**	**R^2**	**q_e (mg/g)**	**k_2 (g/mg/min)**	**R^2**
ATTP@PVP	1.02	0.006	0.72	4.68	0.03	0.99
ATTP@PEG	2.32	0.050	0.90	4.74	0.02	0.99

best described by pseudo-second order (PSO) and fractal-like-pseudo-second order (FL-PSO) kinetic models, and it was suggested that these two micro-pollutants were bound to the adsorbent with relatively stronger forces (Thanhmingliana et al., 2015). Moreover, the kinetic sorption of tetracycline using SBA15, N,N-SBA15 and Fe-N,N-SBA15 adsorbents were also well fitted to the pseudo-second order kinetic model where the tetracycline specifically sorbed by these adsorbents (Zhang et al., 2018).

Table 3.10. Predicted kinetic parameters for pseudo-first order (PFO) and pseudo-second order (PSO) kinetic models in the sorption of tetracycline by the ATTP@PEG and ATTP@PVP solids.

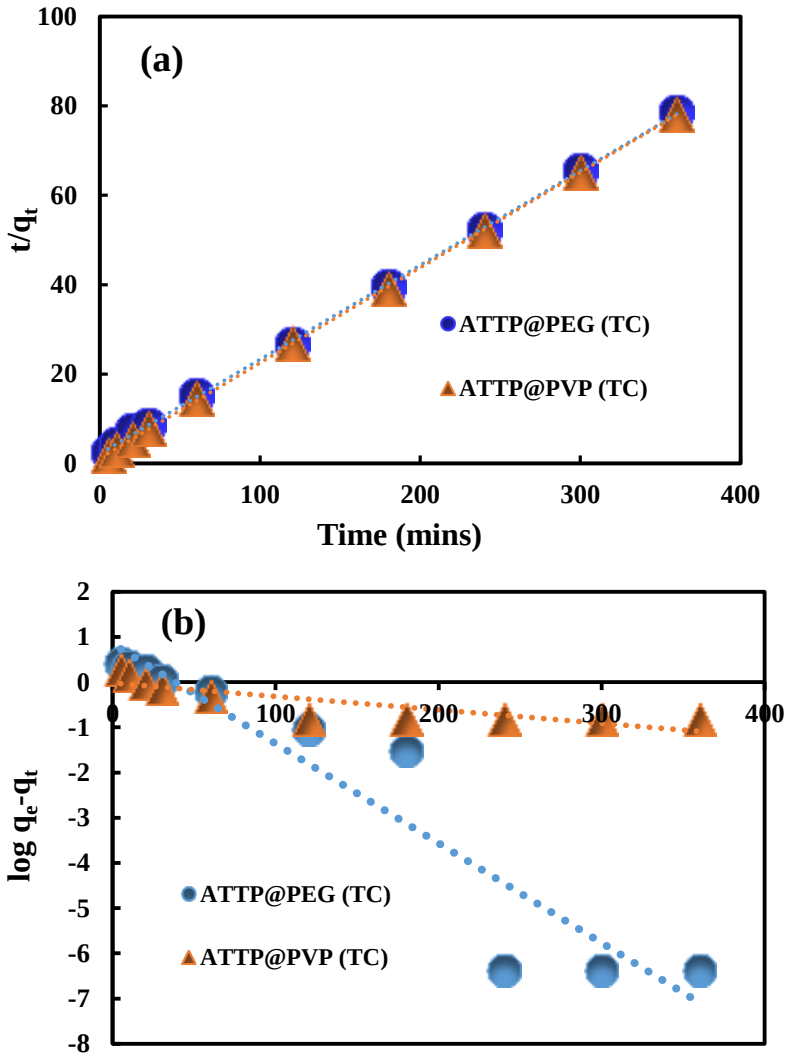

Figure 3.34: Plots of (a) PSO and (b) PFO kinetic models for the sorption of tetracycline by ATTP@PEG and ATTP@PVP solids ([TCH]: 10.0 mg/L; pH: 3.5; Solid dose: 2.0 g/L; Temperature: 25°C).

3.3.5.2. Triclosan (TCS)

The kinetic data of triclosan using ATTP@PEG and ATTP@PVP solids were modeled with the known pseudo-first-order (PFO) and pseudo-second-order (PSO) kinetic models. The linear fitting results for the PFO and PSO models are given in Figure 3.35. The rate constants and uptake capacity along with the least square sums were obtained and included in Table 3.11. The results indicated that the sorption of triclosan by these solids followed better with the PSO model as compared to the PFO model since higher correlation coefficients (R^2) were seen for the PSO model. The fitting of the PSO model indicated that the triclosan species were sorbed by these solids with relatively stronger forces. It was reported previously that the removal of triclosan using *Phaeodactylum tricornutum* follows pseudo-second-order kinetic model (Santaeufemia et al., 2019). Chitosan/Poly composite membrane was employed for the sorption of triclosan and it was reported that the sorption kinetics fitted well to the pseudo-second-order kinetics (R^2>0.986) as compared to the pseudo-first-order kinetics (Liu & Xu, 2014).

Table 3.11. Predicted kinetic parameters for pseudo-first order (PFO) and pseudo-second order (PSO) kinetic models in the sorption of triclosan by ATTP@PEG and ATTP@PVP solids.

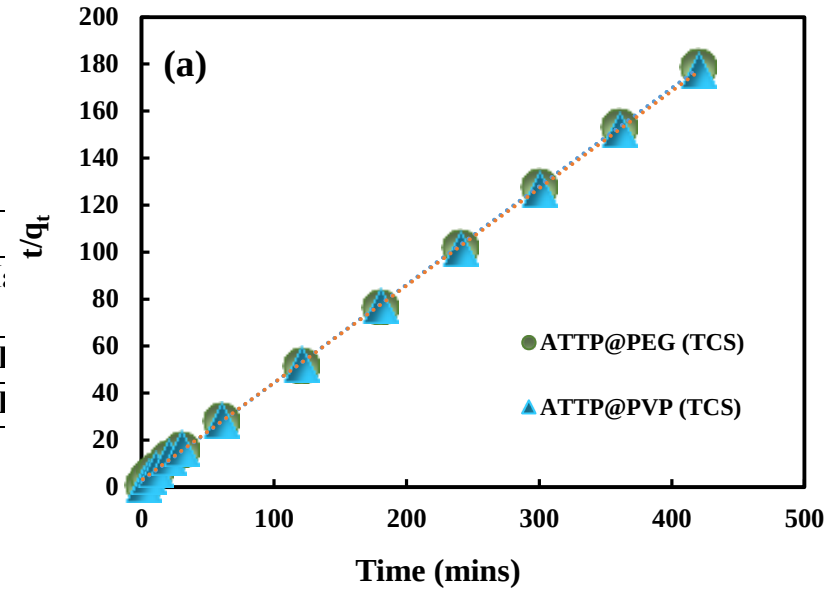

M			R^2
AT			0.99
AT			0.99

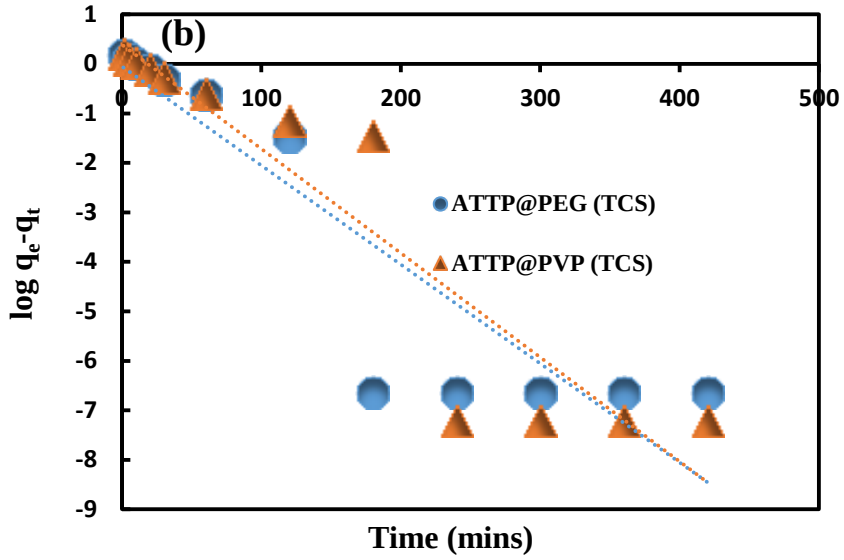

Figure 3.35: Plots of (a) PSO and (b) PFO kinetic models for the sorption of triclosan by ATTP@PEG and ATTP@PVP solids ([TCS]: 10.0 mg/L; pH: 4.0; Solid dose: 2.0 g/L; Temperature: 25°C).

3.3.5.3. 17α-ethinylestradiol (EE2)

The sorption kinetics of EE2 using ATTP@PEG and ATTP@PVP solids employing pseudo-first order (PFO) and pseudo-second order (PSO) kinetic models and the linear simulation results are presented in Figure 3.36. Further, the optimized results are shown in Table 3.12. The results showed that PSO model is fitted well since the R^2 is significantly high compared to the PFO model. The sorption of EDCs (trimethoprim (TMP), estrone (E1), 17β-estradiol (E2) and 17α-ethinylestradiol (EE2)) using -SnO_2 pillared montmorillonite also followed PSO kinetic model (Vidal et al., 2015). Electrospun poly(butylene adipate-co-terephthalate) (PBAT) fibers were employed for the sorption of estrone (E1), 17β-estradiol (E2), and 17α-ethynylestradiol (EE2). The experimental kinetic data is well described by PSO model compared to the PFO model. Further, the difference between calculated and experimental

sorption capacities indicated that PSO model is more favourable. Hence, the sorption of E1, E2 and EE2 onto the PBAT microfiber surfaces occurred predominantly through the chemical interactions (Westrup et al., 2021).

Table 3.12. Predicted kinetic parameters for the pseudo-first order (PFO) and pseudo-second order (PSO) kinetic models in the sorption of EE2 by ATTP@PEG and ATTP@PVP solids

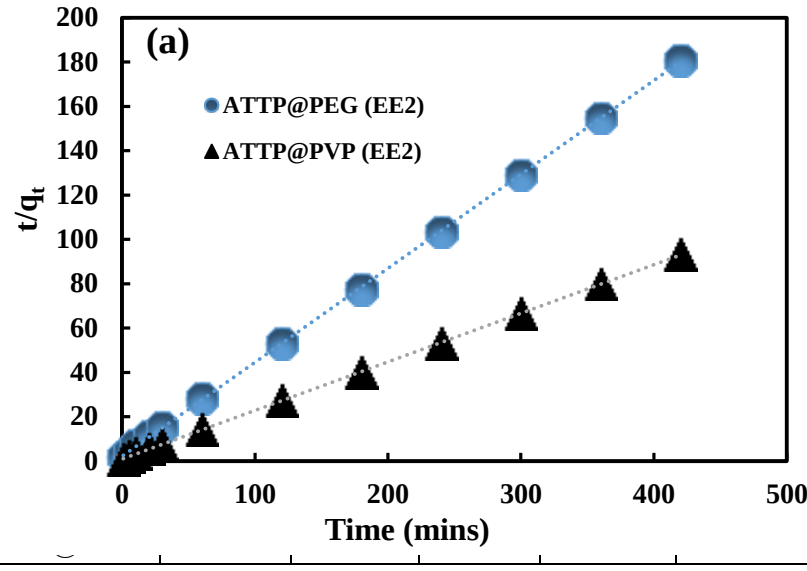

M							R^2
Al							0.99
Al							0.99

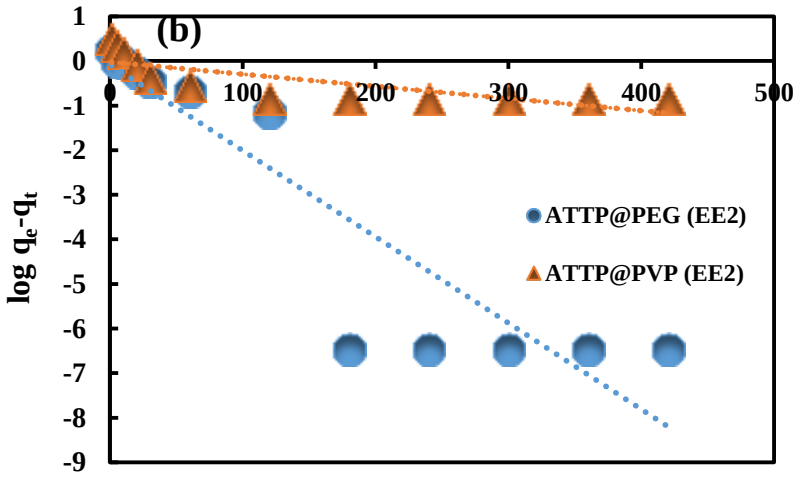

Figure 3.36. Plots of the (a) PSO and (b) PFO kinetic models for the sorption of EE2 by ATTP@PEG and ATTP@PVP solids ([EE2]: 10.0 mg/L; pH: 6.08; Solid dose: 2.0 g/L; Temperature: 25°C).

3.3.5.4. Ciprofloxacin (CIP)

The adsorption kinetics of ciprofloxacin by ATTP@PEG and ATTP@PVP is employed to perform the two linear kinetic models viz., pseudo-first-order (PFO) and pseudo-second-order (PSO) models, and the results are illustrated graphically in Figure 3.37. The calculated least square sum and unknown parameters were included in Table 3.13. These results clearly inferred that the kinetic data is well fitted to the PSO model compared to the PFO model since R^2 is reasonably high for the PSO model. These results further showed that CIP is bound to ATTP@PEG and ATTP@PVP with strong chemical forces. Further, the sorption capacity estimated for CIP by ATTP@PEG and ATTP@PVP was found to be 7.34 and 7.37 mg/g, respectively. The results showed that the materials possessed very high sorption capacity for the CIP. Furthermore, the magnetized powdered activated carbon efficiently removes the ciprofloxacin and agrees well with the PSO adsorption model (Al-Musawi et al., 2021).

Table 3.13. Predicted kinetic parameters for the pseudo-first-order (PFO) and pseudo-second-order (PSO) kinetic models in the sorption of CIP by ATTP@PEG and ATTP@PVP solids

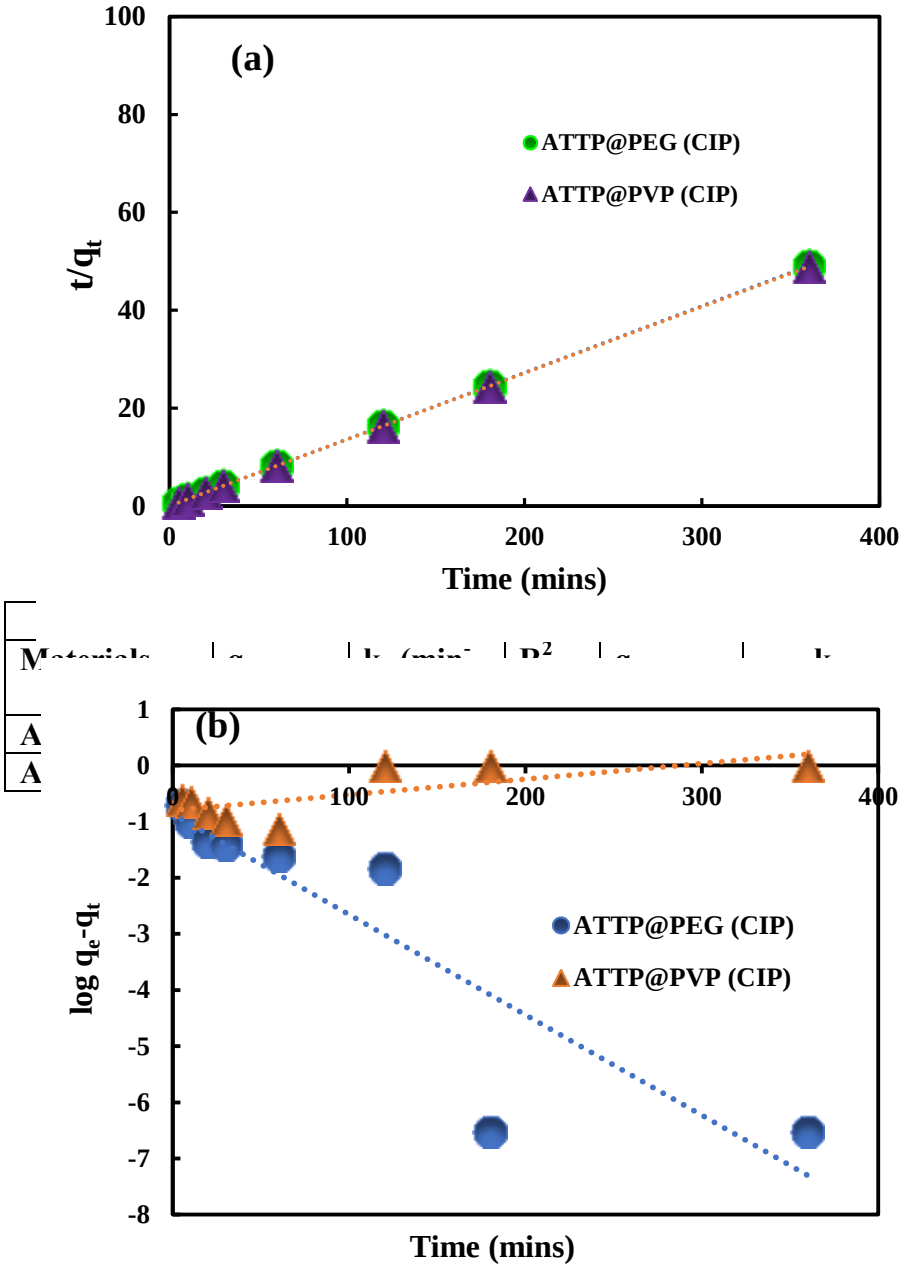

Materials						R^2
A						1
A						1

Figure 3.37: Plots of the (a) PSO and (b) PFO kinetic models for the sorption of CIP by ATTP@PEG and ATTP@PVP solids ([CIP]: 10.0 mg/L; pH: 7.0; Solid dose: 2.0 g/L; Temperature: 25°C).

3.3.5.5. Bisphenol A (BPA)

The time dependence data for the sorption of BPA by the ATTP@PEG and ATTP@PVP is employed for the kinetic modeling viz., PFO and PSO kinetic models. The least-square fitting results are shown graphically in Figure 3.38. Further, the uptake capacity, rate constants, and correlation coefficients were estimated and returned in Table 3.14. It is evident from the results that the PSO model is relatively better fitted to the sorption of BPA by the ATTP@PEG and ATTP@PVP since the correlation coefficients is reasonably high for PSO model. The removal capacity thereby found to be 4.60 and 4.75 for BPA using the ATTP@PEG and ATTP@PVP solids. Further, the fitting of PSO model suggested that the chemical interactions are involved in the adsorption of BPA using ATTP@PEG and ATTP@PVP from aqueous solutions. In the study of goethite iron-oxide impregnated activated carbon (GPAC), was tested for its adsorption capacity to remove BPA from aqueous solutions. The pseudo-second-order model was followed by the adsorption kinetics (Reddy et al., 2016).

	PFO Model			PSO Model		
Materials	**q_e (mg/g)**	**k_1 (min^{-1})**	**R^2**	**q_e (mg/g)**	**k_2 (g/mg/min)**	**R^2**
ATTP@PVP	1.36	0.046	0.847	4.75	0.02	0.99
ATTP@PEG	1.17	0.003	0.195	4.60	0.01	0.99

Table 3.14. Predicted kinetic parameters for the pseudo-first order (PFO) and pseudo-second order (PSO) kinetic models in the sorption of BPA by ATTP@PEG and ATTP@PVP solids

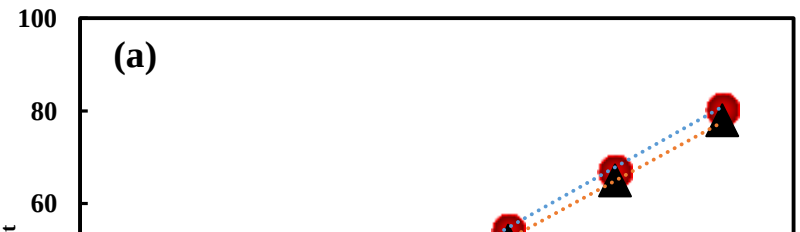

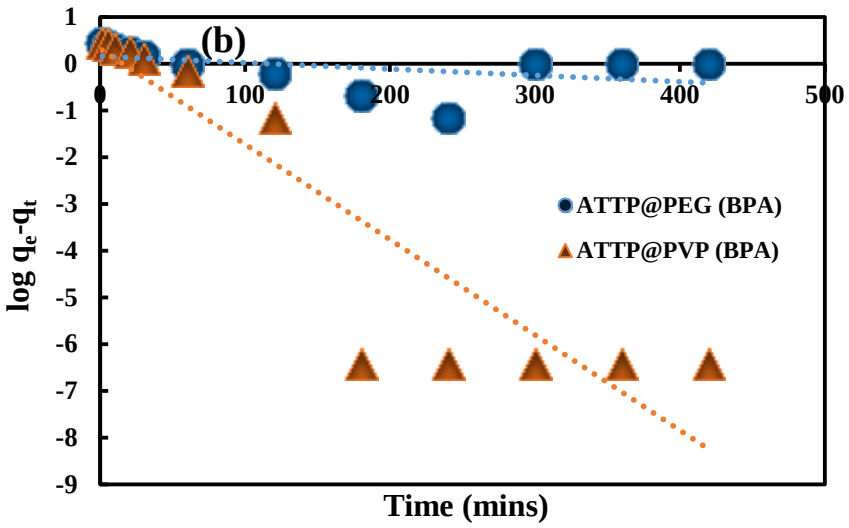

Figure 3.38. Plots of the (a) PSO and (b) PFO kinetic models for the sorption of BPA by ATTP@PEG and ATTP@PVP solids ([BPA]: 10.0 mg/L; pH: 6.06; Solid dose: 2.0 g/L; Temperature: 25°C).

3.3.6. Effect of background electrolyte concentrations

The effect of background electrolyte concentration is an important factor to study the binding nature of sorbate species onto the solid materials (Sonnefeld, 2001). The specific and non-specific sorption of tetracycline, triclosan, ciprofloxacin, bisphenol A and EE2 onto these functionalized materials is studied by collecting the sorption data at different background

electrolyte concentrations. It is reported that the sorption through the outer-sphere complexation is sensitive to the change in background electrolyte concentrations whereas the inner sphere complexes are not altered with the change in background electrolyte concentrations since the adsorbed ions are residing at the plane which is closer to surface where usually background electrolyte ions are not located (Qu et al., 2017). Therefore, the studies were extended to vary the background electrolyte concentrations in the removal of these pollutants by the functionalized materials.

3.3.6.1. Tetracycline (TCH)

The concentration of background electrolyte (NaCl) concentrations was studied in the removal of tetracycline by the ATTP@PEG and ATTP@PVP solids. The background electrolyte concentration was increased from 0.0001 to 0.1 mol/L having the initial tetracycline concentration of 10.0 mg/L and the pH were adjusted to pH 3.5. The results are shown as in Figure 3.39. It is evident from the figure that 1000 times increase in NaCl concentration did not affect significantly the removal of tetracycline by the ATTP@PEG and ATTP@PVP solids. Quantitatively, the percentage removal of tetracycline was decreased from 84.2 to 82.2% for ATTP@PEG while the percentage removal of tetracycline by ATTP@PVP remained constant while increasing the NaCl concentrations from 0.0001 to 0.1 mol/L. These results infer that the TCH is preferentially accumulated at the surface, with stronger forces penetrating within the Stern layer at the surface (Das et al., 2022). These results align with the pH dependence studies, which demonstrated that the TCH aggregated at the surface of ATTP@PEG and ATTP@PVP with relatively stronger Van der Waals forces. However, increasing the concentration of NaCl (0.01 to 0.5 mol/L), the extent of tetracycline removal was increased from 132.4 to 172.7 mg/g using activated carbon produced from tomato waste (TAC) which was due to the inability of big tetracycline molecules aggregated at high ionic strength to enter adsorption sites in the pores of TAC in which electrostatic interaction has overcome by the hydrophobic interaction of tetracycline

(Sayğili & Güzel, 2016). Similarly, an increase in the concentrations of NaCl did not significantly affect the removal of tetracycline using Cu-immobilized alginate beads (Wang et al., 2022), HDTMA modified bentonite and local clay and Al pillared HDTMA modified bentonite and local clay (Thanhmingliana et al., 2015) and MOF/graphite oxide pellets (Yu et al., 2018).

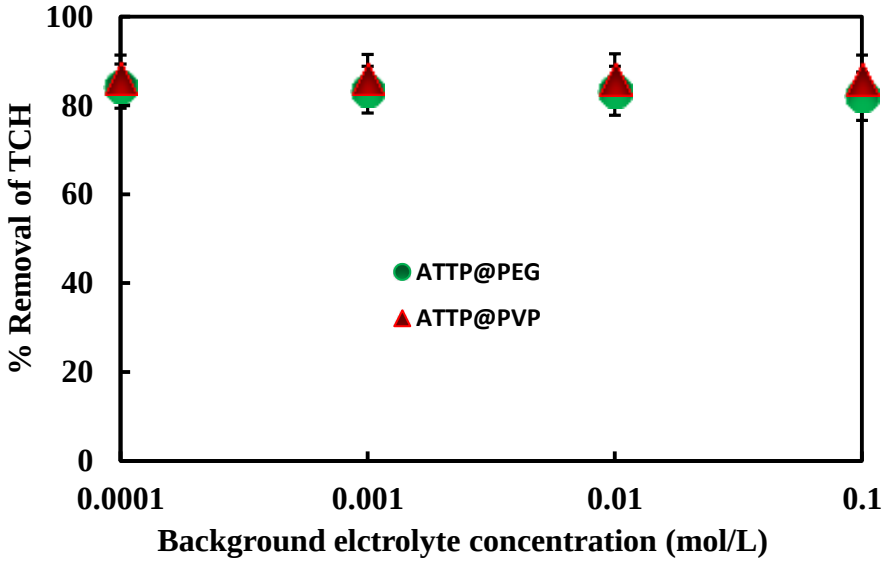

Figure 3.39. Effect of background electrolyte concentrations (NaCl) in the removal of tetracycline by the ATTP@PEG and ATTP@PVP solids ([TCH]: 10.0 mg/L; pH: 3.5; Solid dose: 2.0 g/L; Temperature: 25˚C).

3.3.6.2. Triclosan (TCS)

Similarly, the effect of background electrolyte (NaCl) concentrations on the removal of triclosan by ATTP@PEG and ATTP@PVP solids was performed and the background electrolyte (NaCl) concentration was increased from 0.0001 to 0.1 mol/L. The percentage removal efficiency of triclosan by ATTP@PEG and ATTP@PVP as a function of background electrolyte concentrations is shown in Figure 3.40. Figure 3.40 showed that the percentage uptake of triclosan was remained, almost, constant while the background

electrolyte concentration was increased from 00001 to 0.1 mol/L. In brief, the percentage removal of triclosan was decreased from 90.0 to 88.0% using ATTP@PEG and 94.0 to 91.27% using ATTP@PVP, increasing the NaCl concentrations from 0.0001 to 0.1 mol/L, respectively. These results indicated that triclosan are adsorbed by the stronger forces, perhaps van der Waals, at the surface of functionalized materials. These results are in a line to the pH dependence studies concluded that the strong interactions occurred between the ATTP@PEG or ATTP@PVP solids and the triclosan sorbate species. Previously, it was reported that the sorption of triclosan by polystyrene microplastic was not affected by increasing the concentration of background electrolyte (NaCl) from 0.0 to 0.1 mol/L (Li et al., 2019).

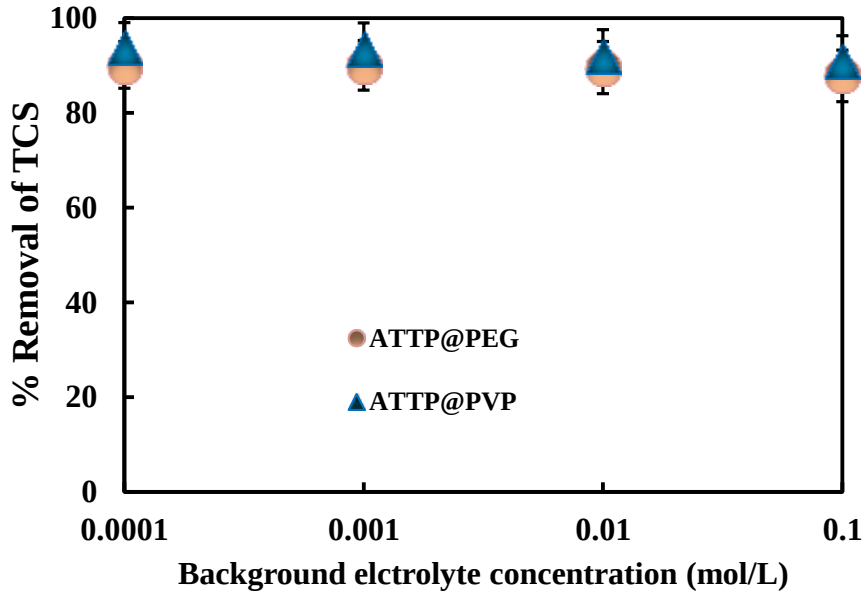

Figure 3.40. Effect of background electrolyte concentrations (NaCl) in the removal of triclosan by the ATTP@PEG and ATTP@PVP solids ([TCS]: 10.0 mg/L; pH: 4.0; Solid dose: 2.0 g/L; Temperature: 25ºC).

3.3.6.3. 17α-ethinylestradiol (EE2)

The impact of background electrolyte (0.0001 to 0.1 mol/L NaCl), concentrations on the adsorption of EE2 by ATTP@PEG and ATTP@PVP materials are conducted as this enables to deduce the type of interactions involved between the sorbate species and the sorbent. Percentage elimination of EE2 using the ATTP@PEG and ATTP@PVP materials is unaffected by increasing the background electrolyte (NaCl) concentrations from 0.0001 to 0.1 mol/L (1000 times) (*Cf* Figure 3.41.). These results inferred that 1000 times increase in background electrolyte concentration has unaffected the percentage sorption of EE2 by ATTP@PEG and ATTP@PVP solids. The outcome infers that EE2 adsorbs by the ATTP@PEG and ATTP@PVP solid surface with stronger forces. The pH dependence studies reveals the possible interactions between the EE2 and the ATTP@PEG/ATTP@PVP solids. Since EE2 is a neutral species at pH below 10.5, substantially EE2 adsorbed through the hydrophobic interactions (Malsawmdawngzela & Tiwari, 2022).

Increasing ionic strength of NaCl from 0 to 320 mM in leachate solutions has not affected sorption of bisphenol A and EE2 by single-walled carbon nanotubes (SWCNTs) (Joseph et al., 2011). Sorption of estrone (E1), 17β-estradiol (E2) and 17α-ethinyl estradiol (EE2) using n-propyl functionalized mesoporous material (30% Pr-MCM-41) on increasing the concentration of NaCl from 0.001 to 0.1 mol/L did not significantly affect the elimination of E1, E2 and EE2. The result is due to the same contribution produced by salting effect for estrogens and squeezing-out effect for 30%Pr-MCM-41 in presence of co-existed ions. The high removal of estrogens was due to the π-π and hydrophobic interaction between a 30% Pr-MCM-41 and estrogens (Gao et al., 2019).

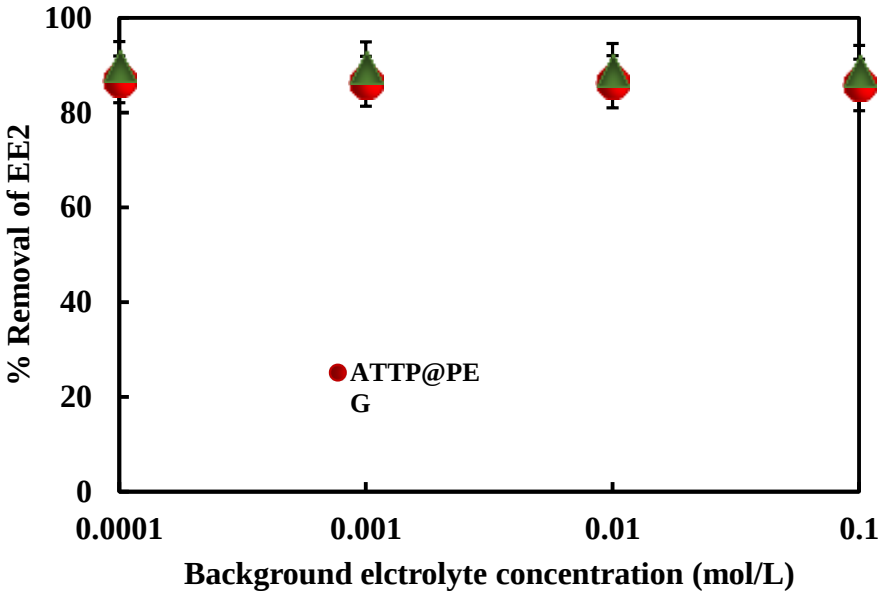

Figure 3.41. Effect of background electrolyte concentrations in the removal of EE2 by the ATTP@PEG and ATTP@PVP solids ([EE2]: 10.0 mg/L; pH: 6.08; Solid dose: 2.0 g/L; Temperature: 25ºC).

3.3.6.4. Ciprofloxacin (CIP)

The sorption of CIP is conducted by varying background electrolyte (NaCl) concentrations from 0.0001 to 0.1 mol/L at a constant pH of 7.0 and initial concentration of CIP 10.0 mg/L. The results are shown in Figure 3.42. It is evident from the figure that increasing the concentration of background electrolyte from 0.0001 to 0.1 mol/L (i.e., 1000 times), the percentage uptake of CIP by ATTP@PEG and ATTP@PVP was not affected. The results show that the functionalized attapulgite has a strong affinity towards the CIP and the CIP molecules are attracted with relatively stronger forces at the surface of ATTP@PEG and ATTP@PVP. The strong binding between CIP and the

adsorbent occurred due to the formation of hydrogen bonding, resulting in specific adsorption of CIP onto ATTP@PEG and ATTP@PVP conducted at pH 7.0. According to prior investigations, the elimination of CIP was not significantly affected by an increased in NaCl concentrations from 0.0001 to 0.1 mol/L using the graphene hydrogel (Ma et al., 2015).

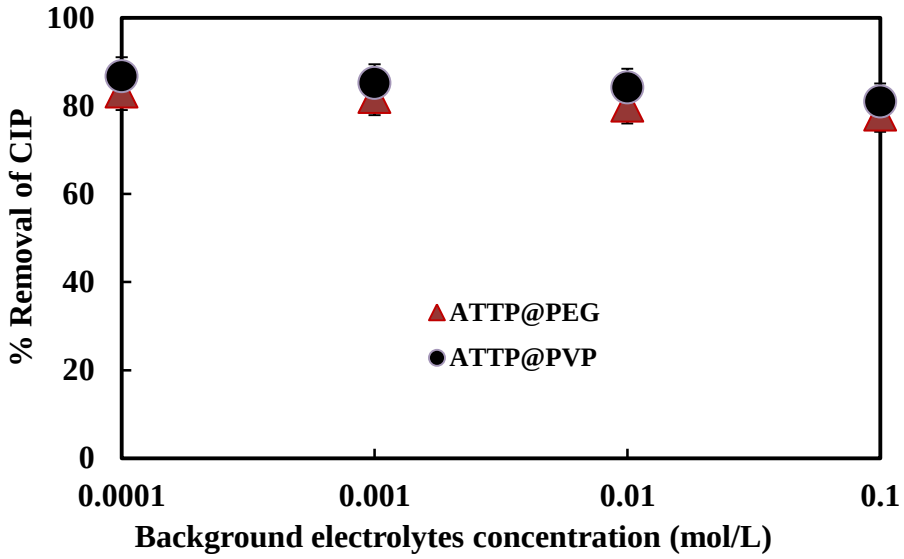

Figure 3.42. Effect of background electrolyte concentrations in the removal of CIP by the ATTP@PEG and ATTP@PVP solids ([CIP]: 10.0 mg/L; pH: 7.0; Solid dose: 2.0 g/L; Temperature: 25ºC).

3.3.6.5. Bisphenol A (BPA)

The background electrolyte concentration dependence adsorption of BPA is obtained by increasing the NaCl concentrations from 0.0001 to 0.1 mol/L. The initial concentration of BPA was taken as 10.0 mg/L and pH 6.06. The percentage of BPA eliminated as a function of background electrolyte concentrations is presented in Figure 3.43. It is clear from the figure that increasing the background electrolyte concentration (0.0001 to 0.1 mol/L, NaCl), the percentage removal of BPA remained unaffected. These results infer

that BPA is preferentially accumulated at the surface with stronger forces penetrating within the Stern layer at the surface (Das et al., 2022). These results align with the pH dependence studies, which demonstrated that the BPA aggregated at the surface of the solids with relatively stronger van der Waals forces. Similarly, the removal of BPA using Palm Shell activated carbon (PAC) was not affected significantly even in the presence of 0.5 mol/L NaCl (Soni & Padmaja, 2014).

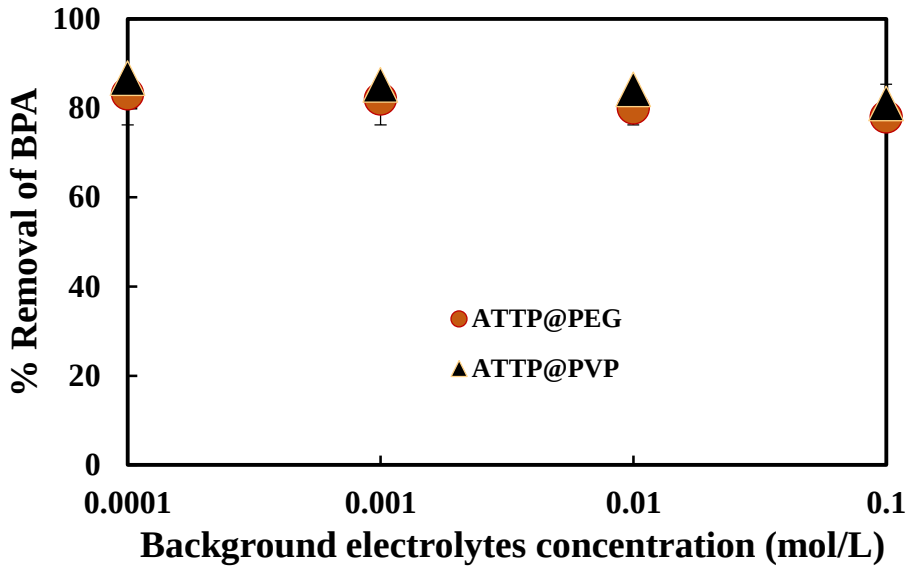

Figure 3.43. Effect of background electrolyte concentrations in the removal of BPA by the ATTP@PEG and ATTP@PVP solids ([BPA]: 10.0 mg/L; pH: 6.0; Solid dose: 2.0 g/L; Temperature: 25ºC).

3.3.7. Effect of co-existing ions in the removal of tetracycline, triclosan, EE2, ciprofloxacin, and bisphenol A

The presence of co-existing ions (cations and anions) in the removal of tetracycline by the ATTP@PEG and ATTP@PVP composite solids was studied with initial tetracycline and co-ions concentrations 10.0 mg/L and 50.0 mg/L,

respectively at pH 3.5. The results are shown in Figure 3.44 and 3.45. The cations chosen were Mn(II), Mg(II), Ca(II), and Ni(II); whereas the anions were taken as ethylenediaminetetraacetate (EDTA), oxalic acid, phosphate and glycine. Figure 3.44. showed that the removal efficiency of tetracycline by both the functionalized solids was almost unaffected in presence of these co-existing cations viz., Mn(II), Mg(II), Ca(II), and Ni(II), which confers the selectivity of the pollutant molecule at the surface. Moreover, it indicates further that the hydrophobic interactions are the driving forces in the aggregation of sorbate species at the solid surface (Makowski & Bogunia, 2020). Moreover, the competitive adsorption ability varies between metal cations and depends on several factors, including the metals' hydration energy, molecular mass, ion charges, and hydrated ionic radius (Ni et al., 2019). However, a slight decrease in percentage uptake of tetracycline was observed in presence of anions viz., glycine, phosphate and oxalic using the ATTP@PEG solid (*Cf* Figure 3.45). Similarly, the presence of EDTA effected significantly the percentage removal of tetracycline by the ATTP@PEG and ATTP@PVP solids. The results apparently indicated therefore, that the presence of EDTA considerably suppressed the uptake and the percentage removal of tetracycline and the sorption of TCH is decreased from 88.9 to 76.0% for ATTP@PEG and from 91.5 to 77.6% for ATTP@PVP. The EDTA aggregates at the surface of these solids through the hydrophobic interactions and occupies the surface active sites hence, suppresses the removal of tetracycline by these solids (DiBlasi et al., 2021). The effect of Cl^{-}, NO^{3-}, SO_4^{2-} anions in the sorption of tetracycline by modified biochar was studied in real water samples and it was observed that these anions could not affect the removal percentage of tetracycline, however, the presence of PO_4^{3-} showed a considerable influence in the removal percentage of tetracycline by modified biochar. Since PO_4^{3-} were easily adsorbed onto modified magnetic biochar (MSABC) compared to TCH due to strong electrostatic interactions between the MSABC and PO_4^{3-}; thus, the actives sites are preferentially occupied by PO_4^{3-} (Dai et al., 2020). On the other hand, the cations such as Mg^{2+} and Ca^{2+} caused a slight decrease in the adsorption capacity of tetracycline while the K^{+} and Na^{+} did not affect the

sorption of tetracycline by $NiFe_2O_4$-COF-chitosan-terephthalaldehyde (NCCT) nanocomposite films implying that the species of TC possibly forms coordinate bonds with the Mg^{2+} and Ca^{2+}. It was further assumed that the Na^{+} or K^{+} bonded to NCCT surface and occupied only one empty seat on the surface of NCCT, while Mg^{2+} and Ca^{2+} as divalent cation captured two empty seat, limiting the effective adsorption of TC on NCCT (Li et al., 2020).

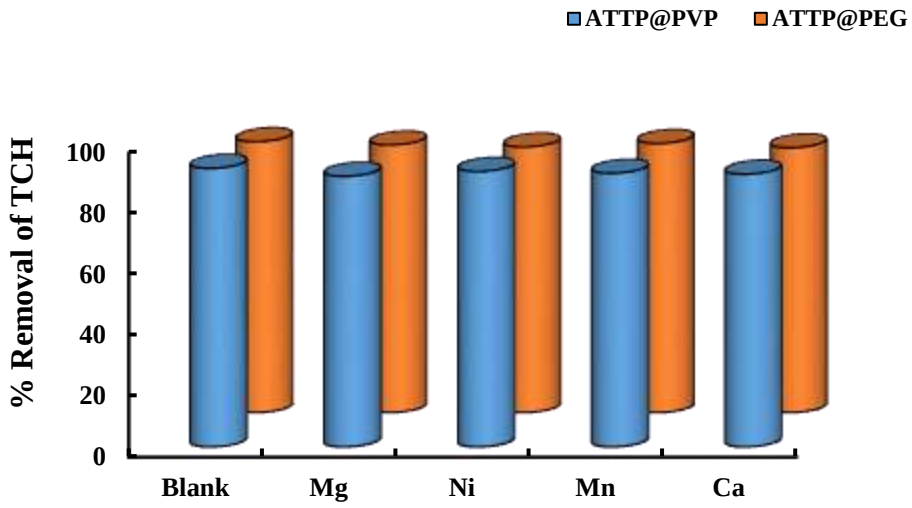

Figure 3.44. Effect of co-existing cations in the removal of tetracycline by ATTP@PEG and ATTP@PVP solids ([TCH]: 10.0 mg/L; [Cations]: 50.0 mg/L; pH: 3.5; Solid dose: 2.0 g/L; Temperature: 25°C).

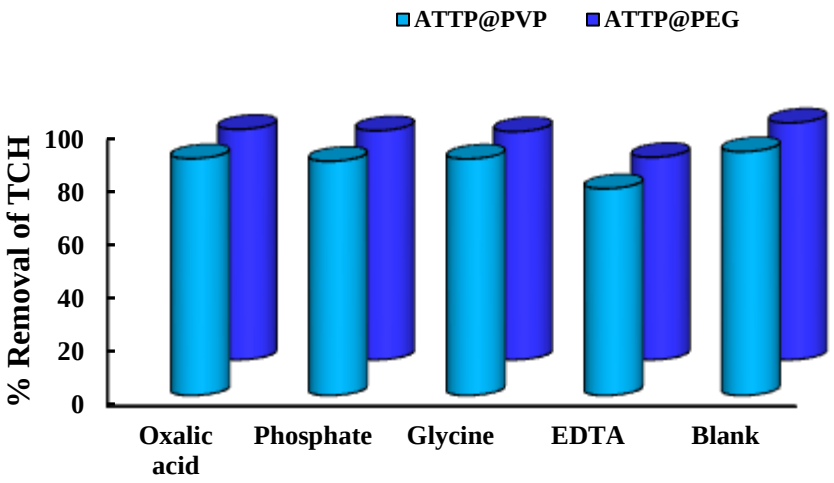

Figure 3.45. Effect of co-existing anions in the removal of tetracycline by ATTP@PEG and ATTP@PVP solids ([TCH]: 10.0 mg/L; [Anions]: 50.0 mg/L; pH: 3.5; Solid dose: 2.0 g/L; Temperature: 25°C).

Similarly, the sorption of triclosan by ATTP@PEG and ATTP@PVP was conducted in simultaneous presence of several coexisting ions. The initial concentration of triclosan was taken 10.0 mg/L at pH 4.0. The cations are included as Mn(II), Mg(II), Ca(II) and Ni(II) whereas the anions are chosen as ethylenediaminetetraacetic acid (EDTA), glycine, phosphate and oxalic acid. The concentration of co-ions was maintained as 50.0 mg/L. Further, the results are presented in Figure 3.46 and 3.47. Results showed that these co-existing ions showed no effect in the sorption efficiency of ATTP@PEG and ATTP@PVP for triclosan except the presence of EDTA. The presence of EDTA had suppressed the removal efficiency of triclosan from 90.6 to 74.5% using ATTP@PEG and 93.6 to 78.9% using ATTP@PVP. Both EDTA and triclosan is adsorbed onto the solid surfaces. EDTA, with its multiple carboxyl and amine groups, leads strong interactions with adsorption sites through hydrogen bonding and reduces the number of available active sites of solid for triclosan. Previously, it was reported that the sorption of triclosan using MIL-53(Al) and

MIL- 53(Al)-1 was not affected in presence of several co-existing ions. However, the presence of humic acid (HA) affected the sorption of triclosan by the solid since the percent removal of triclosan was decreased in presence of HA. Since HA molecules are negatively charged at the studied solution pH (6.5), hence, preferentially occupied the surface active sites by electrostatic attractions, thereby hindering the TCS adsorption. Moreover, HA is highly hydrophobic and has exceptionally large molecular size, the pores on the surface of the MOFs is blocked and restricted adsorption of TCS by the MOF (Dou et al., 2017).

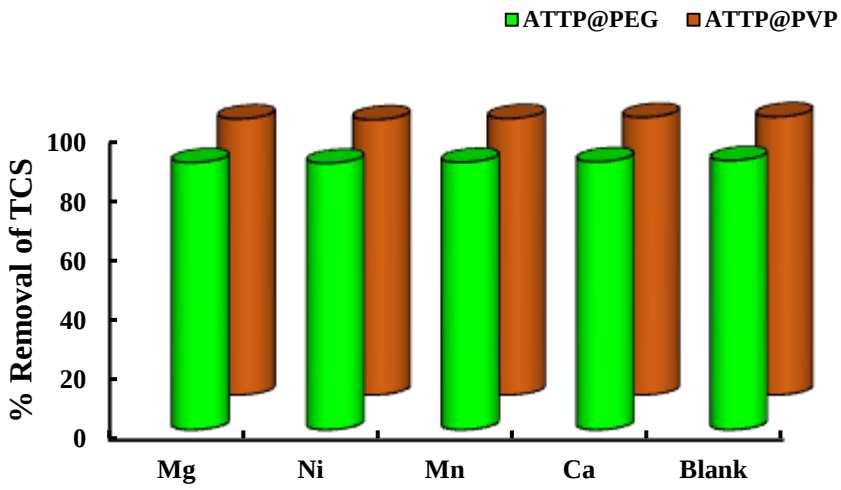

Figure 3.46. Effect of co-existing cations in the removal of triclosan by ATTP@PEG and ATTP@PVP solids ([TCS]: 10.0 mg/L; [Cations]: 50.0 mg/L; pH: 4.0; Solid dose: 2.0 g/L; Temperature: 25°C).

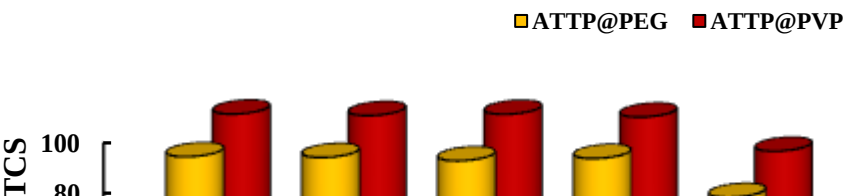

Figure 3.47. Effect of co-existing anions in the removal of triclosan by ATTP@PEG and ATTP@PVP solids ([TCS]: 10.0 mg/L; [Anions]: 50.0 mg/L; pH: 4.0; Solid dose: 2.0 g/L; Temperature: 25°C).

Co-ions (cations: Mn(II), Mg(II), Ca(II) and Ni(II) or anions: ethylenediaminetetraacetic acid (EDTA), oxalic acid, glycine and phosphate) effect in the elimination of EE2 by ATTP@PEG and ATTP@PVP was extensively studied. The concentration of EE2 and co-ions are taken as 10.0 mg/L and 50.0 mg/L, respectively at pH 6.08. Results are shown as percentage elimination of EE2 in presence these co-existing ions and presented in Figure 3.48 and 3.49. The percentage removal of EE2 was not changed in presence of these co-ions except EDTA which significantly affected the removal of EE2 from 86.84 to 70.2% using ATTP@PEG and 88.9 to 69.8% using ATTP@PVP. The larger molecular size and structure of EDTA blocks the active sites of the solid surfaces and results in competitive adsorption. This caused a decrease in the sorption of EE2 by ATTP@PEG and ATTP@PVP (You et al., 2020). It was previously reported that the sorption of EE2 using PA612 was unaffected in presence of cations (0.1 mol/L) viz., Zn(II), K(I) or Ca(II) however, only a

slight reduction in sorption was recorded in presence of Mg(II) (Gao et al., 2019).

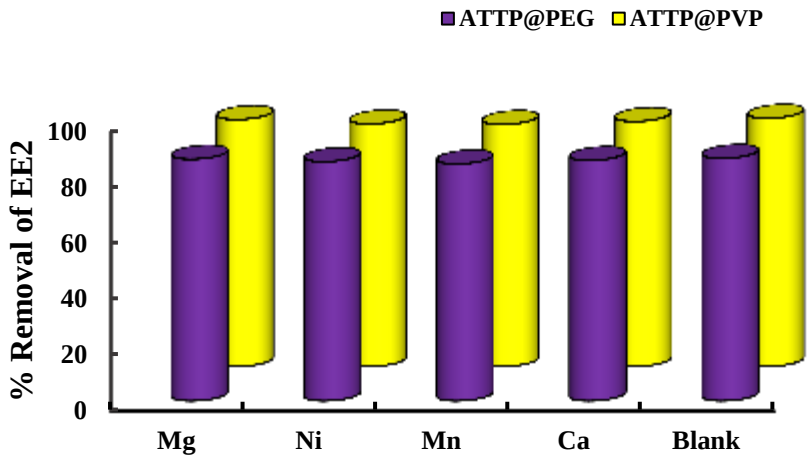

Figure 3.48. Effect of co-existing cations in the removal of EE2 by ATTP@PEG and ATTP@PVP solids ([EE2]: 10.0 mg/L; [Cations]: 50.0 mg/L; pH: 6.08; Solid dose: 2.0 g/L; Temperature: 25°C).

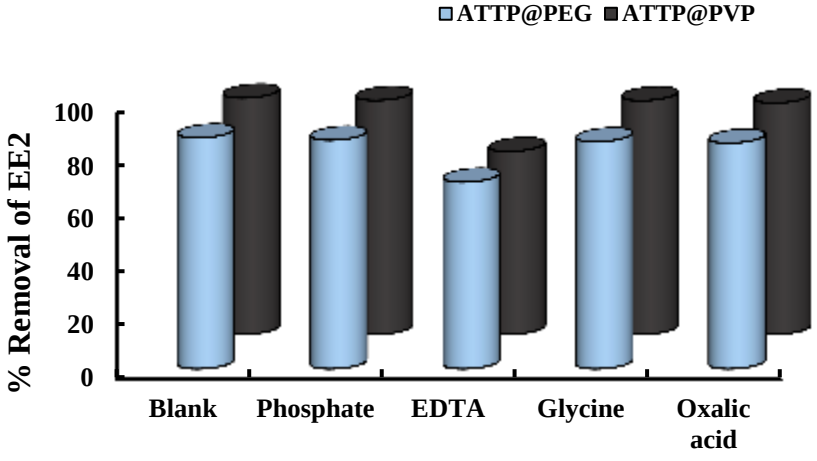

Figure 3.49. Effect of co-existing anions in the removal of EE2 by ATTP@PEG and ATTP@PVP solids ([EE2]: 10.0 mg/L; [Anions]: 50.0 mg/L; pH: 6.08; Solid dose: 2.0 g/L; Temperature: 25°C).

The removal of ciprofloxacin using ATTP@PEG and ATTP@PVP is studied in presence of several co-existing cations (Mg(II), Mn(II), Ca(II) and Ni(II)) and anions Ethylenediaminetetraacetic acid (EDTA), oxalic acid, glycine, and phosphate). The co-existing ions concentration was taken 50.0 mg/L and CIP concentration 10.0 mg/L at pH 7.0 and the results are shown in Figure 3.50. and 3.51. for cations and anions, respectively. The presence of EDTA significantly suppressed the removal of CIP due to the organophilic interactions of the organic EDTA with the solid surface. On the other hand, it is observed that the presence of other cations or anions did not affect the removal of CIP from aqueous solutions. Therefore, the findings further showed the selectivity and the efficiency of ATTP@PEG and ATTP@PVP towards CIP in presence of several cations/anions. Similarly, magnetic acid-activated carbons (MAAC) also showed similar removal trends for CIP removal in the presence of Mg(II), Mn(II), Ca(II) and Ni(II) (A. Kumar et al., 2022).

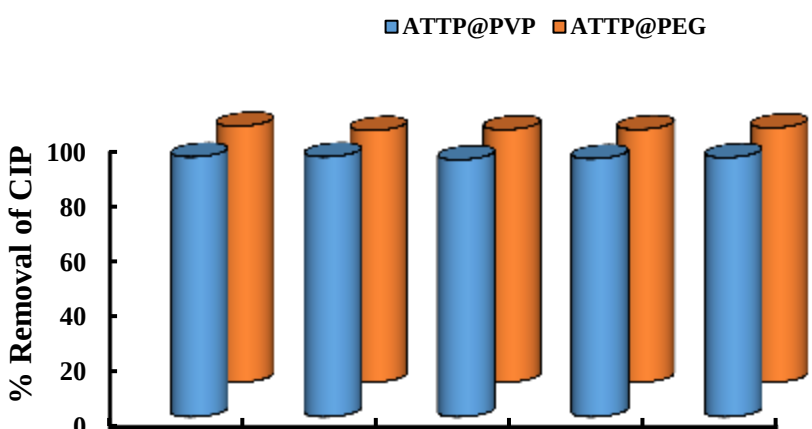

Figure 3.50. Effect of co-existing cations in the removal of CIP by ATTP@PEG and ATTP@PVP solids ([CIP]: 10.0 mg/L; [Cations]: 50.0 mg/L; pH:7.0; Solid dose: 2.0 g/L; Temperature: 25°C).

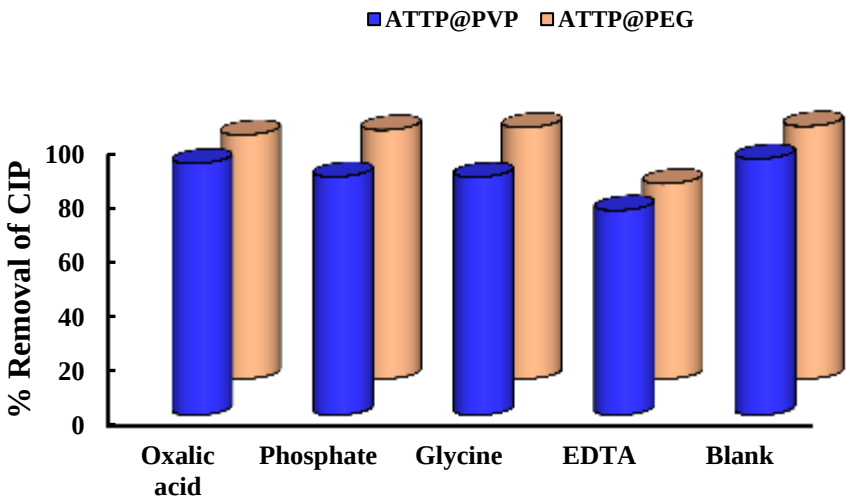

Figure 3.51. Effect of co-existing anions in the removal of CIP by ATTP@PEG and ATTP@PVP solids ([CIP]: 10.0 mg/L; [Anions]: 50.0 mg/L; pH: 7.0; Solid dose: 2.0 g/L; Temperature: 25°C).

The presence of several co-existing ions in the removal of BPA by the ATTP@PEG and ATTP@PVP solids, respectively was conducted by keeping the initial concentration of BPA at 10.0 mg/L, co-existing ions concentration of 50.0 mg/L at constant pH 6.06. The cations chosen are Mn(II), Mg(II), Ca(II), and Ni(II) whereas the anions are ethylenediaminetetraacetic acid (EDTA), glycine, phosphate, and oxalic acid. Results are shown in Figures 3.52 and 3.53 for cations and anions respectively. Figure 3.52. shows that none of those cations had a significant effect on BPA removal by ATTP@PEG and ATTP@PVP, which might be due to the strong binding affinity between BPA and the solids. In agreement with our results, a previous study showed that Ca(II) did not affect BPA removal by soil column experiments (Li et al., 2008). It was reported that the competitive adsorption ability differs from one metal ion to another and is associated with numerous factors, e.g., molecular mass, ion charges, hydrated ionic radius, and hydration energy of the metals (Ni et al., 2019). Thus, the coexisting cations did not compete with BPA for the active sites on the ATTP@PEG and ATTP@PVP nanocomposites, proposing multi-surface adsorption. The presence of co-existing anions slightly inhabited the sorption of BPA. The adsorption of BPA with ATTP@PVP decreased significantly in the presence of phosphate ions. This decrease in percentage removal maybe due to the hydrolysis reaction of PVP molecules since phosphate ions (PO_4^{3-}) can indirectly produce hydroxide ions (OH^-) in aqueous solutions. Further, the presence of EDTA reduced the removal efficiency of BPA by ATTP@PEG from 86.5% to 75.5% and 88.5% to 77.8% by ATTP@PVP respectively. These results show that EDTA preferentially occupies the active sites of the solid and suppresses the uptake of BPA in aqueous medium.

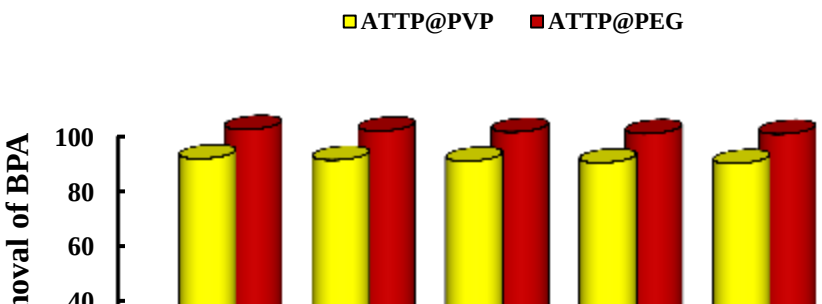

Figure 3.52. Effect of co-existing cations in the removal of BPA by ATTP@PEG and ATTP@PVP solids ([BPA]: 10.0 mg/L; [Cations]: 50.0 mg/L; pH: 6.0; Solid dose: 2.0 g/L; Temperature: 25°C).

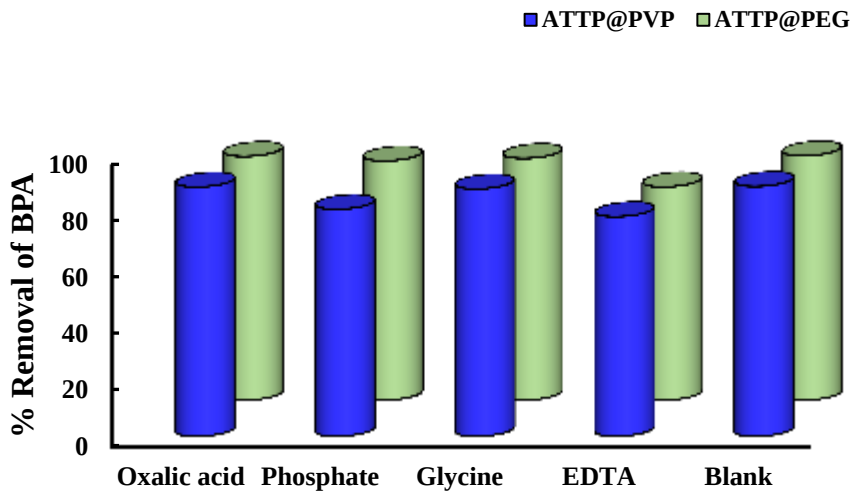

Figure 3.53. Effect of co-existing anions in the removal of BPA by ATTP@PEG and ATTP@PVP solids ([BPA]: 10.0 mg/L; [Anions]: 50.0 mg/L; pH: 6.06; Solid dose: 2.0 g/L; Temperature: 25°C).

3.3.8. Column reactor studies

To determine the removal/loading capacity and the applicability of ATTP@PEG and ATTP@PVP in real water treatment, a fixed bed column

experiment was conducted under dynamic conditions. Therefore, column studies were conducted for the removal of tetracycline, ciprofloxacin, bisphenol A, and EE2 from aqueous solutions. The detailed experimental procedures are followed as described previously (Chapter 2.4.8).

3.3.8.1. Tetracycline, bisphenol A, ciprofloxacin and EE2

The micro-pollutant removal was obtained under the fixed-bed column operations and the loading capacity of ATTP@PEG and ATTP@PVP was assessed for the tetracycline, bisphenol A, ciprofloxacin and EE2 under the dynamic conditions. Tetracycline and bisphenol A concentrations were taken as 10.0 mg/L at pH 3.5 and pH 6.06, respectively, and the column was packed with the 0.25 g of solid i.e., ATTP@PVP beads. The breakthrough curves were obtained for both these pollutants and shown in Figure 3.54. It is noted that a high breakthrough volume was achieved using the material. Further, a complete breakthrough volume is obtained at throughput volume of 2.08 L for tetracycline and 1.51 L for bisphenol A. The breakthrough results are fitted to the Thomas equation and the unknown parameters i.e., the Thomas constants (K_T), loading capacity (q_o) was optimized. The fitting results are shown in Table 3.15. The column results indicated that very high loading capacity was achieved using the ATTP@PVP beads for the removal of both TCH and BPA under the continuous flow system. These results further pointed the potential of the solid for practical implacability in the decontamination of tetracycline or bisphenol A from aqueous wastes.

It was reported earlier that increasing the bed height of modified silica from 3 to 10 cm for the sorption of tetracycline in column experiments leads to enhance the removal capacity from 388.5 to 412.7 mg/g (Liu et al., 2013). Moreover, bentonite modified with hexadecyltrimethylammonium bromide (BH), aluminium pillared bentonite modified with hexadecyltrimethylammonium bromide (BAH), local clay modified with hexadecyltrimethylammonium bromide (LCH) and aluminium pillaring local

clay modified with hexadecyltrimethylammonium bromide (LCAH) showed high removal capacity 111.979, 97.987, 86.965, 64.996 mg/g for tetracycline under fixed bed column operations (Thanhmingliana et al., 2015).

Table 3.15. Thomas constants estimated for the removal of tetracycline and bisphenol A by ATTP@PVP beads ([TCH/BPA]: 10.0 mg/L; Flow rate: 1.0 mL/min; pH: 3.5 and 6.06; Amount of solid loaded: 0.25 g; Temperature: 25°C).

Pollutant	Amount of ATTP@PVP beads (g)	Thomas constant		Least square sum (s^2)
		q_o (mg/g)	K_T (L/min/mg)	
TCH	0.25	3.50±0.04	$4.8 \pm 0.06 \times 10^{-4}$	1.1×10^{-1}
BPA	0.25	3.0± 0.04	$6.09 \pm 0.04 \times 10^{-4}$	1.2×10^{-1}

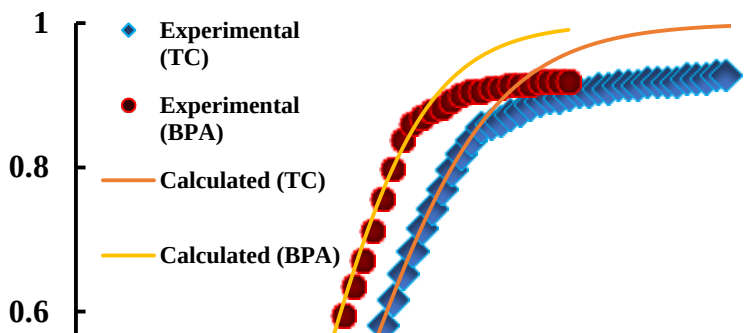

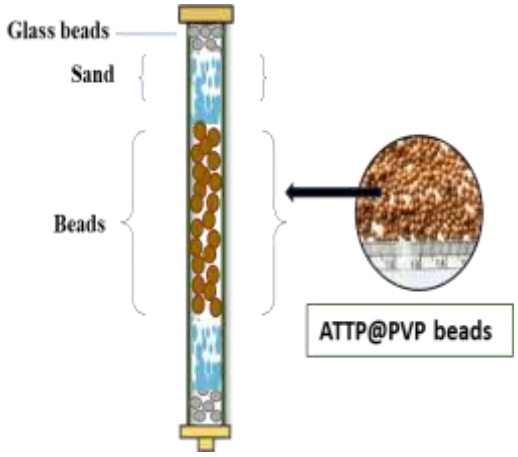

Figure 3.54. Breakthrough curves for the removal of tetracycline and bisphenol A by ATTP@PVP beads (Pollutant concentrations: 10.0 mg/L; flow rate: 1.0 mL/min; pH: 3.5 for tetracycline, and pH: 6.06 for bisphenol A; the amount of solid loaded: 0.25 g; Temperature: 25°C).

The loading capacity of ATTP@PEG beads for CIP and EE2 was obtained under the fixed-bed column reactor operations. The breakthrough results are shown in Figure 3.55. It is evident from the breakthrough curves that the material possessed relatively high breakthrough volumes for both the micro-pollutants i.e., CIP and EE2. A complete breakthrough for EE2 was achieved having a throughput volume of 1.21 L using 0.25 g ATTP@PEG beads. Similarly, a complete breakthrough for CIP is attained at the volume of 1.51 L using 0.25 g of ATTP@PEG beads, respectively. Breakthrough data is intended to be utilized for a non-linear least square fitting using the Thomas equation. The fitting results are illustrated in Figure 3.55. Moreover, optimized constants are returned in Table 3.16. Results showed that under the dynamic conditions, the ATTP@PEG possessed a very high loading capacity for EE2 and CIP. This again reaffirmed that ATTP@PEG has the potential to eliminate

EE2 and CIP from aqueous wastes. The removal of EE2 by aliphatic polyamides612 (PA612) fixed-bed adsorption column could remove EE2 from 10,700-bed volumes (24.1 L) of EE2 concentration (30 µg/L) to non-detectable levels by the HPLC analysis before column breakthrough. On increasing the concentration of EE2 by 10- and 100-fold, the treatment capacity reduced to 6600-bed volumes (14.9 L) and 3800-bed volumes (8.6 L), respectively before the column breakthrough. The results further reveal the efficiency and large treatment capacities of fixed-bed PA612 particles for the removal of EE2 from water on a continuous flow basis (Han et al., 2012).

Table 3.16. Thomas constants for EE2 and CIP using ATTP@PEG beads ([EE2/CIP]: 10.0 mg/L; Flow rate: 1.0 mL/min; pH: 6.08 and 7.0; Amount of solid loaded: 0.25 g; Temperature: 25°C).

Pollutant	**Amount of ATTP@PEG beads (g)**	**Thomas constant**		**Least square sum (s^2)**
		q_o (mg/g)	**K_T (L/min/mg)**	
CIP	0.25	2.7±0.04	$6.5 \pm 0.06 \times 10^{-4}$	1.2×10^{-1}
EE2	0.25	2.3± 0.04	$7.09 \pm 0.04 \times 10^{-4}$	1.1×10^{-1}

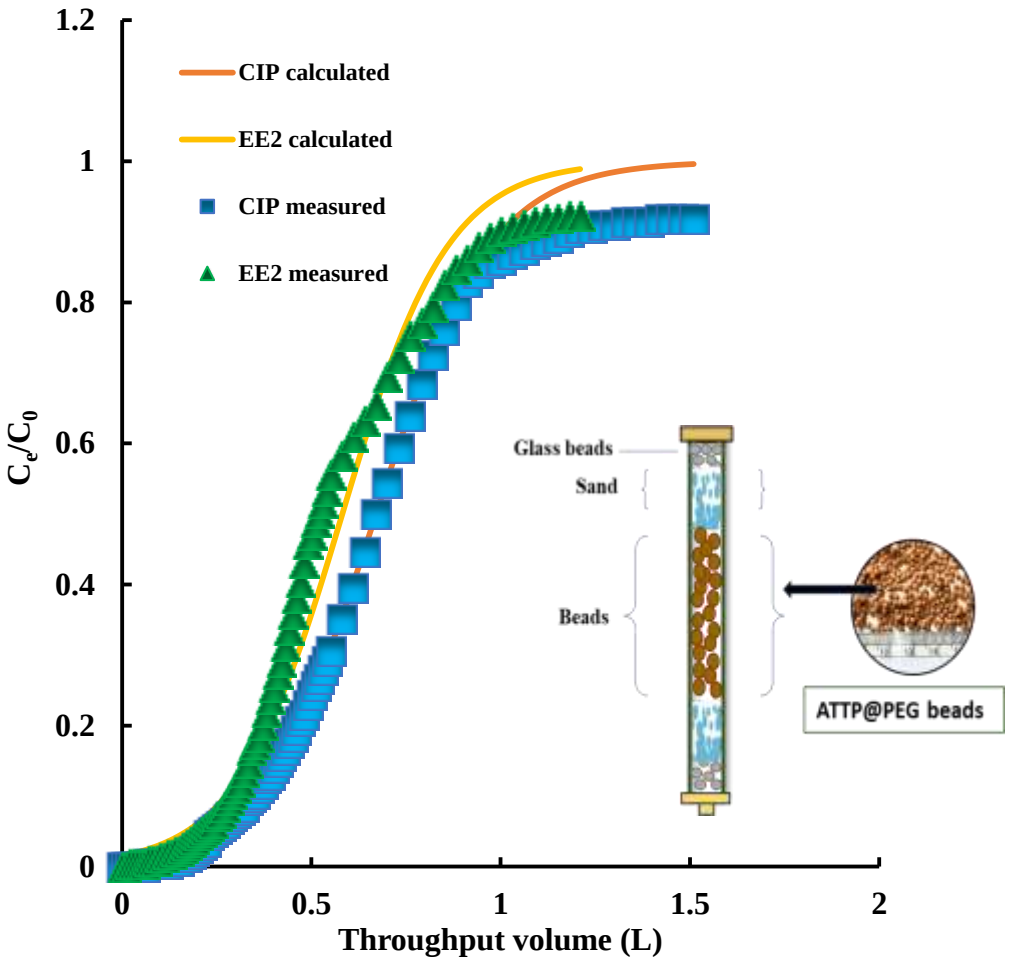

Figure 3.55. Breakthrough curves obtained for the removal of CIP and EE2 using nanocomposite ATTP/PEG [CIP (10.0 mg/L, pH 7.0) and EE2 (10.0 mg/L, pH 6.08); Flow rate: 1.0 mL/min].

3.3.9. Desorption and reusability of the solids

It is important to find a suitable eluent for desorption with appropriate concentrations that allow the adsorbent's reusability. It was found that 0.01 mol/L HCl is a suitable eluent to desorb the pre-adsorbed tetracycline, bisphenol A, ciprofloxacin, triclosan and EE2 from ATTP@PEG and ATTP@PVP solids.

The percentage desorption of tetracycline using 0.01 mol/L HCl from ATTP@PEG and ATTP@PVP was found to be 96.3 and 97.4%, respectively within 120 mins. The reusability of ATTP@PEG and ATTP@PVP for the removal of tetracycline is graphically shown in Figure 3.56. The percentage removal of tetracycline was decreased from 85.9 to 82.0% using ATTP@PEG and 86.4 to 81.9% using ATTP@PVP for six adsorption-desorption cycles. A slight decrease in the sorption of TCH in successive operations is due to the destruction of active sites or loss of solids in repeated HCl washings. Both the pH of the solution and the electrostatic attraction between the sorbate species and the composite material are weakened by the concentration of HCl. Furthermore, at low pH levels, the hydroxyl groups on the solid surface become undissociated and obstruct the hydrogen bonding. Furthermore, the sorbate species desorb from the surface as a result of the HCl-induced weakening of the organophilic contacts between the sorbate species and the solids. Previously, the reusability of activated carbon (TAC) for tetracycline was conducted using 0.05 mol/L NaOH eluent. The adsorption-desorption experiments showed that the adsorption capacity of TAC was decreased from 98.57 mg/g to 53.80 mg/g at the end of five cycles of operations (Sayğili & Güzel, 2016).

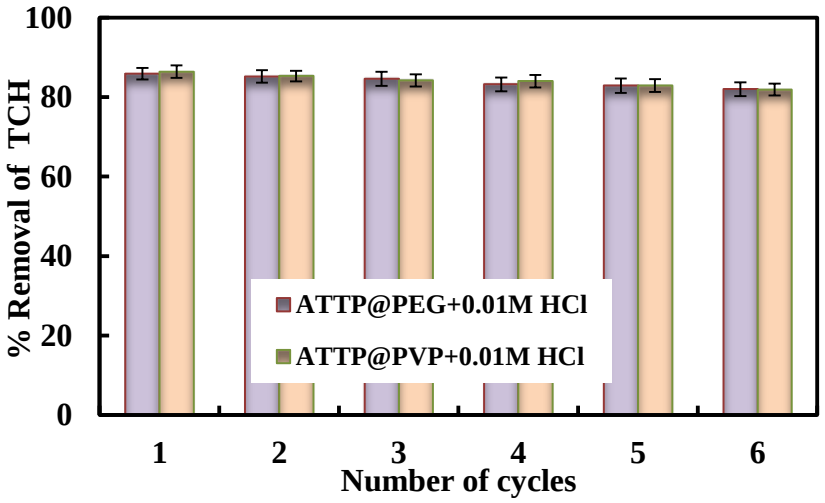

Figure 3.56: Reusability of ATTP@PEG and ATTP@PVP for the removal of tetracycline ([TCH]:10.0 mg/L; Solid dose: 2.0 g/L; [HCl]: 0.01 mol/L; pH: 3.5).

The percentage desorption of triclosan using 0.01 mol/L HCl from ATTP@PEG and ATTP@PVP was found to be 92.3.5 and 94.4%, respectively within 60 mins. The reusability of ATTP@PEG and ATTP@PVP for the removal of triclosan is shown in Figure 3.57. Results showed that the percentage removal of triclosan decreased from 92.3 to 86.3% using ATTP@PEG and 94.4 to 87.2% using ATTP@PVP while the material was utilized for six cycles of adsorption-desorption. This might be because some active adsorption sites were lost when ATTP@PEG and ATTP@PVP were desorbed with 0.01 mol/L HCl. The reusability of bentonite modified with dioctadecyldimethylammonium (2C18-BT) was performed using n-hexane as a desorbing agent for five adsorption/desorption cycles for triclosan. It was found that more than 98% of triclosan was desorbed from 2C18-BT after washing with n-hexane. Triclosan was fully adsorbed and desorbed from 2C18-BT for the first cycle. The amount of triclosan adsorbed slightly decreased after subsequent adsorption/desorption cycles, however, the removal percentage was 98.7% after the fifth cycle. The quantity of residual triclosan increased slightly upon repeating the adsorption/washing cycles (Phuekphong et al., 2020). In another study, it was reported that the removal percentage of triclosan using chitosan/poly (vinyl alcohol) 158 (CS/PVA) composite nanofibrous membranes was above 67% after five regeneration cycles when treated with 95% ethyl alcohol for 240 mins which revealed the good reusability of nanofibrous membranes (Liu et al., 2013).

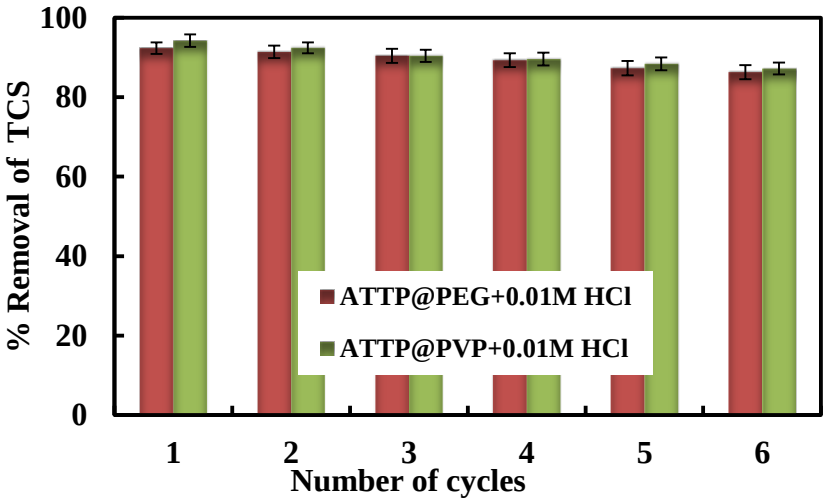

Figure 3.57. Reusability of ATTP@PEG and ATTP@PVP for the removal of triclosan ([TCS]:10.0 mg/L; Solid dose: 2.0 g/L; [HCl]: 0.01 mol/L; pH: 4.0).

Similarly, the percentage desorption of EE2 using 0.01 mol/L HCl from ATTP@PEG and ATTP@PVP were found to be 87.2 and 89.6%, respectively within 120 mins of contact. The reusability of ATTP@PEG and ATTP@PVP for the removal of EE2 is shown in Figure 3.58. It was observed that the percentage removal of EE2 decreased from 87.2 to 82.7% using ATTP@PEG and 89.6 to 84.0% using ATTP@PVP while the materials were employed for six adsorption-desorption cycles. The lack of irreversible partial-adsorption site filling on the ATTP@PEG and ATTP@PVP outer layer causes a decrease in the

removal rate. Previously, it was also reported that acetonitrile was used to desorb the pre-adsorbed 17α-ethinylestradiol (EE2) onto montmorillonite intercalated with cetyltrimethylammonium cation (CTA^+). Results showed that this material is favourably regenerated using acetonitrile and is reused without substantial loss of adsorption capacity even after five reuses (Burgos et al., 2016).

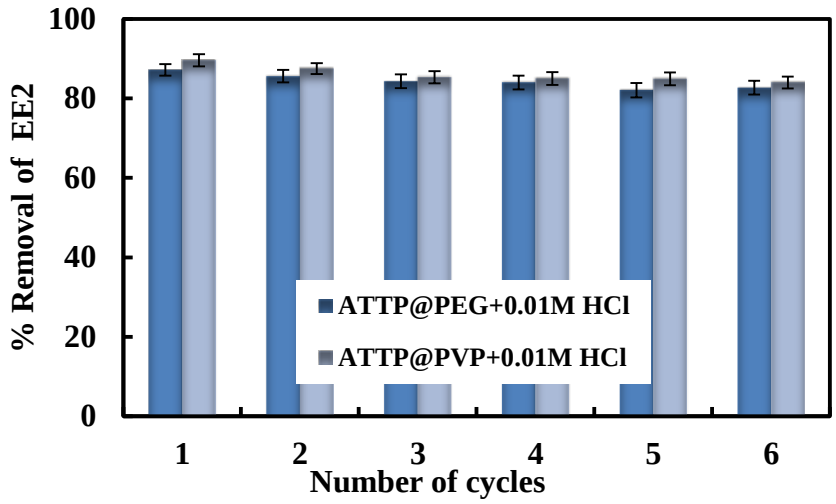

Figure 3.58. Reusability of ATTP@PEG and ATTP@PVP for the removal of EE2 ([EE2]:10.0 mg/L; Solid dose: 2.0 g/L; [HCl]: 0.01 mol/L; pH: 6.08).

The percentage desorption of ciprofloxacin using 0.01 mol/L HCl from ATTP@PEG and ATTP@PVP was found to be 98% and 96% within 60 mins of contact. The reusability of ATTP@PEG and ATTP@PVP for the removal of CIP is graphically shown in Figure 3.59. It was found that the percentage removal of CIP was found to decrease from 93.2 to 89.9% using ATTP@PVP and from 89.0 to 86.5% using ATTP@PEG with six replicates adsorption-desorption cycles. The HCl concentration lowers the pH of the solution and weakens the electrostatic attraction between the sorbate species and the

composite material. Additionally, the hydroxyl groups at the solid surface are undissociated at low pH conditions and hinders the hydrogen bonding. Moreover, the presence of HCl weakens the organophilic interactions between the sorbate species and the solid, which results in the desorption of sorbate species from the surface.

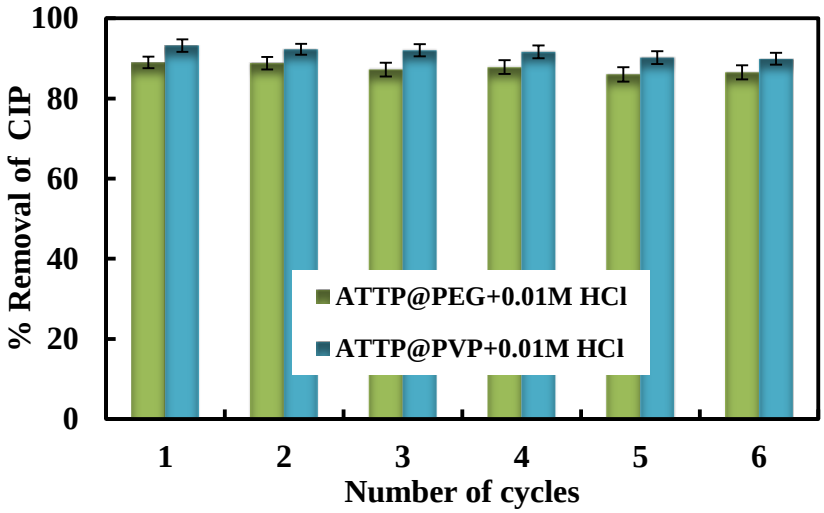

Figure 3.59. Reusability of ATTP@PEG and ATTP@PVP for the removal of CIP [CIP]:10.0 mg/L; Solid dose: 2.0 g/L; [HCl]: 0.01 mol/L; pH: 7.0).

For the stability and reuse of ATTP@PEG and ATTP@PVP in a repeated cycle of sorption/desorption operations, it is necessary to consider the material's potential for reuse. The results indicated that the 0.01 M HCl effectively removes the pre-sorbed BPA from the ATTP@PEG and ATTP@PVP solids. The desorption was conducted by equilibrating the pre-sorbed ATTP@PEG and ATTP@PVP with the desorption solutions for 120 mins of contact. The results revealed that the percentage removal of BPA

decreased from 88.8 to 86.2% from the 1st to the 5th cycle of operation with ATTP@PVP. Similarly, from the 1st to the 5th cycle of sorption/desorption, experiments showed that the BPA percentage removal decreased from 85.5 to 83.0% with ATTP@PEG, respectively. This could be an indication that treatment of the adsorbent with HCl increases the positive sites on the surface of the material. Slight decrease as the reuse-regeneration cycles continues to 5th cycle. The decrease could be due to inadequate regeneration of the sorption sites. Another study showed that after five cycles (adsorption/desorption), the adsorption removal percentage of BPA using methanol, was slightly declined from 100 to 83%, which points out that activated carbon synthesized from the shrimp shell plus cellulose (SS@C-AC) is a promising renewable adsorbent (Zafar et al., 2022).

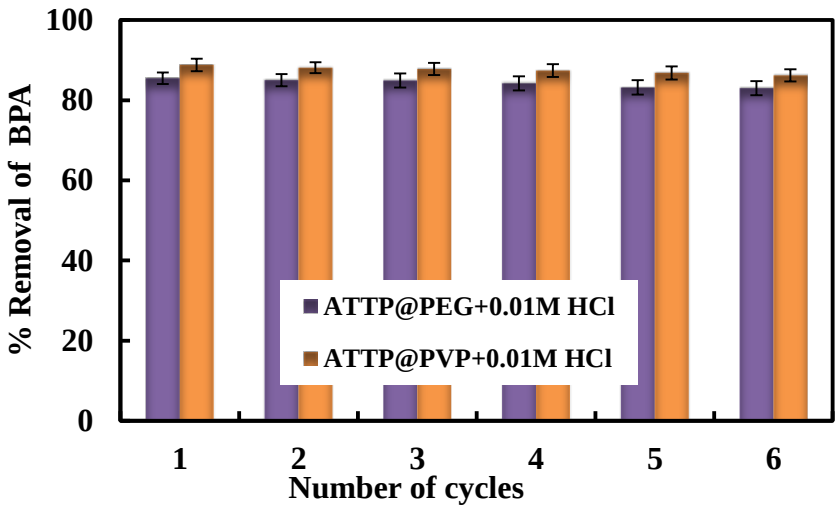

Figure 3.60. Reusability of ATTP@PEG and ATTP@PVP for the removal of BPA ([BPA]:10.0 mg/L; Solid dose: 2.0 g/L; [HCl]: 0.01 mol/L; pH: 6.06).

3.3.10. Applications of ATTP@PEG and ATTP@PVP materials in real water samples

A treated wastewater sample was collected from the SIPMUI Treated water and employed in removing tetracycline and bisphenol A using ATTP@PVP to simulate the studies for real matrix treatment. The water sample was studied for various physico-chemical parametric analyses and the results are returned in Table 3.1. of Chapter 3. The analyses revealed that Cu, Ni, and Al level in the treated water is below detection limit and Pb is 0.35 mg/L. However, the content of Ca and Mg were relatively high as 136.0 and 16.0 mg/L, respectively. Similarly, the TOC analysis of the water showed high inorganic carbon (14.506 mg/L) and with moderate non-purgeable organic carbon (NPOC: 1.679 mg/L). Additionally, the water sample contained with sulphate (2.0 mg/L), phosphate (2.50 mg/L), and nitrates (5.7 μ/L). The real water sample was spiked with known concentrations of tetracycline and bisphenol A at pH 3.5 (for tetracycline) and 6.06 (for bisphenol A). Figure 3.61 displays the concentration-dependent ATTP@PVP removal efficiency for tetracycline and bisphenol A in a natural water matrix. Figure 3.61 also compares the percentage removal of these pollutants in treated water with the purified water as well. The findings showed that, in comparison to purified water, the removal efficiency of ATTP@PVP is not significantly affected at least in the removal of tetracycline and bisphenol A in natural water samples. The pollutant removal at 1.0 mg/L is 95.8% and 92.8% for TCH and BPA in distilled water (DW) compared to SIPMUI water (STW) showed a percentage removal of 94.8% and 91.8% for TCH and BPA, respectively. Therefore, the ATTP@PVP exhibits good selectivity and applicability in attenuating the tetracycline and bisphenol in real water samples.

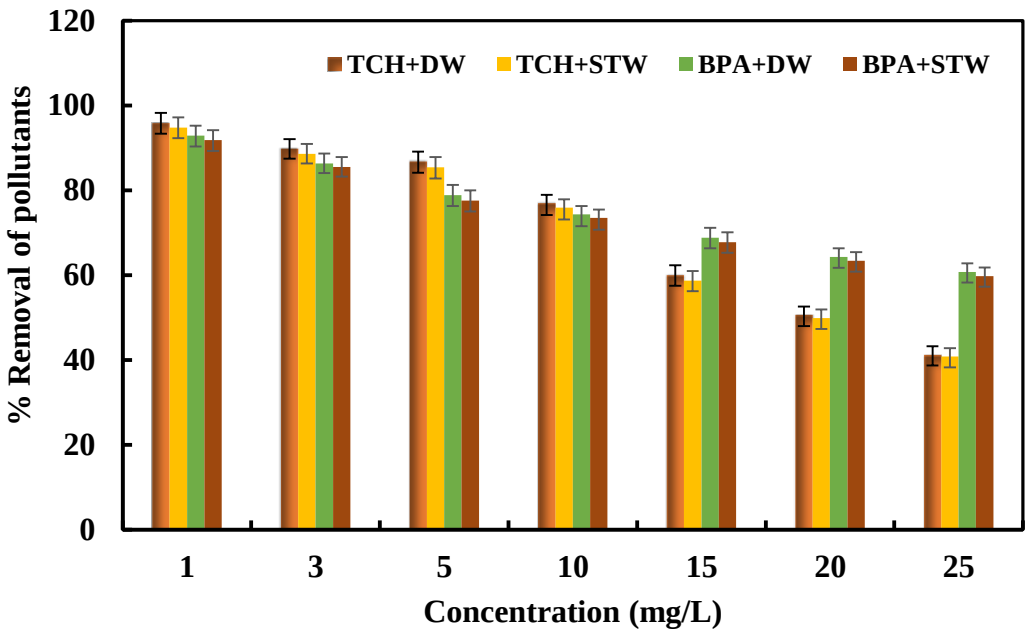

Figure 3.61: Removal of TCH and BPA in distilled water (DW) and SIPMUI treated water (STW) samples using ATTP@PVP nanocomposite at varied sorptive concentrations.

A natural water sample was collected from the Tlawng River, Aizawl, and employed in the removal of ciprofloxacin and triclosan using ATTP@PEG to simulate the studies for real matrix treatment. The water sample was studied for various physico-chemical parametric analyses and the results are returned in Table 3.1. of Chapter 3. The analyses revealed that the Cu, Ni, and Al level in the river water is below detection limit and Pb is 0.10 mg/L. However, the content of Ca and Mg were relatively high as 35.0 and 4.5 mg/L, respectively. Similarly, the TOC analysis of the stream water showed high inorganic carbon (16.004 mg/L) and with moderate non-purgeable organic carbon (NPOC: 1.043 mg/L). Additionally, the water sample contained with sulphate (4.0 mg/L), phosphate (0.4 mg/L), and nitrates (4.0 µ/L). The river water was spiked with known concentrations of ciprofloxacin and triclosan at pH 7.0 (for ciprofloxacin) and 4.0 (for triclosan). Figure 3.62 displays the concentration-dependent ATTP@PEG removal efficiency for ciprofloxacin and triclosan in a natural water matrix. Figure 3.62 also compares the percentage removal of

these pollutants in river water with the purified water as well. The findings showed that, in comparison to purified water, the removal efficiency of ATTP@PEG is not significantly affected at least in the removal of ciprofloxacin and triclosan in natural water samples. The pollutant removal at 1.0 mg/L is 95.6% and 93% for CIP and TCS in distilled water (DW) compared with Tlawng river water (TW) showed a percentage removal of 88.6% and 85.5% for CIP and TCS, respectively. Therefore, the ATTP@PEG exhibits good selectivity and applicability in attenuating the ciprofloxacin and triclosan in real water samples.

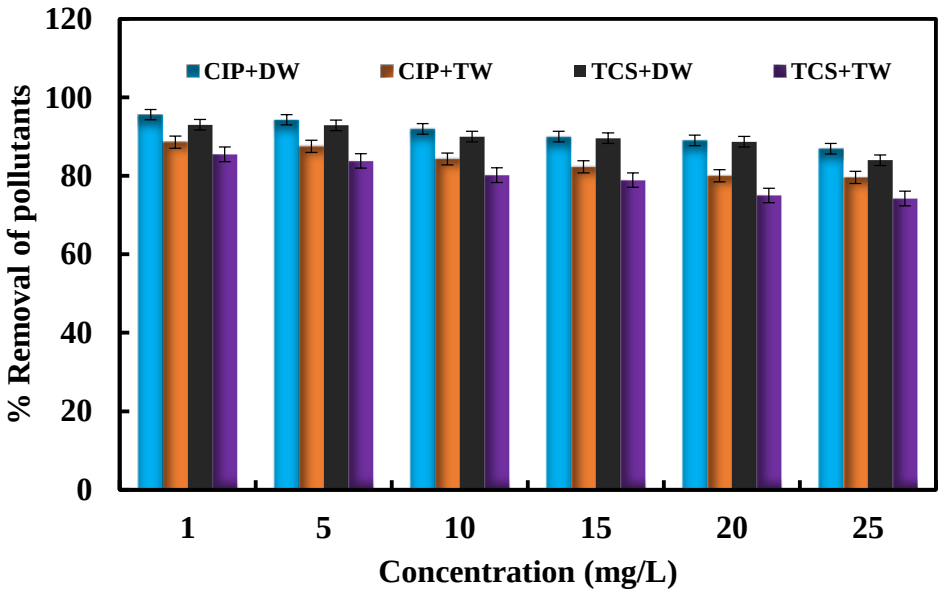

Figure 3.62: Removal of CIP and TCS in distilled water (DW) and Tlwang water (TW) samples using ATTP@PEG nanocomposite at varied sorptive concentrations.

3.3.11. Adsorption mechanism of TCH, BPA, CIP, EE2 and TCS by nanocomposites

The plausible mechanism for the removal of TCH and BPA using the ATTP@PVP composite is given in Figure 3.63 (a). The hydroxyl (-OH) group present in TCH will likely form hydrogen bonds with the carbonyl group in the ATP@PVP composite (Giubertoni et al., 2020). The speciation studies show previously that the hydroxyl groups of TCH dissociate and form the anionic species (TCH^{-} or $TCH^{+\ -\ -}$) of TCH at pH>7.6, which further dissociated to anionic species (TCH^{2-} or $TCH^{0\ -\ -}$) at pH> 9.7. Though the TCH dissociated at a higher pH to form anionic species, the percentage removal of TCH remains relatively high (Figure 3.9) due to the presence of -OH remaining undissociated in the TCH molecule. Figure. 3.63 (b-c) shows the XPS spectra of O1s and C1s before and after adsorption of TCH and BPA. Figure. 3.63 (b) shows that the binding energy of O1s shifted from 531.8 to 532.7 eV after the adsorption of TCH, which indicates the interactions of TCH and BPA with the material through the carbonyl group suggesting the formation of hydrogen bond (He et al., 2020).

In the adsorption of BPA, the binding energy of O1s is shifted from 531.8 to 532.5 eV, indicating that the adsorption of BPA mainly occurs through the hydrogen bonding between the C=O of the composite and two hydroxyl groups presents in BPA (Sun et al., 2020). The speciation study shows that BPA dissociates by losing the H atom to form anionic species. Due to this, the number of hydrogen bonding decreases, and consequently, the removal of TCH declines as the pH of the solution increases. Furthermore, the binding energy of C1s (Figure. 3.63(c)) occurs at 285.44 eV, and the same occurs at 284.7 to 284.05 eV after the adsorption of TCH and BPA, respectively. Moreover, as shown in section 3.2.7, the contact angle test showed the degree of 64.0º and 102.9º for pristine attapulgite clay (ATTP) and ATTP@PVP, respectively, showing the hydrophobicity of the composite material (Yadav et al., 2023). Similarly, the contact angle of ATTP@PEG is 100.9º. Therefore, the TCH and BPA mainly adsorbed to ATTP@PEG composite through hydrophobic interactions. These results indicate that hydrophobic interactions between the ATTP@PVP composite and TCH and BPA. Furthermore, the XPS analysis

showed the binding energy of C1s Figure 3.63. (c) occurred at 285.44 eV, and shifted to 284.7 to 284.05 eV after the adsorption of TCH and BPA, respectively. This analysis results again confirm the strong hydrophobic interactions between the TCH and BPA and ATTP@PVP solid (Hotaby et al., 2017). In addition, the terminal hydroxyl groups in PEG molecule contributed for the formation of hydrogen bonding between the TCH and BPA and ATTP@PEG solid (Ibrahim et al., 2022). Therefore, the hydrogen bonding and hydrophobic interactions are the major pathways of removing TCH and BPA using ATTP@PEG/ATTP@PVP composite.

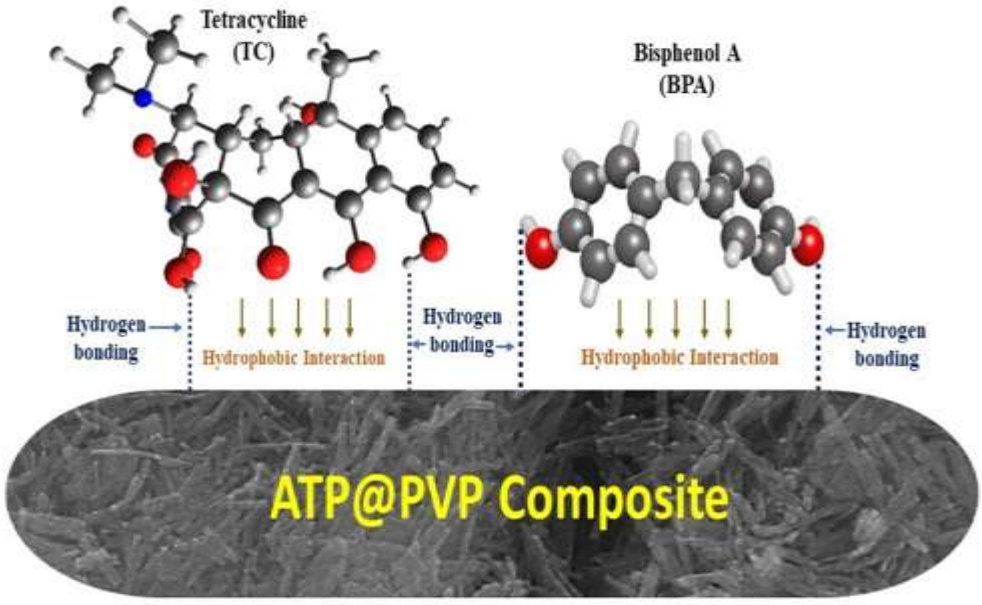

Figure 3.63 (a). Probable mechanism of adsorption of TCH and BPA onto ATTP@PVP solid.

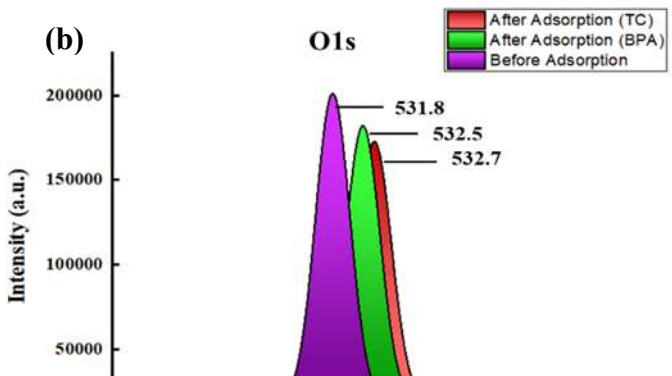

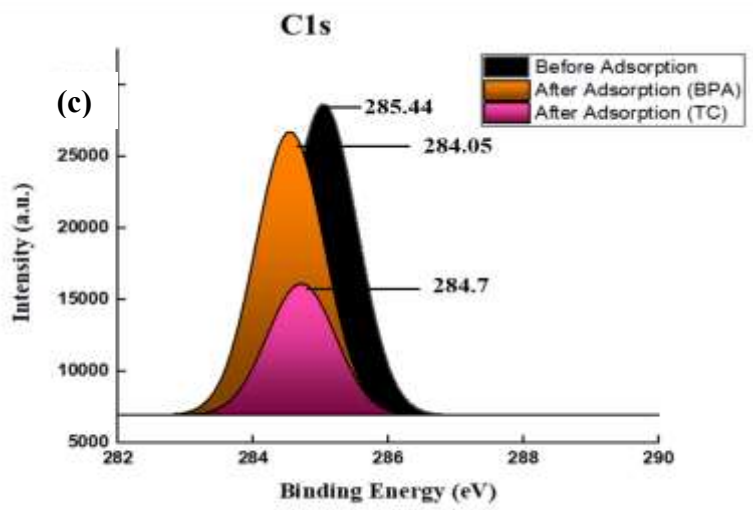

Figure 3.63. High-resolution XPS spectra for **(b)** O1s for before and after adsorption of TCH and BPA **(c)** C1s for before and after adsorption of TCH and BPA.

On the other hand, the adsorption mechanism of CIP, EE2 and TCS onto the ATTP@PEG composite had been investigated and shown in Figure 3.63 (d). The pH studies demonstrate the adsorption mechanism of CIP and EE2 onto ATTP@PEG and the pollutant species' speciation studies. The ATTP@PEG has a pH_{PZC} of 7.8, and the surface of the material possesses a positive charge due to protonation at pH < pH_{PZC}, and the deprotonation leads

to the negative charge of the surface at pH > pH_{PZC}. CIP produces three distinct species at various pHs: the zwitterion ($CIP^{\pm}$) between 6.1 and 8.7. pH 1.0-6.1 forms positively charged species CIP^{+} and CIP^{-} at pH>8.7 (Peng et al., 2015). Therefore, the high percentage removal of CIP mainly resulted from the attraction of CIP^{+} by the negatively charged surface of ATTP@PEG at lower pH and CIP^{-} and positively charged surface of ATTP@PEG at pH>8.7. Additionally, the relatively strong binding between CIP and the adsorbent occurred due to the formation of hydrogen bonding in this pH range, resulting in specific adsorption of CIP onto ATTP@PEG, which is in line with the effect of the background electrolytes study conducted at pH 7.0. Similarly, the impact of the background electrolytes study indicated that the ATTP@PEG specifically adsorbs EE2. Since EE2 is a neutral species at pH below 10.5, EE2 substantially adsorbed EE2 through the hydrophobic interactions (Luo et al., 2017). However, at pH above 8.0, the hydroxyl group in the composite surface dissociates, forming the hydrogen bond with the EE2 (A. da S. V. de Almeida et al., 2022). The contact angle measurement showed 100.9º for ATTP@PEG composite. This result again confirms the hydrophobicity of the material and showed the significant role of hydrophobic interactions in the removal of CIP/EE2/TCS using ATTP@PEG composite (Hazarika et al., 2023; Yadav et al., 2023). Further, the adsorption of TCS onto the ATTP@PEG composite occurred through the formation of hydrogen bond between the hydroxyl group of TCS and the ether group in the PEG chain of ATTP@PEG composite (Petersen et al., 2015). Moreover, the speciation showed triclosan mostly present as uncharged species at pH<7.9 and anionic species (i.e., TCS^{-}) predominate when the pH is greater than 7.9. Therefore, the hydrophobic interaction is between the ATTP/PEG and TCS is the main cause for high adsorption of triclosan from aqueous media (Liu & Zhang, 2013; Shrestha et al., 2020). Furthermore, the successful removal of CIP using the ATTP@PVP composite is mostly due to the hydrophobic interaction as well as electrostatic interactions between carbonyl group of ATTP@PVP composite of the amine group the of CIP (Olasupo et al., 2022). Similarly, the EE2 and TCS adsorption

using ATTP@PVP composite occurred with the combination of hydrophobic interaction and hydrogen bonding (Gui et al., 2020).

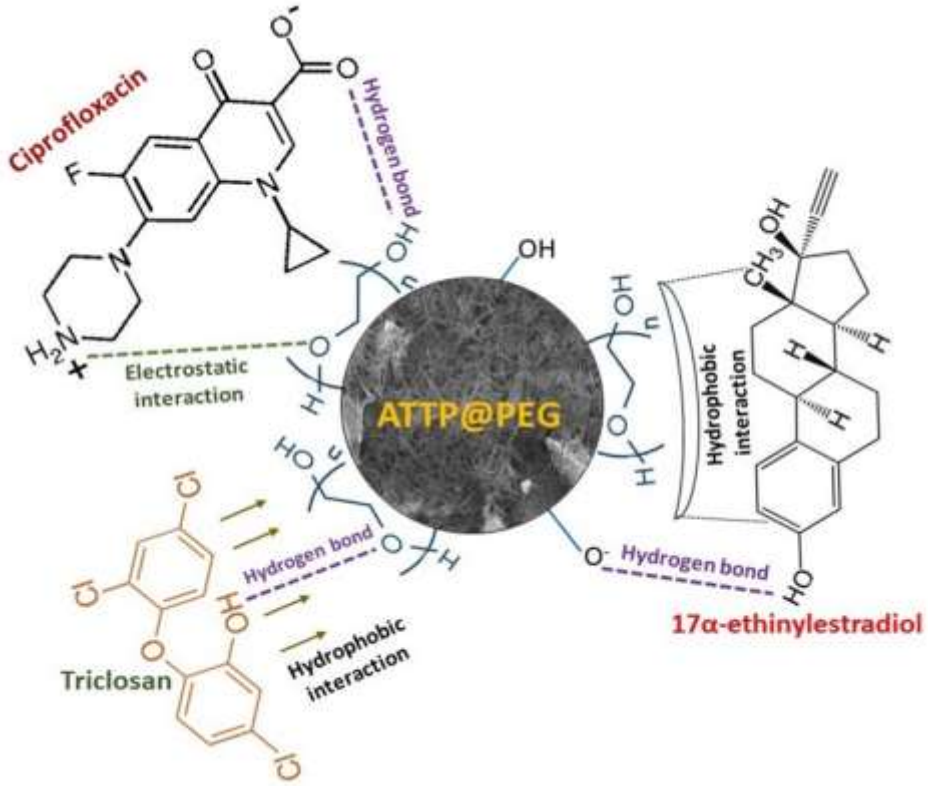

Figure. 3.63 (d). The plausible interactions of CIP, EE2 and TCS with ATTP@PEG

3.3.12. Inhibitory effect: Plate assay method

The findings of the ATTP@PEG/Ag˚ inhibiting effect against *Pseudomonas aeruginosa* and *Bacillus subtilis*, as well as the zones of inhibition (mm) around each well containing ATTP@PEG/Ag^0 and pure attapulgite clay as shown in Figure 3.64. The effectiveness of the material as a possible antibacterial agent is thus significantly revealed by the diameter of the zone of inhibition (Table 3.17).

The zone of inhibition against *P. aeruginosa* had a diameter of 13.6±0.3, 15.3±0.3, 19.3±0.2, and 23.2±0.6 mm for doses of 2.0, 4.0, 6.0, and 8.0 mg of ATTP@PEG/Ag^0, respectively. The measured diameter of the zone of inhibition against *B. subtilis* at the same ATTP@PEG/Ag^0 concentrations was 10.1±0.3, 13.4±0.4, 17.2±0.3 and 20.3±0.2 mm. However, the attapulgite (without Ag) did not inhibit the *P. aeruginosa* and *B. subtilis* (Figure 3.64). According to these findings, ATTP@PEG/Ag^0's antibacterial properties can be due to their broad surface area, which allows for more surface interaction with microbes.

Similarly, Figure 3.65. shows the photograph of zone of inhibition of pristine attapulgite clay and ATTP@PVP/Ag^0 nanocomposite against both Gram negative (*E. coli*) and Gram positive (*S. pyogenes*) bacteria. It is clearly observed that unlike pristine attapulgite clay, the clay/polymer/Ag nanocomposite shows good antibacterial activity against two model bacteria. Generally, the mean zone of inhibition of the ATTP@PEG/Ag^0 nanomaterial ranged between 3.2±0.9 mm and 8.1±0.5 mm for *E. coli* and 4.4±0.3 mm and 10.2±0.6 mm for *S. pyogenes*, and the most susceptible bacterium was *S. pyogenes* (Table 3.18.).

Table 3.17. Results of zone of inhibition for *P. aeruginosa* and *B. subtilis* (mean

+ standard error)

Bacterial	**Dosage of ATTP@PEG/Ag^0 (mg)**			
strain	2.0	4.0	6.0	8.0

P. aeruginosa	13.6 ± 0.3	15.3±0.3	19.3±0.2	23.2±0.6
B. subtilis	10.1±0.3	13.4±0.4	17.2±0.3	20.3±0.2

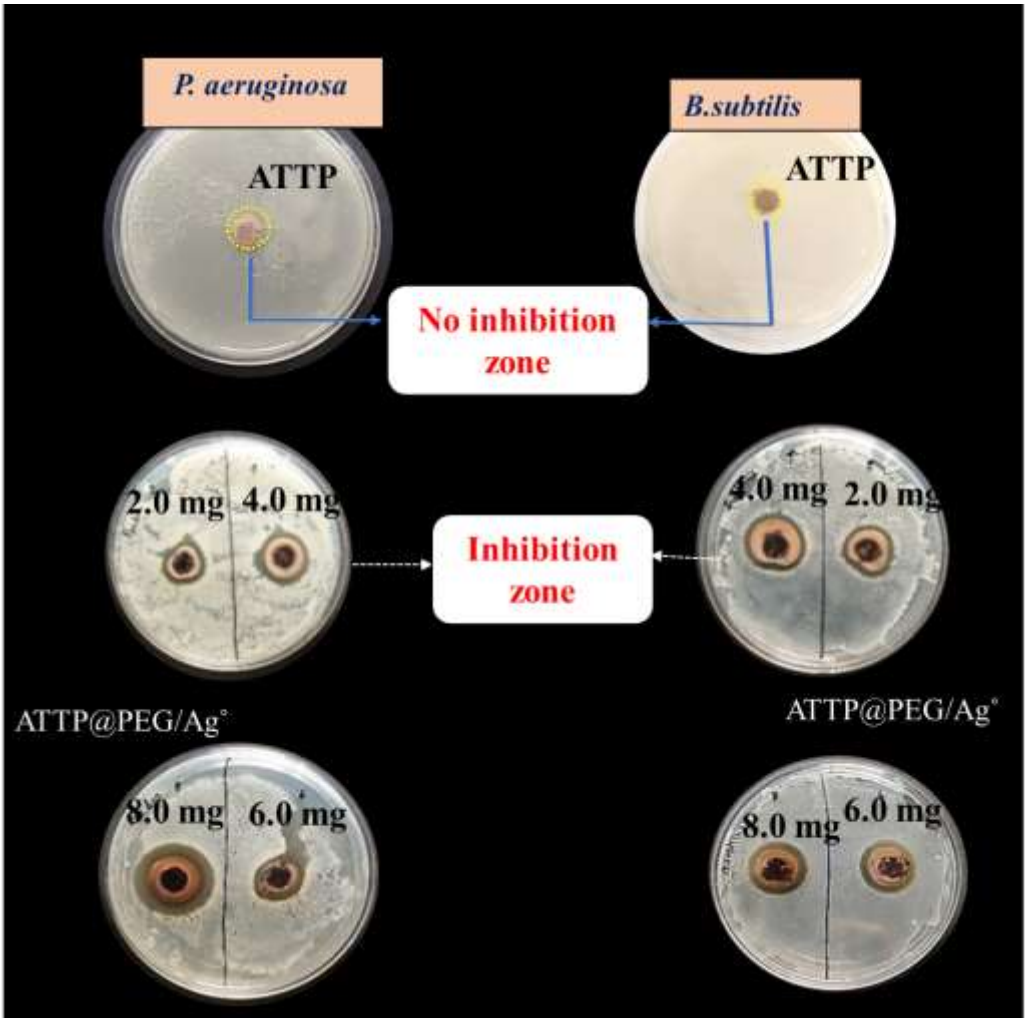

Figure 3.64. Zone of inhibition with ATTP clay and ATTP@PEG/Ag^0 against *P. aeruginosa* and *B. subtilis.* are shown using the disc diffusion technique via culture plates, illustrating the connection between material dosage and zone of inhibition.

Table 3.18. Results of zone of inhibition for *E. coli* and *S. pyogenes* (mean + standard error)

Bacterial strain	**Dosage of ATTP@PVP/Ag^0 (mg)**			
	2.0	4.0	6.0	8.0
E. coli	3.2 ± 0.9	4.1±0.2	6.2±0.3	8.1±0.5
S. pyogenes	4.4±0.3	6.4±0.4	8.3±0.3	10.2±0.2

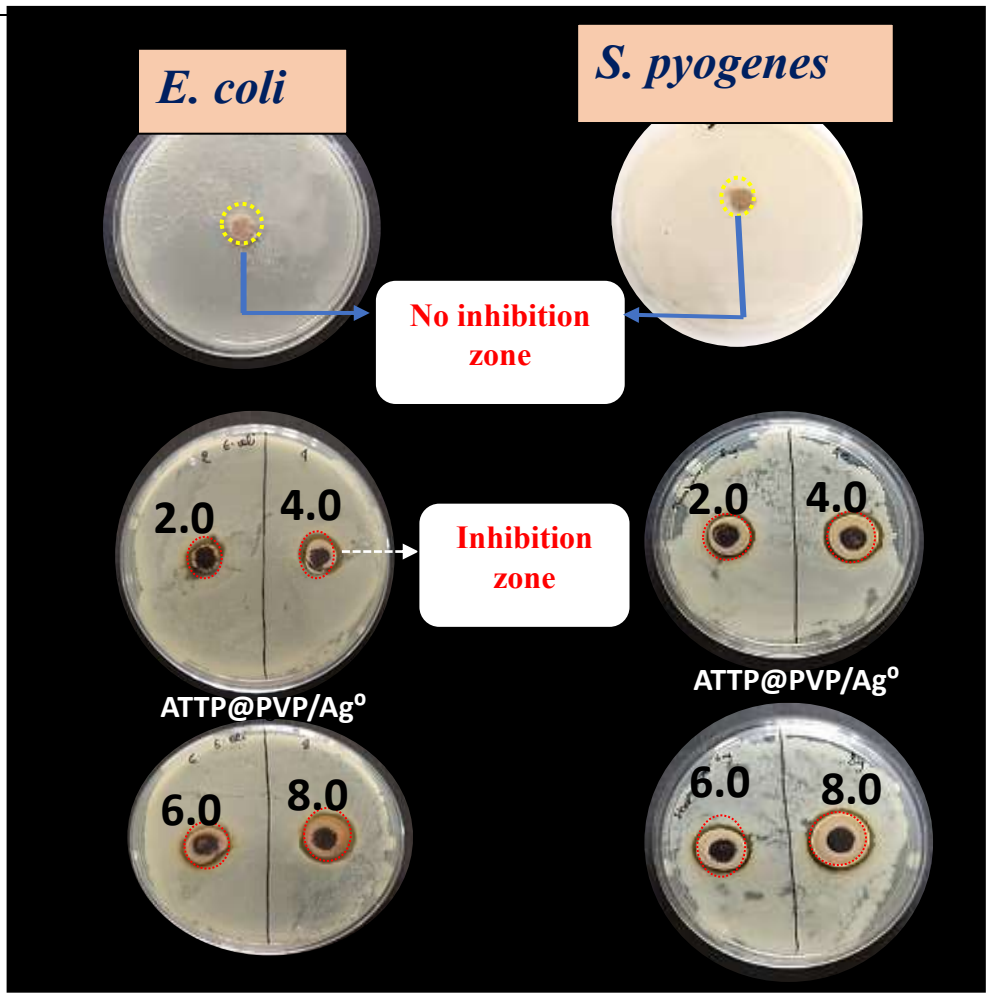

Figure 3.65. Zone of inhibition with ATTP clay and ATTP@PEG/Ag^0 against *E. coli* and *S. pyogenes* are shown using the disc diffusion technique via culture plates, illustrating the connection between material dosage and zone of inhibition.

3.3.13. Quantitative assessment of antibacterial activity of ATTP@PEG/Ag^0 and ATTP@PVP/Ag^0 nanocomposites

The antibacterial effect for different ATTP@PEG/Ag^0 concentrations against *P. aeruginosa* and *B. subtilis* was obtained under dynamic conditions using equation (2.8) of Chapter 2., and Table 3.19. shows the outcomes. The outcomes demonstrate that after contacting for 24 hrs, ATTP@PEG/Ag^0 eliminated all bacterial cells, demonstrating the bactericidal efficacy of ATTP@PEG/Ag^0 towards the two pathogenic bacteria *P. aeruginosa* and *B. subtilis*.

To optimize the doses of ATTP@PEG/Ag^0 towards both microbial strains, the initial dosage increased from 2.0 to 8.0 mg. Furthermore, the pristine attapulgite clay does not remove the investigated bacteria. Using a low dose of solid, i.e., 2.0 mg, *Pseudomonas aeruginosa* and *Bacillus subtilis* elimination were considerably influenced, with 95.0 and 94.0% reductions, respectively. The removal rate improved to 97.0 and 96.0%, respectively, for the increase in dose to 4.0 mg. The removal rate improved by 99.0% and 98.0% at 6.0 mg dosage. After a day of incubation with 100 mL of contaminated solution, the 8.0 mg of ATTP@PEG/Ag^0 eliminates both *P. aeruginosa* and *B. subtilis*, with a 100% decline in bacterial count. In comparison to *B. subtilis*, *P. aeruginosa* is more susceptible to ATTP@PEG/Ag^0 due to a combination of the structural vulnerability of its

Gram-negative cell wall, higher sensitivity to silver-induced reaction oxygen species (ROS), metabolic factors, and differences in biofilm dynamics. These factors collectively render *P. aeruginosa* more prone to the antimicrobial effects of silver nanoparticles.

Light, temperature, and oxygen levels strongly influence the redox behavior and, thus, the bactericidal impact of Ag in a material. Light irradiations reduce Ag (Yin et al., 2012), and rising temperatures hasten Ag^0 dissolution; hence, the testing performs at an ideal temperature of about 38˚C (Sadrnezhaad et al., 2006). Because of this, investigations examining the bactericidal impact of silver (Ag) consider the medium's physical properties. The Ostwald-Freundlich equation is another theoretical formula that describes the effect of particle form and size on silver ion release into the environment (Ely et al., 2014). Smaller silver nanoparticles with rounded or quasi-spherical forms possess greater surface space, as evidenced in the material's TEM examination results, and are more likely to release silver quickly (Jiménez et al., 2022).

Furthermore, the nanoparticles, generate silver ions at a lower rate than isolated nanoparticles. PEG decreases surface energy, stops grain development, and stops particle agglomeration. It offers electrostatic and steric stabilization effects for the Ag(NP) distribution in suspensions. The environment affects the dissolution of silver ions in addition to these inherent silver nanoparticles (Almatroudi, 2020). Organic or inorganic elements in media affect the dissolution of silver nanoparticles by associating with them or interacting with silver ions.

Silver nanoparticles produce silver ions that destroy pathogens through various mechanisms. Ag(NP) assemble in the pockets on the cell membrane after adhering to the cell surfaces, where they denaturize the cell membrane. Silver particles potentially permeate the cell walls of bacteria due to their nano size, changing the chemical composition of the cell membrane (Yin et al., 2020). The free silver ions taken by cells respiratory enzymes become inactive,

which produces ROS, which can function as a critical cause for both the membrane rupture and DNA modification and halting the production of adenosine triphosphate. The silver ions' interaction with phosphorus and sulfur in DNA interferes with cell development, replication of DNA, or even results in the death of bacteria. Additionally, silver nanoparticles are used in the signalling processes of bacteria (Anees Ahmad et al., 2020). Ag(NP) potentially dephosphorylated tyrosine residues on peptide substrates, and the phosphorylation process of protein substrates impacts how bacteria transmit signals. Dephosphorylation leads to cell apoptosis, and the cessation of cell division also results from signal transduction disruption. Silver ions also denaturize the cytoplasmic ribosomes, which potentially stops the synthesis of proteins.

Table 3.19. Antibacterial test results using dynamic contact method.

ATTP@PEG/Ag^0 concentration (mg)	**Percentage removal of *P. aeruginosa***	**Percentage removal of *B. subtilis***
Control	No removal	No removal
2.0	94.0	95.0
4.0	96.0	97.0
6.0	98.0	99.0
8.0	99.90	99.98

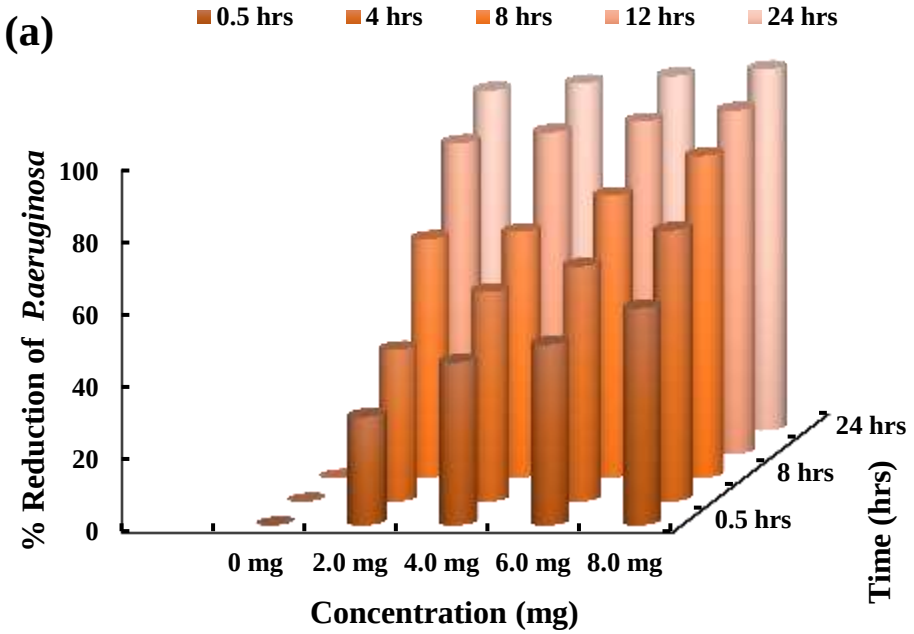
(a)
0.5 hrs
4 hrs
8 hrs
12 hrs
24 hrs
% Reduction of P.aeruginosa
100
80
60
40
20
0
0 mg
2.0 mg
4.0 mg
6.0 mg
8.0 mg
Concentration (mg)
24 hrs
8 hrs
0.5 hrs
Time (hrs)

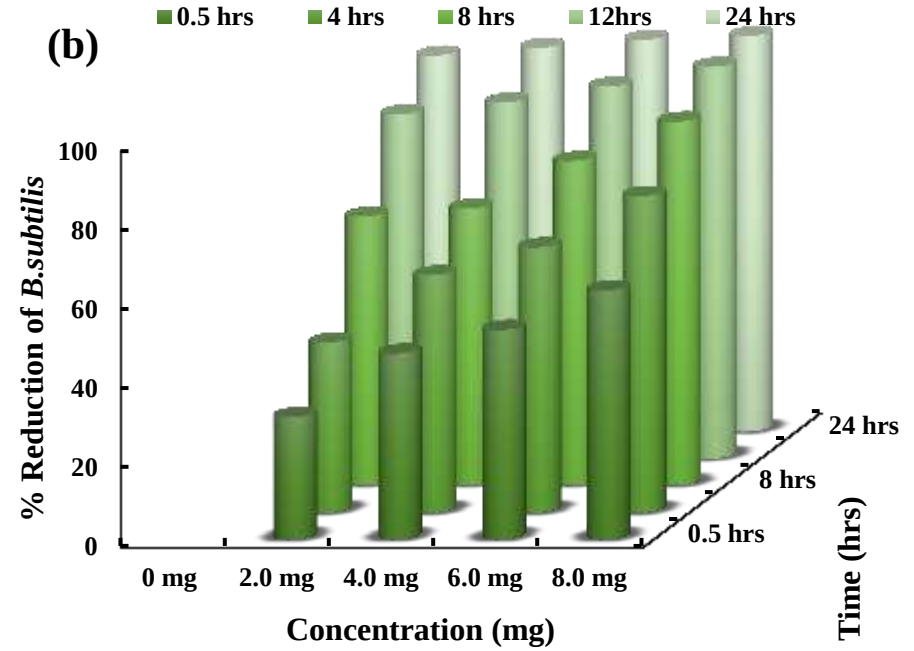
(b)
0.5 hrs
4 hrs
8 hrs
12hrs
24 hrs
% Reduction of B.subtilis
100
80
60
40
20
0
0 mg
2.0 mg
4.0 mg
6.0 mg
8.0 mg
Concentration (mg)
24 hrs
8 hrs
0.5 hrs
Time (hrs)

Figure 3.66. (a) *P. aeruginosa,* and (b*) B. subtilis* percentage reduction by ATTP@PEG/Ag^0 nanocomposite.

The time-kill kinetic analysis analyzes the ATTP@PVP/Ag^0 nanocomposite's bactericidal activity and is investigated against *S. pyogenes* and *E. coli*. By measuring the rate of bacterial survival after exposure to the nanocomposite solid is shown in Figure 3.67. (a-b). The figure displays a percentage decrease of *S. pyogenes* and *E. coli* using the nanocomposite solid. The ATTP@PVP/Ag^0 eliminates every *E. coli* and *S. pyogenes* bacterial cell at an exposure of 24 hrs, demonstrating the material's bactericidal properties.

The 2.0 mg of ATTP@PVP/Ag^0 quantitatively eliminates the *E. coli* bacteria of 33.4, 44.2, 65.5, and 86.4% at 0.5, 4, 8, and 12 hrs of exposure. After a 24 hrs incubation period with 100 mL of medium, the reduction in the percentage of *E. coli* is 99.0%. Similarly, the 2.0 mg of ATTP@PVP/Ag^0 eliminates the *S. pyogenes* to 34.4% at 0.5 hrs, and 24 hrs incubation removes 94.2% of the *S. pyogenes*. However, a solid dose of 8.0 mg eliminates 99.99% of *S. pyogenes* within incubation of 24 hrs.

The level of bacterial growth inhibition by the ATTP@PVP/Ag^0 depends upon the inorganic content present in the media, including the Ag^0 nanoparticles and metal oxides in clay. Increasing the dose of solid (i.e., 2.0 to 8.0 mg) enables an increase in the elimination of both the bacterium, i.e., *E. coli*, and *S. pyogenes*, by about 3 log bacterial concentration over an incubation period of 24 hrs. These studies show that the antibacterial activity directly correlates with an increase of nanocomposite (ATTP@PVP/Ag^0) concentrations and reactive oxygen species (O_2^-, H_2O_2, and HO•) generated in response to bacterial invasion and silver ions (Ag^+), which lead to oxidative stress and killing by stress damage. Ag^+ ions generate reactive oxygen species

(ROS) and hydrogen peroxide (H_2O_2) in bacterial cells and DNA. This leads to DNA damage due to the catalytic binding of zinc ions, which acts as a cofactor involved in DNA repair and synthesis, and releases OH radicals when Zn^{2+} is disrupted by Ag^{+} ions. H_2O_2 reacts with the metal to produce DNA strand breaks, base-pair modifications, and deoxyribose fragmentation.

Further, Ag^{+} substitution results in the transfer of Ag^{+} ions into triple and double hydrogen bonds within DNA base-pairing pairs G (guanine)≡C (cytosine), and A(adenine)=T (thymine). Therefore, DNA damage occurs in the ground state due to Ag^{+} two-coordinated complex forms inside DNA base pairs containing triple hydrogen bonds G≡C and double hydrogen bonds A=T. Another important mechanism operates based on the transformation of microorganisms by converting -SH bonds to -SAg bonds. Silver-thiolate compounds are formed by combining the silver ions with the thiol group. Both organic and inorganic thiols form complexes with silver ions by redox reactions with inorganic thiols like HS and S^{2+} to form AgSH, $[Ag(SH)_2]$ and $[Ag_2(SH)_2S]^{2-}$ (Ishida, 2018).

$$Ag^{+} + (\text{-SH})^{-} \rightarrow AgSH \rightarrow [Ag_2(SH)_2S]^{2-}$$

The dispersion and arrangement of nanoparticles inside the ATTP@PVP/Ag⁰ solid affects the accessibility of silver ions to bacteria and their capacity to interact with bacterial cells. The composite material evenly and widely dispersed the Ag^0(NPs) within the pores and surfaces of the nanocomposite, which enhances the interaction and release of silver ions, increasing its antibacterial effectiveness. Furthermore, the porous structure of the composite material provides additional surface area for bacterial interaction. Silver nanoparticles decorated with the ATTP@PVP enable a controlled release of Ag, enhancing antibacterial characteristics.

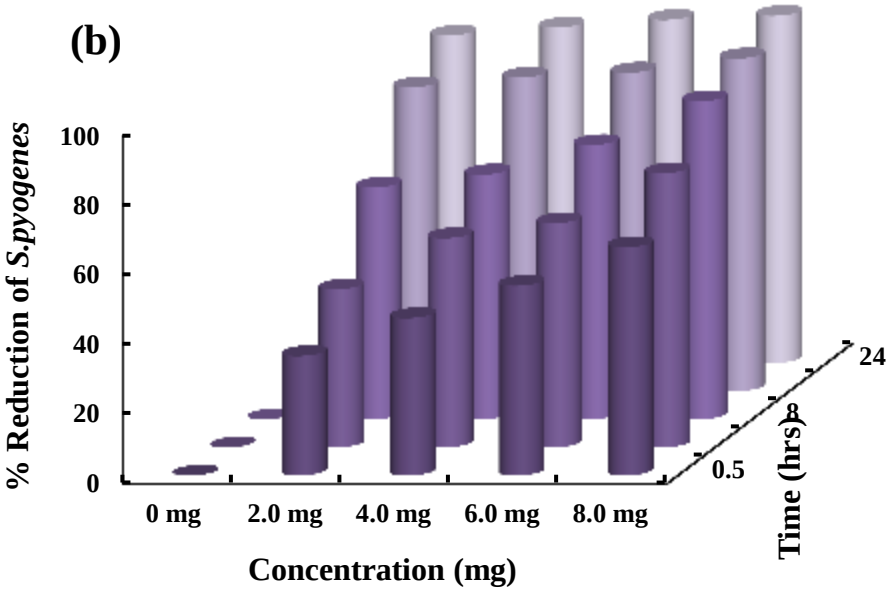

Figure 3.67. (a) *E. coli*, and (b*) S. pyogenes* percentage reduction by ATTP@PVP/Ag^0 nanocomposite.

3.3.14. Effect of pH on the removal of bacteria

The effect of abiotic factors, such as pH, on bacterial elimination from water using ATTP@PVP/Ag^0 was also assessed. The removal efficiency of *E. coli* and *S. pyogenes* increased as pH decreased (Figure 3.68.). After 7 hrs incubation, the log reduction of *E. coli* was 7.6 $\log_{10}$ CFU/ml at pH 4.0, while at pH 7.0 and 9.0 the log reduction of *E. coli* corresponded to 7.0 $\log_{10}$ CFU/ml and 6.7 $\log_{10}$ CFU/ml, respectively. The log reduction of *S. pyogenes* was 7.9 $\log_{10}$ CFU/ml, 7.6 $\log_{10}$ CFU/ml, and 7.0 $\log_{10}$ CFU/ml at pH 4.0, 7.0, and 9.0, respectively. The difference in removal rates between *S. pyogenes* and *E. coli* may be due to their membrane composition and different structures of gram-positive and gram-negative bacteria (e.g., gram-negative bacteria contain a thinner cell wall than gram-positive bacteria) under neutral conditions. In addition, *Streptococcus pyogenes* is highly hydrophobic whereas *E. coli* has a less hydrophobic cell wall, and so there is less tendency to attach to the silver nanoparticles (Oh et al., 2018). Another factor contributing to the difference in removal rates is the pH difference. At all pH levels, silver nanoparticles can release silver ions (Ag^+) into the surrounding environment. These silver ions are highly toxic to bacteria and can disrupt bacterial cell membranes, interfere with cellular processes, and induce oxidative stress, leading to cell death. However, at lower pH levels (pH 4.0), the release of silver ions increases due to the higher solubility of silver nanoparticles, contributing to enhanced antimicrobial activity.

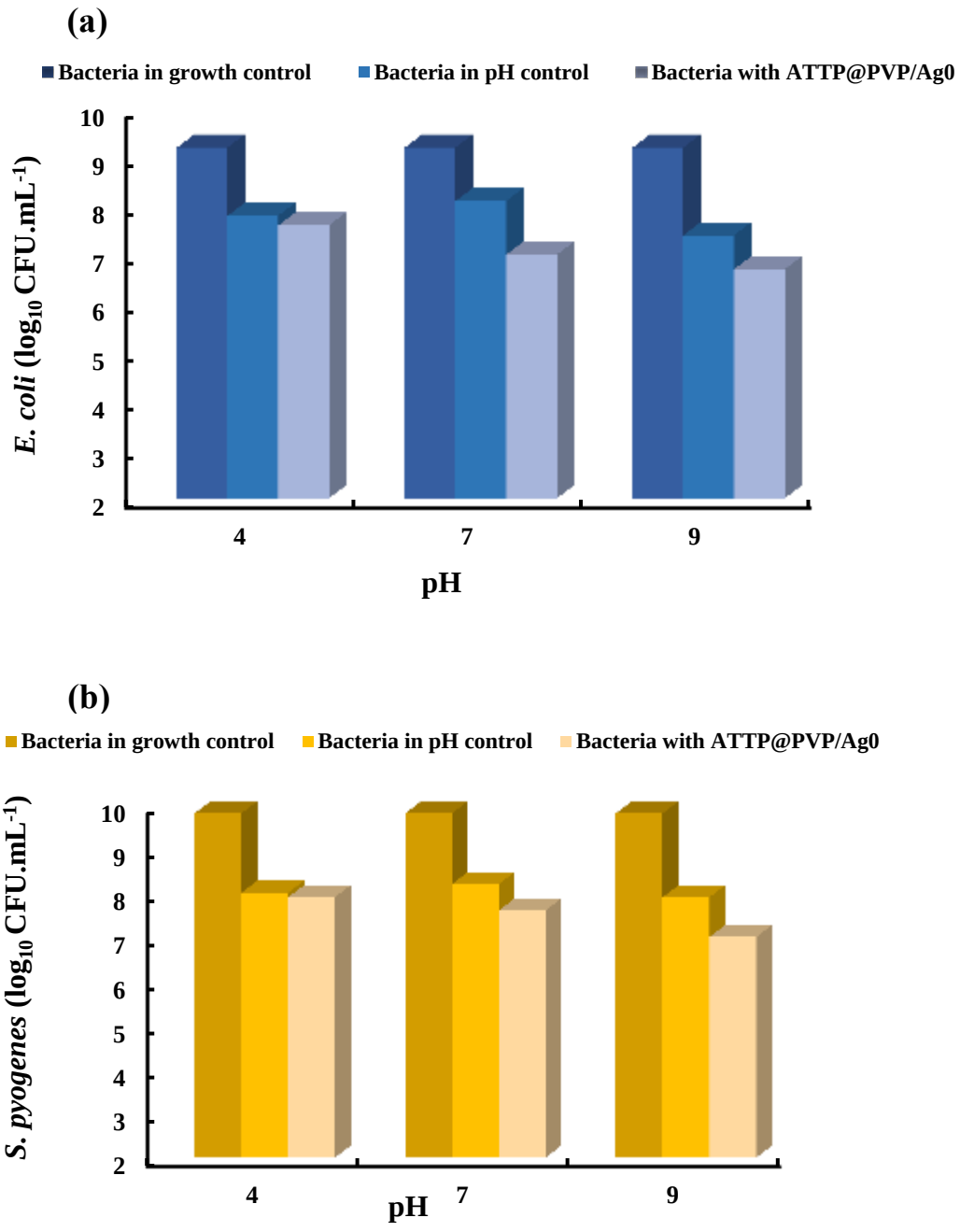

Figure 3.68. Effect of pH in bacterial removal using ATTP@PVP/Ag^0 nanocomposite against (a) *E. coli* and (b) *S. pyogenes*

CHAPTER 4

CONCLUSIONS

4. CONCLUSIONS

The attapulgite clay (ATTP) was incorporated with the Poly(ethylene glycol) (PEG) and Poly(4-vinylpyridine-co-styrene) (PVP) to obtain the novel composite materials, i.e; ATTP@PEG and ATTP@PVP, respectively. Further silver nanoparticles were synthesized using jackfruit leaf extract and incorporated with ATTP@PEG and ATTP@PVP to get the nanocomposites ATTP@PEG/Ag^0 and ATTP@PVP/Ag^0. Then, the materials (ATTP@PEG and ATTP@PVP) were employed in the removal of several micro-pollutants from aqueous solutions under the batch and column reactor studies and the ATTP@PEG/Ag° and ATTP@PVP/Ag° nanocomposites were used for removal of microorganisms. The ATTP@PEG, ATTP@PVP, ATTP@PEG/Ag°, ATTP@PVP/Ag° along with the pristine attapulgite were characterized by the FE-SEM, TEM, XRD, FT-IR, BET, and XPS analytical tools.

The SEM image of attapulgite clay displayed a fibrous crystal structure. The individual fibers are thin and elongated, resembling microscopic needles/rods. Moreover, the EDX results revealed that these solids contained the elements such as Si, Al, Mg, C, O, Na, Ca, N, K and the presence of an additional peak of the Ag is obtained in the EDX spectrum of ATTP@PEG/Ag^o and ATTP@PVP/Ag^o, confirming the successful incorporation of Ag in the nanocomposite solids. The mean size of the silver nanoparticles has been calculated to be 41.18 nm for ATTP@PEG/Ag^o and 30.91 nm for ATTP@PVP/Ag^o. Additionally, the d-spacing was found as 0.24 nm for ATTP@PEG/Ag^o and 0.211 nm for ATTP@PVP/Ag^o, respectively. Further, the XRD pattern of pristine clay demonstrates that the prominent diffraction peaks at 2θ values of 8.3º, 19.7º, and 27.3º inferred the diffraction planes of (110), (040), and (400), respectively, of the attapulgite. The ATTP@PEG showed predominant diffraction peaks at 2θ values of 19.81º and 24.19º having diffraction planes at (120) and (032), due to the presence of PEG. The diffraction peaks shown by ATTP@PEG/Ag^0 at 2θ values of 38.19º, 46.18º, 67.74º, and 77.70º referred to the characteristic planes of (111), (200), (220),

and (311), respectively, for Ag(NPs). Similarly, the ATTP@PVP/Ag^0 showed characteristic diffraction peaks of the Ag(NPs), predominatly occurred at 2θ values of 38.1º, 46.2º, 67.74º and 77.70º corresponding to the planes (111), (200), (220), and (311), respectively. The FT-IR showed a peak located at 1660 cm^{-1} representing the carbonyl (C=O) group whereas the ether groups in PEG's (ATTP@PEG) displayed considerably higher peak at 1092 cm^{-1}due to C-O stretching. The BET analysis revealed that pristine attapulgite and the polymer-incorporated samples exhibited type-IV isotherms having H3 hysteresis loops indicating that the solid materials possessed mesopores. Furthermore, the surface area is significantly increased in the modified samples compared to the raw attapulgite which inferred that the PEG and PVP molecules showed uniform coating and the penetration of a polymeric chain into the clay intergallery, tends to widen the interspacing and therefore enlarge the surface area. The BET-specific surface areas of ATTP, ATTP@PEG, ATTP@PVP, ATTP@PEG/Agº and ATTP@PVP/Ag^0 are 85.55, 100.01, 203.79, 90.46, and 107.37 m^2/g, respectively. However, the surface area decreased comparatively for ATTP@PVP/Agº and ATTP@PEG/Agº since the silver nanoparticles predominantly occupied some of the pores. The XPS analytical graph displayed the peaks of Ag(3d) representing the elemental zerovalent silver's $3d_{5/2}$ and $3d_{3/2}$ energy levels occurred at the binding energies of 368.4 eV and 374.1 eV, respectively, which confirms the presence of silver in its reduced state in ATTP@PEG/Agº and ATTP@PVP/Agº nanocomposites.

Batch studies showed that the synthesized materials ATTP@PEG, ATTP@PVP, ATTP@PEG/Agº and ATTP@PVP/Agº removed tetracycline, bisphenol A, ciprofloxacin, EE2 and triclosan within a wide pH range and the removal percentage are significantly improved after modification of the pristine attapulgite. The concentration dependence data obtained for the studied micro-pollutants followed Langmuir adsorption isotherm. The Langmuir monolayer adsorption capacity obtained for TCH, BPA, CIP, EE2 and TCS are 13.58, 14.08, 28.98, 30.48, and 25.90 mg/L with ATTP@PVP and 10.98, 22.37, 28.17, 29.32, and 39.06 mg/L with ATTP@PEG, respectively.

The effect of contact time in the removal of these micro-pollutants showed the rapid uptake of these pollutants and the kinetic modelling results showed the uptake of these micro-pollutants by the ATTP@PEG and ATTP@PVP fitted well to the PSO model compared to the PFO model. Increasing the background electrolyte (NaCl) concentrations 1000 times had unaffected the removal percentage of these micro-pollutants by the ATTP@PEG and ATTP@PVP solids. Similarly, the presence of various co-existing cations *viz*., Mg(II), Mn(II), Ca(II) and Ni(II) did not affect the percentage uptake of these micro-pollutants whereas the presence of EDTA significantly affected the removal of tetracycline, triclosan, bisphenol A, ciprofloxacin and EE2 using ATTP@PEG and ATTP@PVP. The column reactor experiments resulted a complete breakthrough for TCH and BPA at 2.08 L and 1.51 L using ATTP@PVP beads, and a complete breakthrough for EE2 was achieved having throughput volume of 1.21 L and for CIP is at 1.51 L using ATTP@PEG beads. Additionally, applicability of these novel materials in the removal of micro-pollutants *viz.*, tetracycline, triclosan, ciprofloxacin, bisphenol A and EE2 in real matrix sample was conducted under varied pollutant concentrations (1-25 mg/L). Results showed that the removal of these micro-pollutants was not affected as compared to the results obtained with purified water indicating the selectivity of solids towards these micro-pollutants and possible implacability in real matrix treatment. Furthermore, the materials i.e., ATTP@PEG and ATTP@PVP could be reuse for six adsorption-desorption cycles of TCH, BPA, CIP, EE2 and TCS without significant lost in their efficiency. The reusability test indicated that ATTP@PEG and ATTP@PVP possessed greater stability and could be reutilized for successive operations in the removal of tetracycline, ciprofloxacin, triclosan, bisphenol A and EE2 from aqueous solutions. The studies on insight mechanisms revealed that formation of hydrogen bonding and hydrophobic interactions are the major pathways of removing the studied micropollutants using ATTP@PEG/ATTP@PVP composite.

Further, the silver nanoparticle incorporated nanocomposites i.e., ATTP@PEG/Ag^0 and ATTP@PVP/Ag^0 were used for antibacterial activity

against both gram-positive and gram-negative bacterial strains present in contaminated water. The findings of the ATTP@PEG/Ag^0 inhibiting effect against *Pseudomonas aeruginosa* and *Bacillus subtilis,* showed zone of inhibition against *P. aeruginosa* with a diameter of 13.6±0.3, 15.3±0.3, 19.3±0.2, and 23.2±0.6 mm for doses of 2.0, 4.0, 6.0, and 8.0 mg of ATTP@PEG/Ag^0, respectively. The measured diameter of the zone of inhibition against *B. subtilis* at the same ATTP@PEG/Ag^0 concentrations were 10.1±0.3, 13.4±0.4, 17.2±0.3 and 20.3±0.2 mm while the pristine attapulgite did not inhibit the *P. aeruginosa* and *B. subtilis*. Similarly, the zone of inhibition of pristine attapulgite clay ATTP@PVP/Ag^0 nanocomposite against both Gram negative (*E. coli*) and Gram positive (*S. pyogenes*) bacteria were assessed. It is clearly observed that unlike pristine attapulgite clay, the clay/polymer/Ag nanocomposite shows exceptional antibacterial activity against two model bacteria. Generally, the mean zone of inhibition of the ATTP@PVP/Ag^0 nanomaterial ranged between 3.2±0.9 mm and 8.1±0.5 mm for *E. coli* and 4.4±0.3 mm and 10.2±0.6 mm for *S. pyogenes*. The bactericidal activity of ATTP@PVP/Ag^0 nanocomposite against *E. coli* and S. pyogenes and ATTP@PEG/Ag^0 nanocomposite against *P. aeruginosa* and *B. subtilis* were also assessed by the time kill kinetic analysis. Any reduction in bactericidal activity was evaluated by determination of the bacterial survival rate when exposed to the nanocomposite solid. The result of this study revealed that after 24 hrs, all the bacterial cells of *E. coli* and *S. pyogenes* were removed by ATTP@PVP/Ag^0 and thereby confirming its bactericidal nature. Similarly, the outcomes demonstrate that after contacting for 24 hrs, ATTP@PEG/Ag^0 eliminated all bacterial cells, demonstrating the bactericidal efficacy of ATTP@PEG/Ag^0 towards the two pathogenic bacteria *P. aeruginosa* and *B. subtilis*. The effect of abiotic factor, such as pH, on bacterial elimination from water using ATTP@PVP/Ag^0 was further assessed. The removal efficiency of *E. coli* and S. pyogenes increased as pH decreased. The log reduction of *E. coli* was 7.6 $\log_{10}$ CFU/ml at pH 4.0, while at pH 7.0 and 9.0 the log reduction of *E. coli* corresponded to 7.0 $\log_{10}$ CFU/ml and 6.7 $\log_{10}$ CFU/ml, respectively. The log reduction of *S. pyogenes* was 7.9 $\log_{10}$ CFU/ml, 7.6 $\log_{10}$ CFU/ml and 7.0

$\log_{10}$ CFU/ml at pH 4.0, 7.0 and 9.0, respectively.

Therefore, the studies infer that the clay-polymer composites *viz.,* ATTP@PEG and ATTP@PVP are efficient in the removal of several potential micro-pollutants such as tetracycline, triclosan, ciprofloxacin, bisphenol A and 17α-ethynylestradiol from aqueous solutions. Further, the two nanocomposites *viz;* ATTP@PEG/Ag^0 and ATTP@PVP/Ag^0 shows efficient antimicrobial activity against both gram-positive and gram-negative bacterial strains. The input laboratory data obtained for these studies could be employed for the large-scale operations to decontaminate the water with these emerging water contaminants and microbial activities.

REFERENCES

Abou El-Nour, K. M. M., Eftaiha, A., Al-Warthan, A., & Ammar, R. A. A. (2010). Synthesis and applications of silver nanoparticles. *Arabian Journal of Chemistry*, ***3*(3)**, 135–140. https://doi.org/10.1016/J.ARABJC.2010.04.008

Ahamad, T., Naushad, M., Al-Shahrani, T., Al-hokbany, N., & Alshehri, S. M. (2020). Preparation of chitosan based magnetic nanocomposite for tetracycline adsorption: Kinetic and thermodynamic studies. *International Journal of Biological Macromolecules*, ***147***, 258–267. https://doi.org/10.1016/j.ijbiomac.2020.01.025

Ahn, C., & Jeung, E. B. (2023). Endocrine-Disrupting Chemicals and Disease Endpoints. *International Journal of Molecular Sciences 2023, Vol. **24**, Page 5342*, *24*(6), 5342. https://doi.org/10.3390/IJMS24065342

Akpor, O. B., & OTohinoyi, D. A. (2014). *Pollutants in Wastewater Effluents: Impacts and Remediation Processes*. International Journal of Environmental Research and Earth Science. https://doi.org/10.1007/s10162-014-0441-4

Al-Musawi, T. J., Mahvi, A. H., Khatibi, A. D., & Balarak, D. (2021a). Effective adsorption of ciprofloxacin antibiotic using powdered activated carbon magnetized by iron(III) oxide magnetic nanoparticles. *Journal of Porous Materials*, ***28*(3)**, 835–852. https://doi.org/10.1007/s10934-021-01039-7

Al.Haddabi, M., Vuthaluru, H., Znad, H., & Ahmed, M. (2015). Attapulgite as Potential Adsorbent for Dissolved Organic Carbon From Oily Water. *CLEAN – Soil, Air, Water*, ***43*(11)**, 1522–1530. https://doi.org/10.1002/CLEN.201500073

Alcântara, A. C. S., Darder, M., Aranda, P., & Ruiz-Hitzky, E. (2014). Polysaccharide–fibrous clay bionanocomposites. *Applied Clay Science*, ***96***, 2–8. https://doi.org/10.1016/J.CLAY.2014.02.018

Aliyu, M., Abdullah, A. H., & Tahir, M. I. bin M. (2022). Adsorption tetracycline from aqueous solution using a novel polymeric adsorbent derived from the rubber waste. *Journal of the Taiwan Institute of Chemical Engineers*, ***136***, 104333. https://doi.org/10.1016/J.JTICE.2022.104333

Alizadeh Fard, M., Vosoogh, A., Barkdoll, B., & Aminzadeh, B. (2017). Using polymer coated nanoparticles for adsorption of micropollutants from water. *Colloids and Surfaces A: Physicochemical and Engineering Aspects*, ***531***, 189–197. https://doi.org/10.1016/J.COLSURFA.2017.08.008

Almatroudi, A. (2020). Silver nanoparticles: Synthesis, characterisation and biomedical applications. In *Open Life Sciences* (Vol. ***15***, Issue 1, pp. 819–839). De Gruyter. https://doi.org/10.1515/biol-2020-0094

Almeida, Â., Silva, M. G., Soares, A. M. V. M., & Freitas, R. (2020). Concentrations levels and effects of 17alpha-Ethinylestradiol in freshwater and marine waters and bivalves: A review. *Environmental Research*, ***185***, 109316. https://doi.org/10.1016/J.ENVRES.2020.109316

Almeida, A. da S. V. de, Mastelaro, V. R., da Silva, M. G. C., Prediger, P., & Vieira, M. G. A. (2022). Adsorption of 17α-ethinylestradiol onto a novel nanocomposite based on graphene oxide, magnetic chitosan and organoclay (GO/mCS/OC): Kinetics, equilibrium, thermodynamics and selectivity studies. *Journal of Water Process Engineering*, ***47,*** 102729. https://doi.org/10.1016/J.JWPE.2022.102729

Amari, A., Alzahrani, F. M., Katubi, K. M., Alsaiari, N. S., Tahoon, M. A., & Rebah, F. Ben. (2021). Clay-Polymer Nanocomposites: Preparations and Utilization for Pollutants Removal. *Materials*, *14*(6).

https://doi.org/10.3390/MA14061365

Ambaye, T. G., Vaccari, M., van Hullebusch, E. D., Amrane, A., & Rtimi, S. (2020). Mechanisms and adsorption capacities of biochar for the removal of organic and inorganic pollutants from industrial wastewater. *International Journal of Environmental Science and Technology 2020 18:10*, ***18*(10)**, 3273–3294. https://doi.org/10.1007/S13762-020-03060-W

Anees Ahmad, S., Sachi Das, S., Khatoon, A., Tahir Ansari, M., Afzal, M., Saquib Hasnain, M., & Kumar Nayak, A. (2020). Bactericidal activity of silver nanoparticles: A mechanistic review. *Materials Science for Energy Technologies*, ***3***, 756–769. https://doi.org/10.1016/J.MSET.2020.09.002

Aris, A. Z., Shamsuddin, A. S., & Praveena, S. M. (2014). Occurrence of 17α-ethynylestradiol (EE2) in the environment and effect on exposed biota: a review. *Environment International*, ***69,*** 104–119. https://doi.org/10.1016/J.ENVINT.2014.04.011

Armstrong, B. M., Lazorchak, J. M., Murphy, C. A., Haring, H. J., Jensen, K. M., & Smith, M. E. (2015). Determining the effects of a mixture of an endocrine disrupting compound, 17α-ethinylestradiol, and ammonia on fathead minnow (Pimephales promelas) reproduction. *Chemosphere*, ***120,*** 108–114. https://doi.org/10.1016/J.CHEMOSPHERE.2014.06.049

Awad, A. M., Jalab, R., Benamor, A., Nasser, M. S., Ba-Abbad, M. M., El-Naas, M., & Mohammad, A. W. (2020). Adsorption of organic pollutants by nanomaterial-based adsorbents: An overview. *Journal of Molecular Liquids*, ***301***, 112335. https://doi.org/10.1016/J.MOLLIQ.2019.112335

Azizian, S. (2004). Kinetic models of sorption: A theoretical analysis. *Journal of Colloid and Interface Science*, ***276*(1)**, 47–52. https://doi.org/10.1016/j.jcis.2004.03.048

Bankar, A., Joshi, B., Ravi Kumar, A., & Zinjarde, S. (2010). Banana peel extract mediated synthesis of gold nanoparticles. *Colloids and Surfaces. B, Biointerfaces*, ***80*(1)**, 45–50.

https://doi.org/10.1016/J.COLSURFB.2010.05.029

Barakan, S., & Aghazadeh, V. (2020). The advantages of clay mineral modification methods for enhancing adsorption efficiency in wastewater treatment: a review. *Environmental Science and Pollution Research 2020 28:3*, ***28*****(3)**, 2572–2599. https://doi.org/10.1007/S11356-020-10985-9

Basavegowda, N., & Baek, K. H. (2021). Advances in Functional Biopolymer-Based Nanocomposites for Active Food Packaging Applications. *Polymers*, ***13*****(23)**. https://doi.org/10.3390/POLYM13234198

Behera, S. K., Oh, S. Y., & Park, H. S. (2010). Sorption of triclosan onto activated carbon, kaolinite and montmorillonite: Effects of pH, ionic strength, and humic acid. *Journal of Hazardous Materials*, ***179*****(1–3)**, 684–691. https://doi.org/10.1016/j.jhazmat.2010.03.056

Berber, M. R. (2020). Current Advances of Polymer Composites for Water Treatment and Desalination. *Journal of Chemistry, 2020*. https://doi.org/10.1155/2020/7608423

Bever, C. S., Rand, A. A., Nording, M., Taft, D., Kalanetra, K. M., Mills, D. A., Breck, M. A., Smilowitz, J. T., German, J. B., & Hammock, B. D. (2018). Effects of triclosan in breast milk on the infant fecal microbiome. *Chemosphere*, ***203,*** 467–473. https://doi.org/10.1016/J.CHEMOSPHERE.2018.03.186

Bhattacharyya, R., & Ray, S. K. (2015). Removal of congo red and methyl violet from water using nano clay filled composite hydrogels of poly acrylic acid and polyethylene glycol. *Chemical Engineering Journal*, ***260,*** 269–283. https://doi.org/10.1016/j.cej.2014.08.030

Borst, A. M., Smith, M. P., Finch, A. A., Estrade, G., Villanova-de-Benavent, C., Nason, P., Marquis, E., Horsburgh, N. J., Goodenough, K. M., Xu, C., Kynický, J., & Geraki, K. (2020). Adsorption of rare earth elements in regolith-hosted clay deposits. *Nature Communications 2020 11:1*, ***11*****(1)**, 1–15. https://doi.org/10.1038/s41467-020-17801-5

Brandani, S. (2021). Kinetics of liquid phase batch adsorption experiments. *Adsorption*, ***27*****(3)**, 353–368. https://doi.org/10.1007/S10450-020-00258-9/FIGURES/11

Brouwer, S., Rivera-Hernandez, T., Curren, B. F., Harbison-Price, N., De Oliveira, D. M. P., Jespersen, M. G., Davies, M. R., & Walker, M. J. (2023). Pathogenesis, epidemiology and control of Group A Streptococcus infection. *Nature Reviews Microbiology 2023 21:7*, ***21*****(7)**, 431–447. https://doi.org/10.1038/s41579-023-00865-7

Burdușel, A. C., Gherasim, O., Grumezescu, A. M., Mogoantă, L., Ficai, A., & Andronescu, E. (2018). Biomedical Applications of Silver Nanoparticles: An Up-to-Date Overview. *Nanomaterials*, ***8*****(9).** https://doi.org/10.3390/NANO8090681

Burgos, A. E., Ribeiro-Santos, T. A., & Lago, R. M. (2016). Adsorption of the harmful hormone ethinyl estradiol inside hydrophobic cavities of CTA+ intercalated montmorillonite. *Water Science and Technology*, ***74*****(3)**, 663–671. https://doi.org/10.2166/WST.2016.207

Buttersack, C. (2019). Modeling of type IV and V sigmoidal adsorption isotherms. *Physical Chemistry Chemical Physics*, ***21*****(10)**, 5614–5626. https://doi.org/10.1039/C8CP07751G

Campillo-Cora, C., Conde-Cid, M., Arias-Estévez, M., Fernández-Calviño, D., & Alonso-Vega, F. (2020). Specific Adsorption of Heavy Metals in Soils: Individual and Competitive Experiments. *Agronomy 2020, Vol. **10,** Page 1113, 10*(8), 1113. https://doi.org/10.3390/AGRONOMY10081113

Canesi, L., & Fabbri, E. (2015). Environmental effects of BPA: Focus on aquatic species. *Dose-Response*, ***13*****(3)**. https://doi.org/10.1177/1559325815598304/ASSET/IMAGES/LARGE/10.1177_1559325815598304-FIG2.JPEG

Castro, S. A., & Dorfmueller, H. C. (2021). A brief review on Group A Streptococcus pathogenesis and vaccine development. *Royal Society*

Open Science, ***8*(3)**. https://doi.org/10.1098/RSOS.201991

Celis, R., Adelino, M. A., Hermosín, M. C., & Cornejo, J. (2012). Montmorillonite-chitosan bionanocomposites as adsorbents of the herbicide clopyralid in aqueous solution and soil/water suspensions. *Journal of Hazardous Materials*, ***209–210,*** 67–76. https://doi.org/10.1016/J.JHAZMAT.2011.12.074

Chang, P. H., Jiang, W. T., Li, Z., Kuo, C. Y., Jean, J. S., Chen, W. R., & Lv, G. (2014). Mechanism of amitriptyline adsorption on Ca-montmorillonite (SAz-2). *Journal of Hazardous Materials*, ***277,*** 44–52. https://doi.org/10.1016/j.jhazmat.2013.12.004

Chapla, R., Abed, M. A., & West, J. (2020). Modulating Functionalized Poly(ethylene glycol) Diacrylate Hydrogel Mechanical Properties through Competitive Crosslinking Mechanics for Soft Tissue Applications. *Polymers*, ***12*(12)**, 1–16. https://doi.org/10.3390/POLYM12123000

Cheikh, S., Imessaoudene, A., Bollinger, J. C., Hadadi, A., Manseri, A., Bouzaza, A., Assadi, A., Amrane, A., Zamouche, M., El Jery, A., & Mouni, L. (2023). Complete Elimination of the Ciprofloxacin Antibiotic from Water by the Combination of Adsorption–Photocatalysis Process Using Natural Hydroxyapatite and TiO2. *Catalysts*, ***13*(2)**. https://doi.org/10.3390/catal13020336

Chevalier, S., Bouffartigues, E., Bodilis, J., Maillot, O., Lesouhaitier, O., Feuilloley, M. G. J., Orange, N., Dufour, A., & Cornelis, P. (2017). Structure, function and regulation of Pseudomonas aeruginosa porins. *FEMS Microbiology Reviews*, ***41*(5)**, 698–722. https://doi.org/10.1093/FEMSRE/FUX020

Cooke, E. M. (1974). *Escherichia coli and man*. **96.** http://www.cabdirect.org/abstracts/19742704379.html;jsessionid=0D3FCF364E983E8268DAB6A487C3FCD8

Cunningham, M. W. (2016). Post-Streptococcal Autoimmune Sequelae: Rheumatic Fever and Beyond. *Streptococcus Pyogenes: Basic Biology to Clinical Manifestations*.

Barros, D.,M. A. S., A., P., & A., E. (2013). General Aspects of Aqueous Sorption Process in Fixed Beds. *Mass Transfer - Advances in Sustainable Energy and Environment Oriented Numerical Modeling*. https://doi.org/10.5772/51954

Dai, C. M., Geissen, S. U., Zhang, Y. L., Zhang, Y. J., & Zhou, X. F. (2011). Selective removal of diclofenac from contaminated water using molecularly imprinted polymer microspheres. *Environmental Pollution*, ***159*(6)**, 1660–1666. https://doi.org/10.1016/j.envpol.2011.02.041

Dai, J., Meng, X., Zhang, Y., & Huang, Y. (2020). Effects of modification and magnetization of rice straw derived biochar on adsorption of tetracycline from water. *Bioresource Technology*, ***311***, 123455. https://doi.org/10.1016/j.biortech.2020.123455

Das, D. S., Tadikonda, B. V., Raja, S., & Tripathy, S. (2022). Compressibility Behavior of Bentonites by Stern Theory based on Constant Surface Charge Conditions. *Clays and Clay Minerals*, ***70*(6)**, 916–933. https://doi.org/10.1007/S42860-023-00227-7/METRICS

de Farias, M. B., Silva, M. G. C., & Vieira, M. G. A. (2022). Adsorption of bisphenol A from aqueous solution onto organoclay: Experimental design, kinetic, equilibrium and thermodynamic study. *Powder Technology*, ***395,*** 695–707. https://doi.org/10.1016/j.powtec.2021.10.021

de Farias, M. B., Spaolonzi, M. P., da Silva, T. L., da Silva, M. G. C., & Vieira, M. G. A. (2022). Natural and synthetic clay-based materials applied for the removal of emerging pollutants from aqueous medium. *Advanced Materials for Sustainable Environmental Remediation: Terrestrial and Aquatic Environments*, **359–392.** https://doi.org/10.1016/B978-0-323-90485-8.00012-6

de Paiva, L. B., Morales, A. R., & Valenzuela Díaz, F. R. (2008). Organoclays: Properties, preparation and applications. *Applied Clay Science*, ***42*****(1–2)**, 8–24. https://doi.org/10.1016/J.CLAY.2008.02.006

Dhillon, G. S., Kaur, S., Pulicharla, R., Brar, S. K., Cledón, M., Verma, M., & Surampalli, R. Y. (2015a). Triclosan: current status, occurrence, environmental risks and bioaccumulation potential. *International Journal of Environmental Research and Public Health*, ***12*****(5)**, 5657–5684. https://doi.org/10.3390/IJERPH120505657

Dhillon, G. S., Kaur, S., Pulicharla, R., Brar, S. K., Cledón, M., Verma, M., & Surampalli, R. Y. (2015b). Triclosan: Current Status, Occurrence, Environmental Risks and Bioaccumulation Potential. *International Journal of Environmental Research and Public Health*, ***12*****(5)**, 5657. https://doi.org/10.3390/IJERPH120505657

Dhumale, V. A., Gangwar, R. K., Datar, S. S., & Sharma, R. B. (2012). Reversible aggregation control of polyvinylpyrrolidone capped gold nanoparticles as a function of pH. *Materials Express*, ***2*****(4)**, 311–318. https://doi.org/10.1166/MEX.2012.1082

DiBlasi, N. A., Yalçintas, E., Stanley, F. E., Reed, D. T., & Hixon, A. E. (2021). Influence of ethylenediaminetetraacetic acid on the long-term oxidation state distribution of plutonium. *Chemosphere*, ***274***. https://doi.org/10.1016/J.CHEMOSPHERE.2021.129741

Dolan, F., Lamontagne, J., Link, R., Hejazi, M., Reed, P., & Edmonds, J. (2021). Evaluating the economic impact of water scarcity in a changing world. *Nature Communications 2021 12:1*, ***12*****(1)**, 1–10. https://doi.org/10.1038/s41467-021-22194-0

Dou, R., Zhang, J., Chen, Y., & Feng, S. (2017). High efficiency removal of triclosan by structure-directing agent modified mesoporous MIL-53(Al). *Environmental Science and Pollution Research*, ***24*****(9),** 8778–8789. https://doi.org/10.1007/s11356-017-8583-7

Dubey, S. P., Lahtinen, M., Särkkä, H., & Sillanpää, M. (2010). Bioprospective of Sorbus aucuparia leaf extract in development of silver and gold nanocolloids. *Colloids and Surfaces B: Biointerfaces*, ***80*****(1)**, 26–33. https://doi.org/10.1016/J.COLSURFB.2010.05.024

Earl, A. M., Losick, R., & Kolter, R. (2008). Ecology and genomics of Bacillus subtilis. *Trends in Microbiology*, ***16*****(6)**, 269–275. https://doi.org/10.1016/J.TIM.2008.03.004

Ehling-Schulz, M., Koehler, T. M., & Lereclus, D. (2019). The Bacillus cereus Group: Bacillus species with Pathogenic Potential. *Microbiology Spectrum*, ***7*****(3)**. https://doi.org/10.1128/MICROBIOLSPEC.GPP3-0032-2018

El-sayed, M. E. A. (2020). Nanoadsorbents for water and wastewater remediation. *Science of The Total Environment*, ***739,*** 139903. https://doi.org/10.1016/J.SCITOTENV.2020.139903

El Hotaby, W., Sherif, H. H. A., Hemdan, B. A., Khalil, W. A., & Khalil, S. K. H. (2017). Assessment of in situ-Prepared Polyvinylpyrrolidone-Silver Nanocomposite for Antimicrobial Applications. *Acta Physica Polonica A*, ***131*****(6),** 1554–1560. https://doi.org/10.12693/APHYSPOLA.131.1554

Elbassyoni, S., Kamoun, E. A., Taha, T. H., Rashed, M. A., & ElNozahi, F. A. (2020). Effect of Egyptian Attapulgite Clay on the Properties of PVA-HES–Clay Nanocomposite Hydrogel Membranes for Wound Dressing Applications. *Arabian Journal for Science and Engineering*, ***45*****(6),** 4737–4749. https://doi.org/10.1007/s13369-020-04501-x

Elumalai, E. K., Prasad, T. N. V. K. V., Hemachandran, J., Viviyan Therasa, S., Thirumalai, T., & David, E. (2010). *Extracellular synthesis of silver nanoparticles using leaves of Euphorbia hirta and their antibacterial activities*. Journal of Pharmaceutical Sciences and Research.

Ely, D. R., Edwin García, R., & Thommes, M. (2014). Ostwald–Freundlich diffusion-limited dissolution kinetics of nanoparticles. *Powder*

Technology, ***257***, 120–123. https://doi.org/10.1016/J.POWTEC.2014.01.095

Environmental Quality Standards-Ethinylestradiol. (2011). https://doi.org/10.2772/37258

Errington, J., & van der Aa, L. T. (2020). Microbe Profile: Bacillus subtilis: model organism for cellular development, and industrial workhorse. *Microbiology*, ***166*****(5)**, 425. https://doi.org/10.1099/MIC.0.000922

Etuk, V. E., Oboh, I. O., Etuk, B. R., Ita, B. N., & Bassey, E. E. (2021). Kinetic modelling techniques in industrial wastewater treatment using nanocellulosic adsorbents: A Review of batch and column operations. *J. Mater. Environ. Sci*, *2021*(2), **279–294**.

Ewis, D., Ba-Abbad, M. M., Benamor, A., & El-Naas, M. H. (2022). Adsorption of organic water pollutants by clays and clay minerals composites: A comprehensive review. *Applied Clay Science*, ***229***, 106686. https://doi.org/10.1016/J.CLAY.2022.106686

Feng, P., Weagant, S. D., Grant, M. A., & Burkhardt, W. (2020). *BAM Chapter 4: Enumeration of Escherichia coli and the Coliform Bacteria | FDA*. FDA BAM Chapter 4: Enumeration of Escherichia Coli and the Coliform Bacteria.

Gao, P., Yang, C., Liang, Z., Wang, W., Zhao, Z., Hu, B., & Cui, F. (2019). N-propyl functionalized spherical mesoporous silica as a rapid and efficient adsorbent for steroid estrogen removal: Adsorption behaviour and effects of water chemistry. *Chemosphere*, ***214***, 361–370. https://doi.org/10.1016/j.chemosphere.2018.09.115

Gee, R. H., Charles, A., Taylor, N., & Darbre, P. D. (2008). Oestrogenic and androgenic activity of triclosan in breast cancer cells. *Journal of Applied Toxicology : JAT*, ***28*****(1)**, 78–91. https://doi.org/10.1002/JAT.1316

Geissen, V., Mol, H., Klumpp, E., Umlauf, G., Nadal, M., van der Ploeg, M., van de Zee, S. E. A. T. M., & Ritsema, C. J. (2015). Emerging pollutants

in the environment: A challenge for water resource management. *International Soil and Water Conservation Research*, ***3*(1),** 57–65. https://doi.org/10.1016/j.iswcr.2015.03.002

Ghodake, G., Kim, M., Sung, J. S., Shinde, S., Yang, J., Hwang, K., & Kim, D. Y. (2020). Extracellular synthesis and characterization of silver nanoparticles—antibacterial activity against multidrug-resistant bacterial strains. *Nanomaterials*, ***10*(2)**. https://doi.org/10.3390/nano10020360

Ghosh, B., & Chakraborty, D. (2023). An Overview of the Clay Minerals: Composition, Classification, Internal Structure and Properties. *Clay Minerals*, **1–24**. https://doi.org/10.1007/978-3-031-22327-3_1

Ghosh, S., Ahmad, R., Zeyaullah, M., & Khare, S. K. (2021). Microbial Nano-Factories: Synthesis and Biomedical Applications. *Frontiers in Chemistry*, ***9***. https://doi.org/10.3389/fchem.2021.626834

Giri, A. K., Jena, B., Biswal, B., Pradhan, A. K., Arakha, M., Acharya, S., & Acharya, L. (2022). Green synthesis and characterization of silver nanoparticles using Eugenia roxburghii DC. extract and activity against biofilm-producing bacteria. *Scientific Reports 2022 12:1*, ***12*(1)**, 1–9. https://doi.org/10.1038/s41598-022-12484-y

Giubertoni, G., Sofronov, O. O., & Bakker, H. J. (2020). Effect of intramolecular hydrogen-bond formation on the molecular conformation of amino acids. *Communications Chemistry*, ***3*(1),** 1–6. https://doi.org/10.1038/s42004-020-0329-7

Gopalapillai, Y., Hale, B., & Vigneault, B. (2013). Effect of major cations (Ca2+, Mg2+, Na+, K+) and anions (SO, Cl−, NO) on Ni accumulation and toxicity in aquatic plant (Lemna minor L.): Implications For Ni risk assessment. *Environmental Toxicology and Chemistry*, ***32*(4)**, 810–821. https://doi.org/10.1002/ETC.2116

Gu, H. J., Sun, Q. L., Luo, J. C., Zhang, J., & Sun, L. (2019). A First Study of the Virulence Potential of a Bacillus subtilis Isolate From Deep-Sea

Hydrothermal Vent. *Frontiers in Cellular and Infection Microbiology*, ***9*.** https://doi.org/10.3389/FCIMB.2019.00183

Gui, Q., Zhang, J., Hu, K., Ouyang, Q., Shi, S., & Chen, X. (2020). Hydrogen bonding-induced hydrophobic assembly yields strong affinity of an adsorptive membrane for ultrafast removal of trace organic micropollutants from water. *Journal of Materials Chemistry A*, ***8*(32)**, 16487–16496. https://doi.org/10.1039/D0TA05469K

Guo, X., & Wang, J. (2019). Comparison of linearization methods for modeling the Langmuir adsorption isotherm. *Journal of Molecular Liquids*, ***296***, 111850. https://doi.org/10.1016/J.MOLLIQ.2019.111850

Haerifar, M., & Azizian, S. (2013). An exponential kinetic model for adsorption at solid/solution interface. *Chemical Engineering Journal*, ***215–216,*** 65–71. https://doi.org/10.1016/J.CEJ.2012.11.017

Haider, A., & Kang, I. K. (2015). Preparation of silver nanoparticles and their industrial and biomedical applications: A comprehensive review. *Advances in Materials Science and Engineering*. https://doi.org/10.1155/2015/165257

Hamdi, W., Hamdi, N., Jellali, S., & Seffen, M. (2022). Effect of background electrolytes on the adsorption of phosphorus (P) onto southern Tunisia natural clays. *Physics and Chemistry of the Earth, Parts A/B/C*, ***127***, 103160. https://doi.org/10.1016/J.PCE.2022.103160

Han, J., Qiu, W., Meng, S., & Gao, W. (2012). Removal of ethinylestradiol (EE2) from water via adsorption on aliphatic polyamides. *Water Research*, ***46*(17)**, 5715–5724. https://doi.org/10.1016/j.watres.2012.08.001

Hand, R. M., Snelling, T. L., & Carapetis, J. R. (2020). Group A Streptococcus. *Hunter's Tropical Medicine and Emerging Infectious Diseases*, **429**. https://doi.org/10.1016/B978-0-323-55512-8.00040-5

Hassan, M. S., & El-Nemr, K. F. (2013). Dye sorption characters of gamma

irradiated foamed ethylene propylene diene monomer (EPDM) rubber/clay composites. *Journal of Industrial and Engineering Chemistry*, ***19*****(4)**, 1371–1376. https://doi.org/10.1016/J.JIEC.2012.12.042

Hazarika, B., Ahmaruzzaman, M., Santosh, M. S., Barceló, D., & Rtimi, S. (2023). Advances in polymer-based nanocomposite membranes for water remediation: Preparation methods, critical issues and mechanisms. *Journal of Environmental Chemical Engineering*, ***11*****(6)**, 111401. https://doi.org/10.1016/J.JECE.2023.111401

He, H., Lin, Y., Yang, X., Zhu, X., Xie, W., Lai, C., Yang, S., Zhang, Z., Huang, B., & Pan, X. (2022). The photodegradation of 17 alpha-ethinylestradiol in water containing iron and dissolved organic matter. *Science of the Total Environment*, ***814,*** 152516. https://doi.org/10.1016/j.scitotenv.2021.152516

He, J., Ni, F., Cui, A., Chen, X., Deng, S., Shen, F., Huang, C., Yang, G., Song, C., Zhang, J., Tian, D., Long, L., Zhu, Y., & Luo, L. (2020). New insight into adsorption and co-adsorption of arsenic and tetracycline using a Y-immobilized graphene oxide-alginate hydrogel: Adsorption behaviours and mechanisms. *Science of the Total Environment*, ***701,*** 134363. https://doi.org/10.1016/j.scitotenv.2019.134363

Heath, R. J., Rubin, J. R., Holland, D. R., Zhang, E., Snow, M. E., & Rock, C. O. (1999). Mechanism of Triclosan Inhibition of Bacterial Fatty Acid Synthesis*. *Journal of Biological Chemistry*, ***274,*** 11110–11114. https://doi.org/10.1074/jbc.274.16.11110

Hitzfeld, B. C., Hoger, S. J., & Dietrich, D. R. (2000). Cyanobacterial Toxins: Removal during Drinking Water Treatment, and Human Risk Assessment. *Environmental Health Perspectives*, ***108,*** 113. https://doi.org/10.2307/3454636

Ho, Y. S. (2006). Review of second-order models for adsorption systems.

Journal of Hazardous Materials, ***136*(3),** 681–689. https://doi.org/10.1016/J.JHAZMAT.2005.12.043

Holcomb, D. A., Knee, J., Sumner, T., Adriano, Z., de Bruijn, E., Nalá, R., Cumming, O., Brown, J., & Stewart, J. R. (2020). Human fecal contamination of water, soil, and surfaces in households sharing poor-quality sanitation facilities in Maputo, Mozambique. *International Journal of Hygiene and Environmental Health*, ***226,*** 113496. https://doi.org/10.1016/J.IJHEH.2020.113496

Homburg, M., Rasmussen, Å. K., Ramhøj, L., & Feldt-Rasmussen, U. (2022). The Influence of Triclosan on the Thyroid Hormone System in Humans - A Systematic Review. *Frontiers in Endocrinology*, ***13***. https://doi.org/10.3389/FENDO.2022.883827/FULL

Horcajada, J. P., Montero, M., Oliver, A., Sorlí, L., Luque, S., Gómez-Zorrilla, S., Benito, N., & Grau, S. (2019). Epidemiology and treatment of multidrug-resistant and extensively drug-resistant Pseudomonas aeruginosa infections. *Clinical Microbiology Reviews*, ***32*(4).** https://doi.org/10.1128/CMR.00031-19

Hu, X., Hu, Y., Xu, G., Li, M., Zhu, Y., Jiang, L., Tu, Y., Zhu, X., Xie, X., & Li, A. (2020). Green synthesis of a magnetic β-cyclodextrin polymer for rapid removal of organic micro-pollutants and heavy metals from dyeing wastewater. *Environmental Research*, ***180,*** 108796. https://doi.org/10.1016/J.ENVRES.2019.108796

Ibrahim, M., Ramadan, E., Elsadek, N. E., Emam, S. E., Shimizu, T., Ando, H., Ishima, Y., Elgarhy, O. H., Sarhan, H. A., Hussein, A. K., & Ishida, T. (2022). Polyethylene glycol (PEG): The nature, immunogenicity, and role in the hypersensitivity of PEGylated products. *Journal of Controlled Release*, ***351,*** 215–230. https://doi.org/10.1016/J.JCONREL.2022.09.031

Ifelebuegu, A. O., Ukpebor, J. E., Obidiegwu, C. C., & Kwofi, B. C. (2015). Comparative potential of black tea leaves waste to granular activated

carbon in adsorption of endocrine disrupting compounds from aqueous solution. *Global Journal of Environmental Science and Management*, ***1*(3)**, 205–214. https://doi.org/10.7508/gjesm.2015.03.003

Igwegbe, C. A., Oba, S. N., Aniagor, C. O., Adeniyi, A. G., & Ighalo, J. O. (2021). Adsorption of ciprofloxacin from water: A comprehensive review. *Journal of Industrial and Engineering Chemistry*, ***93,*** 57–77. https://doi.org/10.1016/J.JIEC.2020.09.023

Ishida, T. (2018). Antibacterial mechanism of Ag+ ions for bacteriolyses of bacterial cell walls via peptidoglycan autolysins, and DNA damages. *MOJ Toxicology*, ***4*(5)**. https://doi.org/10.15406/MOJT.2018.04.00125

Ismadji, S., Soetaredjo, F. E., & Ayucitra, A. (2015). *Modification of Clay Minerals for Adsorption Purpose*. **39–56.** https://doi.org/10.1007/978-3-319-16712-1_3

Issaoui, O., Amor, H. Ben, Ismail, M., Pirault-roy, L., & Razak, M. (2020). *Adsorption of Bisphenol A from Aqueous Solution by HDTMA- Tunisian Clay Synthesized Under Microwave Irradiation : A Parametric and Thermodynamic Study*. ***372,*** 361–372.

Jafarpour, M., Aghdam, A. S., Koşar, A., Cebeci, F. Ç., & Ghorbani, M. (2021). Electrospinning of ternary composite of PMMA-PEG-SiO2 nanoparticles: Comprehensive process optimization and electrospun properties. *Materials Today Communications*, ***29***. https://doi.org/10.1016/j.mtcomm.2021.102865

Jayaramudu, T., Raghavendra, G. M., Varaprasad, K., Reddy, G. V. S., Reddy, A. B., Sudhakar, K., & Sadiku, E. R. (2016). Preparation and characterization of poly(ethylene glycol) stabilized nano silver particles by a mechanochemical assisted ball mill process. *Journal of Applied Polymer Science*, ***133*(7)**, 1–8. https://doi.org/10.1002/app.43027

Jha, A. K., & Prasad, K. (2010). Green Synthesis of Silver Nanoparticles Using Cycas Leaf. *International Journal of Green Nanotechnology: Physics*

and Chemistry, ***1*(2)**, P110–P117. https://doi.org/10.1080/19430871003684572

Jiang, W. T., Chang, P. H., Wang, Y. S., Tsai, Y., Jean, J. S., Li, Z., & Krukowski, K. (2013). Removal of ciprofloxacin from water by birnessite. *Journal of Hazardous Materials*, ***250–251,*** 362–369. https://doi.org/10.1016/J.JHAZMAT.2013.02.015

Jiménez, B. C., Bustos, A. R. M., Reyes, R. P., Paniagua, S. A., & Baudrit, J. R. V. (2022). Novel pathway for the sonochemical synthesis of silver nanoparticles with near - spherical shape and high stability in aqueous media. *Scientific Reports*, **1–17.** https://doi.org/10.1038/s41598-022-04921-9

Joseph, L., Zaib, Q., Khan, I. A., Berge, N. D., Park, Y. G., Saleh, N. B., & Yoon, Y. (2011). Removal of bisphenol A and 17α-ethinyl estradiol from landfill leachate using single-walled carbon nanotubes. *Water Research*, ***45*(13),** 4056–4068. https://doi.org/10.1016/J.WATRES.2011.05.015

Kalam, S., Abu-Khamsin, S. A., Kamal, M. S., & Patil, S. (2021). Surfactant Adsorption Isotherms: A Review. *ACS Omega*, ***6*(48)**, 32342–32348. https://doi.org/10.1021/acsomega.1c04661

Kanwal, S., & Vaitla, P. (2023). Streptococcus Pyogenes. *StatPearls*.

Karunakaran, G., Sudha, K. G., Ali, S., & Cho, E. B. (2023). Biosynthesis of Nanoparticles from Various Biological Sources and Its Biomedical Applications. *Molecules*, ***28*(11)**, 4527. https://doi.org/10.3390/MOLECULES28114527

Kasthuri, J., Veerapandian, S., & Rajendiran, N. (2009). Biological synthesis of silver and gold nanoparticles using apiin as reducing agent. *Colloids and Surfaces. B, Biointerfaces*, ***68*(1)**, 55–60. https://doi.org/10.1016/J.COLSURFB.2008.09.021

Kesari, K. K., Soni, R., Jamal, Q. M. S., Tripathi, P., Lal, J. A., Jha, N. K., Siddiqui, M. H., Kumar, P., Tripathi, V., & Ruokolainen, J. (2021).

Wastewater Treatment and Reuse: a Review of its Applications and Health Implications. *Water, Air, and Soil Pollution*, ***232*****(5)**, 1–28. https://doi.org/10.1007/S11270-021-05154-8/FIGURES/5

Kesharwani, J., Yoon, K. Y., Hwang, J., & Rai, M. (2009). Phytofabrication of silver nanoparticles by leaf extract of Datura metel: Hypothetical mechanism involved in synthesis. *Journal of Bionanoscience*, ***3*****(1),** 39–44. https://doi.org/10.1166/JBNS.2009.1008

Khan, F. M., & Gupta, R. (2020). Escherichia coli (e. coli) as an indicator of fecal contamination in groundwater: A review. *Environmental Science and Engineering*, **225–235**. https://doi.org/10.1007/978-3-030-45263-6_21/COVER

Khan, R. M. A., Anwar, S., & Pirzada, Z. A. (2020). Streptococcus pyogenes strains associated with invasive and non-invasive infections present possible links with emm types and superantigens. *Iranian Journal of Basic Medical Sciences*, ***23*****(1)**, 133. https://doi.org/10.22038/IJBMS.2019.38635.9164

Kidd, K. A., Blanchfield, P. J., Mills, K. H., Palace, V. P., Evans, R. E., Lazorchak, J. M., & Flick, R. W. (2007). Collapse of a fish population after exposure to a synthetic estrogen. *Proceedings of the National Academy of Sciences of the United States of America*, ***104*****(21),** 8897. https://doi.org/10.1073/PNAS.0609568104

Klein, E. Y., Van Boeckel, T. P., Martinez, E. M., Pant, S., Gandra, S., Levin, S. A., Goossens, H., & Laxminarayan, R. (2018). Global increase and geographic convergence in antibiotic consumption between 2000 and 2015. *Proceedings of the National Academy of Sciences of the United States of America*, ***115*****(15),** E3463–E3470. https://doi.org/10.1073/PNAS.1717295115

Kora, A. J., Sashidhar, R. B., & Arunachalam, J. (2010). Gum kondagogu (Cochlospermum gossypium): A template for the green synthesis and

stabilization of silver nanoparticles with antibacterial application. *Carbohydrate Polymers*, ***82*****(3)**, 670–679. https://doi.org/10.1016/J.CARBPOL.2010.05.034

Krishnaraj, C., Jagan, E. G., Rajasekar, S., Selvakumar, P., Kalaichelvan, P. T., & Mohan, N. (2010). Synthesis of silver nanoparticles using Acalypha indica leaf extracts and its antibacterial activity against water borne pathogens. *Colloids and Surfaces. B, Biointerfaces*, ***76*****(1),** 50–56. https://doi.org/10.1016/J.COLSURFB.2009.10.008

Kumar, A., Patra, C., Kumar, S., & Narayanasamy, S. (2022). Effect of magnetization on the adsorptive removal of an emerging contaminant ciprofloxacin by magnetic acid activated carbon. *Environmental Research*, ***206,*** 112604. https://doi.org/10.1016/J.ENVRES.2021.112604

Kumar, S. V., Kumar, S. P., Rupesh, D., & Nitin, K. (2011). Journal of Chemical and Pharmaceutical Research preparations. *Journal of Chemical and Pharmaceutical Research*, ***3*****(1)**, 675–684.

Kumari, N., Mohan, C., Kumari, N., & Mohan, C. (2021). Basics of Clay Minerals and Their Characteristic Properties. *Clay and Clay Minerals*. https://doi.org/10.5772/INTECHOPEN.97672

Kurhade, P., Kodape, S., & Choudhury, R. (2021). Overview on green synthesis of metallic nanoparticles. *Chemical Papers, 75:10,* ***75*****(10)**, 5187–5222. https://doi.org/10.1007/S11696-021-01693-W

Lalhmunsiama, Tiwari, D., & Lee, S. M. (2015). Physico-chemical studies in the removal of Sr(II) from aqueous solutions using activated sericite. *Journal of Environmental Radioactivity*, ***147,*** 76–84. https://doi.org/10.1016/j.jenvrad.2015.05.017

Lanrewaju, A. A., Enitan-Folami, A. M., Sabiu, S., & Swalaha, F. M. (2022). A review on disinfection methods for inactivation of waterborne viruses. *Frontiers in Microbiology*, ***13*****.** https://doi.org/10.3389/FMICB.2022.991856

Larsson, D. G. J., & Flach, C. F. (2021). Antibiotic resistance in the environment. *Nature Reviews Microbiology 2021 20:5*, ***20*(5),** 257–269. https://doi.org/10.1038/s41579-021-00649-x

Lee, D. G., Zhao, F., Rezenom, Y. H., Russell, D. H., & Chu, K. H. (2012). Biodegradation of triclosan by a wastewater microorganism. *Water Research*, ***46*(13),** 4226–4234. https://doi.org/10.1016/j.watres.2012.05.025

Li, J., Yang, L., & Wu, Z. (2021). Toxicity of chlortetracycline and oxytetracycline on Vallisneria natans (Lour.) Hare. *Environmental Science and Pollution Research*, ***28*(44),** 62549–62561. https://doi.org/10.1007/S11356-021-14922-2/FIGURES/6

Li, J., Zhou, B., Liu, Y., Yang, Q., & Cai, W. (2008). Influence of the coexisting contaminants on bisphenol A sorption and desorption in soil. *Journal of Hazardous Materials*, ***151*(2–3),** 389–393. https://doi.org/10.1016/j.jhazmat.2007.06.001

Li, N., Fang, J., Jiang, P., Li, C., Kang, H., & Wang, W. (2022). Adsorption Properties and Mechanism of Attapulgite to Graphene Oxide in Aqueous Solution. *International Journal of Environmental Research and Public Health*, ***19*(5),** 2793. https://doi.org/10.3390/IJERPH19052793

Li, X. G., Kresse, I., Springer, J., Nissen, J., & Yang, Y. L. (2001). Morphology and gas permselectivity of blend membranes of polyvinylpyridine with ethylcellulose. *Polymer*, ***42*(16),** 6859–6869. https://doi.org/10.1016/S0032-3861(01)00057-X

Li, Y., Li, M., Li, Z., Yang, L., & Liu, X. (2019). Effects of particle size and solution chemistry on Triclosan sorption on polystyrene microplastic. *Chemosphere*, ***231*,** 308–314. https://doi.org/10.1016/J.CHEMOSPHERE.2019.05.116

Li, Z., Liu, Y., Zou, S., Lu, C., Bai, H., Mu, H., & Duan, J. (2020). Removal and adsorption mechanism of tetracycline and cefotaxime contaminants

in water by NiFe2O4-COF-chitosan-terephthalaldehyde nanocomposites film. *Chemical Engineering Journal*, ***382,*** 123008. https://doi.org/10.1016/j.cej.2019.123008

Lima, É. C., Adebayo, M. A., & Machado, F. M. (2015). Kinetic and equilibrium models of adsorption. *Carbon Nanostructures*, *0*(9783319188744), **33–69.** https://doi.org/10.1007/978-3-319-18875-1_3/COVER

Lin, D., Li, Y., Zhou, Q., Xu, Y., & Wang, D. (2014). Effect of triclosan on reproduction, DNA damage and heat shock protein gene expression of the earthworm Eisenia fetida. *Ecotoxicology*, ***23*(10),** 1826–1832. https://doi.org/10.1007/S10646-014-1320-9

Liu, G., & Zhang, G. (2013). *Interactions between Polymers and Phospholipid Membranes*. **71–81.** https://doi.org/10.1007/978-3-642-39790-5_5

Liu, M., Hou, L. an, Yu, S., Xi, B., Zhao, Y., & Xia, X. (2013). MCM-41 impregnated with A zeolite precursor: Synthesis, characterization and tetracycline antibiotics removal from aqueous solution. *Chemical Engineering Journal*, ***223,*** 678–687. https://doi.org/10.1016/J.CEJ.2013.02.088

Liu, S. J., & Xu, R. (2014). Adsorption characteristics of triclosan on chitosan/poly(vinyl alcohol) composite nanofibrous membranes. *Applied Mechanics and Materials*, ***448–453,*** 134–138. https://doi.org/10.4028/www.scientific.net/AMM.448-453.134

Liu, X., Guan, J., Lai, G., Xu, Q., Bai, X., Wang, Z., & Cui, S. (2020). Stimuli-responsive adsorption behavior toward heavy metal ions based on comb polymer functionalized magnetic nanoparticles. *Journal of Cleaner Production*, ***253,*** 119915. https://doi.org/10.1016/J.JCLEPRO.2019.119915

Liu, Y., Lu, X., Wu, F., & Deng, N. (2011). Adsorption and photooxidation of pharmaceuticals and personal care products on clay minerals. *Reaction*

Kinetics, Mechanisms and Catalysis, ***104*****(1),** 61–73. https://doi.org/10.1007/S11144-011-0349-5

Lodhi, R. S., Kumar, P., Achuthanunni, A., Rahaman, M., & Das, P. (2022). Mechanical properties of polymer/graphene composites. *Polymer Nanocomposites Containing Graphene: Preparation, Properties, and Applications*, **75–105**. https://doi.org/10.1016/B978-0-12-821639-2.00019-7

Luo, Y., Guo, W., Ngo, H. H., Nghiem, L. D., Hai, F. I., Zhang, J., Liang, S., & Wang, X. C. (2014). A review on the occurrence of micropollutants in the aquatic environment and their fate and removal during wastewater treatment. In *Science of the Total Environment* (Vols. **473–474**, pp. 619–641). Elsevier B.V. https://doi.org/10.1016/j.scitotenv.2013.12.065

Luo, Z., Li, H., Yang, Y., Lin, H., & Yang, Z. (2017). Adsorption of 17 α-ethinylestradiol from aqueous solution onto a re duce d graphene oxide-magnetic composite. *Journal of the Taiwan Institute of Chemical Engineers*, ***80,*** 797–804. https://doi.org/10.1016/j.jtice.2017.09.028

Ma, J., Yang, M., Yu, F., & Zheng, J. (2015). Water-enhanced Removal of Ciprofloxacin from Water by Porous Graphene Hydrogel. *Scientific Reports*, ***5,*** 1–10. https://doi.org/10.1038/srep13578

Mailler, R., Gasperi, J., Coquet, Y., Buleté, A., Vulliet, E., Deshayes, S., Zedek, S., Mirande-Bret, C., Eudes, V., Bressy, A., Caupos, E., Moilleron, R., Chebbo, G., & Rocher, V. (2016). Removal of a wide range of emerging pollutants from wastewater treatment plant discharges by micro-grain activated carbon in fluidized bed as tertiary treatment at large pilot scale. *Science of the Total Environment*, ***542*****(**Pt A), 983–996. https://doi.org/10.1016/j.scitotenv.2015.10.153

Makowski, M., & Bogunia, M. (2020). Influence of ionic strength on hydrophobic interactions in water: Dependence on solute size and shape. *Journal of Physical Chemistry B*, ***124*****(46)**, 10326–10336.

https://doi.org/10.1021/ACS.JPCB.0C06399/ASSET/IMAGES/LARGE/JP0C06399_0009.JPEG

Malaeb, L., & Ayoub, G. M. (2011). Reverse osmosis technology for water treatment: State of the art review. *Desalination*, ***267*****(1)**, 1–8. https://doi.org/10.1016/J.DESAL.2010.09.001

Malsawmdawngzela, R., Lalhmunsiama, & Tiwari, D. (2022). Novel and highly efficient functionalized bentonite for elimination of Cu2+ and Cd2+ from aqueous wastes. *Environmental Engineering Research*, ***27*****(6)**, 0–2. https://doi.org/10.4491/eer.2021.355

Malsawmdawngzela, R., & Tiwari, D. (2022a). 17α-Ethinylestradiol elimination using synthesized and dense nanocomposite materials: Mechanism and real matrix treatment. *Korean Journal of Chemical Engineering*, ***39*****(3),** 646–654. https://doi.org/10.1007/s11814-021-0958-2

Maurya, A., Singh, M. K., & Kumar, S. (2020). Biofiltration technique for removal of waterborne pathogens. *Waterborne Pathogens*, **123**. https://doi.org/10.1016/B978-0-12-818783-8.00007-4

Md Ishak, N. A. I., Kamarudin, S. K., & Timmiati, S. N. (2019). Green synthesis of metal and metal oxide nanoparticles via plant extracts: an overview. *Materials Research Express*, ***6*****(11)**, 112004. https://doi.org/10.1088/2053-1591/AB4458

Mekuye, B., & Abera, B. (2023). Nanomaterials: An overview of synthesis, classification, characterization, and applications. *Nano Select*, ***4*****(8),** 486–501. https://doi.org/10.1002/NANO.202300038

Metcalfe, C. D., Bayen, S., Desrosiers, M., Muñoz, G., Sauvé, S., & Yargeau, V. (2022). An introduction to the sources, fate, occurrence and effects of endocrine disrupting chemicals released into the environment. *Environmental Research*, ***207***. https://doi.org/10.1016/J.ENVRES.2021.112658

Mirsoleimani-Azizi, S. M., Setoodeh, P., Zeinali, S., & Rahimpour, M. R.

(2018). Tetracycline antibiotic removal from aqueous solutions by MOF-5: Adsorption isotherm, kinetic and thermodynamic studies. *Journal of Environmental Chemical Engineering*, ***6*****(5),** 6118–6130. https://doi.org/10.1016/J.JECE.2018.09.017

Mittal, A. K., Chisti, Y., & Banerjee, U. C. (2013). Synthesis of metallic nanoparticles using plant extracts. *Biotechnology Advances*, ***31*****(2)**, 346–356. https://doi.org/10.1016/J.BIOTECHADV.2013.01.003

Mohammed, A. A., Abdel Moamen, O. A., Metwally, S. S., El-Kamash, A. M., Ashour, I., & Al-Geundi, M. S. (2020). Utilization of Modified Attapulgite for the Removal of Sr(II), Co(II), and Ni(II) Ions from Multicomponent System, Part I: Kinetic Studies. *Environmental Science and Pollution Research*, ***27*****(7)**, 6824–6836. https://doi.org/10.1007/s11356-019-07292-3

Murray, C. J., Ikuta, K. S., Sharara, F., Swetschinski, L., Robles Aguilar, G., Gray, A., Han, C., Bisignano, C., Rao, P., Wool, E., Johnson, S. C., Browne, A. J., Chipeta, M. G., Fell, F., Hackett, S., Haines-Woodhouse, G., Kashef Hamadani, B. H., Kumaran, E. A. P., McManigal, B., … Naghavi, M. (2022). Global burden of bacterial antimicrobial resistance in 2019: a systematic analysis. *The Lancet*, *399*(10325), **629–655**. https://doi.org/10.1016/S0140-6736(21)02724-0

Murugaiyan, J., Anand Kumar, P., Rao, G. S., Iskandar, K., Hawser, S., Hays, J. P., Mohsen, Y., Adukkadukkam, S., Awuah, W. A., Jose, R. A. M., Sylvia, N., Nansubuga, E. P., Tilocca, B., Roncada, P., Roson-Calero, N., Moreno-Morales, J., Amin, R., Krishna Kumar, B., Kumar, A.,van Dongen, M. B. M. (2022). Progress in Alternative Strategies to Combat Antimicrobial Resistance: Focus on Antibiotics. *Antibiotics (Basel, Switzerland)*, ***11*****(2).** https://doi.org/10.3390/ANTIBIOTICS11020200

Nabikhan, A., Kandasamy, K., Raj, A., & Alikunhi, N. M. (2010). Synthesis of antimicrobial silver nanoparticles by callus and leaf extracts from saltmarsh plant, Sesuvium portulacastrum L. *Colloids and Surfaces. B,*

Biointerfaces, ***79*****(2)**, 488–493. https://doi.org/10.1016/J.COLSURFB.2010.05.018

Natkański, P., Kuśtrowski, P., Białas, A., Piwowarska, Z., & Michalik, M. (2012). Controlled swelling and adsorption properties of polyacrylate/montmorillonite composites. *Materials Chemistry and Physics*, ***136*****(2–3),** 1109–1115. https://doi.org/10.1016/J.MATCHEMPHYS.2012.08.061

Neelakandan, M. S., & Thomas, S. (2018). Applications of Silver Nanoparticles for Medicinal Purpose. *JSM Nanotechnol Nanomed*, ***6*****(1)**, 1063.

Ngo, H. S., Nguyen, T. L., Tran, N. T., & Le, H. C. (2023). Photocatalytic Removal of Ciprofloxacin in Water by Novel Sandwich-like CuFe2O4 on rGO/Halloysite Material: Insights into Kinetics and Intermediate Reactive Radicals. *Water 2023, Vol. 15, Page 1569*, ***15*****(8),** 1569. https://doi.org/10.3390/W15081569

Ni, B. J., Huang, Q. S., Wang, C., Ni, T. Y., Sun, J., & Wei, W. (2019). Competitive adsorption of heavy metals in aqueous solution onto biochar derived from anaerobically digested sludge. *Chemosphere*, ***219***, 351–357. https://doi.org/10.1016/j.chemosphere.2018.12.053

Oh, J. K., Yegin, Y., Yang, F., Zhang, M., Li, J., Huang, S., Verkhoturov, S. V., Schweikert, E. A., Perez-Lewis, K., Scholar, E. A., Taylor, T. M., Castillo, A., Cisneros-Zevallos, L., Min, Y., & Akbulut, M. (2018). The influence of surface chemistry on the kinetics and thermodynamics of bacterial adhesion. *Scientific Reports 2018 8:1*, ***8*****(1)**, 1–13. https://doi.org/10.1038/s41598-018-35343-1

Okoli, C. P., & Ofomaja, A. E. (2019). Development of sustainable magnetic polyurethane polymer nanocomposite for abatement of tetracycline antibiotics aqueous pollution: Response surface methodology and adsorption dynamics. *Journal of Cleaner Production*, ***217,*** 42–55.

https://doi.org/10.1016/J.JCLEPRO.2019.01.157

Olasupo, A., Sadiq, A. C., & Suah, F. B. M. (2022). A novel approach in the removal of ciprofloxacin antibiotic in an aquatic system using polymer inclusion membrane. *Environmental Technology & Innovation*, ***27***, 102523. https://doi.org/10.1016/J.ETI.2022.102523

Ong, L. K., Soetaredjo, F. E., Kurniawan, A., Ayucitra, A., Liu, J. C., & Ismadji, S. (2014). Investigation on the montmorillonite adsorption of biocidal compounds incorporating thermodynamical-based multicomponent adsorption isotherm. *Chemical Engineering Journal*, ***241*,** 9–18. https://doi.org/10.1016/j.cej.2013.12.001

Oram, B. (2020). *Water Research Center - Water Testing Fecal Bacteria Pathogenic Organisms Water*. Fecal Coliform Bacteria in Water.

Oraon, R., De Adhikari, A., Tiwari, S. K., & Nayak, G. C. (2016). Nanoclay-based hierarchical interconnected mesoporous CNT/PPy electrode with improved specific capacitance for high performance supercapacitors. *Dalton Transactions*, ***45*(22),** 9113–9126. https://doi.org/10.1039/c6dt00600k

Osman, A. I., Chen, Z., Elgarahy, A. M., Farghali, M., Mohamed, I. M. A., Priya, A. K., Hawash, H. B., & Yap, P. S. (2024). Membrane Technology for Energy Saving: Principles, Techniques, Applications, Challenges, and Prospects. *Advanced Energy and Sustainability Research*, ***5*(5),** 2400011. https://doi.org/10.1002/AESR.202400011

Osmari, T. A., Gallon, R., Schwaab, M., Barbosa-Coutinho, E., Severo, J. B., & Pinto, J. C. (2013). Statistical analysis of linear and non-linear regression for the estimation of adsorption isotherm parameters. *Adsorption Science and Technology*, ***31*(5),** 433–458. https://doi.org/10.1260/0263-6174.31.5.433

Otieno, M. O. (2018). *How Much Of The Earth Is Covered By Freshwater?* Worldatlas.

Padhi, S., & Behera, A. (2022). Biosynthesis of Silver Nanoparticles: Synthesis, mechanism, and characterization. *Agri-Waste and Microbes for Production of Sustainable Nanomaterials*, **397–440.** https://doi.org/10.1016/B978-0-12-823575-1.00008-1

Pan, B., Pan, B., Zhang, W., Lv, L., Zhang, Q., & Zheng, S. (2009). Development of polymeric and polymer-based hybrid adsorbents for pollutants removal from waters. *Chemical Engineering Journal*, ***151*(1–3),** 19–29. https://doi.org/10.1016/j.cej.2009.02.036

Pang, Z., Raudonis, R., Glick, B. R., Lin, T. J., & Cheng, Z. (2019). Antibiotic resistance in Pseudomonas aeruginosa: mechanisms and alternative therapeutic strategies. *Biotechnology Advances*, ***37*(1),** 177–192. https://doi.org/10.1016/J.BIOTECHADV.2018.11.013

Paprocka, P., Durnaś, B., Mańkowska, A., Król, G., Wollny, T., & Bucki, R. (2022). Pseudomonas aeruginosa Infections in Cancer Patients. *Pathogens*, ***11*(6).** https://doi.org/10.3390/PATHOGENS11060679

Parida, V. K., Saidulu, D., Majumder, A., Srivastava, A., Gupta, B., & Gupta, A. K. (2021). Emerging contaminants in wastewater: A critical review on occurrence, existing legislations, risk assessment, and sustainable treatment alternatives. *Journal of Environmental Chemical Engineering*, ***9*(5),** 105966. https://doi.org/10.1016/J.JECE.2021.105966

Park, Y., Sun, Z., Ayoko, G. A., & Frost, R. L. (2014). Bisphenol A sorption by organo-montmorillonite: Implications for the removal of organic contaminants from water. *Chemosphere*, ***107,*** 249–256. https://doi.org/10.1016/j.chemosphere.2013.12.050

Pellenz, L., de Oliveira, C. R. S., da Silva Júnior, A. H., da Silva, L. J. S., da Silva, L., Ulson de Souza, A. A., de Souza, S. M. de A. G. U., Borba, F. H., & da Silva, A. (2023). A comprehensive guide for characterization of adsorbent materials. *Separation and Purification Technology*, ***305,*** 122435. https://doi.org/10.1016/J.SEPPUR.2022.122435

Petersen, R. C., Richard, J., & Petersen, C. (2015). Triclosan Computational Conformational Chemistry Analysis forAntimicrobial Properties in Polymers. *Journal of Nature and Science*, ***1*(3).**

Petrie, B., Barden, R., & Kasprzyk-Hordern, B. (2015). A review on emerging contaminants in wastewaters and the environment: Current knowledge, understudied areas and recommendations for future monitoring. *Water Research*, ***72*,** 3–27. https://doi.org/10.1016/j.watres.2014.08.053

Philip, D. (2010). Green synthesis of gold and silver nanoparticles using Hibiscus rosa sinensis. *Physica E: Low-Dimensional Systems and Nanostructures*, ***42*(5),** 1417–1424. https://doi.org/10.1016/J.PHYSE.2009.11.081

Phuekphong, A. F., Imwiset, K. J., & Ogawa, M. (2020). Organically Modified Bentonite as an Efficient and Reusable Adsorbent for Triclosan Removal from Water. *Langmuir*, ***36*(31),** 9025–9034. https://doi.org/10.1021/acs.langmuir.0c00407

Pillai, S. B. (2020). Adsorption in Water and Used Water Purification. *Handbook of Water and Used Water Purification*, **1–22.** https://doi.org/10.1007/978-3-319-66382-1_4-1

Pokrajac, L., Abbas, A., Chrzanowski, W., Dias, G. M., Eggleton, B. J., Maguire, S., Maine, E., Malloy, T., Nathwani, J., Nazar, L., Sips, A., Sone, J., Van Den Berg, A., Weiss, P. S., & Mitra, S. (2021). Nanotechnology for a Sustainable Future: Addressing Global Challenges with the International Network4Sustainable Nanotechnology. *ACS Nano*, ***15*(12),** 18608–18623. https://doi.org/10.1021/ACSNANO.1C10919/ASSET/IMAGES/MEDIUM.

Qin, S., Xiao, W., Zhou, C., Pu, Q., Deng, X., Lan, L., Liang, H., Song, X., & Wu, M. (2022). Pseudomonas aeruginosa: pathogenesis, virulence factors, antibiotic resistance, interaction with host, technology advances

and emerging therapeutics. *Signal Transduction and Targeted Therapy 2022 7:1*, ***7*(1),** 1–27. https://doi.org/10.1038/s41392-022-01056-1

Qu, C., Ma, M., Chen, W., Cai, P., & Huang, Q. (2017). Surface complexation modeling of Cu(II) sorption to montmorillonite–bacteria composites. *Science of The Total Environment*, ***607–608,*** 1408–1418. https://doi.org/10.1016/J.SCITOTENV.2017.07.068

Rafa, N., Ahmed, B., Zohora, F., Bakya, J., Ahmed, S., Ahmed, S. F., Mofijur, M., Chowdhury, A. A., & Almomani, F. (2024). Microplastics as carriers of toxic pollutants: Source, transport, and toxicological effects. *Environmental Pollution*, ***343,*** 123190. https://doi.org/10.1016/J.ENVPOL.2023.123190

Raina, N., Singh, A. K., & Islam, A. (2021). Biological Implications of Polyethylene Glycol and PEGylation: Therapeutic Approaches Based on Biophysical Studies and Protein Structure-Based Drug Design Tools. *Innovations and Implementations of Computer Aided Drug Discovery Strategies in Rational Drug Design*, **273–294.** https://doi.org/10.1007/978-981-15-8936-2_11/COVER

Rashed, M. N., & Rashed, M. N. (2013). Adsorption Technique for the Removal of Organic Pollutants from Water and Wastewater. *Organic Pollutants - Monitoring, Risk and Treatment*. https://doi.org/10.5772/54048

Ratola, N., Cincinelli, A., Alves, A., & Katsoyiannis, A. (2012). Occurrence of organic microcontaminants in the wastewater treatment process. A mini review. *Journal of Hazardous Materials*, ***239–240,*** 1–18. https://doi.org/10.1016/j.jhazmat.2012.05.040

Reddy, J., Prasanna, L., Singh, J., & Choo, K. (2016). Effective removal of bisphenol A (BPA) from water using a goethite / activated carbon composite. *Process Safety and Environmental Protection*, ***103,*** 87–96. https://doi.org/10.1016/j.psep.2016.06.038

Reed, B. (2013). Technical Notes on Drinking-Water, Sanitation and Hygiene in Emergencies. *World Health*, ***36*****(2)**, 64.

Regadío, M., Black, J. A., & Thornton, S. F. (2020). The role of natural clays in the sustainability of landfill liners. *Detritus,* ***12,*** 100–113. https://doi.org/10.31025/2611-4135/2020.13946

Revellame, E. D., Fortela, D. L., Sharp, W., Hernandez, R., & Zappi, M. E. (2020). Adsorption kinetic modeling using pseudo-first order and pseudo-second order rate laws: A review. *Cleaner Engineering and Technology*, ***1***, 100032. https://doi.org/10.1016/J.CLET.2020.100032

Richard, J., Boergers, A., vom Eyser, C., Bester, K., & Tuerk, J. (2014). Toxicity of the micropollutants Bisphenol A, Ciprofloxacin, Metoprolol and Sulfamethoxazole in water samples before and after the oxidative treatment. *International Journal of Hygiene and Environmental Health*, ***217*****(4–5),** 506–514. https://doi.org/10.1016/j.ijheh.2013.09.007

Rogers, K. (2023). *Bisphenol A (BPA) | Description, Biological Effects, & Environmental Effects*. https://www.britannica.com/science/bisphenol-A

Rogowska, J., Cieszynska-Semenowicz, M., Ratajczyk, W., & Wolska, L. (2020). Micropollutants in treated wastewater. In *Ambio* (Vol. **49**, Issue 2, pp. 487–503). Springer. https://doi.org/10.1007/s13280-019-01219-5

Sadrnezhaad, S. K., Ahmadi, E., & Mozammel, M. (2006). Kinetics of silver dissolution in nitric acid from Ag-Au0.04-Cu0.10 and Ag-Cu0.23 scraps. *Journal of Materials Science and Technology*, ***22*****(5)**, 696–700.

Sadrolhosseini, A. R., Rashid, S. A., Noor, A. S. M., Kharazmi, A., & Mehdipour, L. A. (2015). Fabrication of silver nanoparticles in pomegranate seed oil with thermal properties by laser ablation technique. *Digest Journal of Nanomaterials and Biostructures,* ***10*****(3),** 1009–1018.

Sailo, L., Tiwari, D., & Lee, S. M. (2017). Degradation of some micro-pollutants from aqueous solutions using ferrate (VI): Physico-chemical studies. *Separation Science and Technology (Philadelphia),* ***52*****(17),**

2756–2766. https://doi.org/10.1080/01496395.2017.1374976

Sajid, M., Nazal, M. K., Ihsanullah, Baig, N., & Osman, A. M. (2018). Removal of heavy metals and organic pollutants from water using dendritic polymers based adsorbents: A critical review. *Separation and Purification Technology*, ***191,*** 400–423. https://doi.org/10.1016/J.SEPPUR.2017.09.011

Samal, K., Mahapatra, S., & Hibzur Ali, M. (2022). Pharmaceutical wastewater as Emerging Contaminants (EC): Treatment technologies, impact on environment and human health. *Energy Nexus*, ***6,*** 100076. https://doi.org/10.1016/J.NEXUS.2022.100076

San-rom, M. F., Sol, C., Schr, S., & Ortiz, I. (2020). *Critical review on the mechanistic photolytic and photocatalytic degradation of triclosan*. ***260***. https://doi.org/10.1016/j.jenvman.2020.110101

Santaeufemia, S., Abalde, J., & Torres, E. (2019). Eco-friendly rapid removal of triclosan from seawater using biomass of a microalgal species: Kinetic and equilibrium studies. *Journal of Hazardous Materials*, ***369,*** 674–683. https://doi.org/10.1016/j.jhazmat.2019.02.083

Sardi, A., Bounaceur, B., Mokhtar, A., Boukoussa, B., Abbes, M. T., Chaibi, W., Nacer, A., Khadidja, K. B., Issam, I., Iqbal, J., Patole, S. P., & Abboud, M. (2023). Kinetics and Thermodynamic Studies for Removal of Trypan Blue and Methylene Blue from Water Using Nano Clay Filled Composite of HTAB and PEG and its Antibacterial Activity. *Journal of Polymers and the Environment*. https://doi.org/10.1007/S10924-023-02927-6

Sarojini, G., Kannan, P., Rajamohan, N., & Rajasimman, M. (2023). *Nanoparticles and Nanocomposites for Heavy Metals Removal*. **139–161**. https://doi.org/10.1007/978-981-99-6924-1_8

Sathishkumar, M., Sneha, K., Won, S. W., Cho, C. W., Kim, S., & Yun, Y. S. (2009). Cinnamon zeylanicum bark extract and powder mediated green

synthesis of nano-crystalline silver particles and its bactericidal activity. *Colloids and Surfaces B: Biointerfaces*, ***73*****(2),** 332–338. https://doi.org/10.1016/J.COLSURFB.2009.06.005

Sayğili, H., & Güzel, F. (2016). Effective removal of tetracycline from aqueous solution using activated carbon prepared from tomato (Lycopersicon esculentum Mill.) industrial processing waste. *Ecotoxicology and Environmental Safety*, ***131*****,** 22–29. https://doi.org/10.1016/J.ECOENV.2016.05.001

Scaria, J., Anupama, K. V., & Nidheesh, P. V. (2021). Tetracyclines in the environment: An overview on the occurrence, fate, toxicity, detection, removal methods, and sludge management. *Science of The Total Environment*, ***771*****,** 145291. https://doi.org/10.1016/J.SCITOTENV.2021.145291

Schäfer, A. I., Akanyeti, I., & Semião, A. J. C. (2010). Edinburgh Research Explorer Micropollutant sorption to membrane polymers: A review of mechanisms for estrogens Micropollutant Sorption to Membrane Polymers: A Review of Mechanisms for Estrogens. *Colloid and Interface Science*, ***164*****(2),** 100–117. https://doi.org/10.1016/j.cis.2010.09.006

Shankar, S. S., Ahmad, A., & Sastry, M. (2003). Geranium Leaf Assisted Biosynthesis of Silver Nanoparticles. *Biotechnology Progress*, ***19*****(6),** 1627–1631. https://doi.org/10.1021/BP034070W

Shankar, S. S., Rai, A., Ahmad, A., & Sastry, M. (2004). *Biosynthesis of silver and gold nanoparticles from extracts of different parts of the geranium plant.* Applied Nanoscience.

Shariati, A., Arshadi, M., Khosrojerdi, M. A., Abedinzadeh, M., Ganjalishahi, M., Maleki, A., Heidary, M., & Khoshnood, S. (2022). The resistance mechanisms of bacteria against ciprofloxacin and new approaches for enhancing the efficacy of this antibiotic. *Frontiers in Public Health*, ***10*****.** https://doi.org/10.3389/FPUBH.2022.1025633

Shetty, S. S., D, D., S, H., Sonkusare, S., Naik, P. B., Kumari N, S., & Madhyastha, H. (2023). Environmental pollutants and their effects on human health. *Heliyon*, ***9*****(9),** 2405–8440. https://doi.org/10.1016/J.HELIYON.2023.E19496

Shi, Y., Sun, B., & Zhu, M. (2011). Preparation and characterization of intercalated Ag/PVP-modified clay hybrids with good antimicrobial activity. *ICAFPM 2011 - Proceedings of 2011 International Conference on Advanced Fibers and Polymer Materials*, **452–455.**

Shirsath, S. R., Patil, A. P., Patil, R., Naik, J. B., Gogate, P. R., & Sonawane, S. H. (2013). Removal of Brilliant Green from wastewater using conventional and ultrasonically prepared poly(acrylic acid) hydrogel loaded with kaolin clay: A comparative study. *Ultrasonics Sonochemistry*, ***20*****(3),** 914–923. https://doi.org/10.1016/J.ULTSONCH.2012.11.010

Shrestha, P., Zhang, Y., Chen, W. J., & Wong, T. Y. (2020). Triclosan: antimicrobial mechanisms, antibiotics interactions, clinical applications, and human health. *Journal of Environmental Science and Health, Part C: Toxicology and Carcinogenesis*, ***38*****(3),** 245–268. https://doi.org/10.1080/26896583.2020.1809286

Skuza, L., Szućko-Kociuba, I., Filip, E., & Bożek, I. (2022). Natural Molecular Mechanisms of Plant Hyperaccumulation and Hypertolerance towards Heavy Metals. *International Journal of Molecular Sciences*, ***23*****(16).** https://doi.org/10.3390/IJMS23169335

So, R. T., Blair, N. E., & Masterson, A. L. (2020). Carbonate mineral identification and quantification in sediment matrices using diffuse reflectance infrared Fourier transform spectroscopy. *Environmental Chemistry Letters*, ***18*****(5),** 1725–1730. https://doi.org/10.1007/S10311-020-01027-4/FIGURES/3

Song, J. Y., & Kim, B. S. (2009). Rapid biological synthesis of silver

nanoparticles using plant leaf extracts. *Bioprocess and Biosystems Engineering*, ***32*(1),** 79–84. https://doi.org/10.1007/S00449-008-0224-6/FIGURES/6

Song, Y. J., Wang, M., Zhang, X. Y., Wu, J. Y., & Zhang, T. (2014). Investigation on the role of the molecular weight of polyvinyl pyrrolidone in the shape control of highyield silver nanospheres and nanowires. *Nanoscale Research Letters*, ***9*(1)**. https://doi.org/10.1186/1556-276X-9-17

Soni, H., & Padmaja, P. (2014). Palm shell based activated carbon for removal of bisphenol A: An equilibrium, kinetic and thermodynamic study. *Journal of Porous Materials*, ***21*(3),** 275–284. https://doi.org/10.1007/s10934-013-9772-5

Sonnefeld, J. (2001). On the influence of background electrolyte concentration on the position of the isoelectric point and the point of zero charge. *Colloids and Surfaces A: Physicochemical and Engineering Aspects*, ***190*(1–2),** 179–183. https://doi.org/10.1016/S0927-7757(01)00677-X

Sreejith, S., Shajahan, S., Prathiush, P. R., Anjana, V. M., Viswanathan, A., Chandran, V., Ajith Kumar, G. S., Jayachandran, R., Mathew, J., & Radhakrishnan, E. K. (2020). Healthy broilers disseminate antibiotic resistance in response to tetracycline input in feed concentrates. *Microbial Pathogenesis*, *149*, 104562. https://doi.org/10.1016/J.MICPATH.2020.104562

Srinivasan, R. (2011). Advances in application of natural clay and its composites in removal of biological, organic, and inorganic contaminants from drinking water. *Advances in Materials Science and Engineering*, *2011*. https://doi.org/10.1155/2011/872531

Steinhilper, R., Höff, G., Heider, J., & Murphy, B. J. (2022). Structure of the membrane-bound formate hydrogenlyase complex from Escherichia coli. *Nature Communications 2022 13:1*, ***13*(1)**, 1–13.

https://doi.org/10.1038/s41467-022-32831-x

Su, Y., Liu, C., Fang, H., & Zhang, D. (2020). Bacillus subtilis: a universal cell factory for industry, agriculture, biomaterials and medicine. *Microbial Cell Factories 2020 19:1*, ***19*****(1),** 1–12. https://doi.org/10.1186/S12934-020-01436-8

Sun, Z., Zhao, L., Liu, C., Zhen, Y., & Ma, J. (2020). Fast adsorption of BPA with high capacity based on Π-Π electron donor-acceptor and hydrophobicity mechanism using an in-situ sp2 C dominant N-doped carbon. *Chemical Engineering Journal*, ***381*****.** https://doi.org/10.1016/j.cej.2019.122510

Swenson, H., & Stadie, N. P. (2019). Langmuir's Theory of Adsorption: A Centennial Review. *Langmuir*. https://doi.org/10.1021/ACS.

Talat, N. (2020). Recent trends and research strategies for treatment of water and wastewater in India. *Water Conservation and Wastewater Treatment in BRICS Nations: Technologies, Challenges, Strategies and Policies*, **139–168.** https://doi.org/10.1016/B978-0-12-818339-7.00007-2

Tang, Z., Liu, Z. hua, Wang, H., Dang, Z., & Liu, Y. (2021a). Occurrence and removal of 17α-ethynylestradiol (EE2) in municipal wastewater treatment plants: Current status and challenges. *Chemosphere*, ***271,*** 129551. https://doi.org/10.1016/J.

Tang, Z., Liu, Z. hua, Wang, H., Dang, Z., & Liu, Y. (2021b). A review of 17α-ethynylestradiol (EE2) in surface water across 32 countries: Sources, concentrations, and potential estrogenic effects. *Journal of Environmental Management*, ***292,*** 112804. https://doi.org/10.1016/J.JENVMAN.2021.112804

Thai, T., Salisbury, B. H., & Zito, P. M. (2023). Ciprofloxacin. *StatPearls*.

Thangamani, N., & Bhuvaneshwari, N. (2022). Synthesis, characterization of Ag nanoparticles using the green approach towards degradation of environmental pollutant. *Journal of Materials Science: Materials in*

Electronics, ***33*****(12),** 9155–9162. https://doi.org/10.1007/S10854-021-07188-4/FIGURES/7

Thanhmingliana, Lee, S. M., Tiwari, D., & Prasad, S. K. (2015). Efficient attenuation of 17α-ethynylestradiol (EE2) and tetracycline using novel hybrid materials: Batch and column reactor studies. *RSC Advances*, ***5*****(58),** 46834–46842. https://doi.org/10.1039/c4ra17197g

Tirtom, V. N., Dinçer, A., Becerik, S., Aydemir, T., & Çelik, A. (2012). Comparative adsorption of Ni(II) and Cd(II) ions on epichlorohydrin crosslinked chitosan–clay composite beads in aqueous solution. *Chemical Engineering Journal*, ***197,*** 379–386. https://doi.org/10.1016/J.CEJ.2012.05.059

Tiwari, A., Shukla, A., Lalliansanga, Tiwari, D., & Lee, S. M. (2020). Synthesis and characterization of Ag0(NPs)/TiO2 nanocomposite: insight studies of triclosan removal from aqueous solutions. *Environmental Technology (United Kingdom)*, ***41*****(26),** 3500–3514. https://doi.org/10.1080/09593330.2019.1615127

Tran, Q. H., Nguyen, V. Q., & Le, A. T. (2013). Silver nanoparticles: synthesis, properties, toxicology, applications and perspectives. *Advances in Natural Sciences: Nanoscience and Nanotechnology*, ***4*****(3),** 033001. https://doi.org/10.1088/2043-6262/4/3/033001

UNESCO. (2023). *The global water quality challenge & SDGs*. Unesco.

Unuabonah, E. I., El-Khaiary, M. I., Olu-Owolabi, B. I., & Adebowale, K. O. (2012). Predicting the dynamics and performance of a polymer–clay based composite in a fixed bed system for the removal of lead (II) ion. *Chemical Engineering Research & Design*, ***90*****(8),** 1105–1115. https://doi.org/10.1016/J.CHERD.2011.11.009

US EPA. (2022). *Triclosan | US EPA*. Ingredients Used in Pesticide Products.

Vanlalveni, C., Lallianrawna, S., Biswas, A., Selvaraj, M., Changmai, B., & Rokhum, S. L. (2021). Green synthesis of silver nanoparticles using plant

extracts and their antimicrobial activities: a review of recent literature. *RSC Advances*, ***11*****(5)**, 2804–2837. https://doi.org/10.1039/D0RA09941D

Veldhoen, N., Skirrow, R. C., Osachoff, H., Wigmore, H., Clapson, D. J., Gunderson, M. P., Van Aggelen, G., & Helbing, C. C. (2006). The bactericidal agent triclosan modulates thyroid hormone-associated gene expression and disrupts postembryonic anuran development. *Aquatic Toxicology (Amsterdam, Netherlands)*, ***80*****(3),** 217–227. https://doi.org/10.1016/J.AQUATOX.2006.08.010

Vidal, C. B., Raulino, G. S. C., Melo, D. Q., Pessoa, G. P., Oliveira, J. T., Santosand, A. B., & Nascimento, R. F. (2015). *Removal of Endocrine Disruptors From Wastewater With Adsorption Onto Tin Pillared Montmorillonite*. *February*, **9146–9153**. https://doi.org/10.5151/chemeng-cobeq2014-1761-17684-145592

Vilchis-Nestor, A. R., Sánchez-Mendieta, V., Camacho-López, M. A., Gómez-Espinosa, R. M., Camacho-López, M. A., & Arenas-Alatorre, J. A. (2008). Solventless synthesis and optical properties of Au and Ag nanoparticles using Camellia sinensis extract. *Materials Letters*, ***62*****(17–18),** 3103–3105. https://doi.org/10.1016/J.MATLET.2008.01.138

Vilela, C. L. S., Bassin, J. P., & Peixoto, R. S. (2018). Water contamination by endocrine disruptors: Impacts, microbiological aspects and trends for environmental protection. *Environmental Pollution*, ***235*****,** 546–559. https://doi.org/10.1016/J.ENVPOL.2017.12.098

Vu, T. H., Ngo, T. M. V., Duong, T. T. A., Nguyen, T. H. L., Mai, X. T., Pham, T. H. N., Le, T. P., & Tran, T. H. (2020). Removal of Tetracycline from Aqueous Solution Using Nanocomposite Based on Polyanion-Modified Laterite Material. *Journal of Analytical Methods in Chemistry*. https://doi.org/10.1155/2020/6623511

Wang, A., & Wang, W. (2019). Palygorskite Nanomaterials: Structure, Properties, and Functional Applications. *Nanomaterials from Clay*

Minerals: A New Approach to Green Functional Materials, **21–133.** https://doi.org/10.1016/B978-0-12-814533-3.00002-8

Wang, H., Tang, H., Liu, Z., Zhang, X., Hao, Z., & Liu, Z. (2014). Removal of cobalt(II) ion from aqueous solution by chitosan–montmorillonite. *Journal of Environmental Sciences*, ***26*(9),** 1879–1884. https://doi.org/10.1016/J.JES.2014.06.021

Wang, J., & Zhang, M. (2020). Adsorption Characteristics and Mechanism of Bisphenol A by Magnetic Biochar. *International Journal of Environmental Research and Public Health*, ***17*(3).** https://doi.org/10.3390/IJERPH17031075

Wang, W. ;, Weng, Y. ;, Luo, T. ;, Wang, Q. ;, Yang, G. ;, Jin, Y., Wang, W., Weng, Y., Luo, T., Wang, Q., Yang, G., & Jin, Y. (2023). Antimicrobial and the Resistances in the Environment: Ecological and Health Risks, Influencing Factors, and Mitigation Strategies. *Toxics 2023, Vol. **11,** Page 185*, *11*(2), 185. https://doi.org/10.3390/TOXICS11020185

Wang, X., Cheng, B., Zhang, L., Yu, J., & Normatov, I. (2022). Adsorption performance of tetracycline on NiFe layered double hydroxide hollow microspheres synthesized with silica as the template. *Journal of Colloid and Interface Science*, ***627*,** 793–803. https://doi.org/10.1016/J.JCIS.2022.07.063

Wang, Y., Liu, A., & Chen, C. (2005). Genetic basis for conversion of rough-to-smooth colony morphology in Actinobacillus actinomycetemcomitans. *Infection and Immunity*, ***73*(6),** 3749–3753. https://doi.org/10.1128/IAI.73.6.3749-3753.2005

Weatherly, L. M., & Gosse, J. A. (2017). Triclosan Exposure, Transformation, and Human Health Effects. *Journal of Toxicology and Environmental Health. Part B, Critical Reviews*, ***20*(8),** 447. https://doi.org/10.1080/10937404.2017.1399306

Westrup, J. L., Bertoldi, C., Cercena, R., Dal-Bó, A. G., Soares, R. M. D., &

Fernandes, A. N. (2021). Adsorption of endocrine disrupting compounds from aqueous solution in poly(butyleneadipate-co-terephthalate) electrospun microfibers. *Colloids and Surfaces A: Physicochemical and Engineering Aspects*, ***611,*** 125800. https://doi.org/10.1016/J.COLSURFA.2020.125800

WHO. (2019). *New report calls for urgent action to avert antimicrobial resistance crisis*.

Wiesner, A. D., Katz, L. E., & Chen, C. C. (2006). The impact of ionic strength and background electrolyte on pH measurements in metal ion adsorption experiments. *Journal of Colloid and Interface Science*, ***301*****(1),** 329–332. https://doi.org/10.1016/J.JCIS.2006.05.011

Williams, L. B. (2019). Natural antibacterial clays: Historical uses and modern advances. *Clays and Clay Minerals*, *67*(1), 7–24. https://doi.org/10.1007/S42860-018-0002-8/METRICS

Wolfe, A. J., & Brubaker, L. (2015). Sterile Urine and the Presence of Bacteria. *European Urology*, ***68*****(2),** 173–174. https://doi.org/10.1016/j.eururo.2015.02.041

Wu, H., Xie, H., He, G., Guan, Y., & Zhang, Y. (2016). Applied Clay Science Effects of the pH and anions on the adsorption of tetracycline on iron-montmorillonite. *Applied Clay Science*, ***119,*** 161–169. https://doi.org/10.1016/j.clay.2015.08.001

Wu, Q., Li, Z., Hong, H., Yin, K., & Tie, L. (2010). Adsorption and intercalation of ciprofloxacin on montmorillonite. *Applied Clay Science*, ***50*****(2),** 204–211. https://doi.org/10.1016/j.clay.2010.08.001

Wu, X., Gao, P., Zhang, X., Jin, G., Xu, Y., & Wu, Y. (2014). Synthesis of clay/carbon adsorbent through hydrothermal carbonization of cellulose on palygorskite. *Applied Clay Science*, ***95,*** 60–66. https://doi.org/10.1016/J.CLAY.2014.03.010

Yadav, D., Karki, S., Gohain, M. B., & Ingole, P. G. (2023). Development of

micropollutants removal process using thin-film nanocomposite membranes prepared by green new vapour-phase interfacial polymerization method. *Chemical Engineering Journal*, ***472,*** 144940. https://doi.org/10.1016/J.CEJ.2023.144940

Yin, I. X., Zhang, J., Zhao, I. S., Mei, M. L., Li, Q., & Chu, C. H. (2020). The Antibacterial Mechanism of Silver Nanoparticles and Its Application in Dentistry. *International Journal of Nanomedicine*, ***15,*** 2555–2562. https://doi.org/10.2147/IJN.S246764

Yin, Y., Liu, J., & Jiang, G. (2012). Sunlight-induced reduction of ionic Ag and Au to metallic nanoparticles by dissolved organic matter. *ACS Nano*, ***6*****(9),** 7910–7919. https://doi.org/10.1021/nn302293r

Yoo, D. K., Bhadra, B. N., & Jhung, S. H. (2021). Adsorptive Purification of Water Contaminated with Hazardous Organics by Using Functionalized Metal-Organic Frameworks. *Metal-Organic Frameworks in Biomedical and Environmental Field*, **269–290**. https://doi.org/10.1007/978-3-030-63380-6_8

You, X., Liu, S., Dai, C., Zhong, G., Duan, Y., Guo, Y., Makhinov, A. N., Júnior, J. T. A., Tu, Y., & Leong, K. H. (2020). Effects of EDTA on adsorption of Cd(II) and Pb(II) by soil minerals in low-permeability layers: batch experiments and microscopic characterization. *Environmental Science and Pollution Research*, ***27*****(33),** 41623–41638. https://doi.org/10.1007/s11356-020-10149-9

Yu, L. ling, Cao, W., Wu, S. chuan, Yang, C., & Cheng, J. hua. (2018). Removal of tetracycline from aqueous solution by MOF/graphite oxide pellets: Preparation, characteristic, adsorption performance and mechanism. *Ecotoxicology and Environmental Safety*, ***164,*** 289–296. https://doi.org/10.1016/J.ECOENV.2018.07.110

Zafar, F. F., Marrakchi, F., Barati, B., Yuan, C., Cao, B., & Wang, S. (2022). Highly efficient adsorption of Bisphenol A using NaHCO3/CO2

activated carbon composite derived from shrimp shell@cellulose. *Environmental Science and Pollution Research*, ***29*****(45),** 68724–68734. https://doi.org/10.1007/s11356-022-20564-9

Zang, L., Qiu, J., Yang, C., & Sakai, E. (2016). Preparation and application of conducting polymer/Ag/clay composite nanoparticles formed by in situ UV-induced dispersion polymerization. *Scientific Reports 2016 6:1*, ***6*****(1),** 1–12. https://doi.org/10.1038/srep20470

Zhang, X. F., Liu, Z. G., Shen, W., & Gurunathan, S. (2016). Silver Nanoparticles: Synthesis, Characterization, Properties, Applications, and Therapeutic Approaches. *International Journal of Molecular Sciences*, ***17*****(9).** https://doi.org/10.3390/IJMS17091534

Zhang, Y., Boyd, S. A., Teppen, B. J., Tiedje, J. M., & Li, H. (2014). Role of tetracycline speciation in the bioavailability to escherichia coli for uptake and expression of antibiotic resistance. *Environmental Science and Technology*, ***48*****(9),** 4893–4900. https://doi.org/10.1021/ES5003428

Zhang, Z., Li, H., & Liu, H. (2018). Insight into the adsorption of tetracycline onto amino and amino–Fe3 + gunctionalized mesoporous silica: Effect of functionalized groups. *Journal of Environmental Sciences*, ***65*****,** 171–178. https://doi.org/10.1016/J.JES.2016.10.020

Zhao, G., Huang, X., Tang, Z., Huang, Q., Niu, F., & Wang, X. (2018). Polymer-based nanocomposites for heavy metal ions removal from aqueous solution: a review. *Polymer Chemistry*, ***9*****(26),** 3562–3582. https://doi.org/10.1039/C8PY00484F

Zhao, M., Huang, L., Babu Arulmani, S. R., Yan, J., Wu, L., Wu, T., Zhang, H., & Xiao, T. (2022). Adsorption of Different Pollutants by Using Microplastic with Different Influencing Factors and Mechanisms in Wastewater: A Review. *Nanomaterials*, ***12*****(13).** https://doi.org/10.3390/NANO12132256/S1

Zhou, C. H., Zhang, D., Tong, D. S., Wu, L. M., Yu, W. H., & Ismadji, S.

(2012). Paper-like composites of cellulose acetate–organo-montmorillonite for removal of hazardous anionic dye in water. *Chemical Engineering Journal*, ***209,*** 223–234. https://doi.org/10.1016/J.CEJ.2012.07.107

Zhou, X. F., Dai, C. M., Zhang, Y. L., Surampalli, R. Y., & Zhang, T. C. (2011). A preliminary study on the occurrence and behavior of carbamazepine (CBZ) in aquatic environment of Yangtze River Delta, China. *Environmental Monitoring and Assessment*, ***173*****(1–4),** 45–53. https://doi.org/10.1007/s10661-010-1369-8

Zidan, H. M., Abdelrazek, E. M., Abdelghany, A. M., & Tarabiah, A. E. (2019). Characterization and some physical studies of PVA/PVP filled with MWCNTs. *Journal of Materials Research and Technology*, ***8*****(1),** 904–913. https://doi.org/10.1016/J.JMRT.2018.04.023

Zuhrotun, A., Oktaviani, D. J., & Hasanah, A. N. (2023). Biosynthesis of Gold and Silver Nanoparticles Using Phytochemical Compounds. *Molecules*, ***28*****(7)**, 3240. https://doi.org/10.3390/MOLECULES28073240

Zulfiqar, M., Lee, S. Y., Mafize, A. A., Kahar, N. A. M. A., Johari, K., & Rabat, N. E. (2020). Efficient Removal of Pb(II) from Aqueous Solutions by Using Oil Palm Bio-Waste/MWCNTs Reinforced PVA Hydrogel Composites: Kinetic, Isotherm and Thermodynamic Modeling. *Polymers 2020, Vol. **12,** Page 430, 12*(2), 430. https://doi.org/10.3390/POLYM12020430

BIO-DATA

1. NAME : Swagata Goswami

2. DATE OF BIRTH : 3rd January, 1997.

3. FATHER'S NAME : Achyut Goswami

4. PERMANENT ADDRESS : House No 40. Pub-Sarania road, Guwahati-781003, Assam.

5. EDUCATIONAL QUALIFICATIONS

Qualification	Year of Passing	Board/University	Subjects	Marks %	Division
HSLC	2013	State Board of Assam	English, Assamese, Mathematics, Science, Adv. Maths Social science.	79.8	First
HSSLC	2015	CBSE	English, Physical education, Physics, Chemistry, Biology	78.9	First
B.Sc	2018	Cotton University	Biotechnology (Major) Zoology & Chemistry (pass course)	70.1	First
M.Sc	2020	VIT University	Applied Microbiology (Specialization)	88.6	First

List of publications

A. Journals

1. **Goswami, S**., Dutta, D., Lalhmunsiama, Dubey, R., Tiwari, D., & Jung, J. (2024). Highly efficient hydrophobic nanocomposite in the decontamination of micropollutants and bacteria from aqueous wastes: A sustainable approach. Science of The Total Environment, 929, 172546. https://doi.org/10.1016/J.SCITOTENV.2024.172546
2. **Goswami, S**., Dutta, D., Pandey, S., Chattopadhyay, P., Lalhmunsiama, Dubey, R., & Tiwari, D. (2024). Novel fibrous Ag(NP) decorated clay-polymer composite: Implications in water purification contaminated with predominant micro-pollutants and bacteria. Journal of Environmental Management, 359,121063. https://doi.org/10.1016/J.JENVMAN.2024.121063
3. Das, P., Devi, N., Gaur, N., **Goswami, S**., Dutta, D., Dubey, R., & Puzari, A. (2023). Acrylonitrile adducts: design, synthesis and biological evaluation as antimicrobial, haemolytic and thrombolytic agent. Scientific Reports, 13(1), 1–16. https://doi.org/10.1038/s41598-023-33605-1
4. Dubey, R., **Goswami, S**., Sharma, S., Dutta, D., & Dwivedi, S. K. (2021). Antibacterial performance evaluation of silver-coated river sand for water decontamination application. Defence Life Science Journal, 6(3), 214–221. https://doi.org/10.14429/DLSJ.6.16031
5. Dutta, D., **Goswami, S.,** Dubey, R., Dwivedi, S. K., & Puzari, A. (2021). Antimicrobial activity of silver-coated hollow poly(methylmethacrylate) microspheres for water decontamination. Environmental Sciences Europe, 33(1). https://doi.org/10.1186/s12302-021-00463-5

B. Conference/ Seminar

1. Presented “Efficient use of hybrid material in the remediation aqueous solutions contaminated with antibiotic tetracycline” at the physical sciences discipline technical session in the 4th Mizoram Science Congress held at Aijal Club, Aizawl during 24-25 November, 2022.

2. Presented “Polymer incorporated clay nanocomposite in the remediation of ciprofloxacin from aquatic environment” at the International Conference on Science and Technology for Innovative and Sustainable Development (STISD-2023), held at Mizoram University during 28-30th June 2023.

Science of the Total Environment 929 (2024) 172546

Contents lists available at ScienceDirect

Science of the Total Environment

journal homepage: www.elsevier.com/locate/scitotenv

Highly efficient hydrophobic nanocomposite in the decontamination of micropollutants and bacteria from aqueous wastes: A sustainable approach

Swagata Goswami [a], Dhiraj Dutta [b], Lalhmunsiama [c], Rama Dubey [b], Diwakar Tiwari [a,*], Jinho Jung [d]

[a] Department of Chemistry, School of Physical Sciences, Mizoram University, Aizawl 796004, India
[b] DRL, Post Bag No 02, Tezpur, Assam 784001, India
[c] Department of Industrial Chemistry, School of Physical Sciences, Mizoram University, Aizawl 796004, India
[d] Division of Environmental Science and Ecological Engineering, Korea University, 145 Anam-ro, Seongbuk-gu, Seoul 02841, South Korea

HIGHLIGHTS

- Poly(4-vinylpyridine-co-styrene) grafted attapulgite decorated with Ag(NP) obtains fibrous nanocomposites
- The nanocomposite show potential in the decontamination of emerging micropollutants viz., tetracycline, and bisphenol A
- The hydrogen bonding and hydrophobic interactions are the deriving foces involved at the interface
- The nanocomposite material show potential in removing the *E. coli* and *S. pyogenes*

GRAPHICAL ABSTRACT

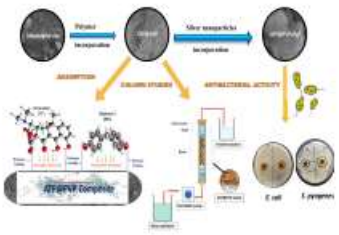

ARTICLE INFO

Editor: Abaslofiok Mark Ibekwe

Keywords:
Emerging micropollutants
Fibrous composites
Poly(4-vinylpyridine-co-styrene)
Sustainable treatment
Bacterial susceptibility

ABSTRACT

Micro-pollutants (specifically antibiotics and personal care products) and potential bacterial contamination pose a severe threat to human health and marine life. The study derives indigenous novel fibrous hydrophobic nanocomposite, efficient in decontaminating the micro-pollutants (tetracycline (TC) and bisphenol A (BPA)) and potential pathogens (*S. pyogenes* and *E. coli*) from aqueous wastes. A facile method synthesizes the fibrous attapulgite (ATP)- poly(4-vinylpyridine-co-styrene) (PVP) framework decorated in situ with the Ag^0 nanoparticles (ATP@PVP/Ag^0). A greener method using the *Artocarpus heterophyllus* leaf extract derives the Ag^0(NPs). Various analytical methods extensively characterize the materials. A comprehensive study that includes pH, concentration, background electrolytes, and ionic strength reveals the sorptive removal insights of TC and BPA utilizing the ATP@PVP solid. The elimination of tetracycline (TC) and bisphenol A (BPA) agrees well with the pseudo-second-order kinetics. The pH 3.07 and 6.06 favor removing TC and BPA with the capacity of 10.86 mg/g and 17.36 mg/g at 25 °C. The hydrogen bonding and hydrophobic interactions predominate the sorption mechanism, and the material shows remarkable stability and reusability in repeated sorption/desorption operations. Similarly, the natural water implications and flow-bed system show fair applicability of solid in

* Corresponding author.
E-mail address: diw_tiwari@yahoo.com (D. Tiwari).

https://doi.org/10.1016/j.scitotenv.2024.172546
Received 9 March 2024; Received in revised form 13 April 2024; Accepted 15 April 2024
Available online 17 April 2024

Journal of Environmental Management 359 (2024) 121063

Contents lists available at ScienceDirect

Journal of Environmental Management

journal homepage: www.elsevier.com/locate/jenvman

Research article

Novel fibrous Ag(NP) decorated clay-polymer composite: Implications in water purification contaminated with predominant micro-pollutants and bacteria

Swagata Goswami [a], Dhiraj Dutta [b], Shreekant Pandey [c], Pronobesh Chattopadhyay [b], Lalhmunsiama [d], Rama Dubey [b], Diwakar Tiwari [a,*]

[a] Department of Chemistry, School of Physical Sciences, Mizoram University, Aizawl, 796004, India
[b] DRL, Post Bag No 02, Tezpur, Assam, 784001, India
[c] Department of Biotechnology, Vinoba Bhave University, Hazaribagh, Jharkhand, 825301, India
[d] Department of Industrial Chemistry, School of Physical Sciences, Mizoram University, Aizawl, 796004, India

ARTICLE INFO

Keywords:
Micro-pollutants
Fibrous composite
Decontamination
Antimicrobial/viral activity
Loading capacity

ABSTRACT

Due to the potential harm caused by emerging micro-pollutants to living organisms, contaminating water supplies by micro-pollutants like EDCs, pharmaceuticals, and microorganisms has become a concern in many countries. Considering both microbiological and micro-pollutant exposure risks associated with water use for agricultural/or household purposes, it is imperative to create a strategy for improving pollutant removal from treated wastewater that is both effective and affordable. Natural clay minerals efficiently remove contaminants from wastewater, though the pristine clay has less affinity to several organic pollutants. Hydrophilic polymers, *viz.*, poly(ethylene glycol) (PEG), improve the dispersion of particles, flocculation processes, and surface properties. In this study, PEG grafted with attapulgite, thereby providing a high-specific surface-area, mesoporous materials for the adsorption of micro-pollutants like ciprofloxacin (CIP) and 17α-ethinylestradiol (EE2) at high rates. A gentle washing process regenerates the clay-polymer material several times with no performance loss, and the natural water implications show fair applicability of solid in decontaminating the CIP and EE2 in an aqueous medium. Further, greenly synthesized silver nanoparticles in situ disperse with the clay polymer efficiently remove the gram-positive and gram-negative bacterium *viz.*, *Bacillus subtilis*, and *Pseudomonas aeruginosa*, which are commonly persistent in aquatic environments. The clay polymer outperformed a modified clay composite to eliminate microorganisms and organic micro-pollutants in significant quantities quickly. These results clearly show the importance of fibrous clay-polymer composite for water purification technologies.

PARTICULARS OF THE CANDIDATE

Name of the candidate : Ms. Swagata Goswami

Department : Department of Chemistry

Title of thesis : Efficient removal of emerging micropollutants and bacteria from treated wastewaters using synthesized novel clay based nanocomposites.

Date of Admission : 6th November, 2020

Approval of research proposal

1. **DRC** : 19th April, 2021
2. **BOS** : 3rd May, 2021
3. **School Board** : 17th May, 2021
4. **PhD registration no. & date** : MZU/Ph.D/1613 of 06.11.2020

Head

Department of Chemistry

ABSTRACT

EFFICIENT REMOVAL OF EMERGING MICROPOLLUTANTS AND BACTERIA FROM TREATED WASTEWATERS USING SYNTHESISED NOVEL CLAY BASED NANOCOMPOSITES

AN ABSTRACT SUBMITTED IN PARTIAL FULFILLMENT OF THE REQUIREMENTS FOR THE DEGREE OF DOCTOR OF PHILOSOPHY

SWAGATA GOSWAMI

MZU REGISTRATION NO.: 2100003

Ph.D. REGISTRATION NO.: MZU/Ph.D./1613 of 06.11.2020

DEPARTMENT OF CHEMISTRY

SCHOOL OF PHYSICAL SCIENCES

JUNE, 2024

EFFICIENT REMOVAL OF EMERGING MICROPOLLUTANTS AND BACTERIA FROM TREATED WASTEWATERS USING SYNTHESISED NOVEL CLAY BASED NANOCOMPOSITES

BY

SWAGATA GOSWAMI

Department of Chemistry

Under the supervision of

Prof. DIWAKAR TIWARI

and

Co-supervision of

Dr. LALHMUNSIAMA

Dr. RAMA DUBEY

Submitted

In partial fulfillment of the requirement of the Degree of Doctor of Philosophy in Chemistry of Mizoram University, Aizawl.

ABSTRACT

Water is a fundamental resource essential for life, encompassing a wide range of uses from drinking and agriculture to industrial processes and recreations. Freshwater is vital for human consumption and ecosystem, constitutes only a small fraction of the total water present on the Earth's surface. The availability of clean, uncontaminated water is crucial for sustaining health, economic development, and ecological balance. Water pollution occurs as the harmful substances, such as chemicals, microorganisms, or waste products, contaminate water bodies, degrading water quality and posing risks to human health and the environment. Major sources of water pollution include industrial discharges, agricultural runoff, wastewater treatment plant effluents, and stormwater. Emerging micro-pollutants *viz.*, endocrine-disrupting chemicals (EDCs), pharmaceuticals, and personal care products have received significant concerns due to their persistence and potential harm even at low concentrations. These pollutants disrupt aquatic ecosystems, bioaccumulate in the ecosystem, and ultimately affect human health through water consumption and food chains. The presence of pathogenic microorganisms in water cause diseases such as cholera, dysentery, hepatitis, and giardiasis in humans. These pathogens proliferate in water bodies, especially in warm conditions, leading to outbreaks of waterborne diseases.

The conventional wastewater treatment plants (WWTPs) are not efficient enough to remove completely many persistent chemicals present in wastewater. The pharmaceuticals, endocrine-disrupting chemicals (EDCs), and personal

care products have received serious concern in recent decades due to their persistency in treated wastewater. Current wastewater treatment plants are not specifically designed to eliminate completely these persistent micropollutants and consequently various micropollutants along with their metabolites and transformation products are often detected in receiving water bodies. Conventional secondary processes such as activated sludge and trickling filters are the most extensively used in the wastewater purification; however, these processes fail to remove several chemical compounds. Therefore, it is necessary to instigate additional treatment technologies to remove these emerging micropollutants from the source i.e., the effluents of the WWTP. In addition, the presence of different microbial pathogens in a partially treated wastewater sample is severe concern and the development of antimicrobial resistance (AMR) has become a serious issue globally. The goal of researchers/environmentalists is to obtain zero fecal coliform in the treated water prior to use it for various purposes. In order to prevent transmission of various diseases, the treated wastewaters need to comply the microbiological quality guidelines.

Several techniques which are in practice for water treatment at small level or domestic scale. But, generally the cost and maintenance of such household water treatment techniques are encompassed with major challenges *viz*., high input cost, and cumbersome operation. However, the adsorptive purification of water is gaining interest globally. Adsorption is one of the tertiary water treatment technique, used for the removal of dissolved organic and inorganic pollutants from water. The adsorbents play a crucial role, and the potential of any adsorbent is determined by its specific surface area, porosity, surface functionality, selectivity, and adsorption kinetics. Nanomaterials (NMs) based adsorbents and nano adsorbents have high specific surface areas, well-defined porosity, and are easy to modify surface properties. All these properties collectively makes nano adsorbents as ideal materials for adsorptive removal of pollutants from water.

The low-cost natural materials are important for cost-effective remediation of water contaminated with a variety of contaminants. Some natural clay materials possess high surface area, well defined porosity and, a large number of active sites; hence, utilized as efficient adsorbents. Clays have unique physicochemical properties, which enables them to use as excellent starting material to obtain the nanocomposite materials. The recent study is an attempt to incorporate efficiently the variety of polymers within the attapulgite clay network. The applicability of clay-polymer composite is manifold due to its stability and functionality. Moreover, the composite materials have greater mechanical strength and show selectivity towards a variety of micro-pollutants. The present study is intended to incorporate the poly(ethylene glycol) (PEG) and poly(4-vinylpyridine-co-styrene) (PVP) onto attapulgite clay to obtain ATTP@PEG and ATTP@PVP composite materials. Further, these materials are employed in efficient elimination of micro-pollutants such as tetracycline (TCH), bisphenol A (BPA), ciprofloxacin (CIP), 17α-ethynylestradiol (EE2) and triclosan (TCS) under batch and column reactor operations. Further, natural phytochemicals obtained from plant extract of Jack fruit leaf (*Artocarpus heterophyllus Lam*) are used to synthesize the Ag nanoparticles, and are incorporated *in situ* with ATTP@PEG and ATTP@PVP. The nanocomposite materials are used to decontaminate the microbial activity of the bacteria present in water.

The pristine attapulgite along with the composite materials were characterized by the Fourier transform-infrared spectrometry (FT-IR), X-ray diffraction (XRD), X-ray photoelectron spectroscopy (XPS), scanning electron microscope (SEM), transmission electron microscope (TEM). Further, the elemental spectra of solids was obtained by the energy-dispersive X-ray spectroscopy (EDX) analyses. The Brunauer-Emmett-Teller (BET) surface area analyzer was employed to obtain the specific surface area, pore size and pore volume of the materials.

The FT-IR data showed the successful grafting of polymers within the clay network. The SEM images showed that ATTP@PEG, ATTP@PVP, ATTP@PEG/Ag^0 and ATTP@PVP/Ag^0 materials possessed more compact structures compared to the pristine attapulgite. The XRD pattern of pristine clay demonstrates that the prominent diffraction peaks at 2θ values of 8.3º, 19.7º, and 27.3º inferred the diffraction planes of (110), (040), and (400), respectively, of the attapulgite. The ATTP@PEG showed predominant diffraction peaks at 2θ values of 19.81º and 24.19º due to the (120) and (032) planes of PEG. The diffraction peaks shown by ATTP@PEG/Ag^0 at 2θ values of 38.19º, 46.18º, 67.74º, and 77.70º referred to the characteristic planes of (111), (200), (220), and (311), respectively, of Ag(NPs). Similarly, the ATTP@PVP/Ag^0 showed characteristic diffraction peaks of the Ag(NPs), predominatly occurred at 2θ values of 38.1º, 46.2º, 64.4º and 77.69º corresponding to the planes (111), (200), (220), and (311), respectively. The average particle sizes of ATTP@PEG/Agº and ATTP@PVP/Agº are 0.24 nm and 0.21 nm, respectively. The BET analysis revealed that all these materials possessed type IV isotherm with mesoporous structure and the specific surface area of the composite materials is increased significantly due to the grating of polymeric chain within the clay network. However, the surface area decreased comparatively for ATTP@PEG/Agº and ATTP@PVP/Ag^0 due to the silver nanoparticles having predominantly occupied some of the pores of ATTP@PEG and ATTP@PVP. The XPS analytical graph displayed the peaks of Ag(3d) representing the elemental zerovalent silver's $3d_{5/2}$ and $3d_{3/2}$ energy levels occurred at the binding energies of 368.4 eV and 374.1 eV, respectively, which confirms the presence of silver in its reduced state in ATTP@PEG/Agº and ATTP@PVP/Agº nanocomposites. Furthermore, the contact angle measurements for ATTP, ATTP@PEG and ATTP@PVP composites showed the contact angles of 64º, 100.9º and 102.9º, respectively, indicating the composite's hydrophobic nature.

The composite materials along with the pristine attapulgite were employed in the elimination of micro-pollutants *viz*., tetracycline, bisphenol A,

ciprofloxacin, triclosan and 17α-ethynylestradiol from aqueous solutions under the batch and column reactor operations. Batch studies showed that the synthesized materials ATTP@PEG, ATTP@PVP, ATTP@PEG/Ag^0 and ATTP@PVP/Ag^0 removed tetracycline, bisphenol A, ciprofloxacin, EE2 and triclosan within a wide pH range and the removal percentage are significantly improved for the composite solids compared to the pristine attapulgite. The concentration dependence data followed Langmuir adsorption isotherm for these pollutants. The Langmuir monolayer adsorption capacities for TCH, BPA, CIP, EE2 and TCS are 13.58, 14.08, 28.98, 30.48, and 25.90 mg/L, respectively, using the ATTP@PVP and 10.98, 22.37, 28.17, 29.32, and 39.06 mg/L, respectively, for ATTP@PEG. The effect of contact time in the removal of these micro-pollutants showed the rapid uptake of these pollutants and the kinetic modelling showed the uptake of these micro-pollutants by the ATTP@PEG and ATTP@PVP fitted well to the PSO model compared to the PFO model. Increasing the background electrolyte (NaCl) concentrations (1000 times) had unaffected the removal percentage of these micro-pollutants by the ATTP@PEG and ATTP@PVP solids. Similarly, the presence of various co-existing cations *viz*., Mg(II), Mn(II), Ca(II) and Ni(II) did not affect the percentage uptake of these micro-pollutants, whereas the presence of EDTA affected the removal of tetracycline, triclosan, bisphenol A, ciprofloxacin and EE2 using ATTP@PEG and ATTP@PVP solids.

The column reactor experiments resulted a complete breakthrough for TCH and BPA at 2.08 L and 1.51 L using ATTP@PVP beads, and a complete breakthrough for EE2 was achieved having throughput volume of 1.21 L and for CIP is at 1.51 L using ATTP@PEG beads. Additionally, applicability of these novel materials in the removal of micro-pollutants *viz.*, tetracycline, triclosan, ciprofloxacin, bisphenol A and EE2 in real matrix sample was conducted under varied pollutant concentrations (1-25 mg/L). Results showed that the removal of these micro-pollutants is not affected as compared to the results obtained with purified water indicating the selectivity of these composite solids towards the studied micro-pollutants and showed potential in

real implications. Furthermore, the materials i.e., ATTP@PEG and ATTP@PVP is reused for six adsorption-desorption cycles of TCH, BPA, CIP, EE2 and TCS without significant loss in their efficacy. The reusability test indicated that ATTP@PEG and ATTP@PVP possessed greater stability and could be reutilized for successive operations in the removal of these micro-pollutants from aqueous solutions.

The insight mechanisms on the removal of these micropollutants was investigated with the help of XPS data and contact angle test of the solid sample. The formation of hydrogen bonding and hydrophobic interactions are the major pathways of removing these micropollutants using the ATTP@PEG and ATTP@PVP composites.

The ATTP@PEG/Ag^0 and ATTP@PVP/Ag^0 were used for antibacterial activity against both Gram-positive and Gram-negative bacterial strains present in contaminated water. The ATTP@PEG/Ag^0 inhibits the *Pseudomonas aeruginosa* and *Bacillus subtilis*, zones against *P. aeruginosa* had a diameter of 13.6±0.3, 15.3±0.3, 19.3±0.2, and 23.2±0.6 mm for doses of 2.0, 4.0, 6.0, and 8.0 mg of ATTP@PEG/Ag^0, respectively. The measured diameter of the zone of inhibition against *B. subtilis* using the ATTP@PEG/Ag^0 concentrations was 10.1±0.3, 13.4±0.4, 17.2±0.3 and 20.3±0.2 mm. However, the attapulgite (without Ag) did not inhibit the *P. aeruginosa* and *B. subtilis*. Similarly, the zone of inhibition using the ATTP@PVP/Ag^0 nanocomposite against both Gram negative (*E. coli*) and Gram positive (*S. pyogenes*) bacteria were assessed. It is clearly observed that nanocomposite showed good antibacterial activity against two model bacteria. Generally, the mean zone of inhibition of the ATTP@PVP/Ag^0 nanomaterial ranged between 3.2±0.9 mm and 8.1±0.5 mm for *E. coli* and 4.4±0.3 mm and 10.2±0.6 mm for *S. pyogenes*. The bactericidal activity of ATTP@PVP/Ag^0 nanocomposite against *E. coli* and *S. pyogenes* and ATTP@PEG/Ag^0 nanocomposite against *P. aeruginosa* and *B. subtilis* were also assessed by the time kill kinetic analysis. The result of this study revealed that after 24 hrs, all the bacterial cells of *E. coli* and *S. pyogenes* were removed by ATP@PVP/Ag^0 and thereby confirming its bactericidal

nature. Similarly, the outcomes demonstrate that ATTP@PEG/Ag^0 eliminated all bacterial cells, demonstrating the bactericidal efficacy of ATTP@PEG/Ag^0 towards the two pathogenic bacteria *P. aeruginosa* and *B. subtilis*. The effect of abiotic factor, such as pH, on bacterial elimination from water using ATTP@PVP/Ag^0 was also assessed. The removal efficiency of these solids towards the *E. coli* and *S. pyogenes* increased as pH was decreased. The log reduction of *E. coli* was 7.6 $\log_{10}$ CFU/mL at pH 4.0, while at pH 7.0 and 9.0 the log reduction of *E. coli* corresponded to 7.0 $\log_{10}$ CFU/mL and 6.7 $\log_{10}$ CFU/mL, respectively. The log reduction of *S. pyogenes* was 7.9 $\log_{10}$ CFU/mL, 7.6 $\log_{10}$ CFU/mL and 7.0 $\log_{10}$ CFU/mL at pH 4.0, 7.0 and 9.0, respectively. These studies show that the materials, i.e., ATTP@PEG/Ag^0 and ATTP@PVP/Ag^0 possesses potential in large-scale treatment of wastewaters contaminated with both micro-pollutants and biological pollutants.